Crystal structure determination and prediction of simple organic molecules, using powder diffraction methods, and modern computational techniques

by

HARCHARN S CHANA

A thesis submitted to
The University of Birmingham
For the degree of
DOCTOR OF PHILOSOPHY

School of Chemistry
The University of Birmingham
June 2006

For my better half - Jasbir

'Gravitation is not responsible for people falling in love'

--Albert Einstein (14 March 1879-1955)

CONTENTS

List of Figures

Figure 5.7.9: Adipamide (form II) structure 13 showing ladders running along the [001] direction.

Figure 5.7.10: Comparison of the experimental X-ray diffraction pattern of adipamide (form II) with the simulated powder patterns for adipamide (form II) structures 1, 2, and 13.

Figure 5.7.10a: End-on view of adipamide (form I) structure 1 showing the sheets along the (110) plane (green shaded area).

Figure 5.7.11: View of an infinite hydrogen bonded sheet in adipamide (form I) structure 1.

Figure 5.7.12: End-on view of adipamide (form I) structure 2 showing the adipamide sheets along the (101) plane within.

Figure 5.7.13: View of an infinite hydrogen bonded sheet in adipamide (form I) structure 2.

Figure 5.7.14: End-on view of adipamide (form I) structure 19 showing the adipamide sheets along the (201) plane.

Figure 5.7.15: View of an infinite hydrogen bonded sheet in adipamide (form I) structure 19. The $R_2^2(8)$ dimer is illustrated in the green shaded area.

Figure 5.7.16: Comparison of the experimental X-ray diffraction pattern of adipamide form (I and II) with the simulated powder patterns for adipamide (form I) structures 1, 2, and 19.

Figure 5.8.1: View of pimelamide (VIII) showing the ladders extending along the [110] direction.

Figure 5.8.2: View of pimelamide (VIII) illustrating the infinite sheets in the [001] direction.

Figure 5.9.1: View suberamide (IX) showing a combination of dimers and chains to form the hydrogen bonded sheet. The $R_2^2(8)$ and $R_1^2(8)$ motifs are shown using green and yellow shading respectively.

Figure 5.9.2: End-on view of hydrogen bonded sheets in suberamide (IX) as illustrated by the yellow shading.

Figure 5.9.3: View of suberamide structure 1 showing ladders in the [201] direction (yellow shaded area).

Figure 5.9.4: End on view of suberamide structure 1 showing the sheets along (101) plane.

Figure 5.9.5: Suberamide structure 2 showing the combination of dimers and chains giving the illusion of ladders.

Figure 5.9.6: View of suberamide structure 2 (aliphatic carbon atoms omitted for clarity) showing the hydrogen bonded sheet along (011). The $R_6^8(24)$ motif is illustrated using green shading.

Figure 5.9.7: View of suberamide structure 9 showing the combination of dimers and chains giving the illusion of ladders.

Figure 5.9.8: View of suberamide structure 9 (aliphatic carbon atoms omitted for clarity) showing the hydrogen bonded sheet along (011). The $R_6^8(24)$ motif is illustrated using green shading.

Figure 5.9.9: View of suberamide structure 10 showing the combination of dimers and chains to form the hydrogen bonded sheet.

Figure 5.9.10: End-on view of suberamide structure 10 showing hydrogen bonded sheets along (110).

List of Tables

Acknowledgements

The work contained within this thesis would not have been possible if not for the people who made the working environment pleasant and educational. I would like to start by expressing my gratitude to my supervisor Dr. Maryjane Tremayne for firstly giving me the opportunity to pursue a PhD and secondly for all her support and positive encouragement throughout the course of the three years. Her commitment and enthusiasm towards the research project has been truly exceptional such that it has allowed me to strive for more knowledge and allowed my research to excel to new levels. I am also indebted to Dr. Colin Cormack who furnished me with oodles of structural information and for making the task of learning the programming language 'perl' just a little less baffling. Other members of the theoretical chemistry group include Dr. Eugene Cheung and Dr. Benson Kariuki for all their crystallographic knowledge and general help and guidance they provided throughout the three years. Finally, I would like to take this opportunity to thank all my friends and family who have supported me over the last four years.

Abstract

The research presented within this thesis highlights aspects of crystal structure determination from the combined use of powder X-ray, synchrotron and neutron diffraction and also computational crystal structure prediction from molecular structure only.

The use of DE enabled the crystal structure of 2,4-dichloro-5-sulfamoylbenzoic acid and oxamic acid to be examined from conventional laboratory X-ray diffraction.

In the case of 2,4-dichloro-5-sulfamoylbenzoic acid two comparable structures were identified each of which refined to similar extents. To correctly identify the correct crystal structure it was necessary to obtain and refine a powder neutron dataset. This presented before obscured information on the relative positions of hydrogen atoms and inevitably led to the successful elucidation of the crystal structure of 2,4-dichloro-5-sulfamoylbenzoic acid. With reference to oxamic acid two conformations, namely '*cis*' and '*trans*' were identified from the refinement of laboratory X-ray diffraction. Infrared analysis and lattice energy calculations were also used to distinguish between the two conformations with some success.

With respect to computational crystal structure prediction, presented here is a new computational strategy for crystal structure prediction from molecular structure only. The traditional lattice energy output from a polymorph prediction sequence is re-ranked in terms of hydrogen bonding and graph set merit points. My research here has to a certain extent managed to combine these attributes and enabled the successful prediction of 8 out of the initial 11 chosen test structures obtained from the Cambridge Structural Database (CSD).

1.0 Introduction

The design and preparation of crystalline materials with specific physical and chemical properties has to a certain extent benefited and shaped our society and the way we live our everyday lives. The study of organics and pharmaceuticals has enabled us to manufacture various chemicals and life saving drugs, the semiconducting properties of silicon has given us the unlimited power of the computer chip. Structural properties of polymers and pigments have brought about the creation of ultra strong carbon fibre plastics and paint. Materials scientists are now discovering and creating entirely new types of materials, such as nanotubes and zeolites; taking materials science into a new dimension, leading to properties and performance never before imagined [Harris. K.D.M. et al 2001]. It is this principal reason why solid state chemists devote so much time exploring the correlations between internal architecture (structure) and performance (properties). This relationship between material structure and performance is governed primarily by the atomic arrangement of atoms, ions and molecules within the crystalline material, and is fundamentally governed by intermolecular interactions such as hydrogen bonding. Understanding these interactions is therefore a crucial tool for the design and synthesis of new materials with desired properties.

Crystal structure determination and more recently crystal structure prediction have been areas of great interest to a wide range of scientific fields and industries that use materials in the solid state, including pharmaceuticals, [Dunitz J. D. 1991] [Caira. M. R. 1998] zeolites, [Thomas J. M. 1998, 1988] [Thomas. J. M. 1994] [Thomas. J. M. 1999] polymers, [Hanna. S. et al. 1995] [Pazur. R. J. et al. 1998] pigments, dyes [Zollinger. H. 1991] and explosives [Millar. G. R. 2001]. In the case of the pharmaceutical industries, it is of grave importance that knowledge of crystal structures

of drug products is accurately acquired. Nearly all drug substances are administered as polycrystalline powders and optimising their pharmaceutical properties such as solubility, dissolution rate, bioavailability, shelf life and the conditions for handling and administration can only be exploited if accurate structural information is available.

The research contained within this thesis is therefore separated into these two main areas, crystal structure determination and prediction. With respect to structure determination, the crystal structures of two organic materials, namely 2,4-dichloro-5-sulfamoylbenzoic acid and oxamic acid were investigated from the combined use of powder X-ray and neutron diffraction data. In the case of crystal structure prediction, a computational strategy was developed that was capable of automatically examining a traditional theoretical polymorph prediction output and re-rank structurally favourable crystal structures.

1.1 Definition of the crystalline State

The fundamental characteristic of a perfectly crystalline solid is the presence of long-range, three dimensional periodic order. This attribute is brought about as a direct consequence of the precise nature in which atoms, ions and molecules are distributed within a crystalline material. At a molecular level interactions and forces (such as Van der Waals and electrostatics) between the molecules, in particular hydrogen bonding give rise to long range periodic order generating structural motifs or repeat units, which interact in all directions to form the overall geometrical arrangement of the crystalline solid. The repeating motif within a crystal structure is represented simply by a translationally repeating unit cell as illustrated in figure 1.1. Unit cells are divided into seven distinct crystal systems (Table 1.1) depending upon the constraints placed upon them by a minimum characteristic symmetry. In addition to these seven crystal systems there are also four independent lattice types, Primitive (P), Face-Centered (F), Body-Centered (I) and Side-Centered (A), (B) or (C), see figure 1.2.

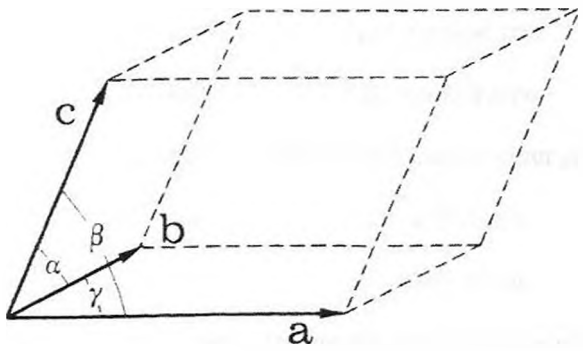

Figure 1.1: A three-dimensional repeating unit cell from which, the entire crystal structure can be translationally constructed. Parallelepiped defined by three lengths, {a, b, c}, and three angles {α, β, γ}.

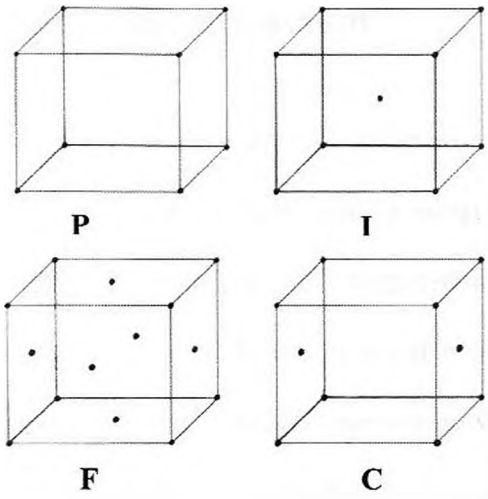

Figure. 1.2: Illustrations of the four lattice types P, I, F and C.

Additional symmetry elements such as rotational and translational symmetry, mirror planes and centres of inversion are used to define the relationships between structural units within the unit cell with 230 distinct combinations of symmetry elements giving rise to the 230 crystallographic space groups.

Crystal Class	Unit Cell	Symmetry	Bravais Lattice
Cubic	$a = b = c$, $\alpha = \beta = \gamma = 90°$	Four threefold axes	P, F, I
Tetragonal	$a = b \neq c$, $\alpha = \beta = \gamma = 90°$	One fourfold axes	P, I
Orthorhombic	$a \neq b \neq c$, $\alpha = \beta = \gamma = 90°$	Three twofold axes or mirror planes	P, F, I, C
Hexagonal	$a = b \neq c$, $\alpha = \beta = 90°$, $\gamma = 120°$	One sixfold axes	P
Trigonal	$a = b \neq c$, $\alpha = \beta = 90°$, $\gamma = 120°$	One sixfold axes	P
Monoclinic	$a \neq b \neq c$, $\alpha = \gamma = 90°$, $\beta \neq 90°$	One twofold axes or mirror planes	P, C
Triclinic	$a \neq b \neq c$, $\alpha \neq \beta \neq \gamma \neq 90°$	None	P

Table 1.1: The Seven crystal systems

1.2 Fundamentals of X-ray diffraction

X-rays are electromagnetic waves of wavelength of the order 1Å (10^{-10}m) and are produced by decelerating fast moving electrons onto a metal target (Mo, Cu, Fe, Cr), thereby converting their energy of motion into characteristic wavelengths of X-ray radiation. On striking a crystalline solid, X-rays will either travel straight through the crystal or be scattered in all directions through interactions with the periodic electron charge distribution surrounding the atomic nuclei. This scattering process is more commonly known as diffraction and is the most widely used method for the precise determination of the atomic positions of atoms in crystalline solids. According to the Bragg model (figure 1.3) this phenomena can be considered as the 'reflection' of incident X-ray radiation by parallel planes of atoms. These crystalline planes, which are defined as the *hkl* lattice planes or Miller indices will only give rise to constructive interference when the path difference between radiation scattered from adjacent planes is equal to a whole number of wavelengths (Bragg angle). This is known as Bragg's law and is expressed in equation 1.

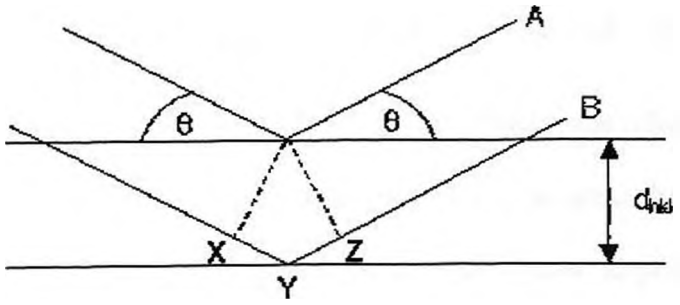

Figure 1.3: Illustration of the Bragg model which gives rise to constructive interference by parallel *hkl* planes.

$$n\lambda = 2d_{hkl}\sin\theta_{hkl} \qquad \textit{equation 1}$$

where λ is the wavelength of incident radiation, $2\theta_{hkl}$ is the angle between the incident X-rays and the crystal surface (*glancing angle*) and n is the order of diffraction. The term d_{hkl} is referred to as the inter-planar spacing for the crystal planes with Miller indices *hkl* and is expressed as in equation 2:

$$d_{hkl} = V\,[h^2b^2c^2\sin^2\alpha + k^2a^2c^2\sin^2\beta + l^2a^2b^2\sin^2\gamma + 2hlab^2c(\cos\alpha\cos\gamma - \cos\beta) + 2hkabc^2(\cos\alpha\cos\beta - \cos\gamma) + 2klab2c(\cos\beta\cos\gamma - \cos\alpha)]^{1/2}$$

equation 2

where V defines the unit cell volume and a, b, c, α, β, γ are the unit cell parameters.

1.2.1 The crystallographic phase problem

An image of the scattering matter (electron density in the case of X-rays and nuclei in the case of neutrons) at a point x,y,z in a unit cell of volume V_c can be expressed as in equation 3:

$$\rho(xyz) = \frac{1}{v_c}\sum_h\sum_k\sum_l |F|\cos\left[2\Pi(hx + ky + lz) - \alpha\right] \qquad \textit{equation 3}$$

where ρ(xyz) is the electron density and α is the associated phase information.

From equation 3, it is clear that the crystal structure is represented by ρ(xyz) and may be determined directly from knowledge of the structure factor amplitudes |F(s)| and the relative phases α(s) of the scattered radiation. The intensity of the scattered radiation is

directly proportional to the square of the structure factor amplitudes |F(s)| as illustrated in equation 4.

$$I(s) \propto | F(s) |^2 \qquad \textit{equation 4}$$

where I(s) is the intensity of the scattered radiation.

However, an experimental diffraction pattern gives only information on intensities and hence the structure factor amplitudes |F(s)|, no information can be obtained directly about the associated phases $\alpha(s)$. This is the fundamental problem in structural crystallography and is known as the 'phase problem'. If phase information could be extracted directly from diffraction data, structure determination would be straightforward using equation 3. In traditional structure determination programs, the phase problem is addressed by mathematically estimating the phases of proposed trial crystal structures. Calculated structure factor amplitudes $|F_c(s)|$, can then be directly compared with the observed amplitudes $|F_o(s)|$, and if comparable then the structural agreement will be good.

1.3 Powder vs single-crystal X-ray diffraction

Within a fine powdered sample, crystallites (microscopic crystals) will be present in every conceivable orientation, as will their corresponding lattice planes [West A. R. 1999]. Some crystallites will be at the correct Bragg angle and some will not; the sample is therefore rotated in the path of the X–ray beam to bring as many crystallite planes into the diffraction condition. Each set of lattice planes gives rise to a particular cone of radiation and is recorded over a particular 2θ range (figure 1.4). This differs fundamentally from single-crystal diffraction data whereby a single crystal of sufficient size and quality is orientated within the path of X-ray radiation. This fundamentally produces a three dimensional diffraction pattern that represents the relative positions of atoms within a crystal. Powder diffraction data can consequently be considered as being single crystal X-ray diffraction data but collapsed and distributed into a single dimension. This 1-dimensional compression of data gives rise to considerable peak overlap, obscuring vital structural information, making all stages of the structure determination process difficult and sometimes intractable.

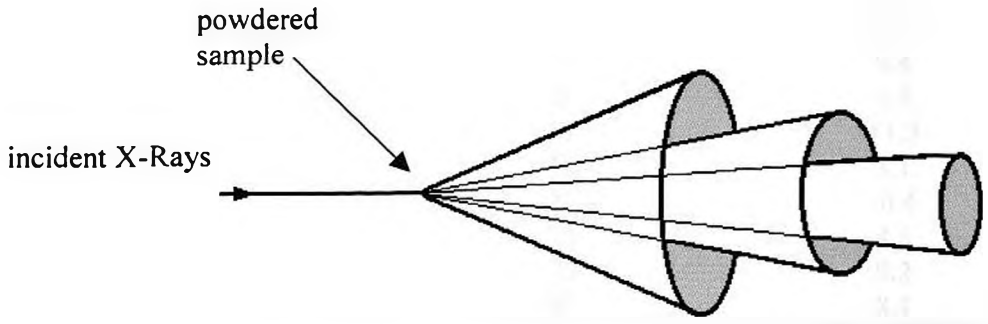

Figure 1.4: Debye diffraction cones produced by X-ray powder diffraction.

1.4 Neutron vs X-ray powder diffraction

The three-dimensional spatial location of hydrogen atoms (or any relatively light atoms in a structure) can be of paramount importance in the rationalisation of a crystal structure and can be a vital stage of the crystal structure determination process. However, the scattering power of X-rays is directly proportional to atomic number and hence the position of hydrogen atoms can be difficult to see by X-rays. A complementary tool, neutron diffraction is commonly used by crystallographers for the accurate location of weak X-ray scattering atoms because of the difference in the nature of their individual scattering mechanisms. X-rays are scattered almost entirely by the atomic shell of an atom, the power of which consequently drops with increasing scattering angle ($\sin\theta/\lambda$). Neutrons are predominately scattered by the atomic nuclei and therefore their coherent scattering power does not fall with increasing scattering angle nor it is directly proportional to the atomic number of the crystalline solid. The difference in scattering factors of a range of atom types is illustrated in table 1.2 [Cheetham. A. K. and Day. P. 1987].

Atom	X-ray	Neutron
H	1	-3.7
D	1	6.7
C	6	6.6
N	7	9.4
O	8	5.8
^{35}Cl	17	11.7
^{37}Cl	17	3.1
V	23	-0.4
W	74	4.8
Re	75	9.2
U	92	8.4

Table 1.2: Comparison of the diffracting powers of different isotopes with X-ray and neutron radiation.

Table 1.2 also illustrates the fact that isotopes of the same element can have different scattering powers allowing them to be readily distinguished. Hydrogen produces a high intensity of negative (incoherent) neutron scattering whereas deuterium shows positive (coherent) scattering power. Thus it is common practice to substitute hydrogen with deuterium in organic materials to reduce background scattering. However, neutron diffraction can have a number of practical difficulties, it is very expensive and is often used only if it offers exceptional advantages over X-ray diffraction in the elucidation of the details of a crystal structure.

1.5 The hydrogen Bond

1.5.1 Classification of the hydrogen bond

The hydrogen bond is without doubt the most frequently studied intermolecular interaction in solid-state chemistry and is fundamental in determining molecular conformation and aggregation. Being present in both chemical and biological systems has led scientists to define and structurally characterise hydrogen bonds since 1920, when Latimer and Rodebush, [Latimer. M. W. and Rodebush. 1920] investigating the proton conductivity of water, described hydrogen bonding as the "force a free pair of electrons on a water molecule exerts on an adjacent water molecule to bind the two together". A modern and more common description of a hydrogen bond is a short ranged intramolecular cohesion force that possesses a high degree of strength and directionality; created when an electronegative donor (D) atom covalently bonded to a 'available' hydrogen (H) atom forms a weak electrostatic interaction with an electron-rich acceptor (A) atom.

Hydrogen bonds are classified as strong, moderate or weak; this categorical representation of the hydrogen bond being directly related to the acidic and basic nature of the hydrogen and acceptor atoms respectively [Gordy. W. and Stanford. S. C. 1940] [Hammett. L. P, 1940] [Gordy. W. and Stanford. S. C. 1941] [Curran. C. 1945] [Jeffrey. G. A. 1997]. If the acidity of the hydrogen atom and the basicity of the acceptor atom are insufficient, the hydrogen bond is usually very weak. The contrary is also true, whereby the hydrogen and acceptor atoms undergo an acid-base type reaction and the formation of a covalent bond is usually evoked.

The basis for identification and classification of a hydrogen bond is often the interatomic distance H...A, and the angle θ (D-H...A). If the interatomic distance between the hydrogen and the acceptor atom is shorter then the sum of their Van der Waals radii

[Nyburg. S. C. and Faerman. C. H. 1985] and, if θ is larger than 90°, then the interaction is classed as a hydrogen bond. Typically hydrogen bond strengths for neutral (moderate) molecules fall in the region of 4 – 15kcal mol^{-1} and for ionic (strong) species the strength can increase to around 14 - 40 kcal mol^{-1}. Table 1.3 summarises the properties of these three categories of hydrogen bonds [Jeffrey. G. A. 1997]. Strong hydrogen bonds can therefore be compared to weak covalent bonds, whereas weak hydrogen bonds are closer to Van der Waals type interactions [Aakeroy. C. B. and Seddon. K. R. 1993].

	STRONG	MODERATE	WEAK
D-H---A interaction	mostly covalent	mostly electrostatic	electrostatic
Bond lengths	D-H ~ H---A	D-H < H---A	D-H << H---A
H---D (Å)	1.2 – 1.5	1.5 – 2.2	2.2 – 3.2
D---A (Å)	2.2 – 2.5	2.5 – 3.2	3.2 – 4.0
Bond angles (°)	175 – 180	130 – 180	90 – 150
Bond energy (kcal mol-1)	14 – 40	4 – 15	< 4
Examples	Gas phase dimers with strong acids or strong bases. Acid salts HF complexes	Acids Alcohols Phenols All biological molecules	Gas phase dimers with weak acids or weak bases. C-H---O/N bonds O/N-H---pi bonds

Table 1.3: Showing some properties of weak, moderate and strong hydrogen bonds.

1.5.2 Graph set analysis

The hydrogen bond interconnectivity within the solid state can range in complexity, and the accurate description of an extended hydrogen bonded structural network can prove to be a formidable challenge. A system of nomenclature to classify and rationalise the diversity of hydrogen-bonded networks within a crystal structure was initially suggested by Kuleshova and Zorky [Zorky. P. M. and Kuleshova. L. N. 1980] and developed to its current form by Etter and Bernstein [Etter. C. E. 1990] [Etter. C. E. et al. 1990]. This notation, known as Graph Set, has now been integrated into the language of structural chemistry and has enjoyed ever-

increasing use since its initial development [Berstein. J. et al. 1995]. The main feature of this graph set approach is the representation of even the most complex of three dimensional networks using only four simple patterns, each specified by a designator: chains (C), rings (R), intramolecular hydrogen bonded patterns (S) and other finite patterns (D). These four designators are combined with a superscript denoting the number of acceptors (a) and a subscript denoting the number of hydrogen bonded donors (d). The total number of atoms (n) included in the pattern, is termed the degree of the pattern and is specified in parenthesis and is usually the minimum atom route. Augmentation of all these terms gives the total graph set descriptor $G_d^a(n)$, where G depicts one of the four possible designators. Examples of graph set descriptors are illustrated in figure 1.5.

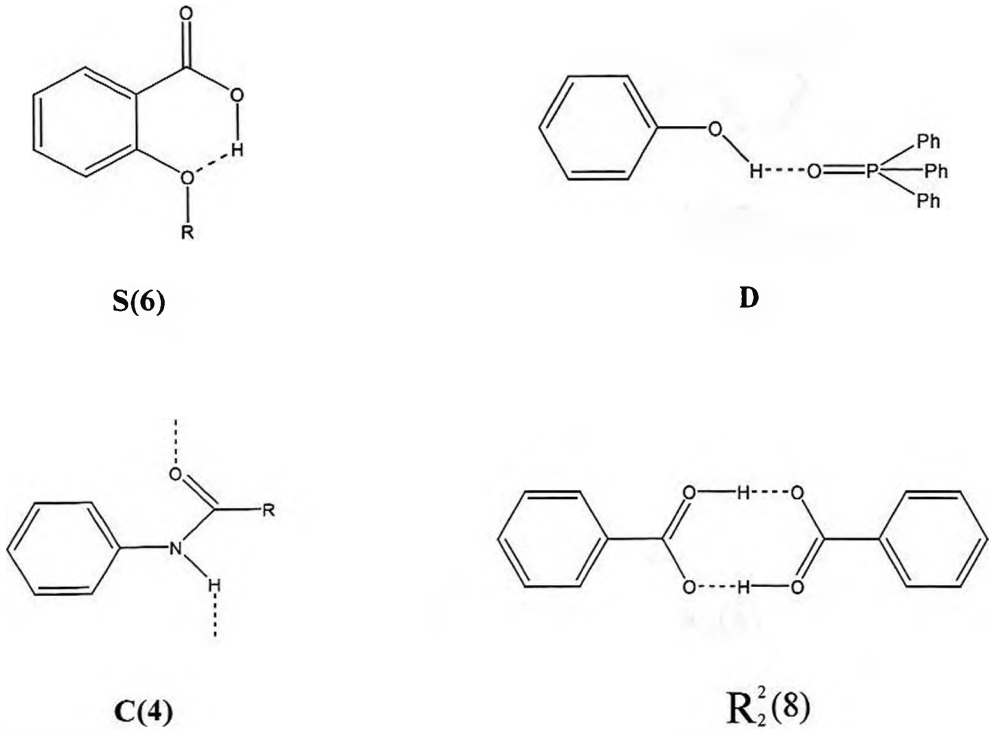

Figure 1.5: Graph set assignments to common hydrogen bond networks.

These first level graph sets are collectively known as unitary graph sets (N_1) and involve only the recognition of the basic motif (that includes only one crystallographically distinct hydrogen bond). Combination of these motif descriptors forms the hierarchal second level or binary graph set (N_2), (illustrated in figure 1.6). Thus, graph set assignment is iterative process, starting with a simple motif, and adding higher and higher order networks until all networks have been described.

The graph set notation certainly was developed using a mathematical basis, most of the notations were based on chemical intuition. In recent years due to the increased use of the graph set tool and the desire for its incorporation into structural databases has led to the basic concepts to be mathematically re-coded and used to develop powerful and sophisticated computer software [Motherwell. W. D. S. et al. 1999] [Grell. J. et al. 1999].

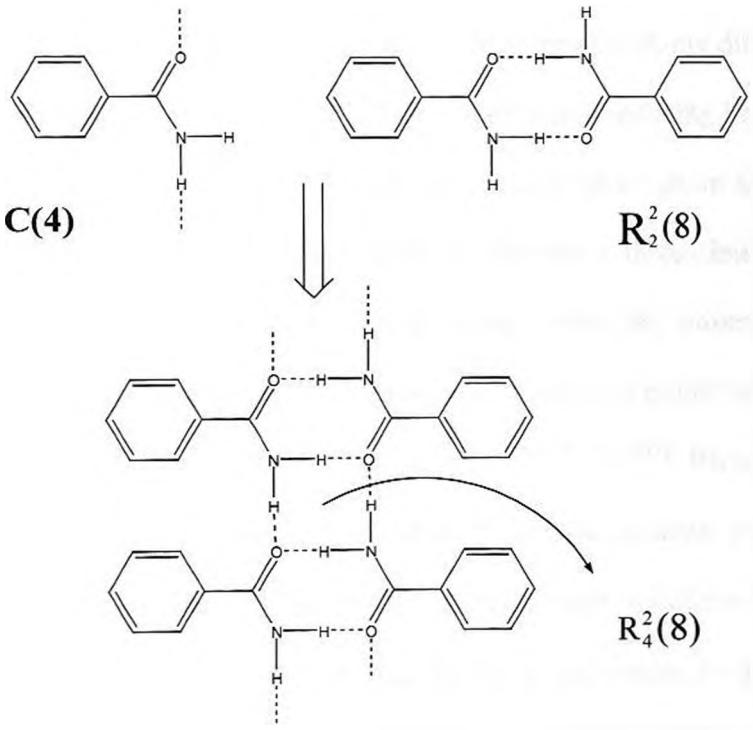

Figure. 1.6: Illustrating the combination of unitary graph sets to generate a binary graph set.

1.6 Crystal structure determination

1.6.1 Crystal structure determination from powder X-ray diffraction

Since the rationalisation of X-ray diffraction using single crystals by Laue, Friedrich and Knipping in 1912, X-ray diffraction has remained the most powerful and most routinely used tool crystallographers have for gaining structural information on crystalline materials. However traditional techniques require the preparation of a single crystal of sufficient size and quality. In many cases preparation of such crystals is not possible resort must be made to powder X-ray diffraction. In a powder diffraction pattern the 2θ positions of the diffraction maxima depend up the periodicity of the structure (i.e. dimensions of the unit cell), whereas the intensities of the diffraction maxima depend on the distribution of scattering matter within the confines of the repeating unit cell (i.e. the atomic positions). Crystal structure determination from powder X-ray diffraction data is carried out in three stages [Harris. K.D.M. et al. 2001]. The first stage is indexing i.e. determination of crystal symmetry, calculation of lattice parameters, and space group assignment. The second stage is structure solution, which aims to generate a three-dimensional crystal model with approximate atomic positions consistent with the observed diffraction maxima. On generating a sufficiently good structural model, this model is further refined in the final stage, known as Rietveld refinement [Rietveld. H. M. 1969]. Rietveld refinement stage aims to adjust the approximate structural model until an accurate representation of the crystal structure is obtained; this is clarified by the comparison of the determined and experimental diffraction pattern quantities R_{wp}, R_p, R_b, χ^2 (equations 5 – 8 page 17). The process of whole profile structure refinement is now quite routine and successful refinements of highly constrained protein molecules have now been carried out [Von Dreele.

R. B. 1999] [Von Dreele. R. B. 2000]. Figure 1.7 illustrates the different stages of the crystal structure determination process from powder X-ray diffraction.

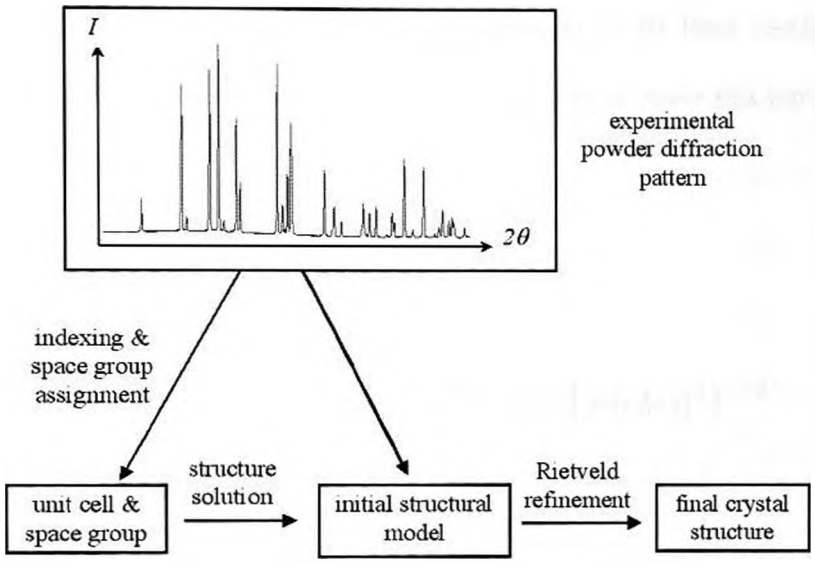

Figure 1.7: Diagram illustrating the different stages involved in the process of crystal structure determination from powder X-ray diffraction data.

In single crystal X-ray diffraction, the peak intensities data I(*hkl*) are distributed in three-dimensional space, whereas the same I(*hkl*) information in powder X-ray diffraction data is collapsed into a single dimension. This compression of data gives rise to considerable peak overlap, obscuring vital peak information and introducing ambiguities in the extraction of intensities of specific peaks. It is this loss of information that makes the determination of crystal structures from powder X-ray diffraction data more difficult, and inherently limits the complexity of materials that can be studied in this way [Harris. K. D. M. and Tremayne. M. 1996].

This loss of data affects every stage of he structure determination process and can make the indexing of a powder diffraction pattern quite challenging. Indeed it is this stage that

can be the bottleneck of the structure determination process and can obstruct further analysis of the powder diffraction pattern. Although a number of indexing programs are available for example, ITO, [Visser, J. W. 1969] TREOR, [Werner, P-E. et al. 1985] DICVOL [Boultif, A., Louer, D. 1991] and CRYSFIRE [Shirley, R. A. 2000] this process is far from routine, and new algorithms are being developed [Neuman, M. A. 2003] which aim to make this intricate process more straightforward.

weighted profile *R*-factor

$$R_{wp} = \{\sum_i w_i[y_i(obs) - y_i(calc)]^2 / \sum_i w_i[y_i(obs)]^2\}^{1/2} \qquad \textit{equation 5}$$

profile *R*-factor

$$R_p = \{\sum_i [y_i(obs) - y_i(calc)]^2 / \sum_i [y_i(obs)]^2\}^{1/2} \qquad \textit{equation 6}$$

χ^2 function

$$\chi^2 = R_{wp}/R_{exp} \qquad \textit{equation 7}$$

Bragg *R*-factor

$$R_b = \sum_{hlk} |I_{hkl}(obs) - I_{hkl}(calc)| / \sum_{hlk} |I_{hkl}(obs)| \qquad \textit{equation 8}$$

Where w_i is the weight, y_i(obs) and y_i(calc) the observed and calculated intensities respectively and R_{exp} the statistically expected *R* value.

1.6.1.1 Direct-space approach to structure solution

Traditional approaches to structure determination aim to extract individual peak intensities I(*hkl*) from the experimental diffraction pattern and use these values in structure solution methods designed for single crystal diffraction data such as the

Patterson method [Patterson, A. L. (1934)] or direct methods [Giacovazzo, C. 1996]. As previously discussed in section 1.6.1, the task of extracting individual peak intensities from a powder pattern is not reliable due to the overlap of reflections at the same value of 2θ. Although a number of techniques have been developed to extract individual I(*hkl*) from overlapping reflections [Pawley, G. S. 1981] [LeBail, A. et al. 1988] the main developments in structure solution of organic materials have resulted from the use of new 'direct-space' methods [Harris, K. D. M. and Tremayne, M. 1996] [Harris, K.D.M. et al. 2001] [David, W. I. F. et al. 2002]. Direct-space powder methods, work on the principle that the best trial structure solution is found by locating the global minimum on the structure solution hypersurface, independently from the experimental powder diffraction data. The suitability of each new trial structure is assessed by directly comparing its powder pattern with the experimental powder data and a weighted profile R factor (R_{wp}) is assigned based on the nature of the fit. As opposed to traditional methods, where individual peak intensities had to be extracted, the direct-space approach, with the application of the R factor utilizes and uses the entire powder diffraction pattern as measured and hence takes peak overlap into account giving rise to more reliable solutions. Inclusion of a structural model in the structure solution process ensures that the resulting structure solution makes chemical sense. Direct space methods require the input of a structural model, (e.g. single molecule of the compound under consideration) which moves around the unit cell to generate trial structures independently of the experimental diffraction data.

Each trial molecule in the calculation is defined by its position (x, y, z), orientation (θ, ϕ, ψ) and intramolecular geometry in the form of n variable torsion angles {τ_1, τ_2,..., τ_n}. The approach of direct-space search methods is to find the global minimum on

the structure solution hypersurface, this minimum corresponds to the structure with the lowest R_{wp} and therefore the most likely candidate for structure refinement on route towards structure determination. There are many optimisation techniques that can be used to search for the global minimum of which simulated annealing [David, W. I. F. et al. 1998] [Andreev, Y. G. et al. 1996], Monte Carlo [Harris, K. D. M. et al. 1998] [Tremayne, M. and Glidewell, C. 2000] [Harris, K. D. M. et al. 1994] and genetic algorithms [Harris, K. D. M. et al. 1998] [Tedesco, E. and Turner, G. W. 2000] are most widely used.

1.6.1.2 Differential Evolution a new direct-space structure solution technique

Differential Evolution (DE) is a relatively new direct space global optimisation algorithm, which like genetic algorithms [Harris, K.D.M. et al. 1998] [Kariuki, B. M. et al. 1997] [Tedesco, E. et al. 2000] uses basic evolutionary principles to recombine and mutate a population of trial structures over a number of generations until convergence upon the global minimum is achieved. However, the processes used to control the evolution of the population are somewhat different between these evolutionary algorithms. In genetic algorithms [Harris, K. D. M. et al. 1998] mating is achieved by crossover of elements of randomly chosen members of the population while maintaining a small number of mutant structures throughout all generations. Selection of new members of the population is then based on probabilistic considerations. However, DE operates in a deterministic manner [Tremayne, M. J. et al. 2002] [Tremayne, M. J and Seaton, C. C. 2002] in which the newly generated child is compared with its parent and the structure with the lowest R_{wp} proceeds into the mass population forming the next generation of structures. The generation of new members in each evolutionary step also differs considerably. Child structures are formed from randomly selected

members of the population by the summation of the weighted differences of the recombination and mutation steps (equation 9).

$$\text{Trial} = \text{Parent} + K(Random_1 - Parent) + F(Random_2 - Random_3) \qquad \textit{equation 9}$$

The term $K(Random_1 - Parent)$ is known as the recombination step and $F(Random_2 - Random_3)$ as the level of mutation. K and F can take values between 0 and 1 and are used to adjust the level of recombination and mutation and hence change the nature in which the R_{wp} hypersurface is explored. Setting K to 0 means that the search criteria will only use mutation to generate the next generation and will inevitably result in a random walk to locate the global minima. The degree of mutation is simply there to disrupt good members of the population and to introduce new information to poorer members, for optimal searching a balance of both these two parameters and the population size is a necessity. Only four parameters are required to control the DE calculation, namely the population size N_p, the total number of generations G_{max} and K and F.

1.6.2 Rietveld structure refinement

The final step in the process of crystal structure determination is a whole profile Rietveld structure refinement [Rietveld. H. M. 1969] [McCusker. L. B. et al. 1999]. Successful refinement requires approximate atomic positions (*from structure solution calculations*). Any major discrepancies or anomalies between the calculated and experimental diffraction patterns can often lead to convergence at an incorrect solution (*or a local minimum*). Rietveld structure refinement uses statistical least squares aiming to obtain an optimal fit (*by*

refinement of both structural and profile parameters) between the experimental and calculated powder patterns. Given that many parameters need to be refined, several successive refinement cycles are needed before convergence is achieved and the addition of geometrical restraints in the structure often proves to be advantageous (*and even essential in the case of molecular compounds*) since more parameters can then be varied while maintaining a stable refinement. Many programs are used for Rietveld structure refinement, the most common of which are GSAS [Larson. A. C. and Von Dreele. R. B. 1987], FULLPROF [Carvajal-Rodriguez. J. 1990], PROFIL [Cockcroft. J. K. 1994], DBWS [Wiles. D. B. and Young. R. A. 1981], RIETAN [Izumi. F. et al. 1987] and TOPAS [Coelho. A. A. 2000].

1.6.3 Polymorphism

Polymorphism is encountered in any field where materials are used in the crystalline solid state, and introduces severe complications during manufacturing, storage and in the design of new crystalline materials with specific solid state properties. "Polymorphic materials are those in which a single molecule can crystallise in two or more crystal structures" [Davey. R. J. 2003]. At any given temperature and pressure only one polymorph is the stable one; all others are termed as 'metastable' polymorphs, of which there could be several. However, the transition from a metastable crystalline form to a stable polymorphic crystalline form can be tipped by minor physical changes, such as grinding, stirring, heating, cooling and nature of solvent [Berstein. J. 2002]. The industrial implications of polymorphism are quite catastrophic, for example within pharmaceuticals different polymorphic forms of drug substances can have quite different solubility, dissolution, bioavailability rates and can as a consequence lead to an ineffective drug, or one that is

extremely toxic to the patient. Already legislation requires drug manufacturers to provide information relating to the occurrence (*or apparent absence*) of polymorphism in their products has been introduced [Hilfiker. R. 2006]. As crystallization is the most common procedure for both purification of solid compounds and the preparation of new polymorphs the sudden loss of control over this simple procedure is a somewhat disturbing thought. Chemists around the world have successfully prepared a particular crystal polymorph on numerous occasions, and to their disbelief, what should have been another routine crystallization has presented a new problem – the appearance of a new polymorphic form of the same compound. In cases of 'disappearing polymorphs' [Dunitz. J. D. and Bernstien. J. 1995] attempts to re-crystallize the original polymorph in the same or even a different laboratory are met with failure. It is not therefore surprising that the study of polymorphism and crystal structure determination is indeed two facets of the same topic.

1.6.3.1 Thermodynamic considerations of polymorphism

Crystallisation of a specific polymorph from melt, solution or vapour commences with nucleation and the factors determining nucleation rate (e.g. the associated Gibbs free energy of activation, molecular volume and interfacial energy) differ for polymorphs of the same substance [Sato. K. 1993]. In a supersaturated solution, nuclei of all possible polymorphs of the dissolved substance can be imagined to exist [Weissbuch. I. et al. 1995] and hence the outcome of crystallisation is governed by the competitive nucleation processes. According to Ostwald's rule of stages [Ostwald. W. 1987] [Khoshkhoo. S. and Anwar. J. 1993] at high supersaturation, the first form, which crystallises is the thermodynamically least stable (most soluble). This sequence continues until only the thermodynamically stable (least

soluble) polymorph remains, however it should be possible to isolate different polymorphs at differing levels of solution supersaturation and hence have some control over the crystallisation process.

1.7 Crystal structure prediction

1.7.1 Overview of structure prediction

Crystal structure prediction is a relatively new challenging field of research and one that is gaining considerable academic and industrial interest. These theoretical techniques aim to predict the three dimensional packing arrangement of a substance on the basis of its molecular structure only [Price. S. 2004].

As discussed earlier, the study of polymorphic form is important in all areas of organic solid state chemistry (see also section 1.0). However, isolating and characterising all the crystalline forms through solvent screening can be very time consuming and costly. Also, knowing when to stop looking for new polymorphs is a major issue since the chances of identifying all the possible polymorphs are very remote [McCrone. W. C. 1965] [Haleblian. J. K., McCrone. W. 1969]. The capability to predict all the possible polymorphs of a given substance by computational methods would clearly be invaluable. Many research groups are aiming towards this goal by development of a range of different software employing different theoretical approaches but as of yet success has been very limited [Lommerse. J. P. M. et al. 2000][Motherwell. W. D. S. et al. 2002][Day. G. M. et al. 2005].

1.7.2 Are crystal structures predictable?

According to Maddox in 1988 "one of the continuing scandals in the physical sciences is that it remains in general impossible to predict the structure of even the simplest crystalline solids from a knowledge of their chemical composition", and according to Gavezzotti [Gavezzotti. A. 1994] in 1994 "No". Prediction programs today aim to find the thermodynamically and kinetically most favourable crystal structure (i.e. the one which is

most likely to exist experimentally) by locating the global minimum on the potential energy hypersurface. However these programs output many hundreds of probable theoretical packing arrangements, all ranked by their relative lattice energies and densities. The Ranking of crystal structures purely on this basis tends to be unreliable, and the probability of even a known experimental crystal structure appearing high in the ranked output is not guaranteed. This problem arises because predictions rely on employment of an empirical force field to assess trial structures, and choice of this force field can in most cases be more important then the actual search method itself. Empirical force fields rely on atom potentials to describe the potential energy surface of a specific molecular species, and do so by using thermodynamic (enthalpic) factors only. As yet, prediction programs are unable to describe kinetic and entropic factors (i.e. nucleation and nature of solvent) and as a result these crucial factors are not taken into account in prediction calculations [Sarma. J.A. and Desiraju. G.R. 2002][Mooij. W. T. M. et al. 1998]. This means that the lattice energy of a predicted structure is assumed to be equivalent to its free energy, and corresponds to the crystal structure which is most likely to be observed experimentally [Pillardy. J. et al. 2001]. Other limitations to the success of structure prediction are the constraints of the number of molecules in the asymmetric unit (only recently have Z' = 2 structures been studied) [Bouke. P. et al. 2000]. Prediction calculations are also restricted to searches using common space groups and molecules having limited flexibility, running a prediction in an alternative packing symmetry or conformation in most cases does require an additional calculation [Beyer. T. et al. 2001]. As of yet most prediction programs are unable to accurately calculate the energy of disordered structures.

1.8 Overview of Molecular Mechanics

Molecular Mechanics is an empirical computational technique, which utilizes classical mechanics theory and represents molecules as point masses (*nuclei*) united by springs (*bonds*). The term 'Molecular Mechanics' was first coined when spectroscopists [Andrews, D. H. 1930] discovered that force fields could be used to describe or predict the vibrational spectra of molecules, and that the energy functions and parameters could be exchanged from one molecule to another. This technique can now be used to simulate properties of both small organic and large biological systems. These simulation calculations require a series of energy functions, which make up what is referred to as a force field. This is simpler than quantum mechanical techniques, in that orbital electrons are not defined explicitly and are assumed to adjust accordingly once the relative positions of the nuclei are known (nuclei and electrons can be treated separately due to their difference in mass). This assumption is based upon the Born-Oppenheimer approximation of the Schrodinger equation. This simplicity is what makes the force field approach such a popular method, with the extension to structure prediction of more and more complex systems possible.

There are four major components to any crystal structure prediction program:

(i) The input molecular model, which may include conformational flexibility.

(ii) A method for generating and searching for initial crystal structures.

(iii) Some sort of energy or fitness function to describe packing efficiency.

(iv) An efficient means of reducing the packing hypersurface by evaluation of fitness function so that a (global) minimum can be located.

Molecular mechanics is generally used to determine the lowest energy conformation (*global minimum on the molecular energy hypersurface*) of a specific molecular system. This process is more commonly referred to as 'geometry optimisation' or 'energy minimization' and uses the information from the force field to make small adjustments to the molecular structure (*atomic coordinates*) to reduce the energy of the system. The procedure to locate the global minimum is an iterative process applied until the change in energy or some step size is reduced to values below some predetermined tolerance i.e. the convergence criteria.

1.8.1 The force field

The basic force field is a set of mathematical potential energy functions that together describe the potential energy surface of a molecular system. The summation of these equations, each of which describes the energy required for distorting a molecule in a particular fashion, permits the calculation of the total energy of a system. Numerous force fields have been developed and there is still debate as to what form a force field should take and how they should be tested [Halgren. T. A. J. 1996]. Some force fields represent additional conformational flexibility or deformations within a molecule, but inevitably they all aim to calculate the total strain energy placed upon a molecule or molecules relative to a hypothetical situation. The total energy calculated by a force field is indicated by equation 10. The terms E_{bond}, E_{bend}, $E_{torsion}$ are all termed as bonded interactions whereas; E_{vdw} and E_{elec} are termed non-bonded interactions.

$$E_{total} = E_{bond} + E_{bend} + E_{torsion} + E_{vdw} + E_{elec} \qquad \textit{equation 10}$$

where E_{bond} is the energy function for stretching a bond between two atoms, E_{bend} represents the energy required for bending an angle, $E_{torsion}$ is the torsion energy for rotation around a bond and E_{vdw} and E_{elec} describe the non-bonded atom-atom interactions. If there are additional mechanisms affecting the energy, such as hydrogen bonding, cross terms are included in E by adding appropriate terms into the above energy function (as illustrated schematically in figure 1.8).

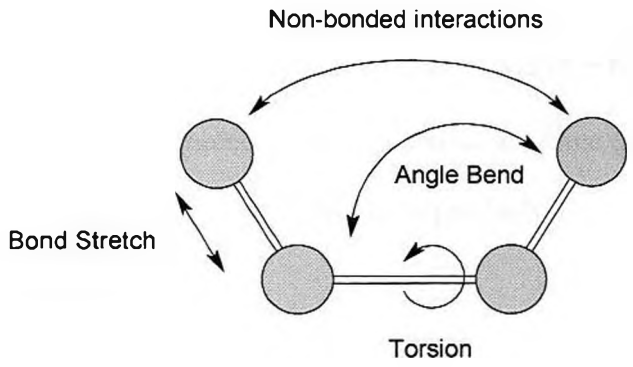

Figure 1.8: Schematic representation of interactions that are included in force field calculations.

1.8.1.1 Bond stretching interactions

Whenever a bond is compressed or stretched from its equilibrium position the relative energy of the system will increase. The energy potential for describing this mode of movement is based on Hooke's Law adapted in equation 11 to show the energy term related to bond stretching.

$$E_r = \Sigma_{bonds}\, k_b\, (r - r_o)^2 \qquad \textit{equation 11}$$

Where E_r is energy of the molecule, k_b the force constant and r the length of a bond in a molecule and illustrates the dependence of the energy of a molecule on the length of a

bond within a molecule. As the bond length deviates from its equilibrium position the associated energy will increase at a rate relative to the force constant (k_b) of the bond. When the bond length is equal to the reference bond length (r_o) the change in bond stretching energy is exactly zero. However it is known from quantum mechanics that energies associated with bond stretching are relatively anharmonic, so higher powers are added to the above quadratic approximation, stopping the energy from rising too sharply as the bond is stretched (equation 12).

$$E_r = k_{b2} (r - r_o)^2 + k_{b3} (r - r_o)^3 + k_{b4} (r - r_o)^4 \qquad \textit{equation 12}$$

Where E_r is the energy of the molecule, k_{b2}, k_{b3} and k_{b4} are force constants and r and r_o the final and initial length of a bond in a molecule respectively.

1.8.1.2 Bond bending interactions

As with bond stretching, the energy associated with deforming a valence angle (θ) from its reference bond angle (θ_o) can also be defined by a 'Hooke's law' type quadratic expression (equation 13).

$$E_\theta = \Sigma_{angles}\, k_\theta (\theta - \theta_o)^2 \qquad \textit{equation 13}$$

Where E_θ is the energy of the molecule, k_θ is the force constant and θ and θ_o the final and initial angle of a bond in a molecule respectively.

This works well for angles up to about $\theta = 10°$, but for larger anharmonic deformations additional terms are again required to accurately define the angle bend energies as shown

in equation 14. Some force fields include terms to $(\theta - \theta_o)^6$ in order to get more accurate bending energy terms.

$$E_\theta = k_{\theta 2} (\theta - \theta_o)^2 + k_{\theta 3} (\theta - \theta_o)^3 + k_{\theta 4} (\theta - \theta_o)^4 \qquad \textit{equation 14}$$

Where E_θ is the energy of the molecule, $k_{\theta 2}$, $k_{\theta 3}$ and $k_{\theta 4}$ are force constants and θ and θ_o the final and initial angle of a bond in a molecule respectively.

1.8.1.3 Dihedral interactions

Torsion angles, account for the steric energy associated with twisting a bond within a molecule and hence altering its conformation. The simplest expression is described by a single term Fourier series, (equation 15). However, this fundamental form is usually used only to differentiate between the energy barriers of *cis* and *trans* conformers.

$$E_\tau = \Sigma_{torsion} V [1 + \cos (n\tau - \phi)] \qquad \textit{equation 15}$$

Where E_τ is the energy of the molecule, V is the energy barrier, n is the multiplicity and ϕ is the phase factor.

V controls the amplitude of the curve, i.e. the number of minimum energy points as the bond is rotated through 360°, and ϕ determines where the torsion angle passes its minimum value. E.g.: for a molecule of ethane n=3 (corresponding to rotational angles of +60°, −60° and 180°) and ϕ =0°. More complicated energy expansion with additional torsional potential terms are used in some force fields (equation 16), and found to be especially important for twisting the terminal atoms of flexible bonds and for systems

containing heteroatoms such as halogenated hydrocarbons and molecules containing CCOC and CCNC fragments.

$$E_\tau = \Sigma_{torsion}\, V_1\,(1 + \cos\tau) + V_2\,(1 + \cos 2\tau) + V_3\,(1 + \cos 3\tau)$$

equation 16

1.8.1.4 Van Der Waals non-bonded interactions

Van der Waals interactions describe the combination of repulsion and attraction between two atoms that are in close proximity to one another without forming a defined bond. These interactions include (i) the long range attractive force, (also referred to as the London dispersion force) arising from fluctuations in the charge distribution in the electron clouds, giving rise to a induced dipole – induced dipole attraction between the atoms. (ii) The repulsive (or exchange repulsive) force that dominates at short distances, resulting from the *Pauli exclusion* principle when two atoms with electron clouds intercept and the clouds repel one another, both being negatively charged. The Lennard-Jones empirical [12–6] function is the expression most commonly used to model Van der Waals interactions between two atoms (equation 17).

$$v(r) = 4\varepsilon\left[\left(\frac{\sigma}{r}\right)^{12} - \left(\frac{\sigma}{r}\right)^{6}\right]$$

equation17

where v(r) is the repulsive force, r^{-12} and r^{-6} represent the repulsive and attractive components respectively, σ is the collision diameter and ε is the well depth.

Many force fields adopt a more accurate force field representation in calculations, and it is not uncommon to see force fields utilizing a [9–6] or [14–7] approach for the definition of Van der Waals interactions.

1.8.1.5 Electrostatic non-bonded interactions

The non-bonded electrostatic contribution is also an important term and is always considered in a typical force field as it dominates the total energy of the system in question. This electrostatic interaction is more commonly represented by Coulomb's law (equation 18), which gives the interaction energy between two charges q_i and q_j separated by a distance R in a medium with a dielectric constant D.

$$E_{elec} = \frac{q_i q_j}{DR_{ij}} \qquad \textit{equation 18}$$

where $D = 4\pi\varepsilon_0$ (ε_0 is the well depth).

When two nuclei of differing electronegativity come into close contact with one another; the more electronegative nucleus attracts more electrons than the other resulting in an unequal distribution of charge. The accuracy of the electrostatic term therefore depends on the correct assignment of charges to individual nuclei. The main problem however in reproducing this charge assignment is that molecular mechanics approach treats nuclei as point charges throughout the molecule. The fact that nuclei share electrons is not considered. Thus, the permanent charges assigned to nuclei in the attempt to use them in all situations are not a suitable representation, of the crystal structure under consideration.

A relatively new approach to assignment of charges is called the multipole expansion [Mooij. W. T. M. and Leusen. F. J. J. 2001][Mooij. W. T. M. et al. 1999] [Willock. D. J. et al. 1995] [Price. S. 2000]. This method treats the molecule as a single unit, and is capable of providing a very accurate calculation of the electrostatic interactions. The multipole expansion is based upon electric moments or multipoles, each of which can be represented by an appropriate distribution of charges, i.e. a dipole is represented by 2 charges and a quadrupole by 4 charges. An accurate description of the complete charge distribution around a molecule requires the specification of all moments.

2.0 Crystal structure prediction methodology

Even with use of the most modern and sophisticated experimental, combinatorial and crystallographic techniques, polymorph screening and analysis is a lengthy and complicated procedure. Clearly the prediction of possible polymorphic structures from only a molecular structure would be invaluable. The current dilemma faced by structural chemists is that structure prediction calculations tend to generate many hundreds of plausible theoretical crystal structures all ranked according to their relative lattice energies. Ranking based on this criteria can be unreliable as in many cases even known crystal structures appear unfavoured in the energy rankings. The application of structural schematics is a possible additional consideration in this ranking procedure, and it is the automatic rationalization of structural features and their subsequent use that is discussed here. Clearly what is required is a program that can automatically examine and rationalize the theoretical models from a traditional polymorph prediction output, and encourage structurally favorable models higher up the rankings. This helps to not only eliminate the need to visually inspect every theoretical model but also encourages easier identification of those structures with common structural features.

2.1 Polymorph Prediction

Accelrys Materials Studio (MS) Modelling 3.0 [Accelrys. Cambridge, UK] is a structure modelling and simulation suite designed for the chemicals and materials industries. It contains a wide variety of modules, namely Forcite and Polymorph Predictor. Forcite is an advanced classical molecular mechanics tool that uses a variety of algorithms (steepest decent, Quasi-newton, conjugate gradient or a smart algorithm) to carry out geometry optimisation and single point energy calculations on both molecular and periodic systems. Polymorph Predictor is a suite that allows the prediction of potential polymorphs of a given compound from the molecular structure.

2.1.1 Molecular representation and geometry optimisation

The Geometry optimisation process starts with construction of the molecular structure of the system of interest (or by importing a compatible structure file), and definition of the environment occupied by each atom within the molecular structure by assignment of an empirical force field and suitable atomistic charges. Geometry optimisation itself is then performed via an interactive graphical interface that guides the user through the calculation until convergence is achieved. The module used to carry out the geometry optimisation was Forcite [Accelrys. Cambridge, UK], which is an advanced classical molecular mechanics tool within the MS Modeling package [Accelrys. Cambridge, UK]. This accurate definition of the structural model is vital if the prediction is to be successful; the geometry optimisation parameters used here were the Compass force field using Gasteiger charges, the electrostatic / van der Waals non-bonded interactions were defined using spline and the quality of the optimization was ultra fine.

2.2 Crystal structure prediction

The Polymorph Predictor module (PP) [Leusen, F. J. J. 1996] enables prediction of all the possible crystal packing arrangements of predominantly rigid, non-ionic molecules composed mostly of carbon, nitrogen, oxygen, hydrogen, chlorine and sulphur. However the module has its limitations in that sulphur atoms are not accurately defined. The molecular structure optimised in the Forcite calculation is used as the input structure for a polymorph prediction sequence, an empirical force field such as Dreiding [Mayo. S. L. et al. 1990] is assigned. The Dreiding force field is designed specifically for the purpose to simulate and optimize periodic molecular systems and also has good coverage for organic, biological and main-group inorganic molecules. The first stage of a PP sequence is a Monte Carlo simulated annealing (MC-SA) search of the lattice energy hypersurface. This algorithm treats the molecule as a rigid unit and through random parameter displacement produces often thousands of alternative packing arrangements. Each new configuration is subjected to the Metropolis acceptance algorithm [Metropolis. N. 1953], which is a fundamental procedure of MC-SA. This Metropolis step not only accepts structures with a lower energy than that of the previous state, but also, using probabilistic methods, is able to accept structures of higher energy. In this way the search of the hypersurface is able to move towards the lowest energy state and avoid being trapped in local minima. In the second stage of PP the geometry of each unique structure is optimized with respect to all degrees of freedom, this includes optimization of the molecular species as well as the unit cell in which it is contained, only the symmetry elements of the user defined space group are retained. The final stage in the PP sequence is clustering; out of the thousands of crystal arrangements generated by the MS-SA algorithm there is a strong

possibility that some structural arrangements will be similar, if not the same. The clustering process is therefore a valuable step that calculates the dissimilarity between structures by comparing the interatomic distances between different atom types based on the information provided by the force field. A predefined cut-off distance is then used to determine whether a structure is to be accepted or rejected within the clustering process; accepted structures that are of similar constitution are deposited in the same cluster. The final list of possible polymorphic structures is written to a spreadsheet ranked according to relative lattice energy. Table 2.1 lists the parameters used in each PP sequence in this project. The structure packing and geometry optimization parameters were all default Polymorph Prediction parameters, however the clustering parameters originally used were default in which the quality of the search was fine. This consequently discriminated between similar structures using a large cut off distance, giving rise to a smaller number of bins and hence a less varied number of structures to examine. Therefore the search was changed to medium, which lowered the cut off distance slightly and also increased the number of bins into which similar structures were to be placed.

Polymorph Prediction parameters

Task	Prediction
Quality	Customised
Force field	Drieding
Charges	Gasteiger
Electrostatic / van der Waals	Ewald
1. SRUCTURE PACKING	
Quality	Fine
Maximum number of iterations	7000
Steps to accept before cooling	12
Minimum move factor	1.00E-09
Heating factor	0.025
Maximum temperature (K)	1.00E+05
Minimum temperature (K)	300.00
2. GEOMETRY OPTIMISATION	
Algorithm / Quality	Smart / Ultra-fine
Maximum number of iterations	5000
Convergence tolerance	
Energy (kcal/mol)	2.00E-05
Force (kcal/mol/Å)	0.001
Stress (GPa)	0.001
Displacement (Å)	1.00E-05
3. CLUSTERING	
Quality	Medium
Cutoff (Å)	7.0
Tolerance	0.15
Number of bins	140
Maximum number of clusters	250

Table 2.1: Shows the parameters used in a typical polymorph prediction sequence.

2.3 Overview of the re-ranking strategy

The re-ranking strategy developed in the project involved the construction and application of 2 programs, *predictor.pl* and *gset.pl*. Developed using the language perl [L. Wall, T. Christiansen, J. Orwant 2000], the primary aim of this re-ranking strategy is to automatically examine, rationalize and re-rank the top 10 kcalmol^{-1} (or the first 30 theoretical structures) from the traditional polymorph prediction output. The consideration of only 30 structures was deemed as sufficient energy range for testing of our re-ranking strategy, with extension to a larger set of structures possible. Initial rationalization was achieved through the introduction of hydrogen bonding and graph set assignment information using the crystallographic programs Platon [Spek. A. L. 1990][Spek. A. L. 2003] and RPluto [Motherwell. W. D. S. et al. 2000] respectively.

On completion of a PP sequence, Shelx files (*.ins) were manually exported for those theoretical structures corresponding to the top 10 kcalmol^{-1} or for the first 30 predicted structures. This was seen as a viable method of choice, since alternative polymorphic packing arrangements usually occur within 1-2 kcalmol^{-1} of the global minimum structure. Through command line execution *predictor.pl* sequentially runs the program Platon using each Shelx file in turn as input and generating a list file for each structure, containing comprehensive structural information on both intra and intermolecular geometry including possible hydrogen bonding. These files are automatically screened for intermolecular interactions and the specified hydrogen bonding geometry for each structure extracted. It is this geometrical information that is used as a basis for awarding of hydrogen bonding merit points. Structures are then re-ranked according to the number of hydrogen bonding merit points and exported into a text file (*Pmorph_sort_Hbond.txt*). The second stage of the re-ranking strategy

entails the input of the original Shelx files (via command line) in the program RPluto. Rpluto is an X-windows tool for visualising molecular crystal structures; the feature of interest here is the ability for automatic graph set analysis in the form of a list of all the structural motifs (*both unitary and binary*) present within the predicted structures. Execution of the program *gset.pl* compares the motifs located in each theoretical structure with those predefined in the perl code e.g. the characteristic $R_2^2(8)$ dimers and C(4) chains, points are awarded to those structures that contain the characteristic $R_2^2(8)$ and C(4) motifs. As previously this information is used to re-rank the structures and export into a text file (*Pmorph_sort_gset.txt*). Figure 2.1 illustrates by means of a flow chart exactly how the perl code operates. Effectively, this provides 3 different (but equally useful) ways of re-ranking the same set of predicted structures, i.e. ranked according to:

(i) Lattice energy (original polymorph prediction output, $kcalmol^{-1}$).

(ii) Hydrogen bonding merit points.

(iii) Graph set assignment merit points.

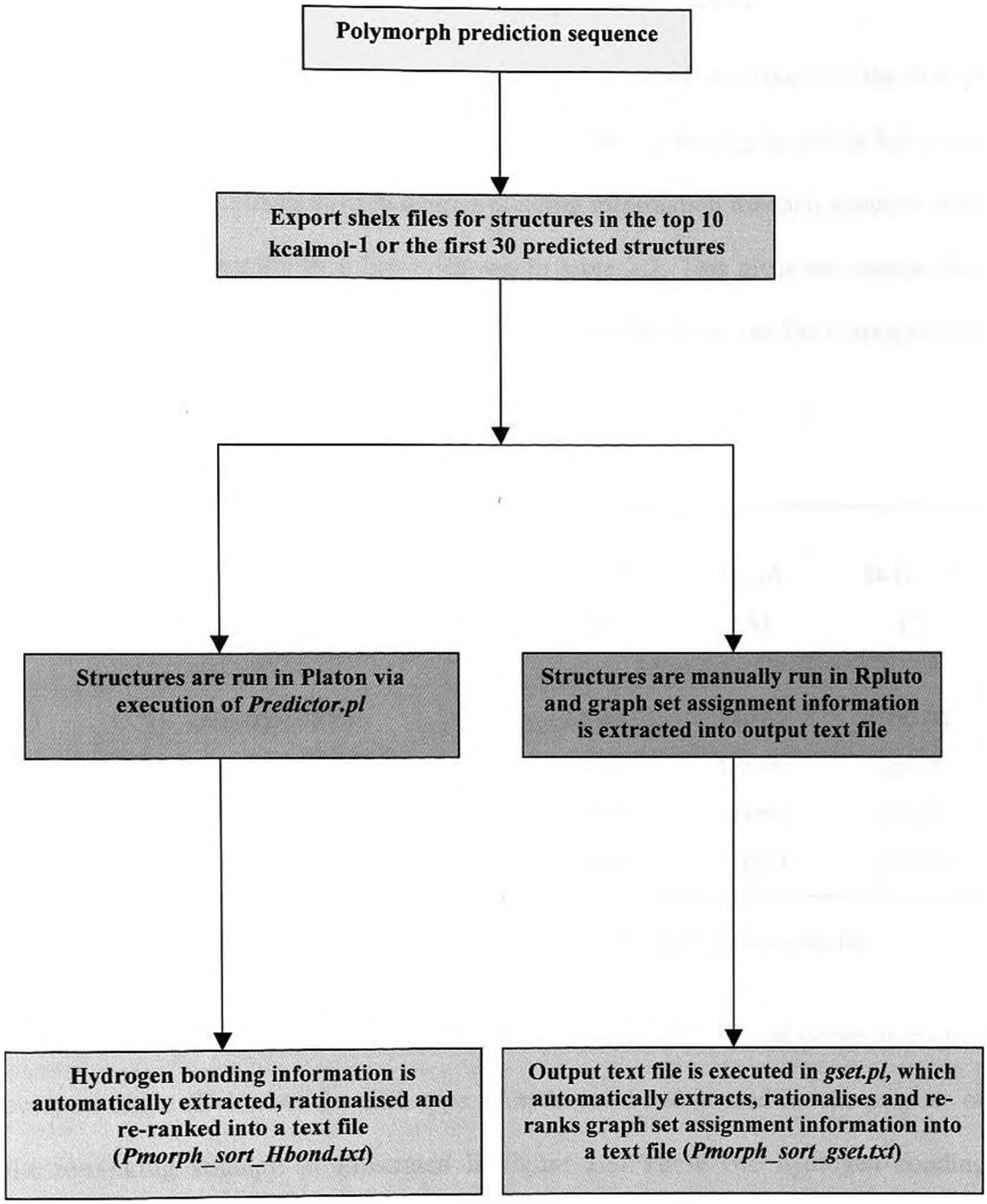

Figure 2.1: Illustration of how the code extracts the hydrogen bonding and graph set information.

2.4 The hydrogen bonding merit point scheme

Assessing the structural suitability of the top 30 theoretical structures (*or the first 10 kcalmol^{-1}*) through the implementation of a point scheme strategy is simple but a very effective method. Extraction of hydrogen bonding information for each structure from the Platon output results in a list as shown in table 2.2. This gives the number and type of hydrogen bonds present within the predicted structure and the corresponding geometrical information for each type.

Nr	Donor---H....Acceptor	D-H (Å)	H...A (Å)	D...A (Å)	D-H...A (°)
1	O(9) --H(10) ..N(8)	1.1900	2.5900	3.0362	100.00
2	O(9) --H(10) ..N(8)	1.1900	2.4100	3.0090	109.00
3	N(8) --H(15) ..O(9)	0.9600	3.0090	3.0090	166.00
4	N(8) --H(16) ..O(9)	0.9700	3.0362	3.0362	165.00

Table 2.2: Example of the hydrogen bonding information extracted from the Platon list file.

It should be noted, only the hydrogen-acceptor distance (H...A) and donor-hydrogen-acceptor angle (D-H...A) for each type of hydrogen bond is used for the purpose of the re-ranking strategy as illustrated in figure 2.3. These two hydrogen bonding geometry parameters were used because they inevitably play a fundamental role in the formation of strong and weak hydrogen bonds. These geometrical values are automatically compared to the predefined limits [Desiraju. G. R. and Steiner. T. 1999] (table 2.3) implemented in the *predictor.pl* code and it is the difference between these values that drives the number of merit points that a particular hydrogen bond is awarded.

	Very strong	Strong	Weak
Examples	$[F...H...F]^-$	O-H...O=C	C-H...O
	$[N...H...N]^+$	N-H...O=C	O-H...Π
	P-OH...O=P	O-H...O-H	O_s-H...O
Bond lengths	H-A ≈ X-H	H...A > X-H	H...A >> X-H
D(X...A) range (Å)	2.2-2.5	2.5-3.2	3.0-4.0
Θ(X-H...A) range (°)	175-180	130-180	90-180

Table 2.3: Properties of very strong, strong and weak hydrogen bonds.

The point system was devised with simplicity in mind, simply awarding a maximum of 10 points to a strong hydrogen bonding distance or angle (e.g. N-H...O) and only 1 point to a weak hydrogen bonding distances and angles (e.g. C-H...O) was seen to be a sufficient way of discriminating between the two types of interactions. This simple yet effective scaling was used to reflect the fact that stronger hydrogen bonds play a more crucial role in the overall formation of the crystal structure, whereas weak hydrogen bonds form across a larger distance a wider angle. Weak hydrogen bonds therefore have more of a stabilizing effect on the overall three dimensional arrangement and hence are awarded fewer merit points. To obtain the maximum number of points, hydrogen bonding distances and angles must be within the predefined limits, with any hydrogen bonding geometry outside the predefined limits awarded a percentage of the maximum via a sliding scale subroutine. The total number of hydrogen merit points is then the summation of all hydrogen bonding contributions in the structure. The pseudo-code for this process is given in figure 2.2 and figure 2.3 outlines a summery of the geometry predefined in the perl code and the associated merit points awarded.

```
#For strong hydrogen bonds: N-H...O, N-H...N, O-H...N, O-H...O

If distance H...A >= 1.5 and <= 2.2 {
     Award 10 points
     #2.2 Å = predefined limit
}
elsif distance H...A < 1.5 or > 2.5 {
     Award 0 points
}
elsif distance H...A > 2.2 and <= 2.5 {
     subroutine_1
     #Subroutine_1 = 10-abs[((trial distance -2.2)**2)*100]
}
If angle D-H...A >= 160 and <= 180 {
     Award 10 points
     #160° = predefined limit
}
elsif angle D-H...A < 130 or > 180 {
     Award 0 points
}
elsif angle  D-H...A >= 130 and < 160 {
     Run subroutine_2
     #Subroutine_2 = 10-abs[((trial angle -160)**2-10)/100]
}
#For weak hydrogen bonds: C-H...O, C-H...N, C-H...C
If distance H...A >= 2.5 and <= 3.0 {
     Award 1 point
     #2.5 Å = predefined limit
}
elsif distance H...A < 2.2 or > 3.0 {
     Award 0 points
}
elsif distance H...A >= 2.2 and < 2.5 {
     Run subroutine_3
     #Subroutine_3 = 0.1*abs[10-(((trial distance-2.5**2)*100)]
}
If angle D-H...A >= 120 and <= 180 {
     Award 1 point
     #120° = predefined limit
}
elsif angle D-H...A < 90 or > 180 {
     Award 0 points
}
elsif angle D-H...A >= 90 and < 120 {
     Run subroutine_4
     #Subroutine_4 = 0.1*abs{10- [((trial angle-20)**2)/100]}
}
```

Figure 2.2: Pseudo perl code for calculating and awarding merit points.

For strong hydrogen bonds			
Distance (Å)	**Points**	**Angle (°)**	**Points**
H...A >= 1.5 and <= 2.2	10	D-H...A >= 160 and <= 180	10
H...A < 1.5 or > 2.5	0	D-H...A < 130 or > 180	0
H...A > 2.2 and <= 2.5	0 to 10	D-H...A >= 130 and < 160	0 to 10
For weak hydrogen bonds			
Distance (Å)	**Points**	**Angle (°)**	**Points**
H...A >= 2.5 and <= 3.0	1	D-H...A >= 120 and <= 180	1
H...A >= 2.2 and < 2.5	0	D-H...A < 90 or > 180	0
H...A >= 2.2 and < 2.5	0 to 10	D-H...A >= 90 and < 120	0 to 10

Figure 2.3: Predefined hydrogen bonding geometry and associated merit points.

Example 1:

Consider a sulphonamide dimer with close to ideal geometry values (figure 2.4).

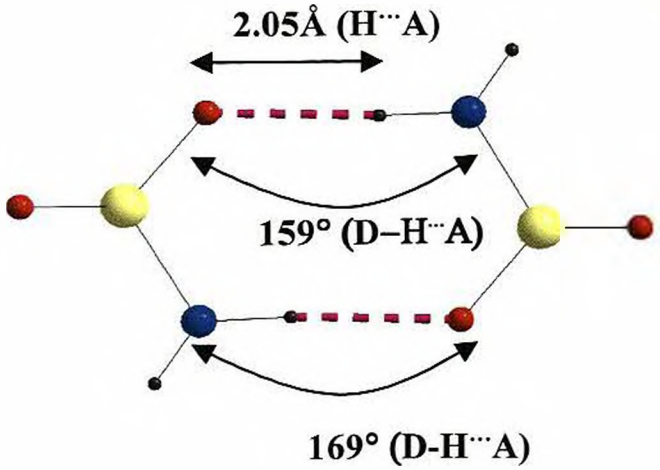

Figure 2.4: Strongly hydrogen bonded sulphonamide dimer with hypothetical geometrical values.

The sulfonamide dimer contains two strong hydrogen bonds with each of hydrogen bonding distances awarded the maximum of 10 points. However one of the corresponding angles lies outside the predefined limits and hence is awarded a lower level of points via the sliding scale subroutine (10 and 9.91). The total number of hydrogen bonding merit points this crystal structure would be awarded is 39.91, as illustrated in table 2.4.

		D-H	H...A	D...A	D-H...A
1	N(56) --H(63) ..O(57)	0.9600	2.0500	2.9980	168.00
2	N(56) --H(64) ..O(57)	0.9700	2.0500	3.0444	159.00

1	N(56) --H(63) ..O(57):	2.05	merit = 10
2	N(56) --H(64) ..O(57):	2.05	merit = 10

1	N(56) --H(63) ..O(57):	168	merit = 10
2	N(56) --H(64) ..O(57):	159	merit = 9.91

TOTAL MERIT = **39.91**

Table 2.4: Total number of points awarded to the hypothetical sulphonamide dimer.

Example 2:

Consider a structure containing non-ideal hydrogen bonding geometry, with distances and angles well beyond the predefined limits. This is illustrated in figure 2.5 and table 2.5 with a structure again containing hypothetical geometrical values. This hypothetical structure contains 4 types of strong hydrogen bonds. Bonds 2 and 4 have an angle that is awarded 6.49 merit points and a distance that is beyond the outer predefined limits for a strong hydrogen bond (<1.5Å or >2.5Å) and consequently awarded 0 points.

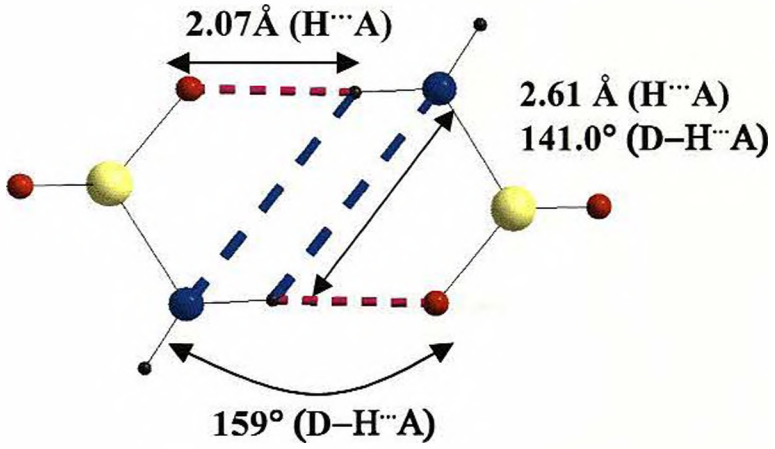

Figure 2.5: Strongly hydrogen bonded sulphonamide dimer with non-ideal hypothetical geometrical values.

In such a case all the merit points awarded to hydrogen bonds 2 and 4 are discounted from the structures total (both distance and angle need to be within predefined limits to count towards final total). This approach is vital as it helps to highlight structures with unfavorable hydrogen bonding geometry and essentially moves them lower down the rankings. This also ensures that clearly incorrect structures that form many non-ideal hydrogen are not credited.

		D-H	H...A	D...A	D-H...A
1	N(28) --H(37) ..O(29)	0.9600	2.0700	3.0092	164.00
2	N(28) --H(37) ..N(28)	0.9600	2.6100	3.4064	141.00
3	N(28) --H(37) ..O(29)	0.9600	2.0700	3.0092	164.00
4	N(28) --H(37) ..N(28)	0.9600	2.6100	3.4064	141.00

1	N(28) --H(37) ..O(29): 2.07	merit = 10
2	N(28) --H(37) ..N(28): 2.61	merit = 0
3	N(28) --H(37) ..O(29): 2.07	merit = 10
4	N(28) --H(37) ..N(28): 2.61	merit = 0

1	N(28) --H(37) ..O(29): 164	merit = 10
2	N(28) --H(37) ..N(28): 141	merit = 6.49
3	N(28) --H(37) ..O(29): 164	merit = 10
4	N(28) --H(37) ..N(28): 141	merit = 6.49

TOTAL MERIT = **40.00**

Table 2.5: Total number of points awarded to a hypothetical structure.

2.5 The graph set assignment merit point scheme

All the aromatic and aliphatic test structures in this project contain the $R_2^2(8)$ and the C(4) unitary graph set motifs, although there are differences in terms of binary networks. These characteristic features of isostructural materials allow the implementation of a graph set assignment point scheme re-ranking strategy. Evoking Rpluto for a structure visually displays the graph set assignments (motifs) present with the crystal structure; information that can be exported into an output file as shown in figure 2.6.

POLYMORPH 1

Output file graphset notation	Standard graphset notation
R 2, 2(8)	$R_2^2(8)$
R 2, 4(8)	$R_4^2(8)$
C 1, 1(4)	C4

Figure 2.6: Graphset assignment information for a polymorphic structure as output into a text file.

Execution of the second perl program *gset.pl* automatically compares the motifs present within each structure as above with predefined expected characteristic motifs. If the structure has both expected motifs present, a maximum of 2 merit points are awarded; presence of only 1 of the expected 2 motifs results in only 1 merit point and the absence of expected motifs awards the structure 0 points. Again this point scheme was chosen due to its simplicity and was seen to be a viable way of discriminating between the occurrence and absence of the expected motifs within predicted structures.

2.6 Re-ranking strategy outputs

Tables 2.6 and 2.7 show typical results from these re-ranking procedures i.e. Pmorph_sort_Hbond.txt and Pmorph_sort_gset.txt, illustrating hydrogen bonding and graph set assignment merit points respectively.

Polymorph number	Lattice energy ($kcalmol^{-1}$)	Awarded hydrogen bonding merit points
17	-6.31	46.49
10	-6.46	42.00
12	-6.38	40.56
3	-7.06	40.00
4	-6.87	40.00
5	-6.68	40.00
6	-6.56	40.00
11	-6.46	40.00
14	-6.37	40.00
15	-6.35	40.00
18	-6.30	40.00
19	-6.29	40.00
20	-6.22	40.00
21	-6.21	40.00
24	-6.18	40.00
25	-6.15	40.00
2	-7.82	39.91
27	-6.12	39.36
1	-7.89	38.79
29	-6.09	36.45
7	-6.55	35.25
9	-6.48	30.85
23	-6.19	30.00
8	-6.50	20.00
13	-6.38	20.00
16	-6.34	20.00
22	-6.20	20.00
26	-6.12	20.00
28	-6.11	20.00
30	-6.08	20.00

Table 2.6: File Pmorph_sort_Hbond.txt illustrating the re-ranked polymorph distribution through the number of hydrogen bonding merit points awarded to each structure.

Polymorph number	Lattice energy ($kcalmol^{-1}$)	Awarded graph set assignment merit points
1	-7.89	2
3	-7.06	2
4	-6.87	2
6	-6.56	2
10	-6.46	2
11	-6.46	2
14	-6.37	2
15	-6.35	2
17	-6.31	2
18	-6.30	2
19	-6.29	2
20	-6.22	2
21	-6.21	2
24	-6.18	2
2	-7.82	1
5	-6.68	1
8	-6.50	1
9	-6.48	1
12	-6.38	1
16	-6.34	1
22	-6.20	1
23	-6.19	1
25	-6.15	1
27	-6.12	1
28	-6.11	1
29	-6.09	1
30	-6.08	1
7	-6.55	0
13	-6.38	0
26	-6.12	0

Table 2.7: File Pmorph_sort_gset.txt illustrating the re-ranked polymorph distribution through the number of graph set assignment merit points awarded to each structure.

3.0 Experimental

3.1 Instrumentation

3.1.1 Powder diffraction

The following powder diffraction instrumentation was used during the course of this project:

1. Bruker AXS D5000 high-resolution powder diffractometer using a Ge-monochromator producing Cu $K\alpha_1$ (λ = 1.54 Å) radiation with a position sensitive detector covering 8° in 2θ.
2. Bruker AXS D5005 powder diffractometer with Gobel mirrors producing radiation of type Cu $K\alpha_{1,2}$ (λ = 1.54 Å). The beam size was set at 0.6 mm x 1 cm and a position sensitive detector used with radial slits covering 8° in 2θ.
3. Synchrotron diffraction data were collected using the high-resolution powder diffractometer at station 2.3 of the synchrotron source, Daresbury Laboratory, UK. The wavelength of the X-rays used was 1.40 Å and the beam size was 1x10 mm^2.
4. Neutron diffraction data were collected using the BT-1 32 detector neutron powder diffractometer at the NIST (Centre for Neutron Research reactor, NBSR). A Cu(311) monochromator with a 90° take-off angle, λ = 1.5402(1) Å, and in-pile collimation of 15 minutes of arc were used. Data were collected over the range of 3 - 168° 2θ with a step size of 0.05°.

Diffraction data were collected at room temperature using two sample preparation strategies:

1. Flat disc

   The sample was ground using a pestle and mortar and placed between two pieces of transparent tape creating a circular area of diameter approximately 1cm. This sample geometry was used on the D5000 diffractometer, running in transmission mode.

2. Glass capillary

   The sample was ground using a pestle and mortar and packed into a 0.5mm glass capillary tube to a depth of approximately 3cm. Data sets were collected using this geometry using the D5005 diffractometer and on station 2.3.

3.1.2 FT-IR spectroscopy

Solid State infrared spectra were recorded at room temperature using the following Fourier transform spectrometer:

Shimadzu model 8300 FT-IR spectrometer (Single beam scanning Michelson Interferometer) with a DLATGS pyroelectric detector. Samples for infrared analysis were used as supplied in the solid state by compression by a diamond tip screw gauge on the instruments sample plate.

3.1.3 NMR spectroscopy

A solution state ^{1}H NMR spectra were recorded at 300.18 MHz on a Bruker AC300 spectrometer with a 5 mm diameter quad probe using residual solvent as reference.

3.2 Sample and data collection

3.2.1 2,4-dichloro-5-sulfamoylbenzoic acid

Anhydrous 2,4-dichloro-5-sulfamoylbenzoic acid was purchased from Aldrich [CAS no. 2736-23-4] as a fine white powder of purity 98%. Powder X-ray diffraction data were collected using the D5000 over the range $8° \leq 2\theta \geq 85°$ in 0.0194° steps over a total of 10hrs.

2,4-dichloro-5-sulfamoylbenzoic acid was re-crystallised from deuterated ethanol (Ethanol-d, 99.5+ atom % D, CAS no. 925-93-9) achieving a final bulk deuteration in the region of 67% ($Ar\text{-}H_1$ $\delta_{(ppm)}$ 8.6, $Ar\text{-}H_2$ $\delta_{(ppm)}$ 7.9, NH_2 $\delta_{(ppm)}$ 7.1). The deuterated sample was prepared for NMR by dissolving in acetone d^6 (Acetone-d, 99.9 atom % D, CAS no. 666-52-4) to a level of 5-10mg of sample in 50mm of solvent (see appendix 1).

3.2.2 Oxamic acid

The sample was purchased from Aldrich as a fine white powder purity 98% [CAS no. 471-47-6]. Powder X-ray diffraction data were collected using the D5000 over the range $15° \leq 2\theta \geq 80°$ in 0.0203° steps over a total of 10hrs. Additional data sets were recorded in capillary mode using the D5005 over the range $10° \leq 2\theta \geq 60°$ in 0.0100° steps for a total 10hrs. Multiple re-crystallisations of oxamic acid were carried out from deuterated ethanol (Ethanol-d, 99.5+ atom % D, CAS no. 925-93-9) and sent for neutron powder diffraction analysis at the NIST (Centre for Neutron Research reactor, NBSR).

The bulk deuteration in oxamic acid was investigate by Fourier transform infra red spectroscopy using the Shimadzu model 8300 FT-IR spectrometer in the 400 – 4000cm^{-1} range using a scan time of 4 seconds. Deuterartion was confirmed by the change in N-H ν = 3200cm^{-1} to N-H ν = 2336cm^{-1} (see appendix 2).

4.0 Crystal structure determination

4.1 2,4-dichloro-5-sulfamoylbenzoic acid

4.1.1 Background

2,4-Dichloro-5-sulfamoylbenzoic acid (I) is commonly known as Halazone (or pantocide and acetamid) and was commercially manufactured in tablet form by Abbott laboratories. The sodium salt of this material is used to disinfectant drinking water due to its ability to release chlorine in aqueous solution. Development of the disinfectant was introduced by Abbot laboratories in 1917, but was stopped in 1989; however it is still manufactured in some parts of the world along with other chloro compounds such as dichloroisocyanurate (as in Kintabs) and trichloroisocyanurate.

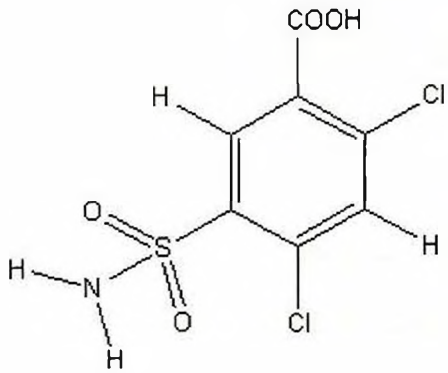

(I)

Crystals of the dihydrate form were prepared by re-crystallization from aqueous ethanol by Dr Phil Cox (Dept of Pharmacy, RobertGordon University, Aberdeen) and the crystal structure determined using conventional single crystal X-ray diffraction. Suitable single crystals of the anhydrous form however could not be prepared and so Laboratory powder X-ray diffraction was used to characterise the material and rationalise its crystal structure.

4.1.2 Structure solution and refinement from laboratory X-ray powder diffraction data

Laboratory powder X-ray diffraction data for (I) was indexed on the basis of the first 20 reflections using the indexing program CRYSFIRE [Shirley. R. A. 2000]. Density considerations indicated that two molecules occupied the unit cell, and structure solution was therefore initially attempted in the space group P-1 (2), Z' = 1. The profile parameters were refined by the LeBail [Le Bail. A. et al. 1988] method within the package GSAS [Larson. A. C. and Von Dreele. R. B. 1987] to establish the peak shape parameters and to improve the initial fit of the lattice parameters and zero point before initiating structure solution (see table 4.2).

Structure solution was carried out using the program POSSUM [Seaton. C.C. and Tremayne. M. 2002], invoking the DE technique. The structural model used in the DE calculation comprised the complete molecule, excluding

the carboxyl and amide hydrogens. The model was constructed using standard bond lengths and angles, the benzene ring and the carboxyl group were maintained as a rigid body, but the sulfonamide group allowed to rotate about the C - S bond. The structure was defined by 7 elements: 3 parameters (θ, ϕ, ψ) to define the orientation of the molecule (bounds 0 – 360°), 3 parameters (x, y, z) to define the overall crystallographic position of the molecule (bounds 0 - 1) and 1 torsion angle (τ_1) to define the sulfonamide conformation (bounds 0 – 360°). The parameters used in the DE calculation were, K = 1, F = 0.3, N_p = 160 and G_{max} = 200. The DE calculation was run 10 times, and convergence was achieved between R_{wp} 8 – 10 % in 9 separate cases, the lowest being R_{wp} 8.01 % for epoch 3 ($R_{wp} \approx$ 24 % for average random trial structures), see figure 4.1.

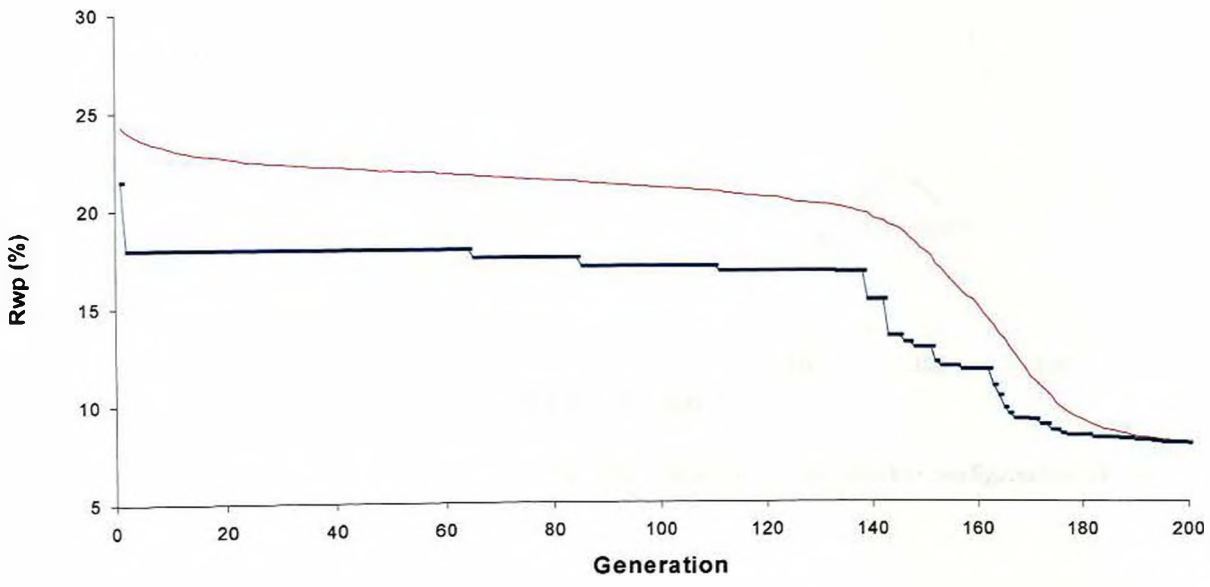

Figure 4.1: Evolutionary progress plot for (I) showing the best R_{wp} (dark blue line) and mean R_{wp} (red line) for epoch 3.

A full search of conformational space around the sulfonamide group was also performed using a grid search procedure also implemented in the program POSSUM. The best DE solution (R_{wp} = 8.01 % - structure A) was used as a starting model to investigate the R_{wp} discrimination on rotation of the carbon-sulphur bond. This bond was systematically rotated through 360° using fixed increments of 5° and R_{wp} calculated for every conformation generated. Starting with the best DE solution at 0°, the grid search method identified two alternative sulfonamide conformations with R_{wp} = 8.24% - stucture C and 8.71 % - structure B, differing from the DE solution by +/- 120° (see figure 4.2). As the R_{wp} discrimination between these structures is relatively small, all three conformations were investigated further.

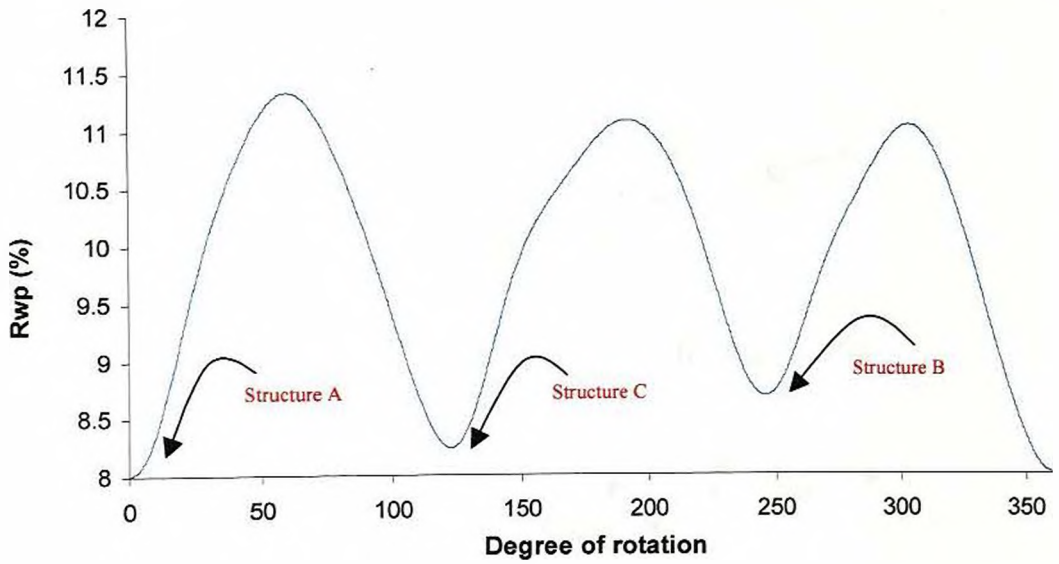

Figure 4.2: Direct space grid search showing the three lowest R_{wp} from possible configurations of the sulfonamide group.

Whereas structure C has the amide in the plane of the ring, structure A and B are similar in that they both have a sulfonyl oxygen in the plane of the ring, with the remaining sulfonyl oxygen and amide hydrogen either above or below the ring (see figure 4.3). In order to investigate whether there is a preferred conformational arrangement of the sulphonamide group in the solid state, a study of molecular geometry was carried out using the crystal structures present in the Cambridge Structural Database (CSD).

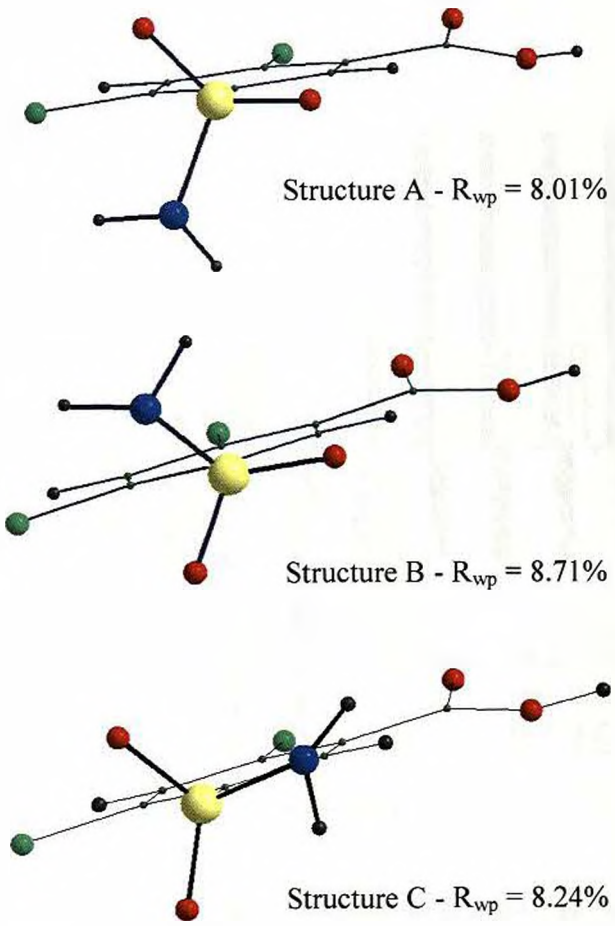

Figure 4.3: Difference in molecular conformation of structures A, B and C about the carbon-sulphur bond.

A search was conducted for aromatic sulphonamides with a chlorine atom on the adjacent carbon atom, hence constraining the search to similar intramolecular interactions and steric considerations as our material. A total of 17 crystal structures were found which contained the aforementioned molecular arrangement. In each case, the geometry of the sulphonamide group was analysed by measuring 3 torsion angles C_2-C_1-S_1-O_1, C_2-C_1-S_1-O_2 and C_2-C_1-S_1-N_1 (as in II) and the results of the conformational study displayed in the form of a histogram (figure 4.4).

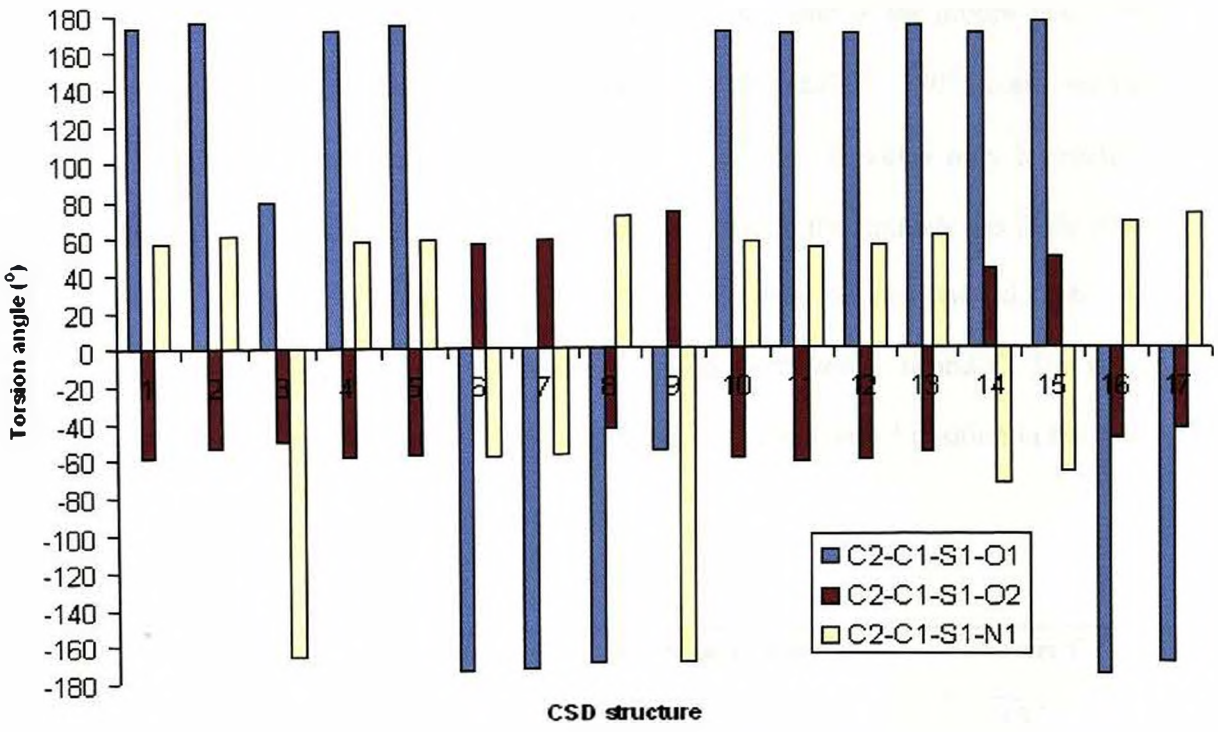

Figure 4.4: Histogram displaying conformation of the sulphonamide group as observed in the structures selected from CSD.

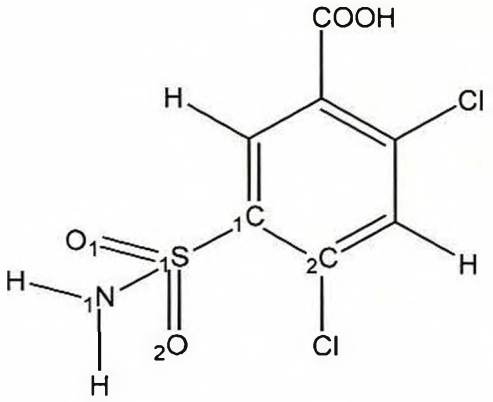

(II)

This clearly shows that in all 17 structures, as expected, one of the groups (either the amine or the sulfonyl oxygen) lies in the plane of the ring (±170° - 180°), corresponding to our 3 conformations identified in our structure solution. However only 2 structures found in the CSD search display the conformation in which the amine N lies in the plane of the ring, implying this geometry (i.e. structure C) may be less favored. Table 4.1 shows the three sulphonamide torsion angles within structures A, B and C. The amide torsion angle was measured at –170.25° highlighting its less favored position in the plane of the ring.

Torsion	Structure A (°)	Structure B (°)	Structure C (°)
C_2-C_1-S_1-O_1	-179.95	175.06	69.75
C_2-C_1-S_1-O_2	-59.47	56.39	-59.18
C_2-C_1-S_1-N_1	63.75	-66.35	-170.25

Table 4.1: torsion angles of the sulphonamide group of structures A, B and C.

The intermolecular packing of all three structures was also examined and their hydrogen bonding suitability considered. At this point structure C was dismissed as the true structure solution, due to having a sulfonamide conformation not conducive for intermolecular hydrogen bonding. Despite the similarity in molecular conformation of structures A and B, these structures differ significantly in their hydrogen bonding arrangements and were hence both used as starting points for two independent Rietveld refinements.

These Rietveld refinements were carried out using GSAS with both models being subjected to the same parameter variation of atomic positions with soft constraints (weighting factor 0.001 for intramolecular bond distances), lattice parameters, zero point and isotropic thermal parameters (refined for non-H atoms constrained according to atom type). The carboxyl and amide hydrogens were placed in positions calculated in accordance with hydrogen bonding positions, but had no significant effect on the refinement. Preferred orientation parameter refinement was also required along the [110] direction. Final agreement factors for the two structures are in table 4.2 and the final Rietveld profile plots are shown in figure 4.5.

Indexing				
Crystal system	Triclinic			
Space group	P-1 (2)			
Initial a / Å	8.3186			
Initial b / Å	8.6928			
Initial c / Å	7.6046			
Initial α / °	106.20			
Initial β / °	112.39			
Initial γ / °	81.23			
Initial V / Å^3	488.61			
Structure solution	X-ray	Neutron		
LeBail R_{wp} / %	3.26	1.78		
LeBail R_p / %	2.26	1.47		
LeBail χ^2	5.25	0.63		
DE elements	7			
K	0.3			
F	1			
Population size	160			
No. of generations	200			
No. of epochs	10			
Average trial R_{wp} / %	24			
Best R_{wp} / %	8.01(*structure A*)	8.71(*structure B*)[a]		
Refinement	X-ray		Neutron	
	Structure A	Structure B	Structure A	Structure B
R_{wp} / %	3.94	4.42	2.91	5.24
R_p / %	2.76	3.08	2.39	4.14
χ^2	7.93	10.05	1.73	27.50
P.O ratio [Dir]	0.8434 [110]	0.8575 [110]	-	-
Final a / Å	8.3223(3)	8.3229(4)	8.3237(3)	8.3237(3)
Final b / Å	8.6960(3)	8.6965(4)	8.6933(4)	8.6933(4)
Final c / Å	7.6062(3)	7.6068(3)	7.6032(3)	7.6032(3)
Final α / °	106.204(2)	106.206(2)	106.208(3)	106.208(3)
Final β / °	112.386(2)	112.386(2)	112.462(3)	112.462(3)
Final γ / °	81.227(2)	81.227(2)	81.187(3)	81.187(3)
Final V / Å^3	488.20(5)	488.12(4)	487.55(4)	487.55(4)

Table 4.2: Initial lattice parameters, DE structure solution parameters, final refined parameters and agreement factors for structures A and B.

[a] – Structure solution from grid search.

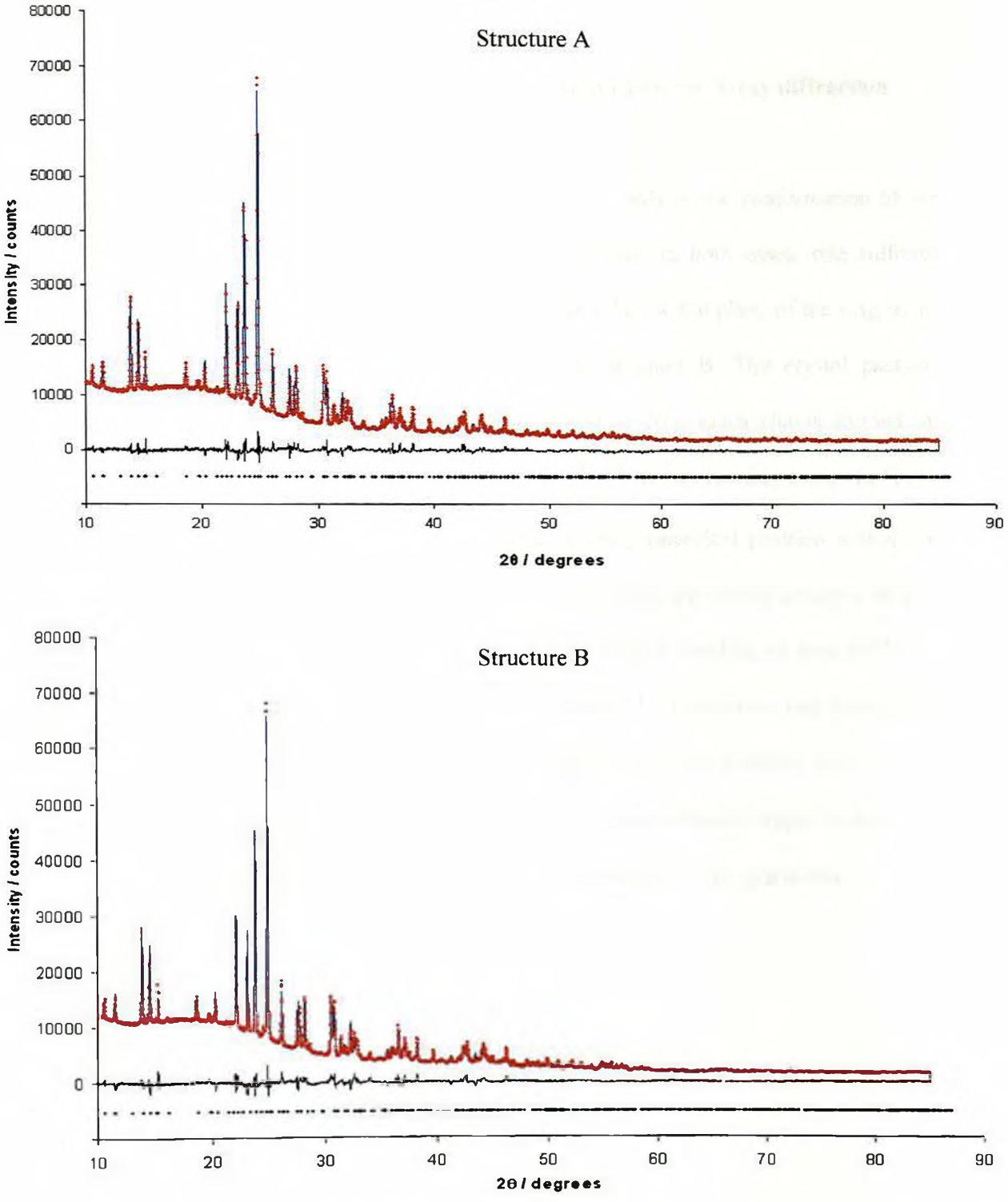

Figure 4.5: Final observed (red), calculated (blue) and difference (below) powder diffraction profile for the Rietveld refinement of Structures A and B. Reflection positions are also shown.

4.1.2.1 Analysis of crystal structures from laboratory powder X-ray diffraction

The two refined molecular structures of A and B differ only in the conformation of the sulfonamide group with respect to the plane of the ring: in both cases, one sulfonyl oxygen is in the plane of the ring with the amide either below the plane of the ring, as in structure A or above the plane of the ring as in structure B. The crystal packing arrangement of structure A (figure 4.6) is comprised of continuous chains formed by sulfonamide N-H···O=S and carboxylate O-H···O=C $R_2^2(8)$ dimers running along the [211] direction. The second amino hydrogen atom, due to its geometrical position within the crystal structure, does not form typical hydrogen bonds with any strong acceptor atoms. However, this amino H may be involved in weak hydrogen bonding of type N-H···Cl, stabilising the hydrogen bonded chains that run in the [211] direction and form a 2D sheet. The amide hydrogen lies between the nitrogen and the chlorine with a N-H distance of 2.71Å and a N-H···Cl angle of 112°. The second sulfonyl oxygen is also in a position that prevents it from forming any strong intermolecular hydrogen bonds.

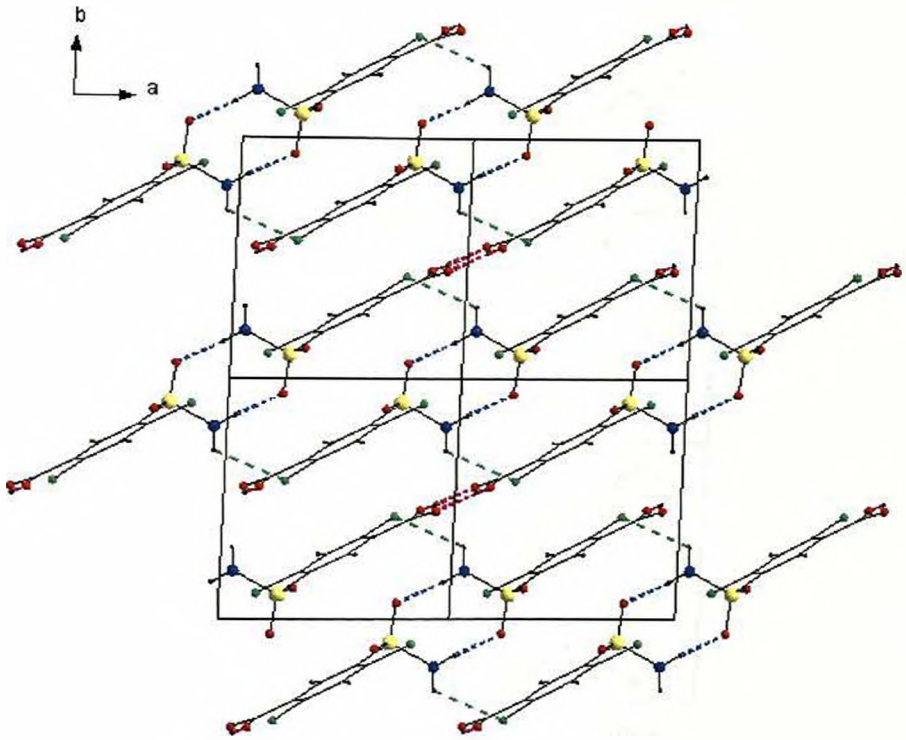

Figure 4.6: View of crystal structure A, where the purple, blue and green hashed lines represent the carboxylate, sulfonamide dimers and the N-H···Cl hydrogen bond respectively. Atoms coloured yellow, blue, red and green signify sulphur, nitrogen, oxygen and chlorine respectively.

The conformation of the sulfonamide group in structure B (see figure 4.7) gives rise to a theoretically more stable hydrogen bonding arrangement, which utilizes all the hydrogen bond donors and acceptors on the sulfonamide and carboxylate groups. This crystal structure contains alternating centrosymmetric sulfonamide N-H···O=S $R_2^2(8)$ dimers (blue hashed lines) forming chains running parallel to the a axis, which are held together by a network of carboxylate O-H···O=C $R_2^2(8)$ dimers (purple hashed lines). Although all hydrogen bonding donors and acceptors are utilized the apparent distortion of the molecule upon refinement, despite the use of geometrical restraints, cannot be overlooked.

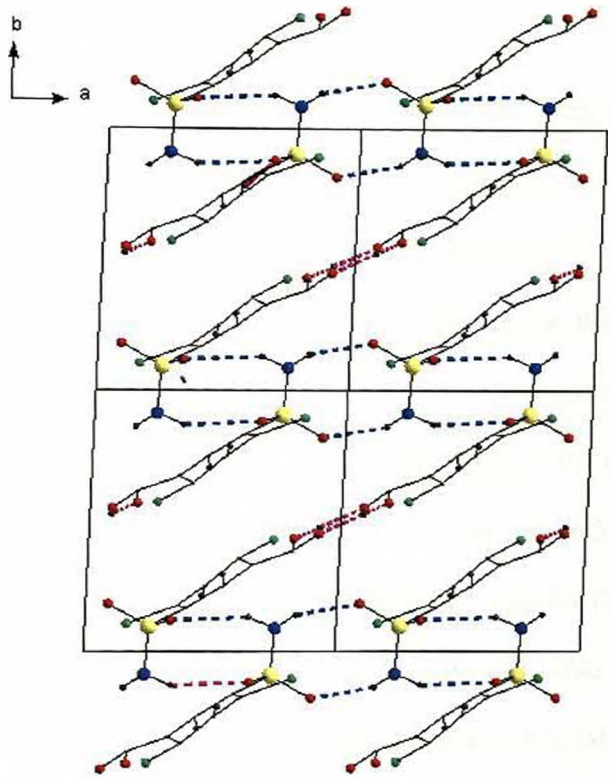

Figure 4.7: View of crystal structure B, where the purple and blue hashed lines represent carboxylate and sulphonamide dimers respectively. Atoms coloured yellow, blue, red and green signify sulphur, nitrogen, oxygen and chlorine respectively.

The structure determination and rationalisation of structures A and B seem at this stage contradictory. Structure B adopts the preferred crystal packing arrangement utilizing all hydrogen bonding donors and acceptors [Etter M. C. 1990], but has become severely distorted during Rietveld refinement. Structure A has remained undistorted but has a sulfonyl oxygen and an amino hydrogen that does not take part in any strong intermolecular interactions.

4.1.3 Infrared analysis

Infrared vibrational spectroscopy can be used to provide evidence for the existence of hydrogen bonding in the solid state and has been used to differentiate between polymorphs [Stockton. G. W. and Godfrey. R. 1998]. An example of this is the structural study of a potent herbicide Pendimethalin; a secondary aromatic amine that exists in triclinic and monoclinic polymorphic forms (orange and bright yellow respectively). Usually the N-H stretching mode appears near 3450 cm^{-1}, but in the case of the triclinic and monoclinic forms the stretching modes appear at 3318.6 cm^{-1} and 3326.5 cm^{-1} respectively. The lower stretching mode in the orange polymorphic form implies the formation of a strong hydrogen bond involving the N-H group. In this study, solid state IR has been used to aid the structural comparison of the anhydrous and dihydrate materials, the latter of which we know has a crystal structure that involves all donor and acceptor atoms in the formation of a complex hydrogen bonding network through two water molecules (see appendix 3). If both amide hydrogen frequencies from the anhydrous material (see figure 4,6 and 4.7) are comparable to the dihydrate, this would indicate that all donors and acceptors are involved in hydrogen bonding and that the correct structure would most likely be structure B. However, if one of the amide hydrogen vibrational stretches is slightly higher in frequency compared to the dihydrate then this would suggest that the amide hydrogen in question is not involved in hydrogen bonding and hence infer that structure A is correct (see table 4.3).

Assignment ν / cm^{-1}	Dihydrate ν / cm^{-1}	Anhydrous ν / cm^{-1}
N - H stretch	1540.1	1549.7
N - H stretch	1578.3	1578.4

Table 4.3: Infrared frequencies for dihydrate and anhydrous 2,4-dichloro-5-sulfamoylbenzoic acid

Comparison of the N-H vibrational stretches of the dihydrate and anhydrous materials shows that one of the amide hydrogen stretches is higher in frequency compared to that of the dihydrate. This would imply that one of the amino hydrogens in the anhydrous material is not involved in structural hydrogen bonding and that structure A is possibly correct.

4.1.4 Analysis of molecular and lattice energy calculations

The Accelrys CERIUS^2 molecular modelling package [Accelrys, Cambridge, UK.] was used to calculate the molecular gas phase energies and the crystal lattice energies for structures A and B using the minimiser module. This was done using two classical force fields; Consistent Valence Force Field_950_1.01 [Dauber-Osguthorpe, P. et al. 1988] and DREIDING 2.21 [Mayo, S. L. et al. 1990] (see Table 4.4).

	FORCEFIELDS			
	CVFF_950_1.01		DREIDING 2.21	
Energy (kcalmol^{-1})	Structure A	Structure B	Structure A	Structure B
Gas phase energy	9.74	9.74	33.77	33.77
Lattice energy	-50.59	-44.63	-73.61	-68.21

Table 4.4: Molecular gas phase and crystal lattice energies of structures A and B.

As expected, the molecular gas phase energies obtained for structures A and B are identical. However, there is a clear difference between the two structures when their lattice energies are considered. Calculations using both force fields show structure A to be the thermodynamically more stable structure, despite the presence of less hydrogen bonding.

4.1.5 Refinement from neutron diffraction powder data

In order to determine the positions of all the atoms in the amine group neutron diffraction studies were carried out on the deuterated anhydrous material (bulk deuteration level 67% - see appendix 1). Structures A and B (obtained from the original structure solution from laboratory powder X-ray data) were again used as starting models for two independent neutron powder refinements. Atomic positions were refined using soft constraints (weighting factor 0.001 for intramolecular bond distances), with the deuterated positions allocated a D:H ratio of 0.33:0.67 in accordance with the measured extent of deuteration, lattice parameters, zero point and isotropic thermal parameters were refined for non-H atoms constrained according to atom type.

The final Rietveld profile plots are shown below in figure 4.8 and the initial LeBail and final refinement agreement factors are shown in table 4.2.

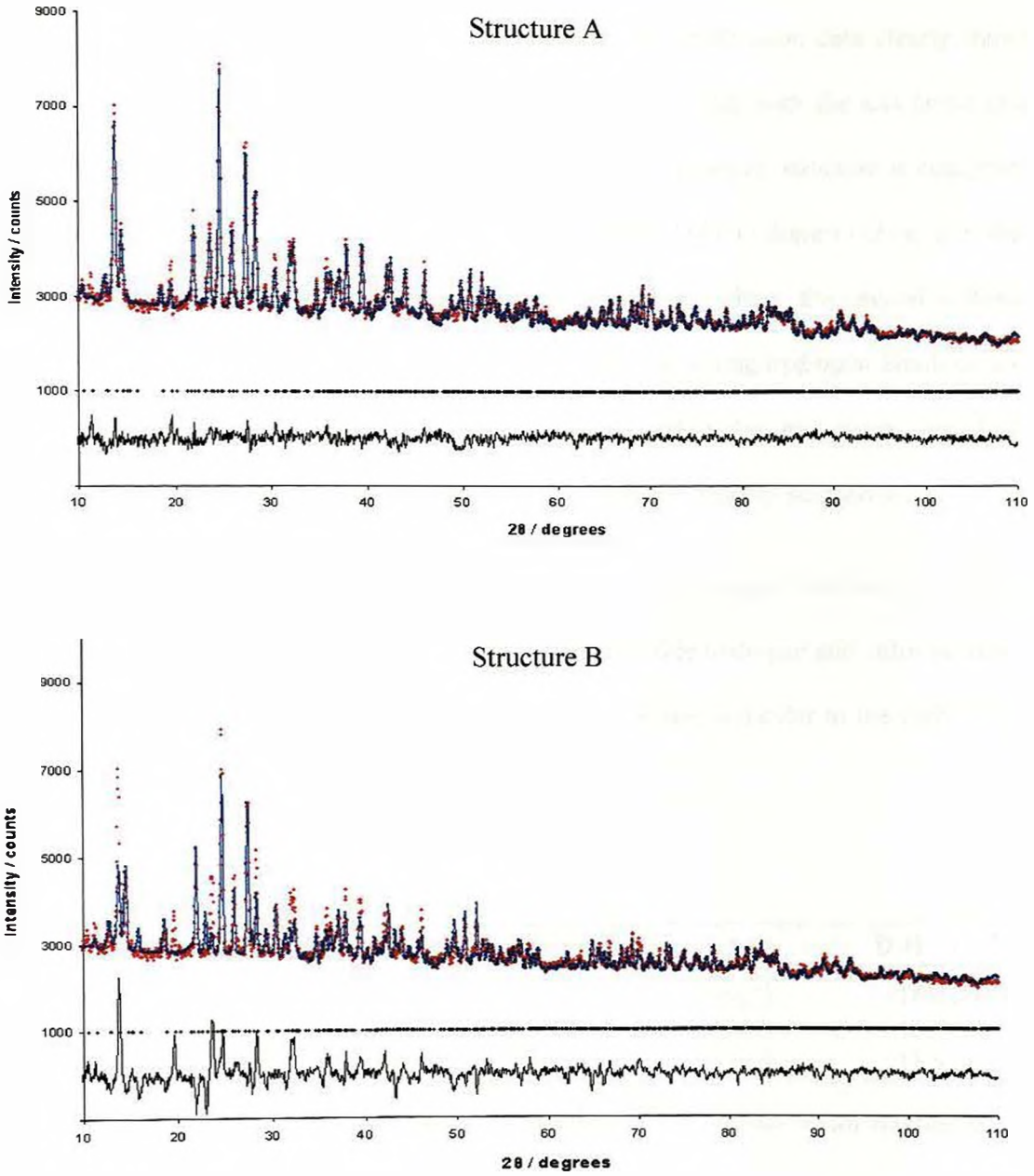

Figure 4.8: Final observed (red), calculated (blue) and difference (below) neutron diffraction profile for the Rietveld refinement of Structures A and B. Reflection positions are also shown.

4.1.5.1 Analysis of crystal structures from neutron powder diffraction

Rietveld refinement of structures A and B using neutron diffraction data clearly shows that structure B is incorrect and that the correct structure is that with the less favourable hydrogen bonding arrangement (structure A). As described earlier, structure A comprises sulfonamide N-H···O dimers (*-x, -y, 1-z*) and carboxylate O-H···O dimers (*-1+x, y, z*) that form continuous chains in the [211] direction. However, neither the second sulfonyl oxygen or the remaining amino hydrogen are involved in strong hydrogen bonding, and the formation of a N-H···π bond with the electron rich carboxylate ring seems unrealistic as the H···Centroid distance is 3.5 – 4.0Å and the groups are slightly staggered.

However, it is feasible that a weak N-H···Cl (*1-x, 1-y, 2-z*) hydrogen bond may be holding the sulfonamide and carboxylate chains together. The amide hydrogen and chlorine atoms lie in the same plane as the sulfonamide dimer, but are perpendicular to the carboxylate dimer.

H···*A*	*D*-H···*A*	Symmetry code of *A*	H···*A* / Å	D-H···*A* / °
$H_{19}\cdots O_1$	$N_1\text{-}H_{19}\cdots O_1$	*-x, -y, 1-z*	1.99(2)	168(1)
$H_{18}\cdots O_3$	$O_4\text{-}H_{18}\cdots O_3$	*-1+x, y, z*	1.41(1)	168(1)
$H_{20}\cdots Cl_2$	$N_1\text{-}H_{20}\cdots Cl_2$	*1-x, 1-y, 2-z*	2.71(3)	112(1)

Table 4.5: Selected intermolecular distances (Å) and angles (°) for the final refined structure of 2,4-dichloro-5-sulfamoylbenzoic acid.

To investigate the plausibility of an N-H···Cl hydrogen bond in this structure, a survey of this type of intermolecular interaction was carried out using CSD and the IsoStar [Bruno, I. J. et al. 1997] interface. This enables selection of a particular chemical group, the '*central group*', and investigation of its non bonded interactions with a second group, the '*contact group*'. The results are displayed in the form of a scatterplot [Rosenfield, R. E. et al. 1984] [Taylor, R. et al. 1990] showing the intermolecular distance and angle distribution of the contact group around the specified central group, as observed in the crystal structures taken from the CSD. Figure 4.9 shows the scatterplot displaying all 106 N-H···Cl interactions identified in the CSD, where the '*central group*' is planer NH_2 and the '*contact group*' is C-Cl.

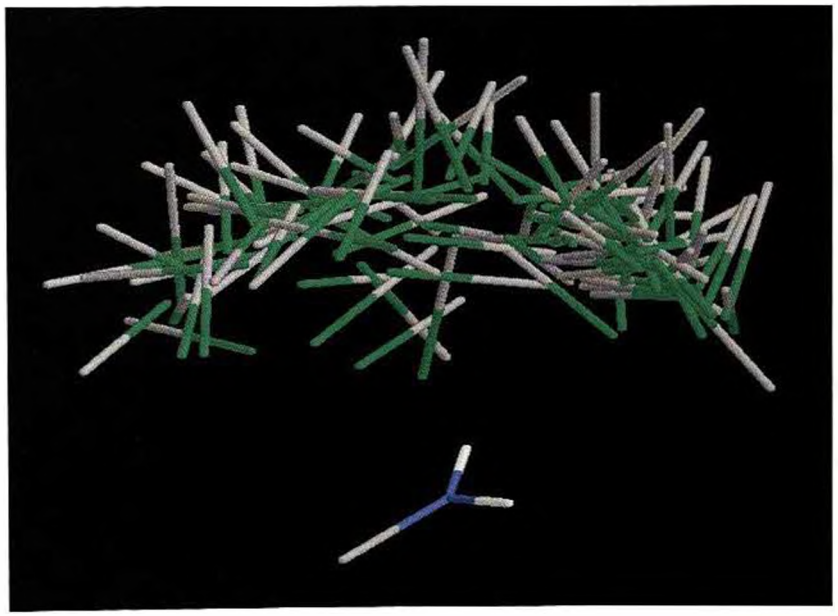

Figure 4.9: Distribution of C-Cl '*contact group*' (green) around the planar NH_2 '*central group*' (blue).

This clearly shows that the N-H···Cl hydrogen bond is not strongly directional, but that the typical hydrogen bonding geometry of this interaction is D-H···A distance between 2.6 – 4.1Å and D-H···A angle between 60 - 134°. The N-H···Cl geometry in structure A is clearly within this range and can be assumed to be a viable hydrogen bond.

4.1.6 Discussion

Laboratory powder X-ray diffraction has been used to solve the crystal structure of anhydrous 2,4-dichloro-5-sulfamoylbenzoic acid. We investigated here the reliability of this data in the discrimination between the three different molecular conformations adopted by the sulfonamide functional group. Although these three structures only varied by 0.7% in R_{wp}, only two of the molecular conformations gave rise to crystal structures that are favourable in terms of hydrogen bonding: structure A with the lowest R_{wp} and structure B with the highest R_{wp} but with a hydrogen bonding typical of sulfonamides. Despite structure B having the preferred crystal packing with all hydrogen bonding donors and acceptors utilised in strong hydrogen bond interactions, the fact that this structure became distorted during refinement gave the impression that structure A may be the correct crystal arrangement, appendix 4 gives the final refined coordinates for anhydrous 2,4-dichloro-5-sulfamoylbenzoic acid.

Gas phase molecular energy calculations showed that structures A and B are equivalent, however, lattice energy calculations showed that structure A is energetically more stable and the most likely structural arrangement.

Infrared spectroscopic analysis offered further supportive evidence in favour of structure A, indicating that one amino hydrogen on the sulfonamide group does not form any strong hydrogen bond interactions when compared to the amide stretches of the dihydrate material, (although other possible weak interactions cannot be overlooked).

Refinement of these structures against neutron powder diffraction data was then used to confirm that structure A was indeed the correct crystal structure for anhydrous 2,4-dichloro-5-sulamoylbenzioc acid. Although this structure contains sulphonamide and carboxylate hydrogen-bonded dimers combined together into chains, the amino hydrogen and sulfonyl oxygen are not involved in traditional strong hydrogen bonds.

However, close examination of the structure revels that these chains are held together by N-H···Cl interactions, the geometry of which falls well within the regions identified in the CSD. With one acceptor still not utilized in the hydrogen-bonding network, this structure differs significantly from that of the dihydrate material. The final crystal packing arrangement of anhydrous 2,4-dichloro-5-sulfamoylbenzoic acid is that of structure A, as illustrated in Figure 4.6.

4.2 Oxamic acid

4.2.1 Background

Oxamic acid powder was purchased from Aldrich [CAS no. 471-47-6] 98% purity in an attempt to re-crystallise the material from solution to obtain suitable single crystals for characterization by single crystal X-ray diffraction. However, all attempts to grow single crystals were unsuccessful, and characterisation of the solids obtained by powder X-ray diffraction only confirmed the presence of the solvate derivative.

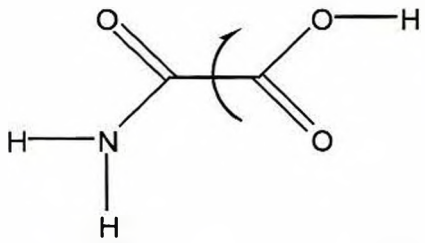

(I)

4.2.2 Structure determination from single crystal X-ray diffraction

The crystals available for this study were of poor quality and although indexing and structure solution were attempted, the lack of quality single crystal X-ray diffraction data was reflected in an unreliable structure with a high R-factor (see appendix 5 for crystal data). The packing arrangement in this solution comprises oxamic acid molecules in the *cis* conformation lining up but not hydrogen bonded along the [010] direction. Figure 4.10 shows the packing arrangement for this structure.

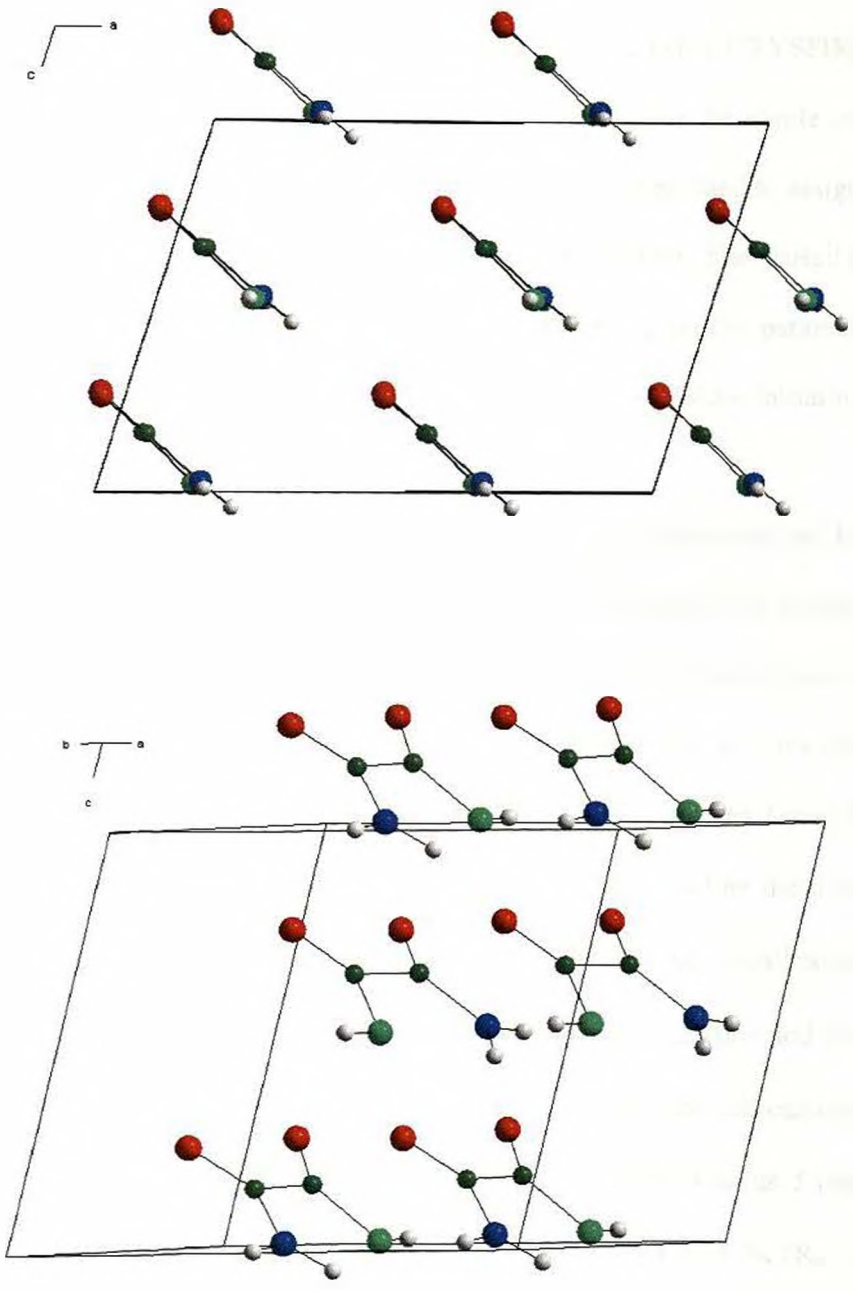

Figure 4.10: Packing arrangement of oxamic acid from the attempted single crystal structure solution, where green, blue and red atoms signify hydroxide oxygen, nitrogen and carbonyl oxygen respectively.

4.2.3 Structure solution and refinement from laboratory powder X-ray diffraction data

The laboratory powder X-ray diffraction data were indexed using CRYSFIRE and unit cell parameters were generated similar to those obtained from the single crystal data, details of which are listed in table 4.6. Systematic absences were used to assign the space group Cc (9) and this was used in subsequent structure solution. The LeBail refinement method (within the package GSAS) was used to establish the profile parameters and to improve the initial fit of the lattice parameters and zero point before initiating structure solution (see table 4.6).

Structure solution was carried out using the DE method implemented in the program POSSUM. The structural model used in the calculation comprised the model shown in figure 4.11 but excluding the carboxyl and amide hydrogens. The model was constructed using standard bond lengths and angles, and the relative conformation of the carboxyl and amide groups allowed to vary by rotation about the C - C bond (see figure 4.11). The structure was defined by 7 elements: 3 parameters (θ, ϕ, ψ) to define the orientation of the molecule (bounds 0 - 360°), 3 parameters (x, y, z) to define the overall position of the molecule (bounds 0 - 1) and 1 torsion angle (τ_1) to define the carboxyl and amide group conformation (bounds 0 - 360°). The control parameters used in the DE calculation were, K = 0.99, F = 0.5, N_p = 70 and G_{max} = 1000. The DE calculation was run 5 times, and in each case convergence was achieved between R_{wp} = 9.6 % and 9.74 %, ($R_{wp} \approx$ 20.12 % for average random trial structures), Figure 4.12 displays the evolutionary progress plot for the optimum DE run.

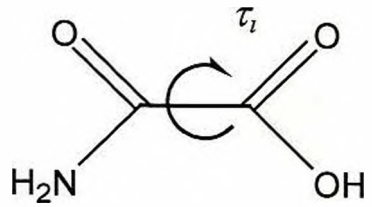

Figure 4.11: Structural model used in the DE structure solution of oxamic acid. The arrow indicates the conformational flexibility allowed in this model.

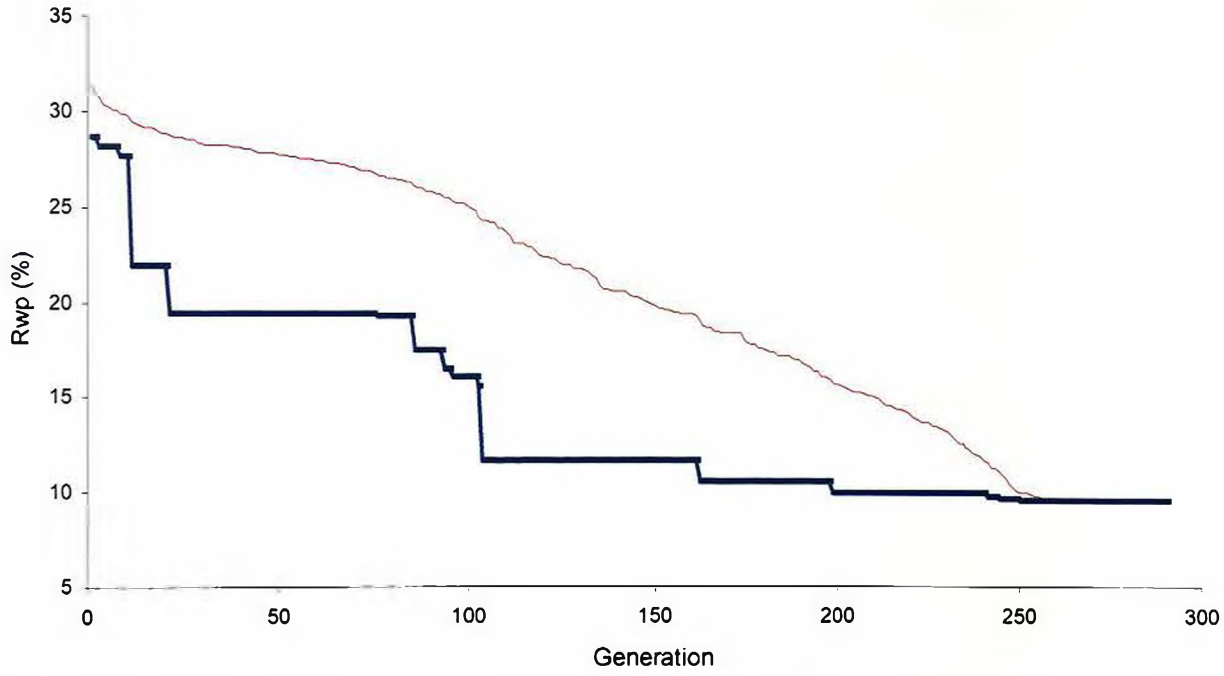

Figure 4.12 Evolutionary progress plot for oxamic acid showing the best R_{wp} (blue line) and mean R_{wp} (red line).

Rietveld refinement was carried out using the best DE solution (R_{wp} = 9.6 %), with variation of atomic positions using soft constraints (weighting factor 0.001 for intermolecular bond distances and angles), lattice parameters, zero point and isotropic thermal parameters refined for non-H atoms (constrained according to atom type and

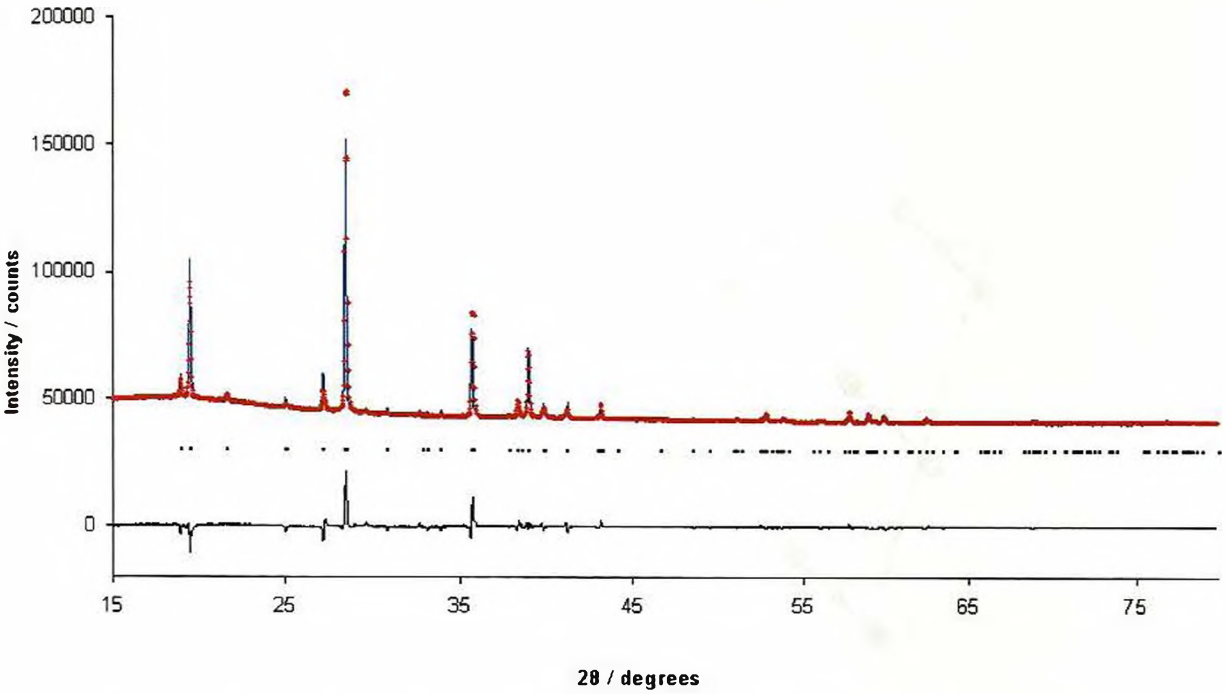

Figure 4.13. Final observed (red), calculated (blue) and difference (below) powder diffraction profile for the Rietveld refinement of oxamic acid. Reflection positions are also shown.

Clearly the fit of this structure with the powder data is not ideal. Although a number of possible considerations have not yet been addressed e.g. the presence of preferred orientation, scattering contribution of hydrogen atoms (still excluded from the refinement), it was felt that it may be informative at this point to compare this structure with that obtained from the single crystal data.

4.2.3.1 Analysis of crystal structure from laboratory powder X-ray diffraction data

All 5 structures obtained from the DE structure solution calculations showed preference for the *trans* conformation. These solutions all exhibited infinite hydrogen bonded chains running along the [010] direction through the formation of N-H...O=C and O-H...O=C

type $R_2^2(8)$ dimers. Figure 4.14 shows the crystal structure of oxamic acid determined from laboratory X-ray diffraction data.

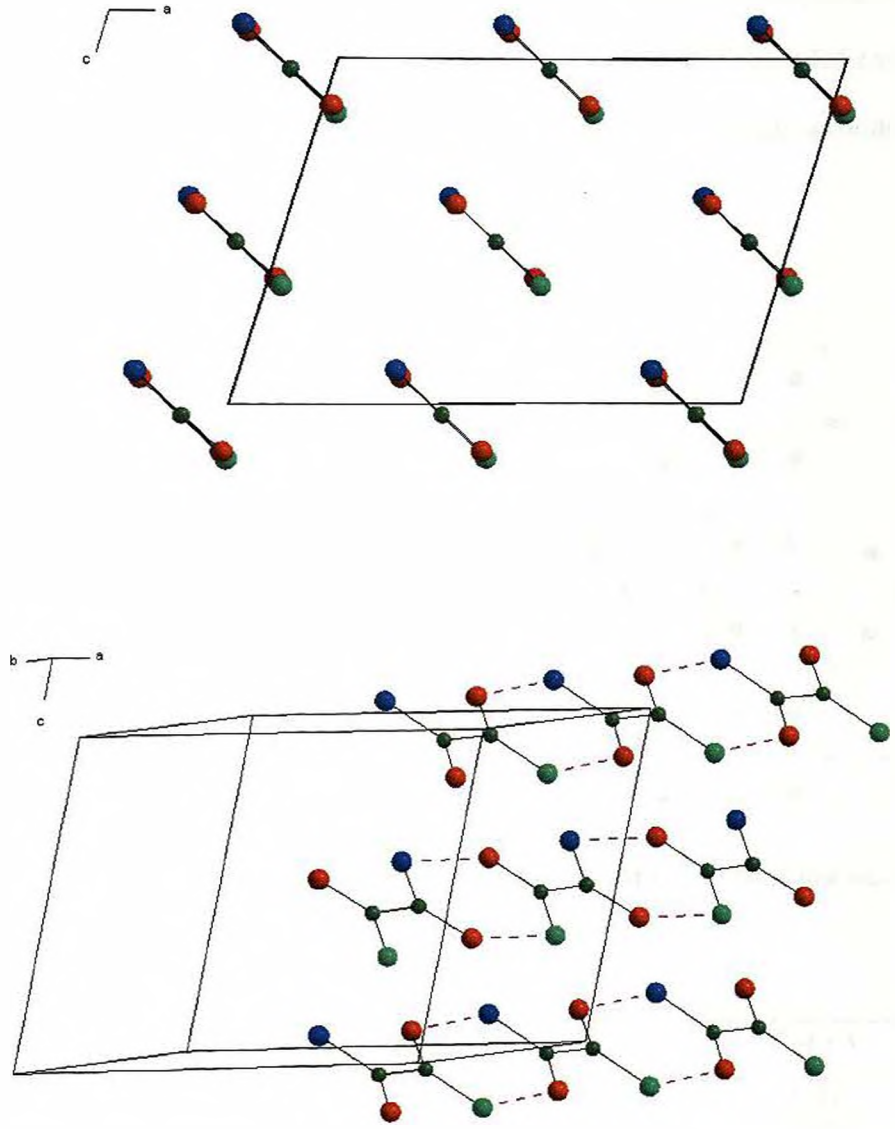

Figure 4.14: Crystal structure of oxamic acid from laboratory powder X-ray diffraction data, atoms depicted as in figure 4.10. The purple hashed lines represent hydrogen bonds.

Figure 4.15 illustrates the possible presence of a further hydrogen bond of type N-H...O holding these chains together in a sheet lying in the (101) plane containing alternating rows of $R_2^2(8)$ and $R_4^4(14)$ motifs (see table 4.7). Calculation of the hydrogen atom positions idealised for the formation of the dimer further support this observation, giving a second amide hydrogen position ideal for formation of this extended hydrogen bond network. Formation of these interactions utilizes the hydroxyl oxygen as both a donor and an acceptor.

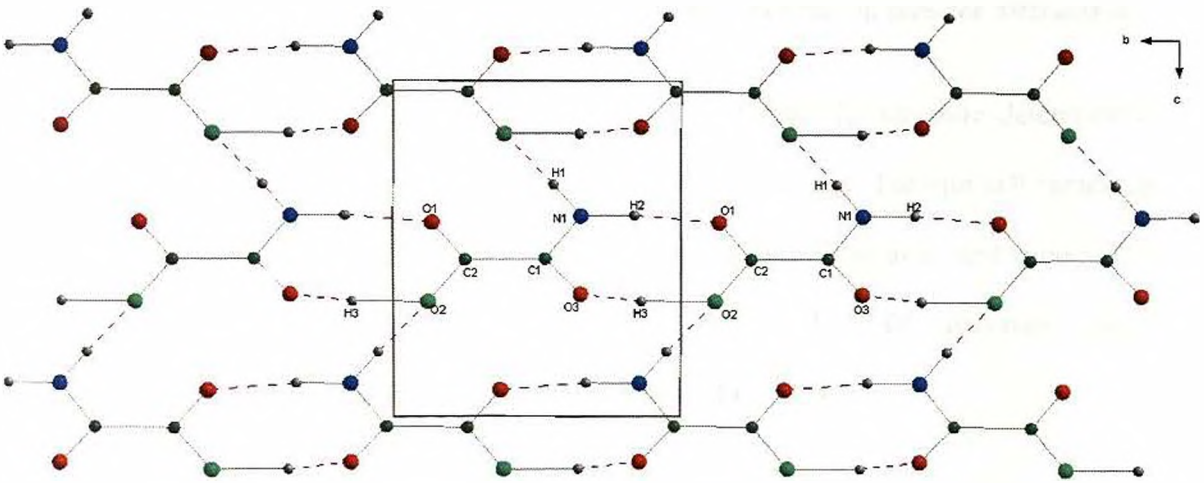

Figure 4.15: Crystal structure of oxamic acid from laboratory powder X-ray diffraction data illustrating the third hydrogen bond (H_1···O_2) network in the (101) plane.

H···*A*	*D*-H···*A*	Symmetry code of *A*	H···*A* / Å	*D*-*A* / Å	D-H···*A* / °
H_1···O_2	N_1-H_1···O_2	*0.5-x, 1.5 -y, 0.5+z*	1.98	2.99	170
H_2···O_1	N_1-H_2···O_1	*x, -1-y, z*	1.64	2.65	173
H_3···O_3	O_2-H_3···O_3	*x, -1-y, z*	1.58	2.60	175

Table 4.7: Hydrogen bonding geometry of oxamic acid from laboratory powder X-ray diffraction data.

The presence of preferred orientation within the oxamic acid sample was investigated by collection of powder data in capillary geometry. However, comparison with the original disc dataset confirmed that there are no preferred orientation effects in this case. Comparison of this powder structure with the single crystal structure illustrates that the two structures are very similar, both in terms of molecular position and overall molecular orientation. However, because the single crystal structure is in the *cis* conformation it cannot form any intermolecular hydrogen bonding interactions.

4.2.4 Structure solution and refinement from synchrotron powder diffraction data

In order to improve the quality of this structure solution, the structure determination process was repeated using synchrotron powder diffraction data. The unit cell parameters and space group from the laboratory powder data study were used as a starting point for a LeBail refinement before initiating structure solution. Two DE structure solution calculations were then carried out using the program POSSUM:

i) Using model A:

The structural model defined in section 4.2.3, i.e. excluding the carboxyl and amide hydrogens and defined by 7 elements (θ, ϕ, ψ, x, y, z, τ_1). The parameters used in the DE calculation were, K = 0.99, F = 0.5, N_p = 70 and G_{max} = 1000. The DE calculation was run 5 times, and in each case convergence was achieved giving an R_{wp} for each calculation between 17.26 % and 17.32%, ($R_{wp} \approx 29.94$ % for average random trial structures), see Table 4.6. The evolutionary progress plot for the best DE run is shown in figure 4.16.

ii) Using model B:

Comprised the complete oxamic acid molecule including the carboxyl and amide hydrogens. This requires 9 elements to define the structure including two additional torsion angles to enable full conformational flexibility (θ, ϕ, ψ, x, y, z, τ_1, τ_2, τ_3), this is illustrated in figure 4.18. The parameters used in the DE calculation were, K = 0.99, F = 0.5, $N_p = 90$ and $G_{max} = 1000$. The DE calculation was also run 5 times, and in each case convergence was achieved giving $R_{wp} = 16.34$ % ($R_{wp} \approx 28.30$ % for average random trial structures), see table 4.6. The evolutionary progress plot for the best DE run is shown in figure 4.17.

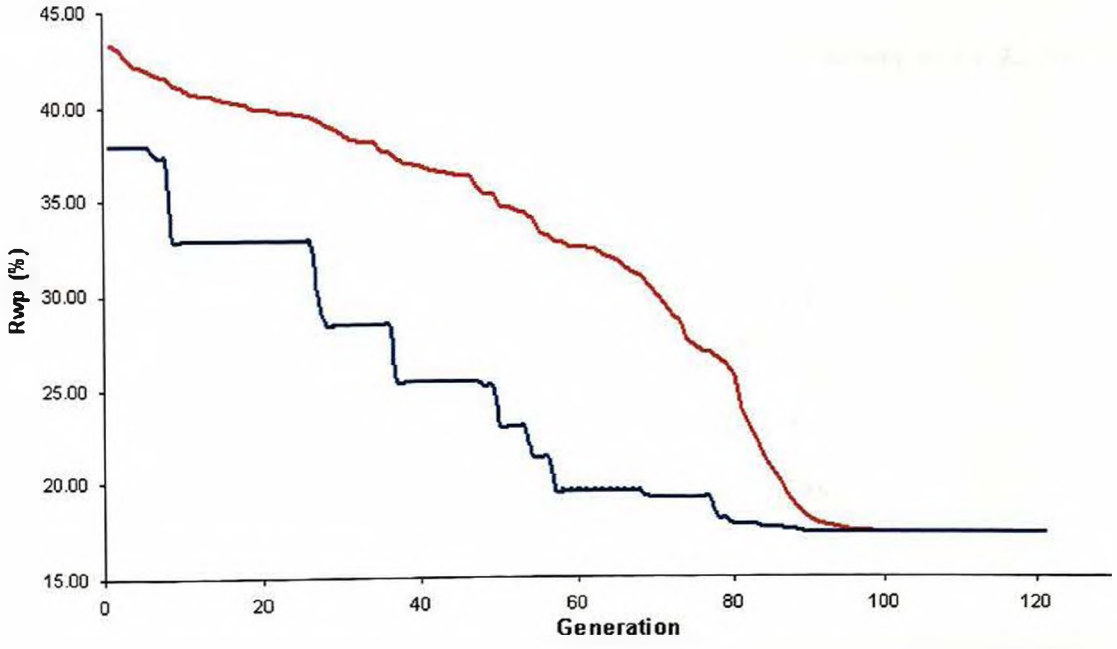

Figure 4.16: Evolutionary progress plot for oxamic acid from synchrotron data showing the best R_{wp} (blue line) and mean R_{wp} (red line) for model A.

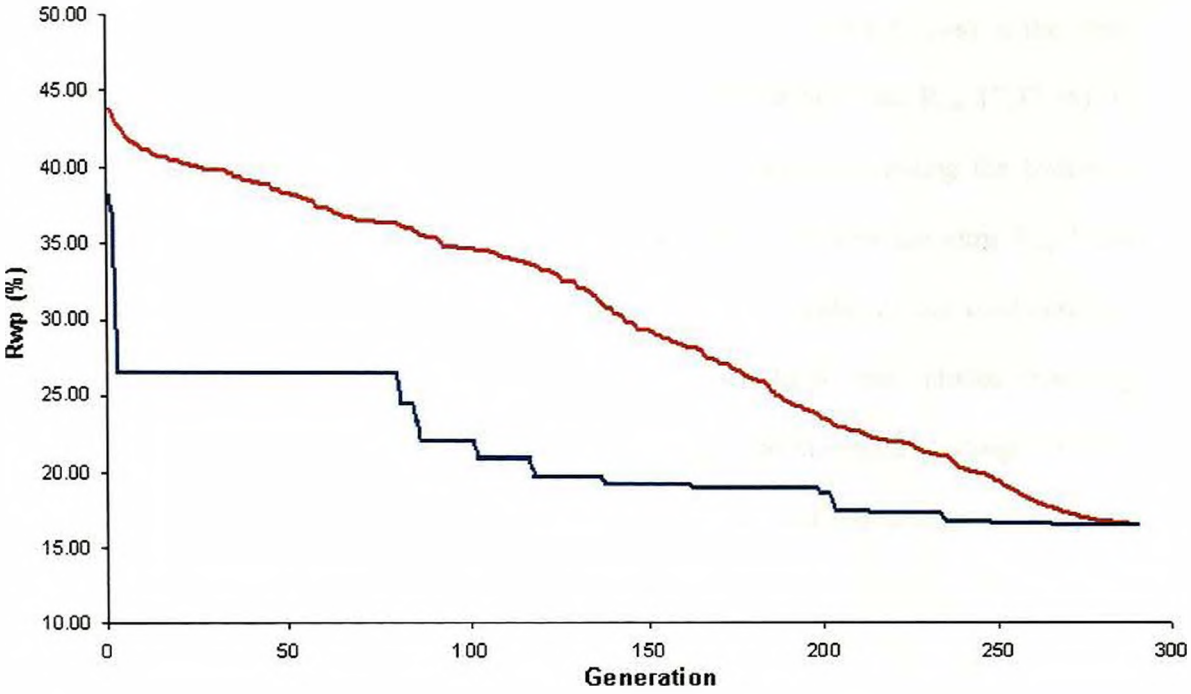

Figure 4.17: Evolutionary progress plot for oxamic acid from synchrotron data showing the best R_{wp} (blue line) and mean R_{wp} (red line) for model B.

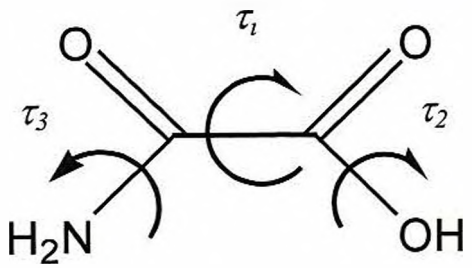

Figure 4.18: Model B used in the DE structure solution of oxamic acid. The arrows indicate the conformational flexibility allowed in this model.

The calculations using model A generated 4 structures (out of the 5 runs) in the *trans* conformation (all R_{wp} 17.26 %) and 1 in the *cis* conformation (with R_{wp} 17.32 %). In contradiction to these results, the calculations using model B (including the hydrogen atoms) all gave rise to structures in the *cis* conformation, all having the same R_{wp} 16.34 %. All three DE solutions (model A: *trans* configuration, model A: *cis* configuration, model B: *cis* configuration) showed molecules in positions to form chains extending along the *b* axis with only the *trans* model forming intermolecular hydrogen bonds. Given the variation in these structures, 3 independent Rietveld refinements were carried out using the 3 different starting structures.

In all cases the parameters varied were atomic positions with soft constraints (weighting factor 0.001 for intermolecular bond distances and angles), lattice parameters, zero point and isotropic thermal parameters (for non H atoms only and constrained according to atom type). All refinements also required variation of asymmetry peak shape parameters. Final agreement factors for these refinements are given in table 4.8 and the final Rietveld profile plots for all three models are shown in figure 4.19.

Structure solution

LeBail R_{wp} / %	15.94
LeBail R_p / %	10.34
LeBail χ^2	2.789

	Model A (excluding hydrogens)	Model B (including hydrogens)
DE elements	7	9
K	0.99	0.99
F	0.5	0.5
Population size	70	70
No. of generations	1000	1000
No. of epochs	5	5
Average trial R_{wp} / %	29.94	28.30
Best R_{wp} / %	17.26	16.34

Refinement

	Model A - *trans*	Model A - *cis*	Model B - *cis*
R_{wp} / %	16.46	16.81	16.46
R_p / %	10.62	10.79	10.58
χ^2	3.424	3.431	3.411
Final a / Å	9.4689(3)	9.4689(3)	9.4689(3)
Final b / Å	5.4316(1)	5.4316(1)	5.4316(1)
Final c / Å	6.8517(2)	6.8517(2)	6.8517(2)
Final α / °	90	90	90
Final β / °	107.084(1)	107.084(1)	107.084(1)
Final γ / °	90	90	90
Final V / Å^3	336.849(4)	336.849(4)	336.849(4)

Table 4.8: DE structure solution parameters, final refined parameters and agreement factors for oxamic acid from synchrotron powder diffraction data.

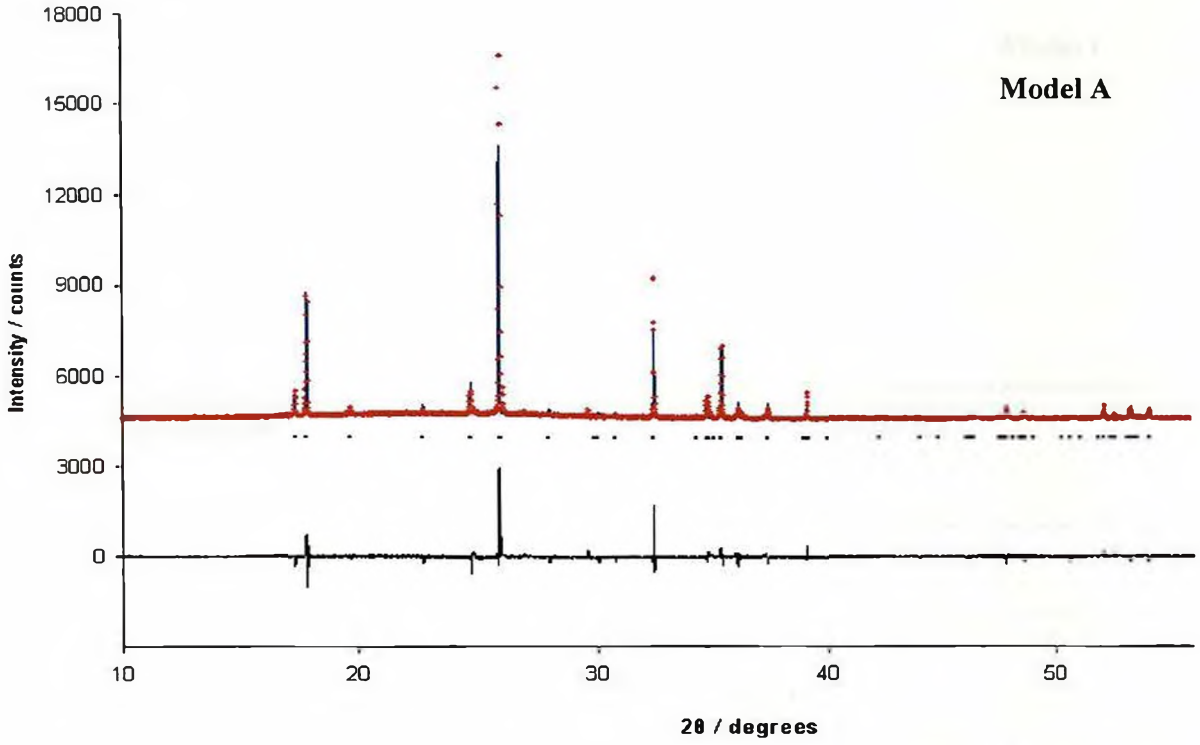
Model A
18000
15000
12000
9000
6000
3000
0
Intensity / counts
10
20
30
40
50
2θ / degrees

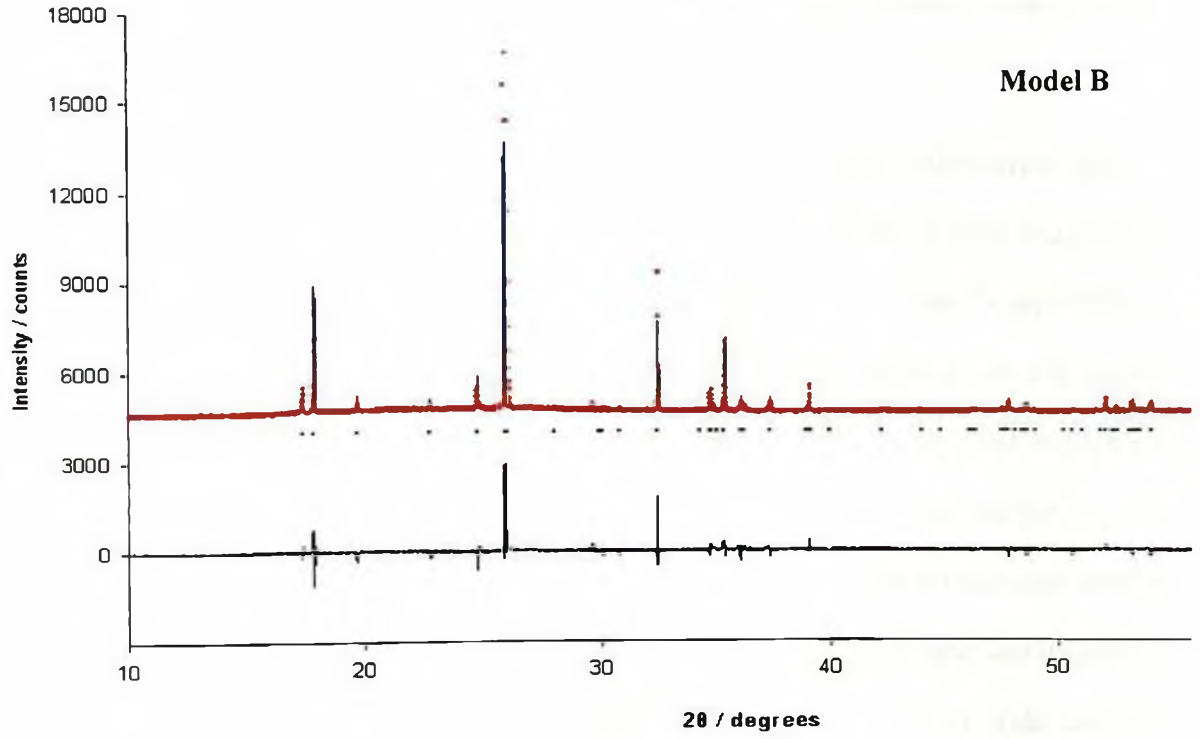
Model B
18000
15000
12000
9000
6000
3000
0
Intensity / counts
10
20
30
40
50
2θ / degrees

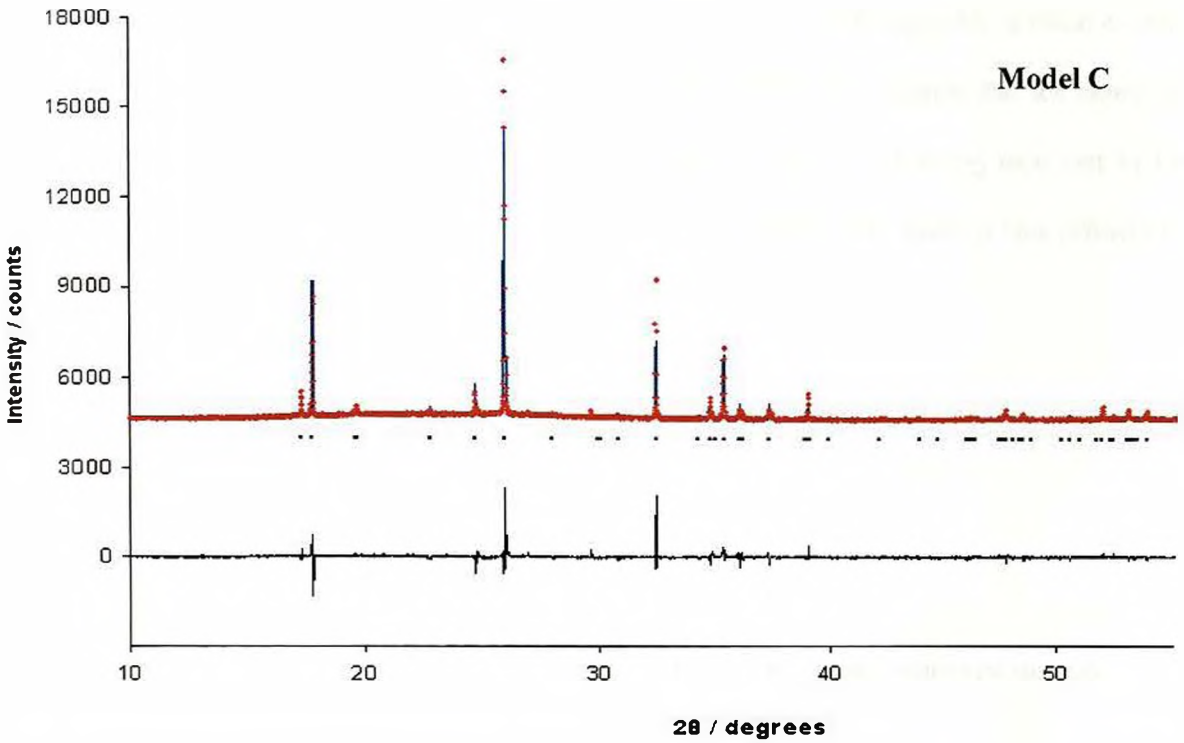

Figure 4.19: Final observed (red), calculated (blue) and difference (below) powder diffraction profiles for the Rietveld refinements of oxamic acid from synchrotron diffraction data, a) model A *trans*, b) model A *cis*, c) model B *cis*. Reflection positions are also shown.

4.2.4.1 Analysis of crystal structures from synchrotron powder diffraction data

Refinement of model A (*trans* configuration, final R_{wp} = 16.46 %) resulted in a hydrogen bonded structure identical to that obtained from the laboratory powder X-ray diffraction data although there is clearly a deficiency in the fit between this structure and the data. Refinement of model A (*cis* configuration, final R_{wp} = 16.81 %) resulted in a packing arrangement similar to the single crystal X-ray structure, (with no feasible hydrogen bonds evident along the b-axis). However, examination of the soft constraint data (see table 4.9) showed that the refinement was 'trying' to lengthen the carbon-carbonyl oxygen (O_6) bond and shorten the carbon-amide nitrogen (N_5) bond. This can be an indication that the molecule has either been restrained incorrectly or that the atom

environments have been miss-assigned [Tremayne. MJ. et al. 1997] (although this is often evident only from high quality synchrotron data). Here, this behaviour implies that the atoms O_6 and N_5 have been assigned incorrectly and that the molecule is trying to revert to the *trans* conformation. Table 4.9 illustrates the soft constraint data used in this refinement and figure 4.20 defines the labelling scheme.

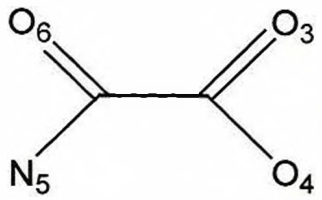

Figure 4.20: Labelling scheme used to define the soft constraint data for the oxamic acid molecule.

Bond	Interatomic distance (initial constraint)	Interatomic distance (after refinement)
$C_1 - C_2$	1.50	1.50
$C_1 - O_6$	1.23	1.33
$C_1 - N_5$	1.33	1.27
$C_2 - O_3$	1.21	1.21
$C_2 - O_4$	1.30	1.34

Table 4.9: Soft constraint data for the refinement of the model A (*cis*) structure highlighting the atoms that may have been assigned incorrectly.

From this, we can assume that this model is actually similar to the model A *trans* configuration and that the *cis* configuration of model A is not a viable structure solution.

Refinement of model B *cis* conformation showed a profile fit of the same quality to those obtained from the model A refinements, despite the presence of the additional 3 hydrogen atoms. The structure is identical to that found from the single crystal data.

4.2.5 Crystal structure prediction of oxamic acid

The weak X-ray scattering of the hydrogen atoms and the similar scattering power of oxygen and nitrogen severely hinders the crystal structure determination of this material from powder X-ray diffraction data (i.e. one could effectively interchange the hydroxyl and carbonyl oxygens as well as the nitrogen atom around the carbon centre). Differentiating between the oxamic acid conformations appears to be very complicated and problematic. Hence, additional methods need to be employed in order to identify the correct structural arrangement of this molecule.

To further explore which of the two possible conformations may be most favorable within the crystalline state, crystal structure prediction studies were carried out using the Forcite module within the Materials Studio software environment. The molecular structure of oxamic acid was constructed in the *cis* conformation and the desired empirical forcefield and atomistic charges assigned. The optimised molecular structure was then used in a polymorph prediction sequence in space group Cc (9). All the resulting crystal structures were in the *cis* conformation and on visual inspection some reasonable crystal structures with sensible hydrogen bonding networks were present, although none appeared comparable to the single crystal solution. Although the

prediction calculations were set up to enable rotation around the C-C bond (i.e. allowing generation of structures in the *trans* conformation) it became apparent that electron charge delocalisation of the two highly acidic oxygen carbonyl groups were essentially restricting rotation of this bond during the final geometry optimisation stage and preventing consideration of the *trans* conformation in the prediction calculation. Figure 4.21 diagrammatically illustrates the delocalisation effect in oxamic acid.

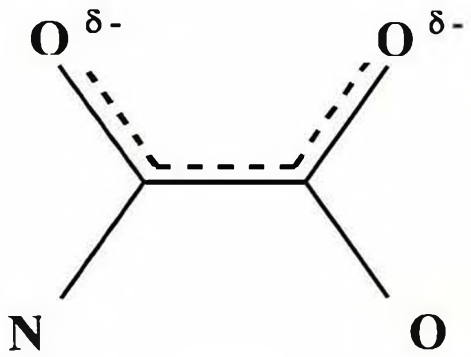

Figure 4.21. Delocalisation of oxamic acid preventing rotation of the molecular conformation.

Hence, a second polymorph prediction sequence was performed using the optimised *trans* conformation as a starting model. This resulted in a set of predicted crystal structures with the *trans* conformation. Which in terms of 'direct space' crystal packing all showed hydrogen bonding arrangements comparable to the experimental structure obtained from laboratory powder X-ray diffraction data. Table 4.13 shows the lattice energy values for the predicted structures. These values clearly demonstrate that the crystal structures formed by the *trans* conformation are relatively more stable then those formed by the *cis* conformation. Figure 4.22 shows the simulated X-ray powder diffraction patterns for the best 3 predicted trans structures compared to the experimental data.

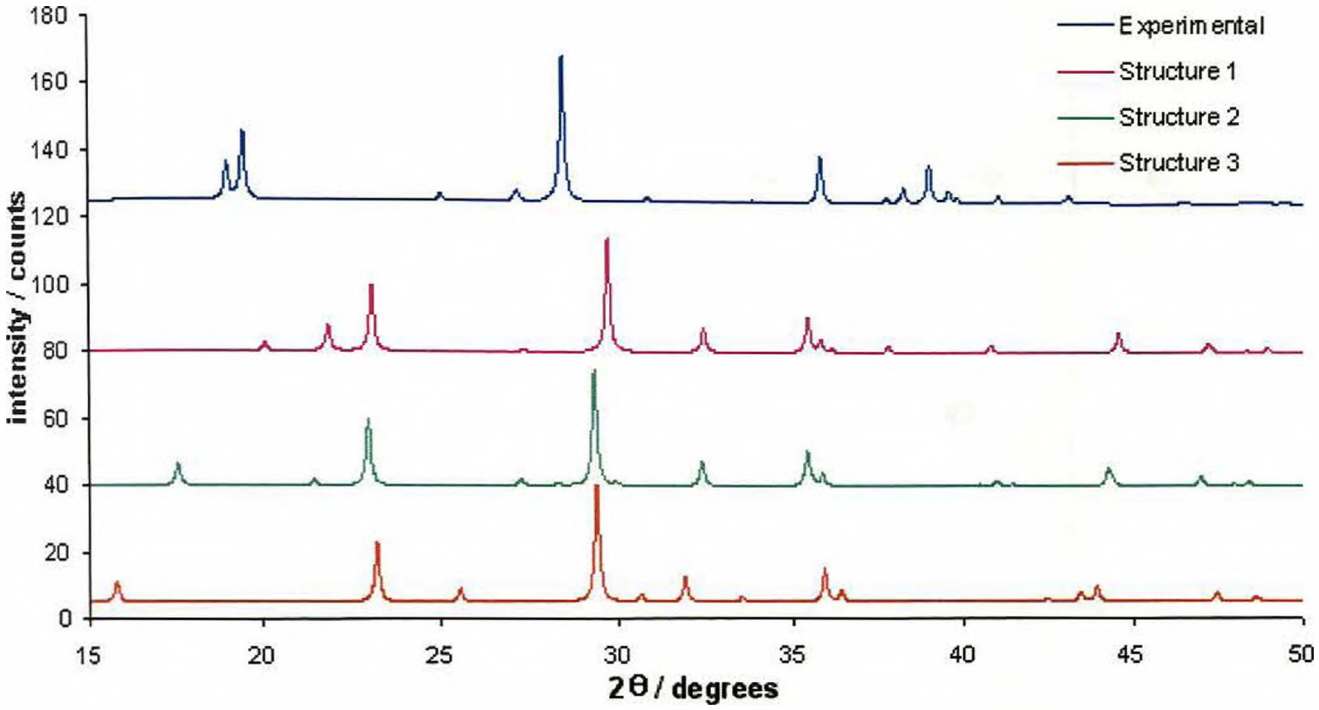

Figure 4.22: Comparison of the experimental powder X-ray diffraction pattern of oxamic acid with the simulated X-ray powder diffraction pattern of *trans* oxamic acid models 1, 2 and 3.

Model 1 contains hydrogen bonded $R_2^2(8)$ dimers, which combine to form infinite hydrogen bonded chains propagating along the [10-1] direction. As in the experimental *trans* structure the hydroxyl oxygen acts as both a donor and acceptor atom generating an infinite sheet in the (101) plane containing alternating rows of $R_2^2(8)$ and $R_4^4(14)$ motifs. Figure 4.23 (a and b) shows the crystal packing for model 1 as described.

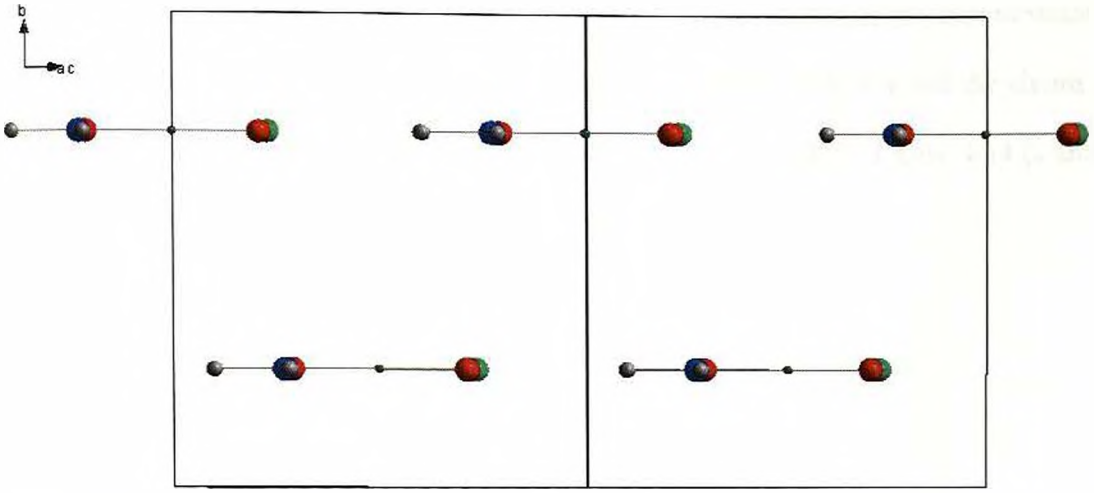

Figure 4.23(a): Predicted (model 1) crystal structure of oxamic acid showing the chains along the [10-1] direction.

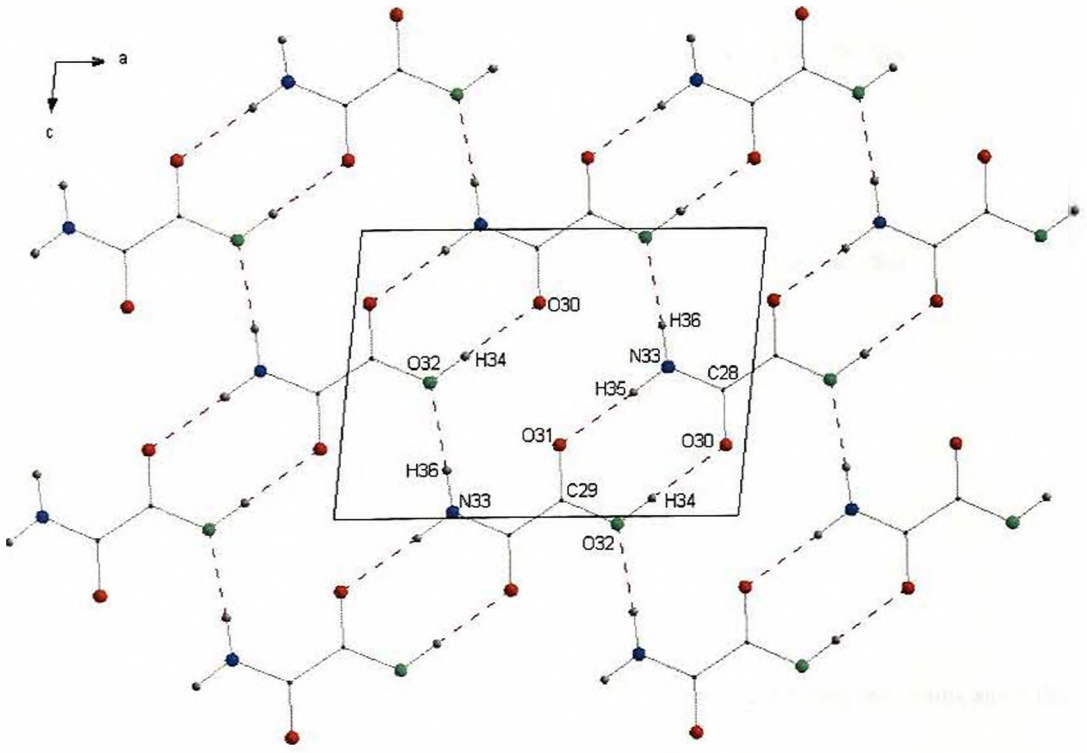

Figure 4.23(b): Predicted (model 1) crystal structure of oxamic acid showing the full hydrogen bonding network.

Model 2 shows a hydrogen bonding scheme also analogous to that of the experimental X-ray powder structure, except the unit cell is doubled along the *b* axis and the chains are generated in the [100] direction, with the sheets in the (101) plane. Figure 4.24 (a and b) shows the crystal packing for model 2 as described.

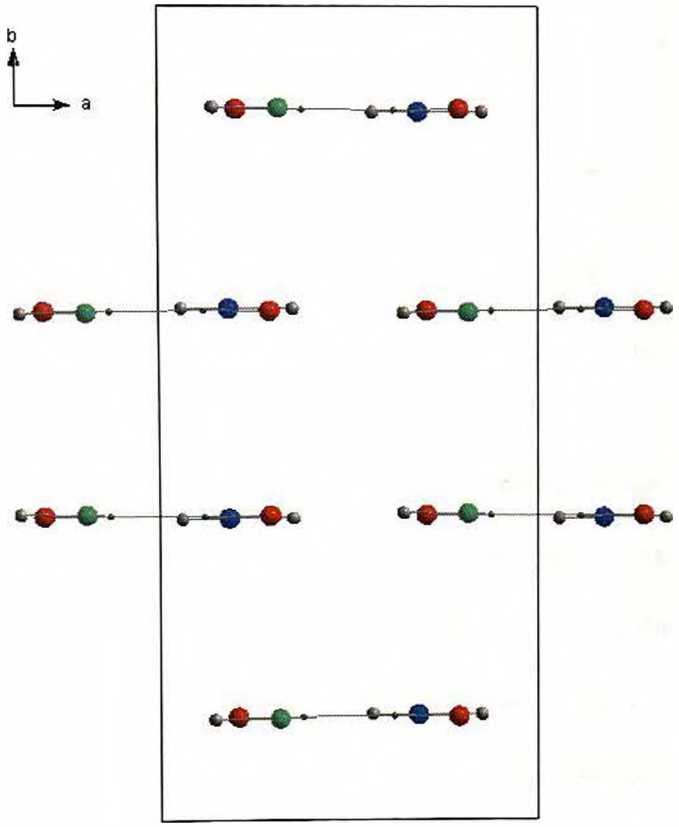

Figure 4.24(a): Predicted (model 2) crystal structure of oxamic acid showing the chains along the [100] direction.

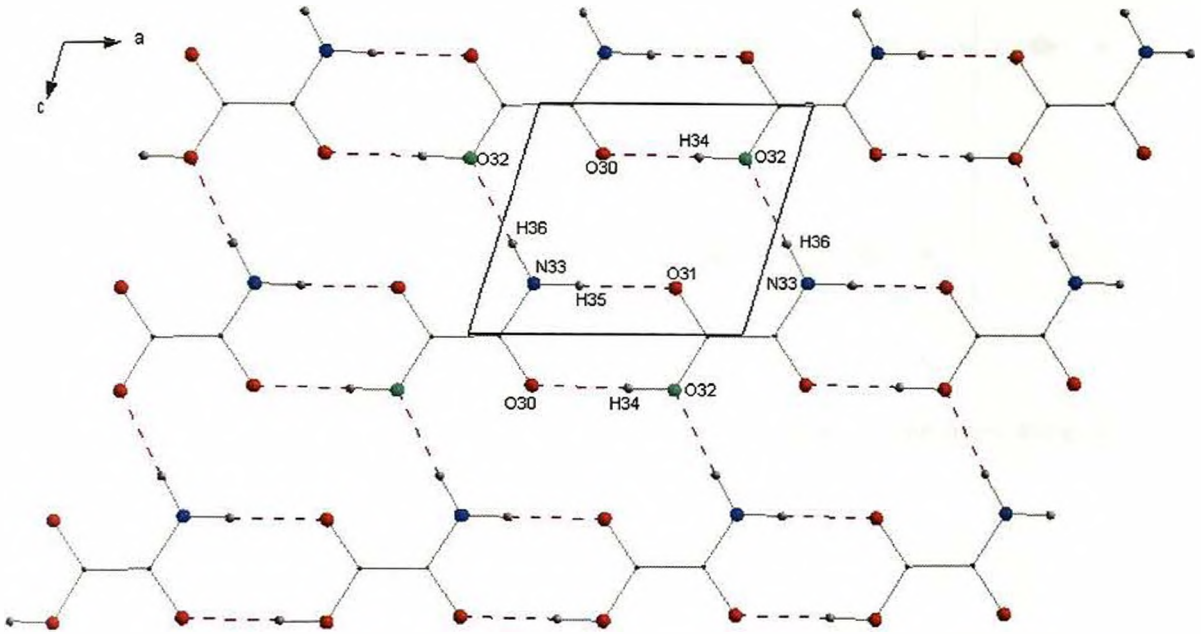

Figure 4.24(b): Predicted (model 2) crystal structure of oxamic acid showing the full hydrogen bonding network.

Model 3 shows an alternative hydrogen bonding arrangement in which the third hydrogen bond interacts with the carbonyl oxygen (rather then the hydroxyl oxygen) generating a network of $R_2^2(8)$ and $R_4^3(14)$ motifs where chains run in the [101] direction and infinite hydrogen bonded sheets are generated along the (101) plane. Figures 4.25 and 4.26 shows the crystal packing for model 3 as described. Details of the hydrogen bonding geometry of the 3 theoretical models are given in tables 4.10, 4.11 and 4.12.

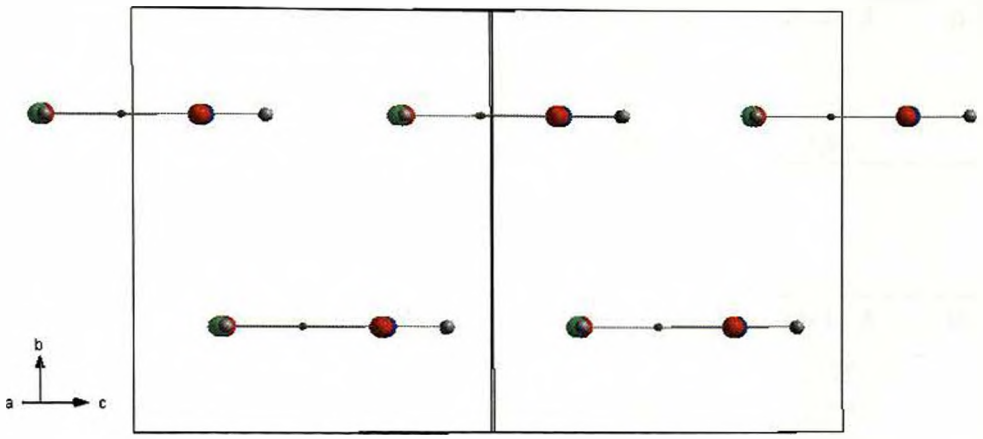

Figure 4.25: Predicted (model 3) crystal structure of oxamic acid showing the chains along the [101] direction.

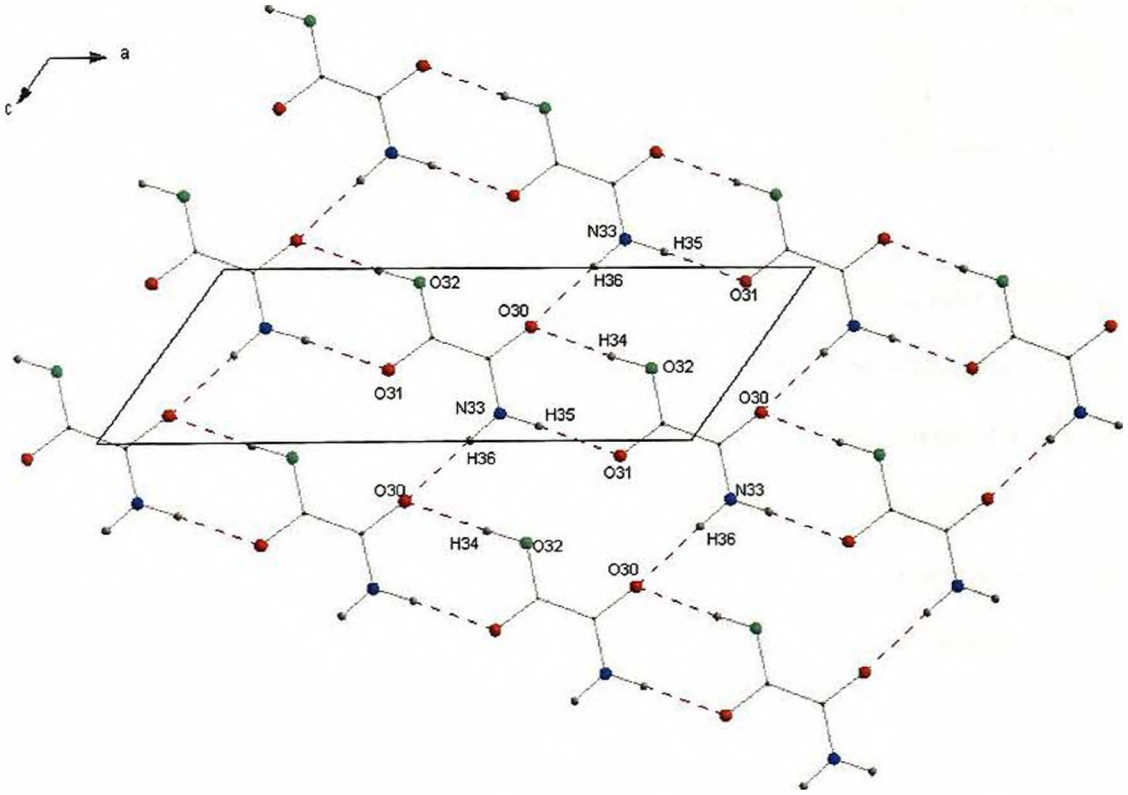

Figure 4.26: Predicted (model 3) crystal structure of oxamic acid showing the third hydrogen bonding with the carbonyl oxygen.

H···*A*	*D*-H···*A*	Symmetry code of *A*	H···*A* / Å	*D*-*A* / Å	D-H···*A* / °
$H_{34}\cdots O_{30}$	O_{32}-$H_{34}\cdots O_{30}$	*-0.5+x, 1.5 -y, 0.5+z*	2.02	2.99	179
$H_{35}\cdots O_{31}$	N_{33}-$H_{35}\cdots O_{31}$	*-0.5+x, 1.5 -y, 0.5+z*	2.02	2.98	179
$H_{36}\cdots O_{32}$	N_{33}-$H_{36}\cdots O_{32}$	*-0.5+x, 1.5 -y, -0.5+z*	2.03	2.99	177

Table 4.10: Hydrogen bonding geometry of model 1.

H···*A*	*D*-H···*A*	Symmetry code of *A*	H···*A* / Å	*D*-*A* / Å	D-H···*A* / °
$H_{35}\cdots O_{31}$	N_{33}-$H_{35}\cdots O_{31}$	*1+x, y, z*	2.02	2.98	178
$H_{36}\cdots O_{32}$	N_{33}-$H_{36}\cdots O_{32}$	*x, y, -1+z*	2.03	2.99	177
$H_{34}\cdots O_{30}$	O_{32}-$H_{34}\cdots O_{30}$	*-1+x, y, z*	2.02	2.99	178

Table 4.11: Hydrogen bonding geometry of model 2.

H···*A*	*D*-H···*A*	Symmetry code of *A*	H···*A* / Å	*D*-*A* / Å	D-H···*A* / °
$H_{36}\cdots O_{30}$	N_{33}-$H_{36}\cdots O_{30}$	*x,-y, 1+z*	2.07	3.03	178
$H_{35}\cdots O_{31}$	N_{33}-$H_{35}\cdots O_{31}$	*0.5+x, 1.5 -y, 0.5+z*	2.03	2.99	178
$H_{34}\cdots O_{30}$	O_{30}-$H_{34}\cdots O_{32}$	*-0.5+x, 1.5 -y, -0.5+z*	2.03	2.99	177

Table 4.12: Hydrogen bonding geometry of model 3.

Certainly all aspects explored in the structure determination of oxamic acid informs us that the most likely conformation to be adopted by oxamic acid is the trans structure. The value for model 3 (*trans*) which hydrogen bonds using the alternative interaction with the carbonyl oxygen is also shown here to be less favourable with an energy of 1.36 kcalmol^{-1} this further reinforcing what we have suspected, that the second amide hydrogen interacts with the hydroxyl oxygen rather then the carbonyl oxygen to give rise to the planes of oxamic acid molecules.

Polymorph	Volume ($Å^3$)	Lattice energy ($Kcalmol^{-1}$)	a (Å)	b (Å)	c (Å)	β (°)
1	347.85	0.90	8.88	6.01	6.55	95.73
2	351.54	1.18	5.77	12.17	5.23	106.95
3	346.33	1.36	13.72	6.07	5.09	125.19
4	345.30	1.46	5.78	7.66	8.22	108.33
5	356.74	1.52	5.22	6.18	13.95	127.53
6	360.73	1.56	5.21	12.48	8.79	140.90
7	348.50	1.64	5.78	12.21	5.08	103.65
8	350.15	1.77	17.30	7.01	9.05	161.41
9	364.10	1.80	3.74	10.93	8.93	93.90
10	364.79	1.83	8.76	12.63	5.77	145.16
11	346.90	1.87	6.77	6.26	8.26	97.91
12	352.34	1.92	6.59	6.94	18.21	155.00
13	357.66	2.01	6.72	12.53	10.42	155.92
14	362.64	2.08	3.89	10.84	9.63	63.29
15	368.08	2.11	6.34	11.19	5.18	90.00
16	346.39	2.11	5.78	16.11	5.31	135.56
17	347.67	2.19	7.89	15.34	5.13	145.97
18	360.50	2.30	5.09	12.62	6.75	123.60
19	347.95	2.59	5.10	19.72	13.46	165.10
20	367.77	2.66	6.30	8.36	8.90	128.24

Polymorph	Volume ($Å^3$)	Lattice energy ($Kcalmol^{-1}$)	a (Å)	b (Å)	c (Å)	β (°)
1	350.91	2.18	4.54	9.22	11.51	133.24
2	347.52	2.28	4.19	9.11	9.55	107.63
3	356.88	2.46	6.17	11.37	8.00	140.51
4	352.64	2.48	3.75	21.98	7.80	146.77
5	347.05	2.48	5.18	11.50	11.88	150.62
6	354.96	2.61	6.48	6.86	12.77	141.35
7	342.68	3.02	8.90	9.12	4.60	66.46
8	372.27	3.13	3.99	9.54	10.32	108.53
9	355.45	3.29	5.17	11.49	5.98	90.00
10	362.94	3.29	6.34	11.26	8.13	141.23
11	358.73	3.39	4.01	20.71	8.02	147.40
12	358.16	3.44	8.87	21.70	4.49	155.52
13	339.01	3.44	5.17	6.42	10.94	68.79
14	341.67	3.45	5.13	6.48	13.34	50.38
15	366.76	3.52	15.57	6.18	5.18	132.54
16	366.72	3.67	5.11	10.33	7.75	116.36
17	339.92	3.68	5.15	20.39	4.10	52.08
18	345.41	3.71	3.64	21.96	5.10	57.73
19	351.99	3.72	11.64	4.38	16.13	154.68
20	370.19	3.73	9.62	12.46	5.17	143.37

Table 4.13: Lattice energies and unit cell parameters for the predicted a) *trans* and b) *cis* conformations of oxamic acid.

4.2.6 Discussion

A combined use of laboratory powder X-ray and powder synchrotron diffraction has been used to elucidate the crystal structure of oxamic acid, investigated in detail the two different molecular conformations that oxamic acid can adopt.

Single crystal data had been recorded on a previous occasion however, the poor quality of the crystals reflected in the single crystal X-ray diffraction data and led to an unreliable structure with a high R-factor. All the oxamic acid molecules adopted the *cis* conformation and lined up in a regular fashion in the [010] direction, but their conformation made it impossible for hydrogen bonding to take place.

Structure solution using DE from powder X-ray diffraction data gave rise to 5 structures, all of which showed preference for the *trans* conformation. In each case convergence was achieved between R_{wp}= 9.6% and 9.74%. The solutions obtained all exhibited infinite hydrogen bonded chains running along the [010] direction through the formation of N-H...O=C and O-H...O=C type $R_2^2(8)$ dimers. In order to improve the structure solution process a synchrotron powder diffraction dataset was recorded and used to initiate two separate structure solutions, excluding and including hydrogen atoms. The DE calculation was run 5 times for each of the two models giving rise to 4 *trans* and 1 *cis* conformation for model A. Refinement of model A (*cis* configuration, final R_{wp} = 16.81%) resulted in a packing arrangement similar to the single crystal X-ray structure. However, examination of the soft constraint data showed that the refinement was trying to revert to the *trans* conformation. All 5 solutions for model B were in the *cis* conformation and as a result formed crystal structures that contained no hydrogen bonding.

Crystal structure prediction was attempted on the *cis* and *trans* conformation using Polymorph Predictor. The cis molecular arrangement resulted in all structures being predicted in the *cis* conformation, none of which were comparable to the powder X-ray structure. Prediction using the *trans* molecular arrangement resulted in structures adopting the *trans* conformation show hydrogen bonding trends comparable to the powder X-ray structure, although the position and orientation of the molecules in the unit cell were evidently different.

Although there is considerable data pointing to the *trans* conformation as being the most likely adopted by oxamic acid a neutron dataset was recorded, which should finally conclude the correct conformation for the oxamic acid molecules. However, the dataset has not been analysed due to time restrictions but it is envisaged that the data will be analysed through structure solution and a structure refinement.

5.0 Crystal structure prediction

A computational strategy that can automatically examine the traditional theoretical polymorph prediction output and re-rank structurally favourable crystal structures has been developed. This re-ranking strategy uses expected hydrogen bonding geometry and graph set assignment to rationalise the predicted crystal structures, effectively eliminating the need to visually inspect every structure from the prediction output, thus reducing the time spent on evaluating the structural features of the predicted structures.

The structures of eleven molecular materials, all containing the amide functional group as the only strong hydrogen bonding donor and acceptor atoms were selected from the Cambridge Crystallographic Database [Allen, F. A. and Kennard, O. 1993] and used as test cases for the development of the re-ranking prediction strategy. The selected structures form two amide families; benzamide (I) and its ortho (II), meta (III), para (IV) methyl derivatives, and oxamide (V) and its aliphatic C_5 (VI), C_6 (VII), C_7 (VIII), C_8 (IX), C_9 (X) and C_{10} (XI) derivatives (see figure 5.1.1). The C_3 derivative was not used as a test case due to it being Z' = 2, the C_5 structure was not present in the Cambridge Crystallographic Database, however it is available from Aldrich, CAS [110-14-5].

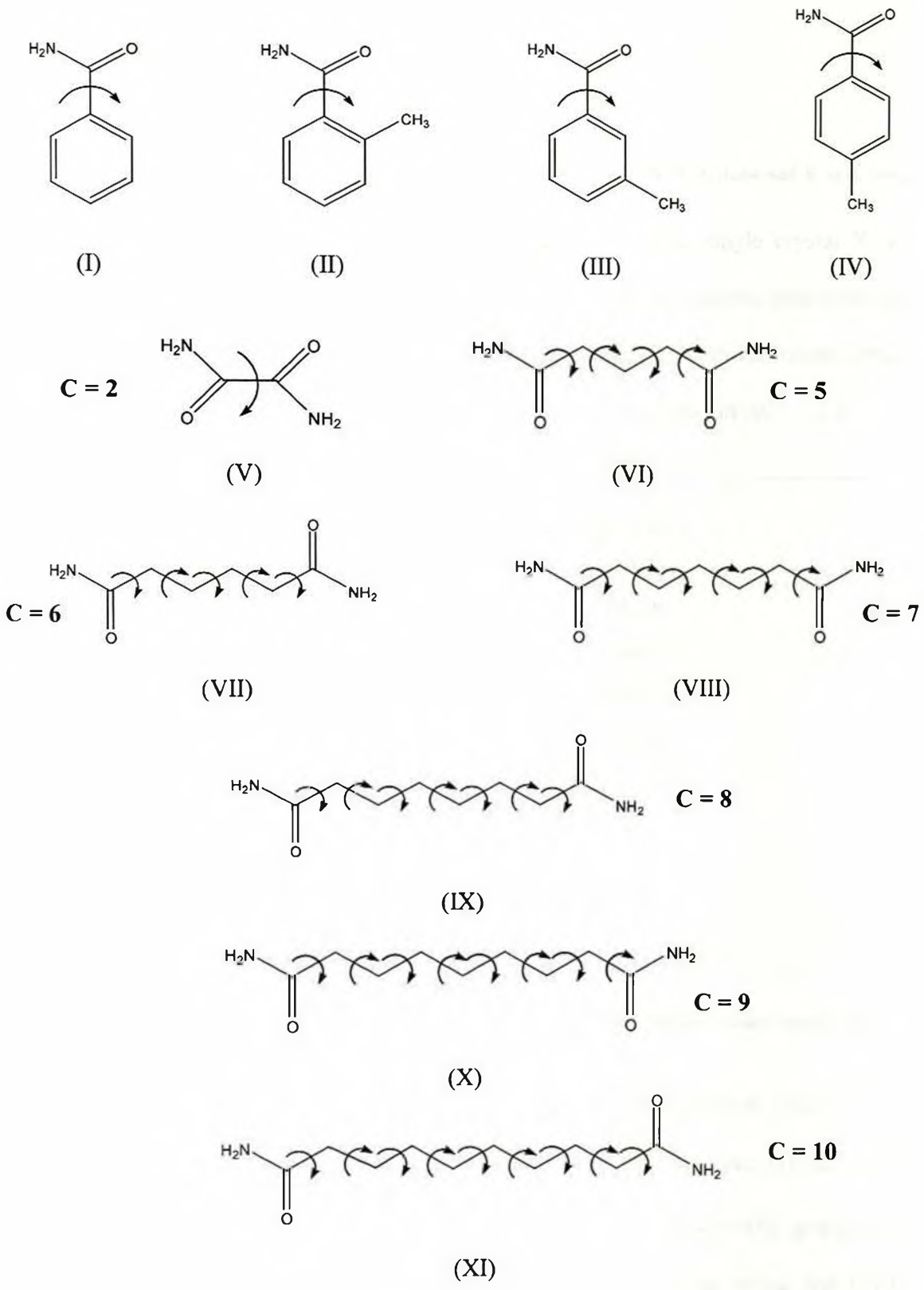

Figure 5.1.1: Molecular structures selected from the Cambridge Structural Database for the development of the re-ranking strategy.

5.1 Benzamide

5.1.1 Experimental crystal structure

The crystal structure of benzamide (I) [Penfold. B. R., White. J. C. B. 1959] [Kobayashi. K. et al. 2003] [David. W. I. F. et al. 2005] has been determined using conventional single crystal X-ray diffraction data, although the hydrogen atoms were placed in idealised positions and not refined. The unit cell parameters, space group and single point minimised lattice energy of the experimentally determined crystal structure are given in table 5.1.1.

a (Å)	5.607(2)
b (Å)	5.046(2)
c (Å)	22.053(8)
β (°)	90.66(3)
Volume ($Å^3$)	623.902(2)
Density (gcm^{-3})	1.289(1)
Space group	$P2_1/c$ (14)
Z	4
Single point minimised lattice energy ($kcalmol^{-1}$)	-6.00

Table 5.1.1: The crystallographic and lattice energy data for experimentally determined benzamide.

This structure displays a three dimensional hydrogen bonding network (figure 5.1.2, 5.1.3 & 5.1.4) consisting of cyclic $R_2^2(8)$ dimers linked by C(4) chains (both motifs being of type N-H...O=C). Combination of these two structural motifs generates a secondary network of $R_4^2(8)$ rings that form ladders extending along the [010] direction. Pairs of ladders are related by an edge to face double herringbone structure.

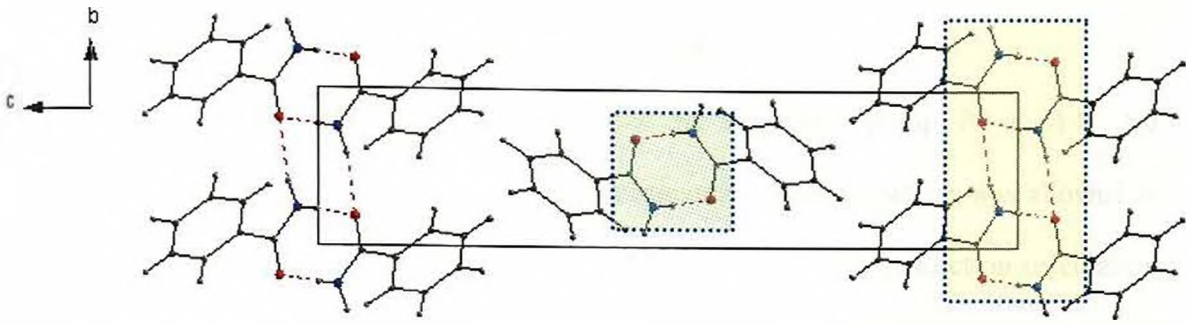

Figure 5.1.2: View of benzamide (I) showing the ladders running along the *b* axis (yellow shaded area). Hydrogen bonds are illustrated using purple dashed lines. The $R_2^2(8)$ motif is illustrated using green shading.

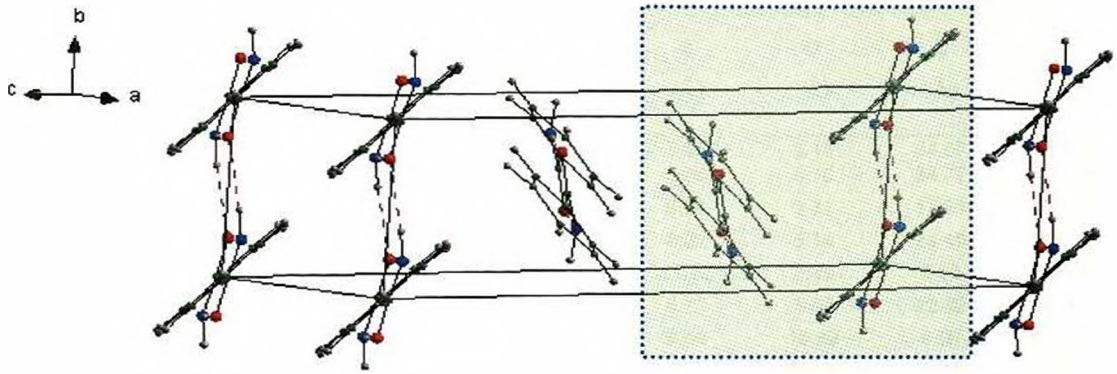

Figure 5.1.3: Illustrates the edge to face orientation of the ladders as indicated by the green shading.

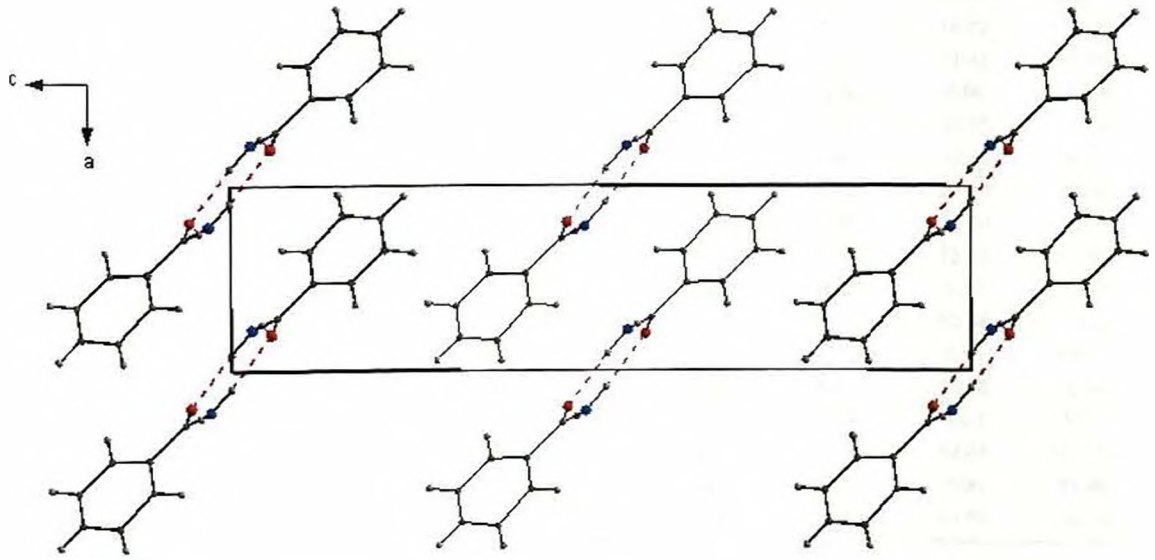

Figure 5.1.4: End-on view of hydrogen bonded sheets in benzamide (I).

5.1.2 Structure prediction analysis - Benzamide

Crystal structure prediction was performed in the space group $P2_1/c$ (14). No geometric restraints were placed upon the molecular structure, which was allowed to rotate through all degrees of freedom (as in figure 5.1.1). The prediction calculation generated 250 theoretical crystal structures, ranging in energy from –6.64 to 3.23 $kcalmol^{-1}$. Table 5.1.2 shows the top 30 predicted structures and their corresponding unit cell parameters.

No.	Volume ($Å^3$)	Density (gcm^{-3})	Lattice energy ($kcalmol^{-1}$)	a (Å)	b (Å)	c (Å)	β (°)
1	615.82	1.31	-6.64	5.09	5.13	24.67	72.87
2	616.97	1.30	-6.59	5.26	5.10	24.77	111.75
3	637.39	1.26	-6.35	8.08	9.31	17.61	151.24
4	623.10	1.29	-6.32	8.32	5.14	24.45	143.38
5	642.38	1.25	-6.10	21.22	7.36	9.55	154.49
6	631.84	1.27	-5.91	5.12	5.49	22.62	96.02
7	646.36	1.24	-5.83	9.59	15.59	8.06	147.57
8	639.01	1.26	-5.82	7.16	24.74	5.07	134.61
9	619.26	1.30	-5.82	9.53	6.27	15.75	138.85
10	635.63	1.27	-5.78	5.48	5.10	25.18	115.57
11	649.34	1.24	-5.76	9.57	15.59	8.09	147.48
12	637.91	1.26	-5.69	13.46	6.77	9.46	132.29
13	643.27	1.25	-5.58	7.31	5.14	17.40	100.26
14	615.77	1.31	-5.57	29.08	3.85	27.25	168.37
15	620.91	1.30	-5.56	8.40	5.11	14.70	79.88
16	646.34	1.24	-5.55	10.99	5.12	11.49	89.15
17	637.26	1.26	-5.54	5.16	19.43	6.96	113.98
18	642.63	1.25	-5.52	7.47	17.31	10.13	150.60
19	629.93	1.28	-5.50	7.70	6.63	19.22	140.07
20	624.20	1.29	-5.48	26.70	3.73	27.79	166.96
21	622.04	1.29	-5.40	29.87	5.96	28.39	172.93
22	652.08	1.23	-5.39	9.27	5.12	13.78	85.67
23	641.04	1.26	-5.38	6.80	25.38	5.10	133.28
24	644.85	1.25	-5.36	31.41	5.20	32.48	173.02
25	666.35	1.21	-5.34	13.23	5.36	9.55	100.37
26	637.59	1.26	-5.34	5.08	4.84	26.78	75.44
27	652.17	1.23	-5.33	15.79	7.04	9.03	139.49
28	656.12	1.23	-5.28	16.65	9.11	14.62	162.79
29	660.37	1.22	-5.28	5.01	26.05	5.06	91.46
30	631.27	1.27	-5.27	3.74	6.23	33.59	126.34

Table 5.1.2: Top 30 predicted structures for benzamide (I).

5.1.3 Re-ranking of structure prediction results - Benzamide

Ranked according to lattice energy ($kcalmol^{-1}$)		Ranked according to Hbonding merit points		Ranked according to graphset merit points	
1	**-6.64**	**1**	**40.00**	**1**	**2**
2	**-6.59**	**2**	**40.00**	**2**	**2**
3	-6.35	3	40.00	3	2
4	-6.32	4	40.00	4	2
5	-6.10	5	40.00	5	2
6	-5.91	6	40.00	6	2
7	-5.83	7	40.00	7	2
8	-5.82	8	40.00	8	2
9	**-5.82**	10	40.00	10	2
10	-5.78	11	40.00	11	2
11	-5.76	12	40.00	**13**	**2**
12	-5.69	**13**	**40.00**	16	2
13	**-5.58**	16	40.00	18	2
14	-5.57	17	40.00	23	2
15	-5.56	18	40.00	25	2
16	-5.55	22	40.00	28	2
17	-5.54	23	40.00	29	2
18	-5.52	24	40.00	**9**	**1**
19	-5.50	25	40.00	12	1
20	-5.48	26	40.00	15	1
21	-5.40	27	40.00	17	1
22	-5.39	28	40.00	19	1
23	-5.38	29	40.00	20	1
24	-5.36	15	38.89	22	1
25	-5.34	19	34.25	24	1
26	-5.34	**9**	**33.85**	26	1
27	-5.33	20	32.08	27	1
28	-5.28	30	30.34	30	1
29	-5.28	14	20.00	14	0
30	-5.27	21	20.00	21	0

Table 5.1.3: Top 30 predicted structures for benzamide (I) re-ranked according to hydrogen bonding and graph set merit points. Highlighted structures show similarity to experimental structure.

The re-ranking procedure (table 5.1.3) shows that a total of 23 predicted structures have the expected maximum 40 hydrogen bonding merit points and 17 structures have 2 graph set merit points highlighting the presence of the characteristic structural motifs expected in amide crystal structures. All theoretical structures with maximum merit points were examined further. However, only structures 1, 2, 9 and 13 are discussed in more detail (highlighted) either due to their similarity to the experimentally determined structure or due to their behaviour in the re-ranking process.

Benzamide structure 1 is clearly the most energetically favourable and has remained at the top of the re-ranking tables with maximum hydrogen bonding and graph set assignment points (see table 5.1.3), but structurally it is not comparable to the experimental crystal structure. Although the structure still contains dimers combining to form ladders, this network runs in the [100] direction (compared with the [010] direction in the experimental crystal structure). Although these ladders are stacked in a similar fashion to the experimental structure they form a herringbone type rather than a double herringbone structural arrangement (figures 5.1.5 and 5.1.6).

		D-H	H...A	D...A	D-H...A
1	N(56) --H(63) ..O(57)	0.9600	2.0500	2.9980	168.00
2	N(56) --H(64) ..O(57)	0.9700	2.1000	3.0444	164.00

1 N(56) --H(63) ..O(57): 2.05 merit = 10
2 N(56) --H(64) ..O(57): 2.10 merit = 10

1 N(56) --H(63) ..O(57): 168 merit = 10
2 N(56) --H(64) ..O(57): 164 merit = 10

TOTAL MERIT FOR POLYMORPH 1 = 40

Table 5.1.4: Hydrogen bonding merit points generated by the re-ranking strategy for benzamide structure 1.

Benzamide structure 2 is another structure whose relative position in the rankings has remained unchanged (see table 5.1.3). The packing arrangement within structure 2 is similar to the experimental crystal structure in that it contains $R_2^2(8)$ dimers. Combination of these two motifs form a secondary hydrogen bonding network of $R_4^4(8)$ rings which lead to the formation of ladders running in the [010] direction. However, the orientation of the dimers along the (101) plane is different compared with the experimental crystal structure (figure 5.1.7 and 5.1.8).

		D-H	H...A	D...A	D-H...A
1	N(56) --H(63) ..O(57)	0.9600	2.0500	2.9980	167.00
2	N(56) --H(64) ..O(57)	0.9700	2.1000	3.0433	164.00

1 N(56) --H(63) ..O(57): 2.05 merit = 10
2 N(56) --H(64) ..O(57): 2.10 merit = 10

1 N(56) --H(63) ..O(57): 167 merit = 10
2 N(56) --H(64) ..O(57): 164 merit = 10

TOTAL MERIT FOR POLYMORPH 2 = 40

Table 5.1.5: Hydrogen bonding merit points generated by the re-ranking strategy for benzamide structure 2.

Benzamide structure 9 has fallen a total of 17 places with respect to hydrogen bonding merit points and 9 places in terms of graph set merit points. Close examination of this structure reveals that it contains C(4) chains forming spirals along the [010] direction with additional N-H...N hydrogen bonds forming dimers (see table 5.1.6) which are not ideal. It is this hydrogen bonding arrangement and the absence of characteristic amide motifs that has resulted in this structure falling down the rankings (figures 5.1.9 and 5.1.10).

		D-H	H...A	D...A	D-H...A
1	N(56) --H(63) ..O(57)	0.9600	2.0300	2.9915	177.00
2	N(56) --H(64) ..N(56)	0.9600	2.4400	3.3226	153.00

1 N(56) --H(63) ..O(57): 2.03 merit = 10
2 N(56) --H(64) ..N(56): 2.44 merit = 4.24

1 N(56) --H(63) ..O(57): 177 merit = 10
2 N(56) --H(64) ..N(56): 153 merit = 9.61

TOTAL MERIT FOR POLYMORPH 9 = 33.85

Table 5.1.6: Hydrogen bonding merit points generated by the re-ranking strategy for benzamide structure 9.

Benzamide structure 13 appears to have the same three dimensional molecular arrangement as the experimental structure (i.e. maximum structural merit points – table 5.1.7), with $R_2^2(8)$ dimers which combine through C(4) chains to generate the secondary $R_4^4(8)$ ladder network in the [010] direction, chains extending in the (101) plane are also still evident. However, on closer inspection, it is clear that the aromatic rings are rotated by approximately 45° with respect to the dimers compared to that of the single crystal structure (figures 5.1.11, 5.1.12 and 5.1.13).

		D-H	H...A	D...A	D-H...A
1	N(56) --H(63) ..O(57)	0.9600	2.0600	3.0091	166.00
2	N(56) --H(64) ..O(57)	0.9700	2.0900	3.0362	165.00

1 N(56) --H(63) ..O(57): 2.06 merit = 10
2 N(56) --H(64) ..O(57): 2.09 merit = 10

1 N(56) --H(63) ..O(57): 166 merit = 10
2 N(56) --H(64) ..O(57): 165 merit = 10

TOTAL MERIT FOR POLYMORPH 13 = 40

Table 5.1.7: Hydrogen bonding merit points generated by the re-ranking strategy for benzamide structure 13.

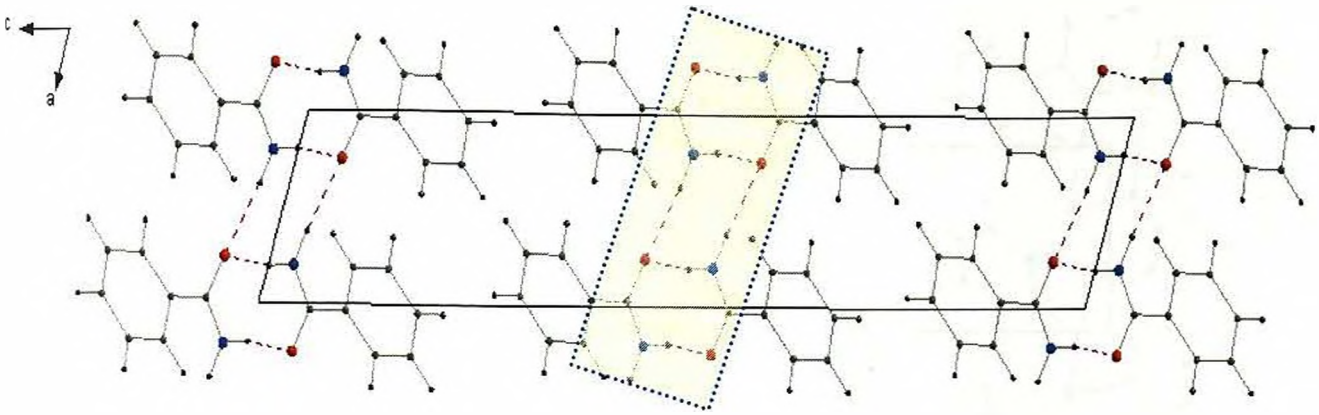

Figure 5.1.5: View of structure benzamide structure 1 showing the ladders running along the *b* axis (yellow shaded area).

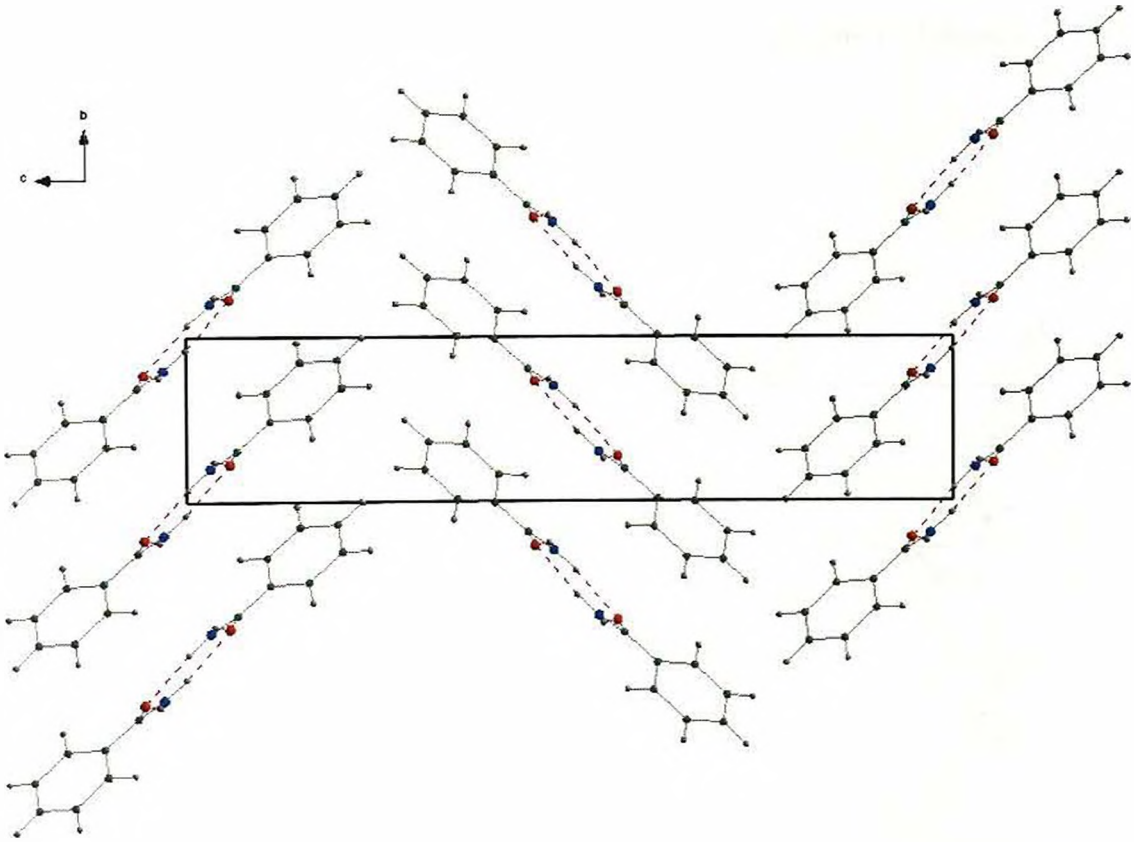

Figure 5.1.6: Herringbone type arrangement of benzamide structure 1.

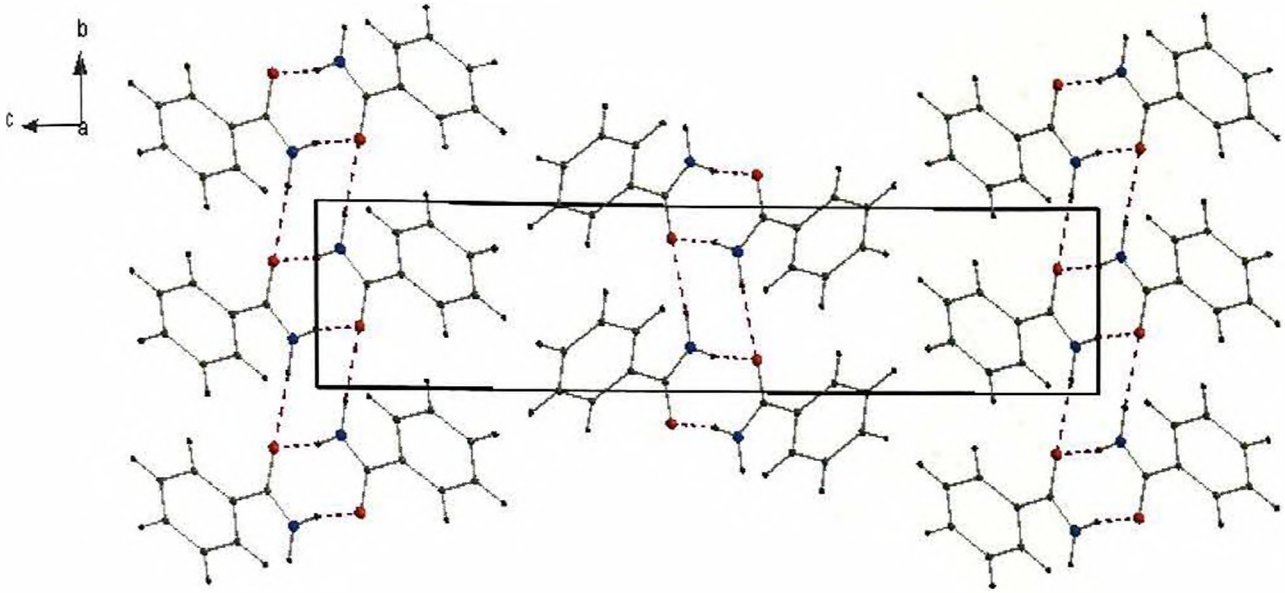

Figure 5.1.7: View of benzamide structure 2 showing ladders running along the [010] direction.

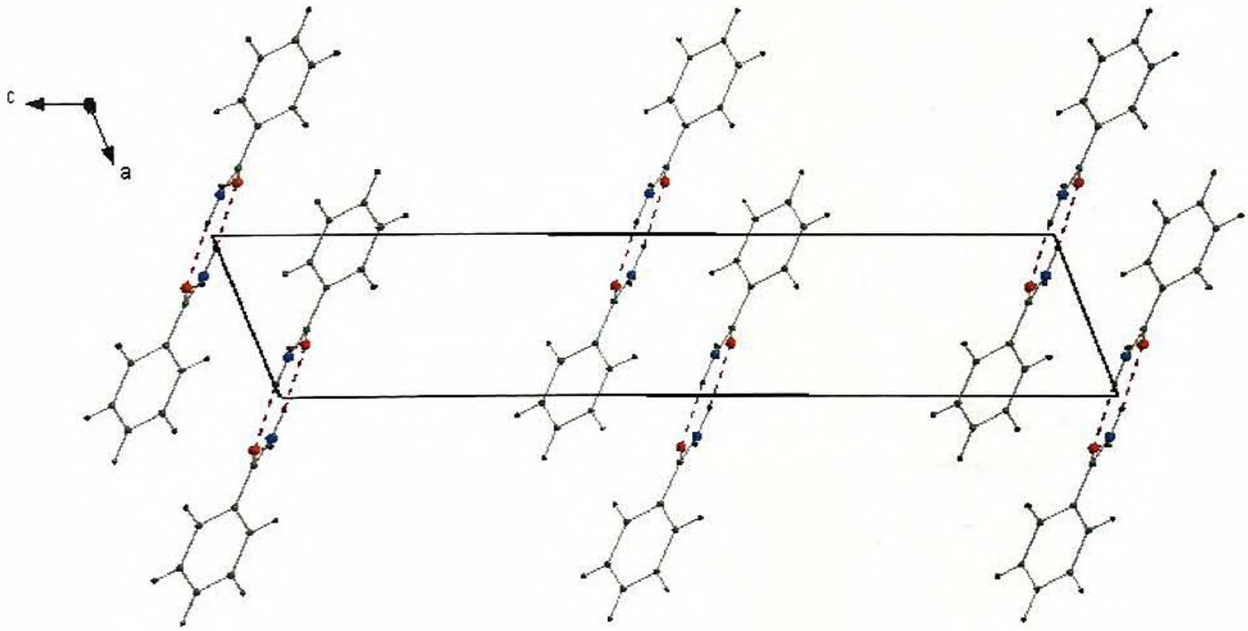

Figure 5.1.8: View of benzamide structure 2 showing the chains that run along the (101) plane.

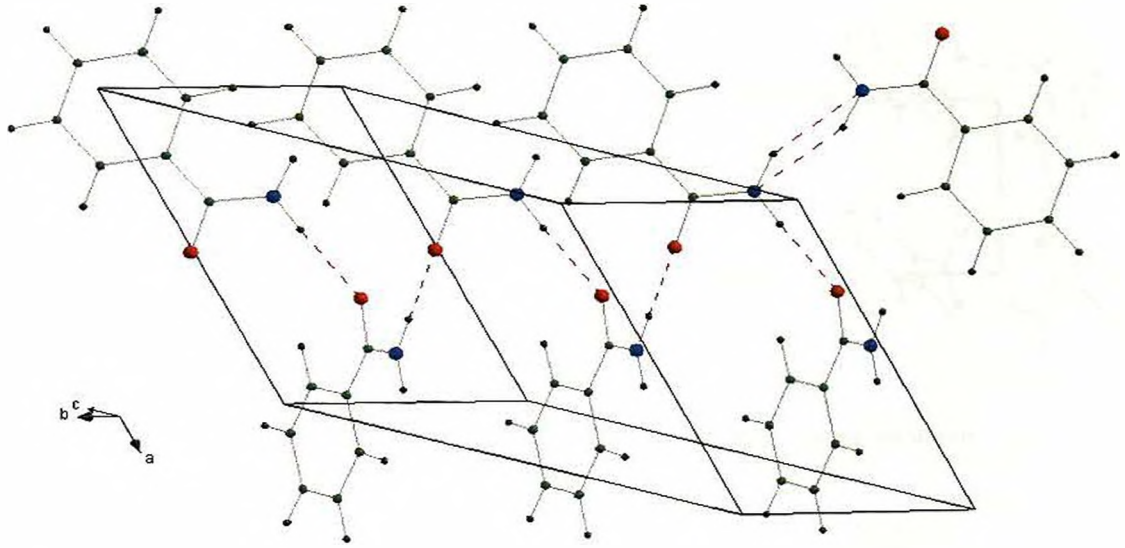

Figure 5.1.9: View of benzamide structure 9 showing the spirals running along the [010] direction.

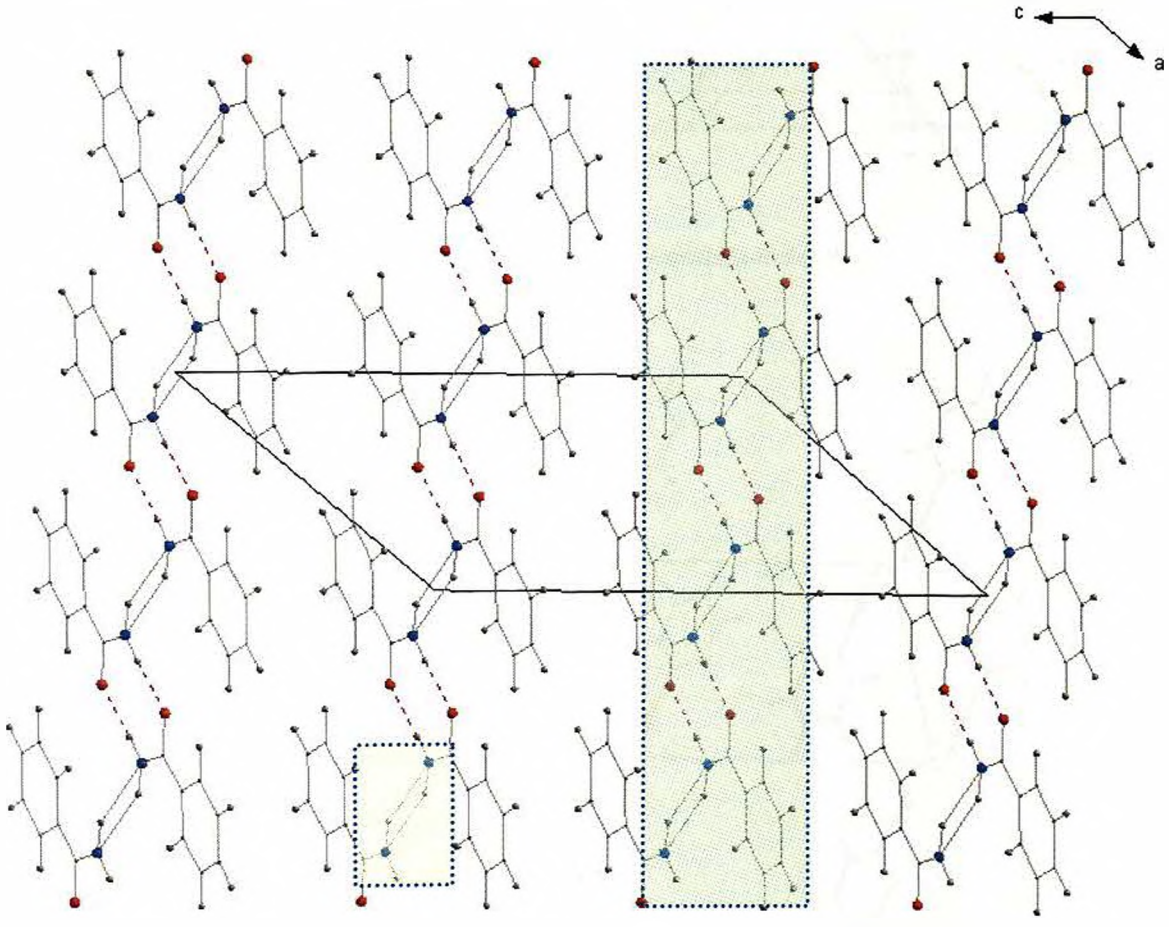

Figure 5.1.10: View of benzamide structure 9 along the (101) plane showing the N-H...N hydrogen bonded dimers (yellow shaded area). Spirals are illustrated using the green shaded are.

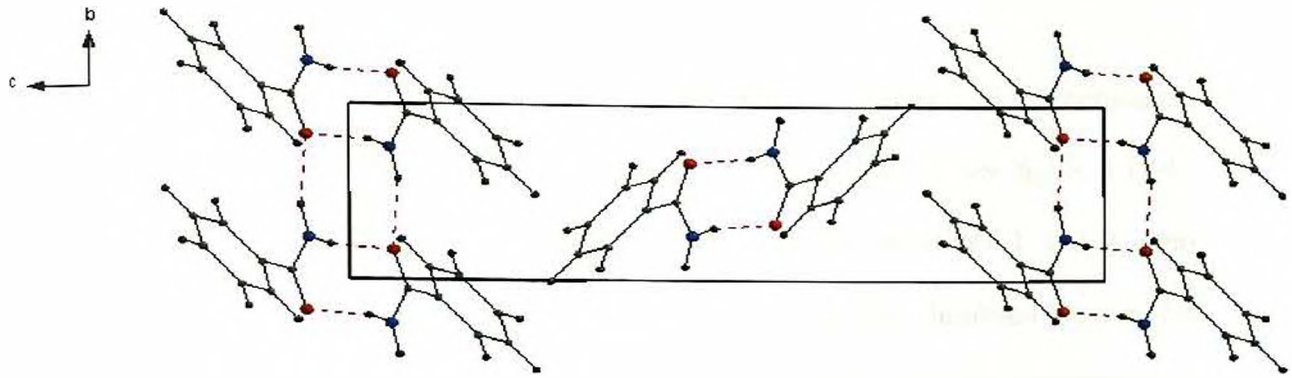

Figure 5.1.11: View of benzamide structure 13 showing the ladders that run along the axis b.

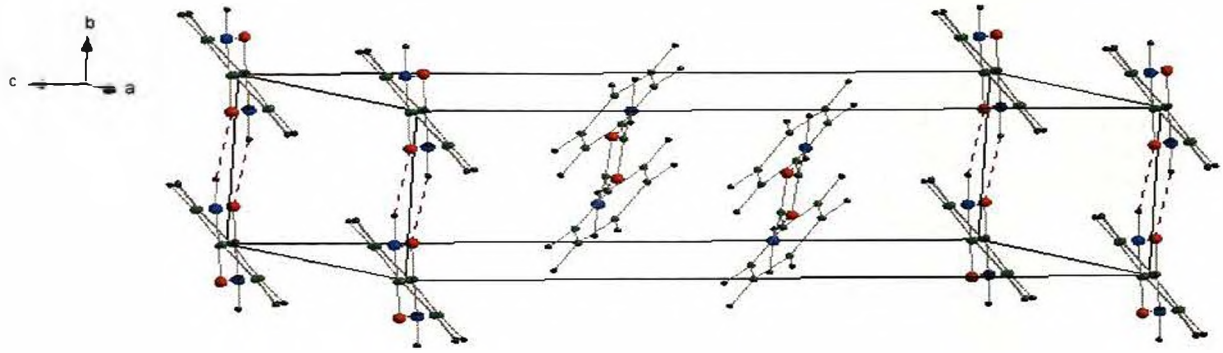

Figure 5.1.12: Illustrates the edge to face orientation of the benzamide molecules.

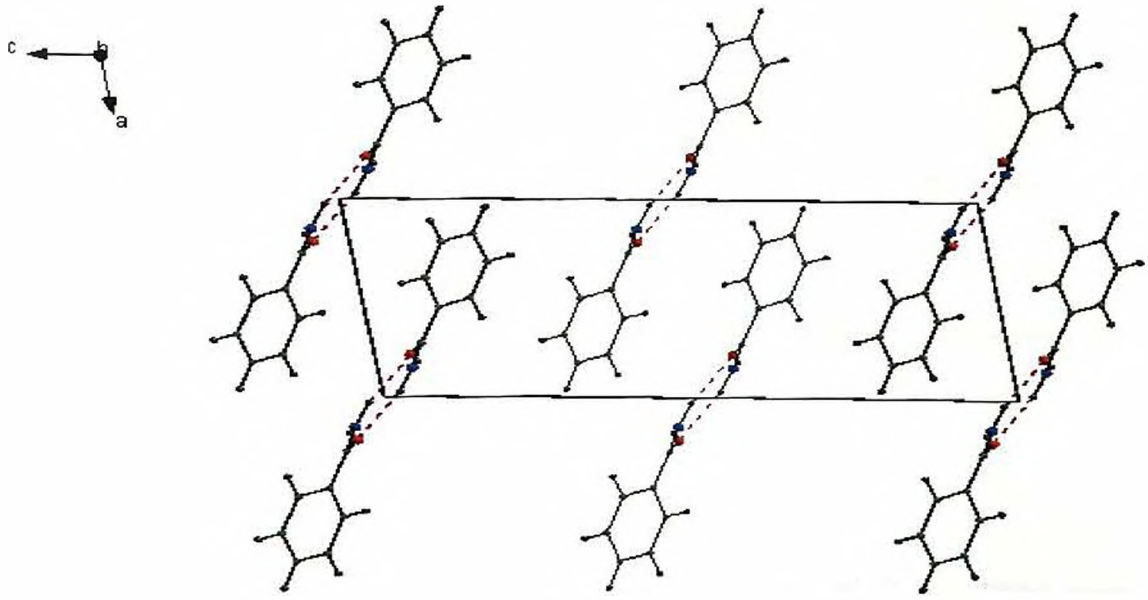

Figure 5.1.13: View of benzamide structure 13 showing the chains that extend along the (101) plane.

Simulated powder X-ray diffraction data were used to compare the experimental structure with the predicted benzamide structures 1, 2, 9 and 13 (see figure 5.1.14). On initial evaluation, the powder patterns of benzamide structures 1 and 2 seem comparable to that of the experimental structure with the simulated pattern for benzamide structures 9 and 13 showing no resemblance. This is not surprising, as structures 1 and 2 display similar features to the experimental structure, although they are clearly not identical.

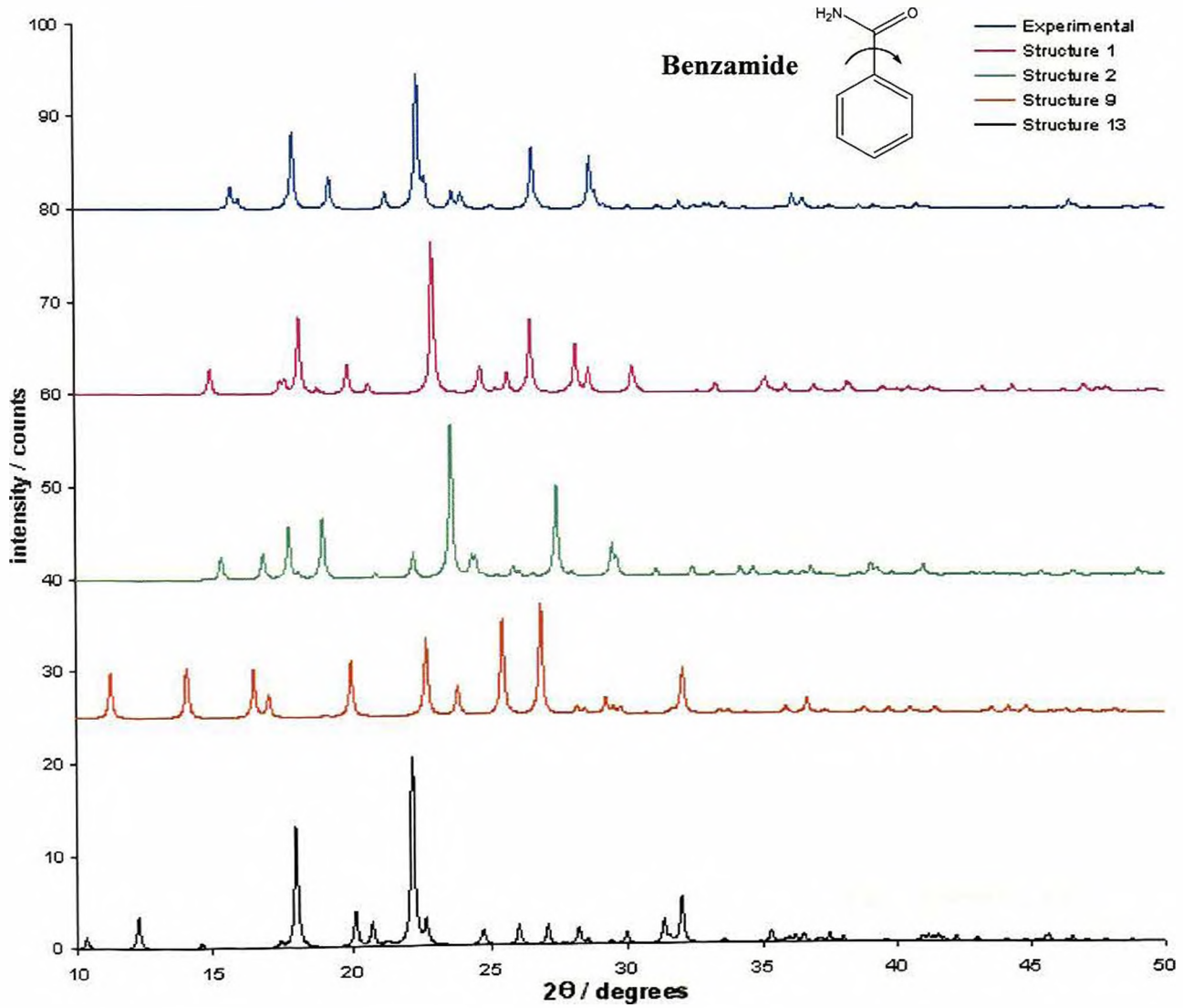

Figure 5.1.14: Comparison of the simulated experimental X-ray diffraction pattern of benzamide with predicted benzamide structures 1, 2, 9 and 13.

5.2 Ortho-methylbenamide

5.2.1 Experimental crystal structure

The crystal structure of ortho-methylbenzamide (II) [Kato. Y. et al. 1979] has been determined using conventional single crystal X-ray diffraction data, although the hydrogen atoms were placed in idealised positions and not refined. The unit cell parameters, space group and single point minimised lattice energy of the experimentally determined crystal structure are given in table 5.2.1.

a (Å)	12.18(3)
b (Å)	6.07(2)
c (Å)	4.99(1)
α (°)	89.92(2)
β (°)	97.09(3)
γ (°)	95.82(1)
Volume ($Å^3$)	364.89(2)
Density (gcm^{-3})	1.236(2)
Space group	P-1(2)
Z	2
Single point minimised lattice energy ($kcalmol^{-1}$)	-1.81

Table 5.2.1: The crystallographic and lattice energy data for experimentally determined ortho-methylbenzamide.

The crystal structure of ortho-methylbenzamide (II) contains pairs of molecules forming $R_2^2(8)$ centrosymmetric amide dimers at each of the unit cell corners of type N-H...O=C. The second amino hydrogen generates a C(4) chain which when combined with the amino dimer produces a secondary hydrogen bonding network of $R_1^2(8)$ rings forming ladders that extend along the *c* axis (figure 5.2.1 and 5.2.2).

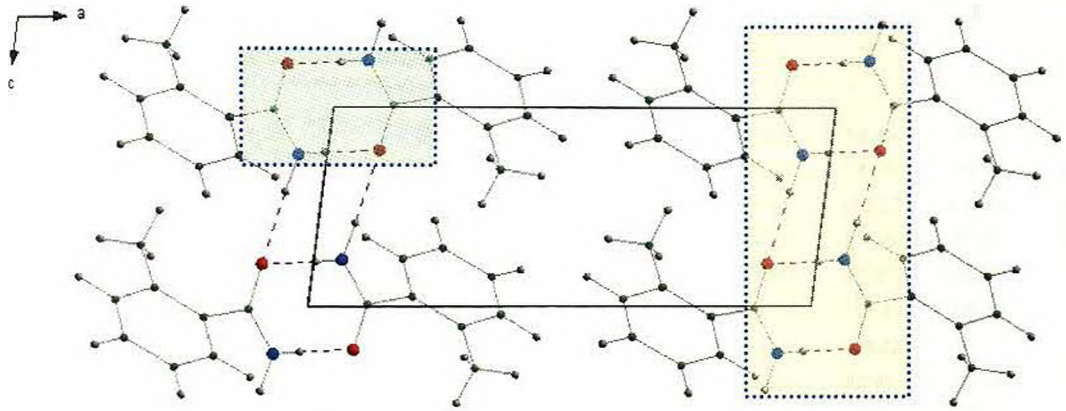

Figure 5.2.1: View of ortho-methylbenzamide (II) showing an $R_2^2(8)$ dimer (green shaded area) and ladders extending along axis *c* (yellow shaded area).

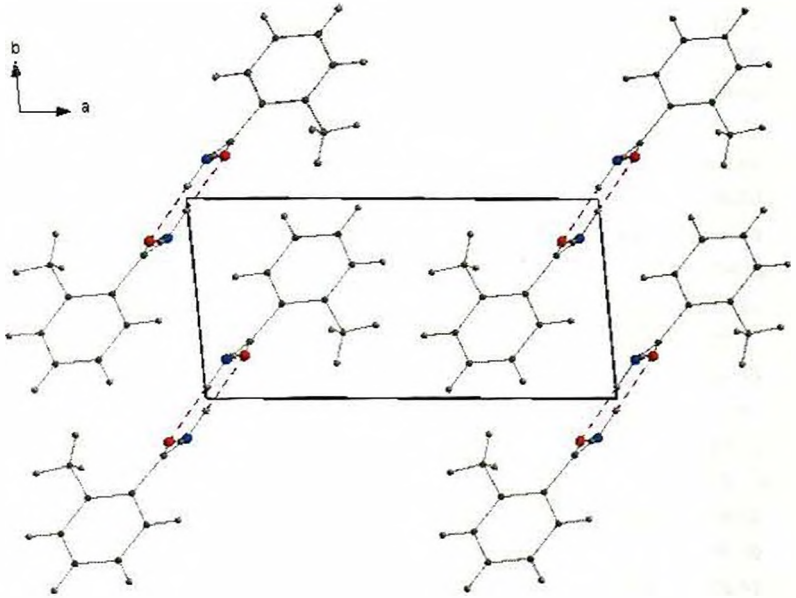

Figure 5.2.2: View of ortho-methylbenzamide (II) showing the orientation of the aromatic rings with respect to the ladders along axis *c*.

5.2.2 Structure prediction analysis - Ortho-methylbenamide

Crystal structure prediction was performed in the space group P-1 (2). No geometrical restraints were placed upon the molecular model, which was allowed to rotate through all degrees of freedom (as in figure 5.1.1). The prediction calculation generated 128 theoretical crystal structures, ranging in energy from –2.06 to +17.84 kcalmol^{-1}. Table 5.2.2 shows the top 30 predicted models and their corresponding unit cell parameters.

No.	Volume (Å^3)	Density (gcm^{-3})	Lattice energy (kcalmol^{-1})	a (Å)	b (Å)	c (Å)	α (°)	β (°)	γ (°)
1	358.89	1.25	-2.06	14.78	5.03	7.83	49.45	88.43	62.53
2	363.76	1.23	-1.64	5.02	7.73	12.87	74.06	86.98	50.17
3	379.97	1.18	-0.39	5.00	14.68	7.47	130.37	103.08	96.82
4	356.90	1.26	-0.18	4.01	14.66	6.98	81.38	85.98	61.51
5	358.03	1.25	-0.06	8.57	10.13	7.96	57.97	56.28	39.38
6	391.97	1.15	0.02	7.74	4.98	14.76	118.99	66.75	127.21
7	357.84	1.25	0.13	7.90	16.33	4.00	123.22	73.76	123.98
8	363.00	1.24	0.14	4.02	16.57	8.31	82.41	57.21	54.18
9	361.15	1.24	0.14	7.78	11.92	4.03	82.52	77.48	85.36
10	383.98	1.17	0.16	6.84	5.01	12.02	84.61	71.27	80.62
11	389.53	1.15	0.18	13.78	6.39	4.99	96.99	114.80	78.13
12	365.26	1.23	0.19	8.55	9.58	7.14	53.29	54.11	79.98
13	361.31	1.24	0.29	6.95	4.07	12.93	83.32	90.87	85.22
14	363.97	1.23	0.48	6.59	7.94	7.10	87.42	79.05	91.47
15	399.01	1.13	0.50	7.53	12.94	5.02	113.60	112.38	94.27
16	360.95	1.24	0.63	16.00	11.87	4.07	86.93	151.88	89.51
17	360.95	1.24	0.68	7.86	15.24	4.03	55.66	74.46	65.16
18	371.77	1.21	0.70	4.00	9.95	13.78	62.63	71.40	49.81
19	370.06	1.21	0.76	7.51	7.67	7.71	75.05	118.61	106.60
20	361.55	1.24	0.80	7.87	13.88	4.05	84.74	74.69	57.96
21	372.87	1.20	0.80	8.73	7.39	7.67	104.52	107.50	117.17
22	367.06	1.22	0.88	12.41	7.83	3.92	76.24	93.57	84.14
23	376.66	1.19	0.94	7.68	7.63	7.80	57.51	84.99	77.70
24	367.10	1.22	0.95	7.78	7.68	11.16	58.13	43.52	54.50
25	370.51	1.21	0.95	7.77	7.24	7.69	61.56	95.59	102.88
26	383.97	1.17	1.18	6.89	4.98	14.72	51.36	76.47	82.18
27	370.27	1.21	1.22	4.85	11.50	7.30	108.15	78.19	82.60
28	380.25	1.18	1.40	4.98	8.19	12.00	74.02	53.99	78.14
29	374.86	1.20	1.44	15.16	7.09	4.10	76.10	81.13	113.90
30	381.58	1.18	1.53	7.31	7.99	6.79	78.58	96.98	82.90

Table 5.2.2: Top 30 predicted structures for ortho-methylbenzamide (II).

5.2.3 Re-ranking of structure prediction results - Ortho-methylbenamide

Ranked according to lattice energy ($kcalmol^{-1}$)		Ranked according to Hbonding merit points		Ranked according to graphset merit points	
1	**-2.06**	**1**	**40.00**	**1**	**2**
2	**-1.64**	**2**	**40.00**	**2**	**2**
3	-0.39	3	40.00	3	2
4	**-0.18**	6	40.00	6	2
5	-0.06	11	40.00	**10**	**2**
6	0.02	15	40.00	11	2
7	0.13	**10**	**39.85**	15	2
8	0.14	26	35.60	**4**	**1**
9	0.14	**4**	**20.00**	5	1
10	**0.16**	5	20.00	7	1
11	0.18	7	20.00	8	1
12	0.19	8	20.00	9	1
13	0.29	9	20.00	12	1
14	0.48	12	20.00	13	1
15	0.50	13	20.00	14	1
16	0.63	14	20.00	16	1
17	0.68	16	20.00	17	1
18	0.70	17	20.00	18	1
19	0.76	18	20.00	19	1
20	0.80	19	20.00	20	1
21	0.80	20	20.00	21	1
22	0.88	21	20.00	22	1
23	0.94	22	20.00	23	1
24	0.95	23	20.00	24	1
25	0.95	24	20.00	25	1
26	1.18	25	20.00	26	1
27	1.22	27	20.00	27	1
28	1.40	28	20.00	28	1
29	1.44	29	20.00	29	1
30	1.53	30	20.00	30	1

Table 5.2.3: Top 30 predicted structures for ortho-methylbenzamide (II) re-ranked according to hydrogen bonding and graph set merit points. Highlighted structures show similarity to experimental structure.

The re-ranking procedure (table 5.2.3) shows that a total of 6 theoretical structures have the expected maximum 40 hydrogen bonding merit points and 7 structures have 2 graph set merit points highlighting the presence of the characteristic structural motifs expected in amide crystal structures. All theoretical structures with maximum merit points were examined further. However, only structures 1, 2, 4 and 10 are discussed in more detail (highlighted) either due to their similarity to the experimentally determined structure or due to their behaviour in the re-ranking process.

Ortho-methylbenzamide structure 1 is clearly the most energetically favourable and has remained at the top of the re-ranking tables with maximum hydrogen bonding and graph set assignment points (see table 5.2.3). Like the experimental crystal structure it contains molecules that form $R_2^2(8)$ amide dimers, which through C(4) chains generate infinite ladders along axis *b*. These dimers are shifted by 0.5 along axis *a* (compared to the experimental structure) and the ladders run along a different direction. However, the relationship between the layers of ladders in the experimental structure and theoretical structure 1 is similar (figures 5.2.3 and 5.2.4).

		D-H	H...A	D...A	D-H...A
1	1 N(28) --H(37) ..O(29)	0.9600	2.0700	3.0092	164.00
2	1 N(28) --H(37) ..N(28)	0.9600	2.6100	3.4064	141.00
3	1 N(28) --H(38) ..O(29)	0.9600	2.0400	3.0022	173.00

1	1 N(28) --H(37) ..O(29):	2.07	merit = 10
3	1 N(28) --H(38) ..O(29):	2.04	merit = 10
2	1 N(28) --H(37) ..N(28):	2.61	merit = 0

1	1 N(28) --H(37) ..O(29):	164	merit = 10
3	1 N(28) --H(38) ..O(29):	173	merit = 10
2	1 N(28) --H(37) ..N(28):	141	merit = 6.49[a]

TOTAL MERIT FOR POLYMORPH 1 = 40.00

Table 5.2.4: Hydrogen bonding merit points generated by the re-ranking strategy for ortho-methylbenzamide structure 1.
[a]These merit points are discounted due to respective bond distance having zero points.

Ortho-methylbenzamide structure 2 also contains $R_2^2(8)$ amide dimers which are linked through C(4) N-H...O chains to form infinite $R_1^2(8)$ rings generating ladders along the *a* axis, compared with axis *b* in the experimental structure. The distance between the layers within structure 2 is 7.73Å compared to 6.07Å in the experimental structure (figures 5.2.5 and 5.2.6).

		D-H	H...A	D...A	D-H...A
1	N(28) --H(37) ..O(29)	0.9600	2.0800	3.0137	163.00
2	N(28) --H(37) ..N(28)	0.9600	2.5800	3.3830	141.00
3	N(28) --H(38) ..O(29)	0.9600	2.0400	2.9994	174.00

1 N(28) --H(37) ..O(29): 2.08 merit = 10
3 N(28) --H(38) ..O(29): 2.04 merit = 10
2 N(28) --H(37) ..N(28): 2.58 merit = 0

1 N(28) --H(37) ..O(29): 163 merit = 10
3 N(28) --H(38) ..O(29): 174 merit = 10
2 N(28) --H(37) ..N(28): 141 merit = 6.49 => 0

TOTAL MERIT FOR POLYMORPH 2 = 40.00

Table 5.2.5: Hydrogen bonding merit points generated by the re-ranking strategy for ortho-methylbenzamide structure 2.

Ortho-methylbenzamide structure 4 has been re-ranked down 5 places after being awarded only 20 hydrogen bonding merit points and 4 places with only 1 graph set assignment point. This reflects the presence of only one structural motif; $R_2^2(8)$ amide dimers are present, but no C(4) N-H…O chains are generated and consequentially no ladders are formed. Figures 5.2.7 and 5.2.8 show the crystal packing of structure 4.

		D-H	H...A	D...A	D-H...A
1	N(28) --H(37) ..O(29)	0.9600	2.0400	3.0022	174.00
2	N(28) --H(38) ..N(28)	0.9600	2.5700	3.5315	175.00

1 N(28) --H(37) ..O(29): 2.04 merit = 10
2 N(28) --H(38) ..N(28): 2.57 merit = 0

1 N(28) --H(37) ..O(29): 174 merit = 10
2 N(28) --H(38) ..N(28): 175 merit = 0

TOTAL MERIT FOR POLYMORPH 4 = 20

Table 5.2.6: Hydrogen bonding merit points generated by the re-ranking strategy for ortho-methylbenzamide structure 4.

Ortho-methylbenzamide structure 10 has moved significantly up the table following re-ranking. Like the experimental crystal structure it contains $R_2^2(8)$ amide dimers at each of the unit cell corners and through the generation of C(4) chains, ladders are formed along axis *b*. However, the orientation of the aromatic ring with respect to the $R_2^2(8)$ amide dimers is significantly different from the experimental crystal structure (figures 5.2.9 and 5.2.10).

		D-H	H...A	D...A	D-H...A
1	N(28) --H(37) ..O(29)	0.9600	2.1200	3.0205	155.00
2	N(28) --H(37) ..N(28)	0.9600	2.5100	3.3118	140.00
3	N(28) --H(38) ..O(29)	0.9600	2.0300	2.9905	172.00

1 N(28) --H(37) ..O(29): 2.12 merit = 10
3 N(28) --H(38) ..O(29): 2.03 merit = 10
2 N(28) --H(37) ..N(28): 2.51 merit = 0

3 N(28) --H(38) ..O(29): 172 merit = 10
1 N(28) --H(37) ..O(29): 155 merit = 9.85
2 N(28) --H(37) ..N(28): 140 merit = 0

TOTAL MERIT FOR POLYMORPH 10 = 39.85

Table 5.2.7: Hydrogen bonding merit points generated by the re-ranking strategy for ortho-methylbenzamide structure 10.

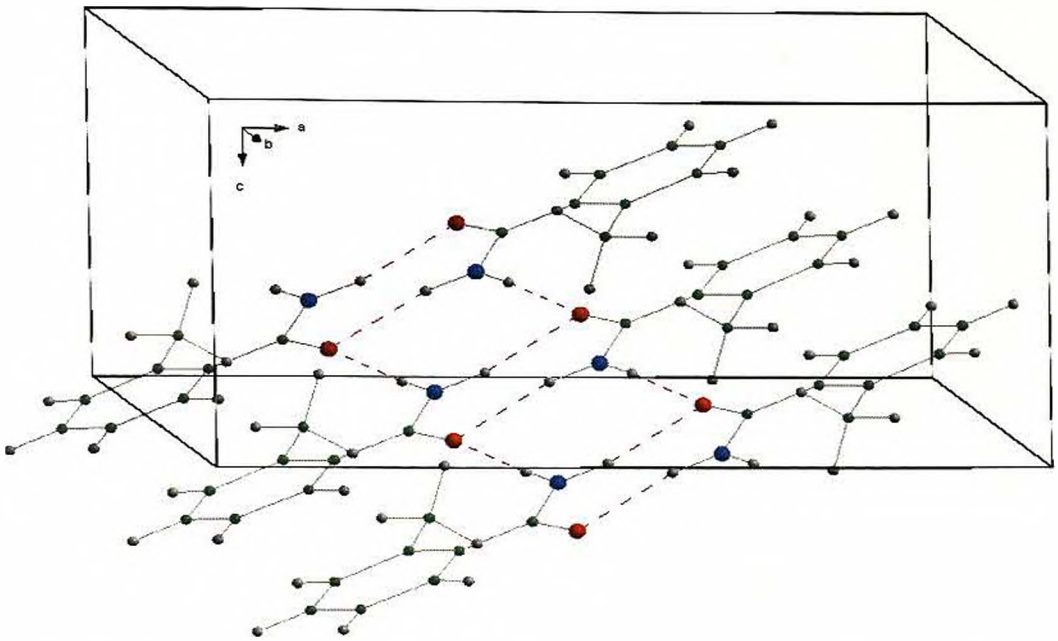

Figure 5.2.3: View of ortho-methylbenzamide structure 1 showing ladders running along the *b* axis, illustrated using purple dashed lines.

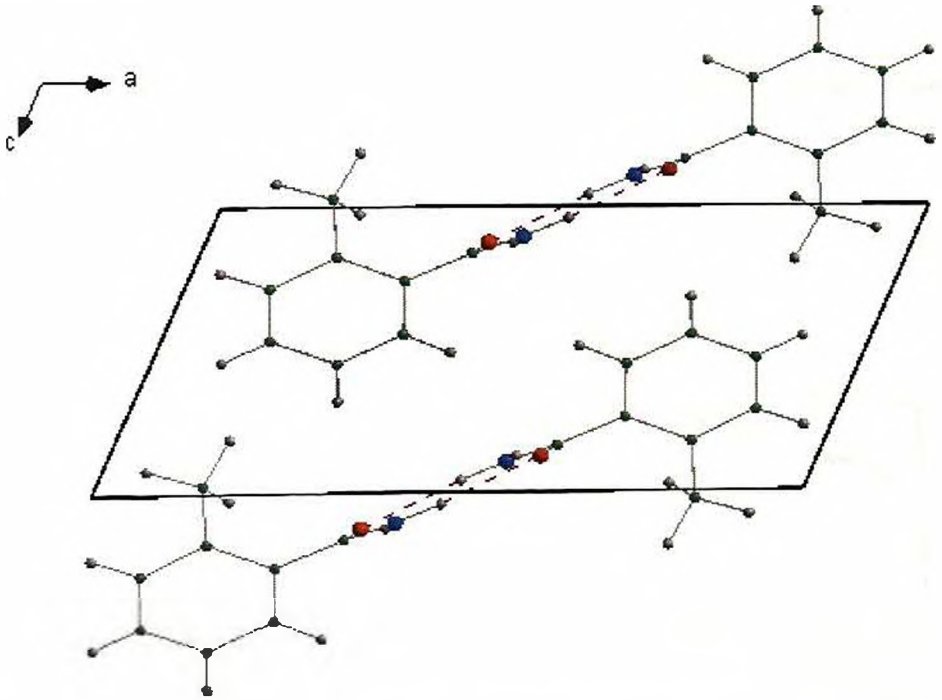

Figure 5.2.4: View of ortho-methylbenzamide structure 1 showing the perpendicular orientation of the aromatic rings with respect to the ladders along axis *b*.

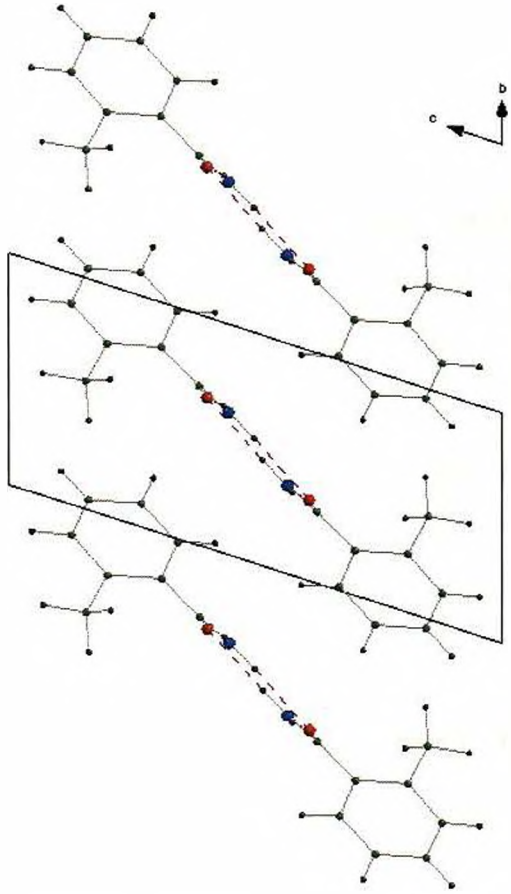

Figure 5.2.5: View of ortho-methylbenzamide structure 2 showing the perpendicular orientation of the aromatic rings with respect to the ladders along axis a.

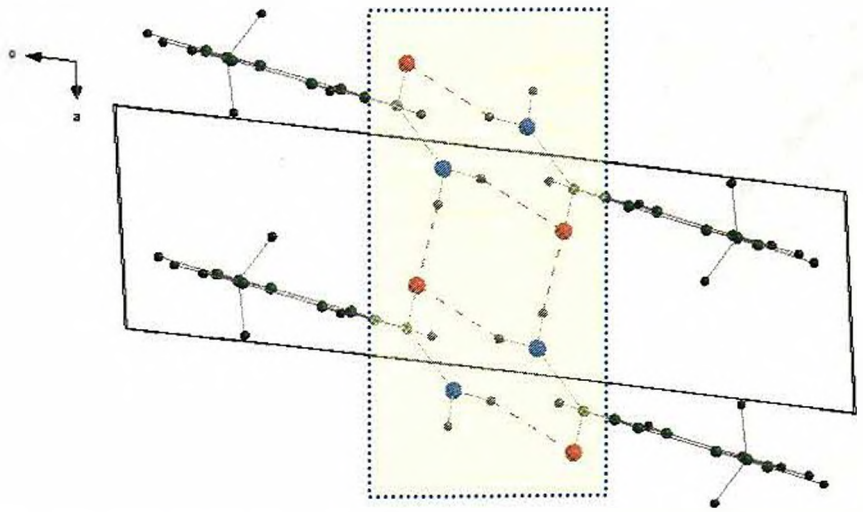

Figure 5.2.6: View of ortho-methylbenzamide structure 2 showing the ladders formed along axis a (yellow shaded area).

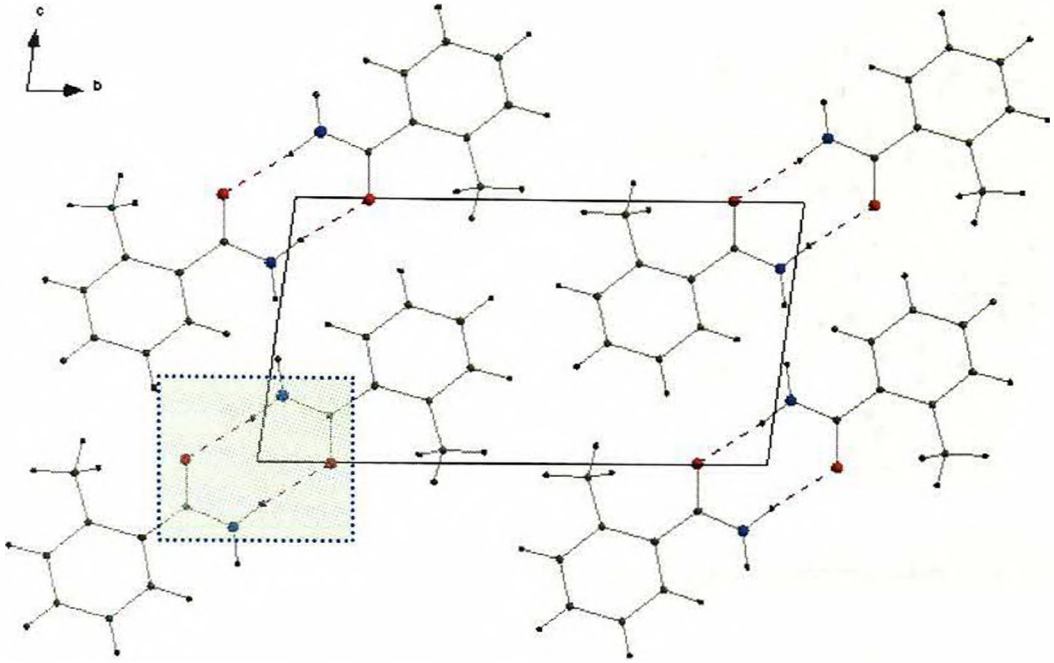

Figure 5.2.7: Packing arrangement of ortho-methylbenzamide structure 4 showing the staggered amide dimers along the [001] direction (green shaded area).

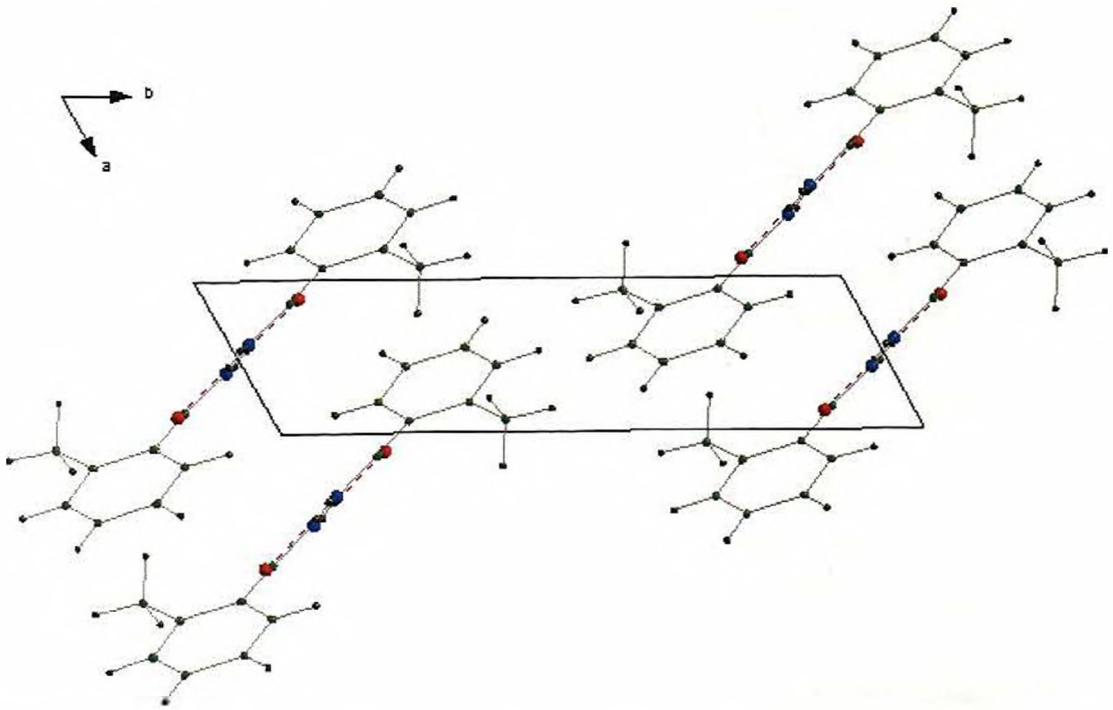

Figure 5.2.8: View of ortho-methylbenzamide structure 4 showing the amide dimers stacked along axis *a*.

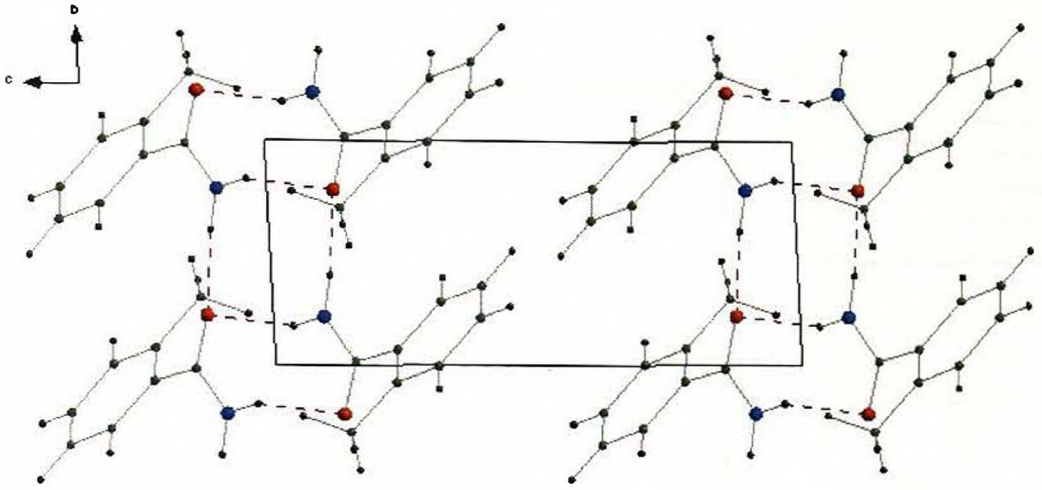

Figure 5.2.9: Packing arrangement of ortho-methylbenzamide structure 10 showing ladders along the axis *b*.

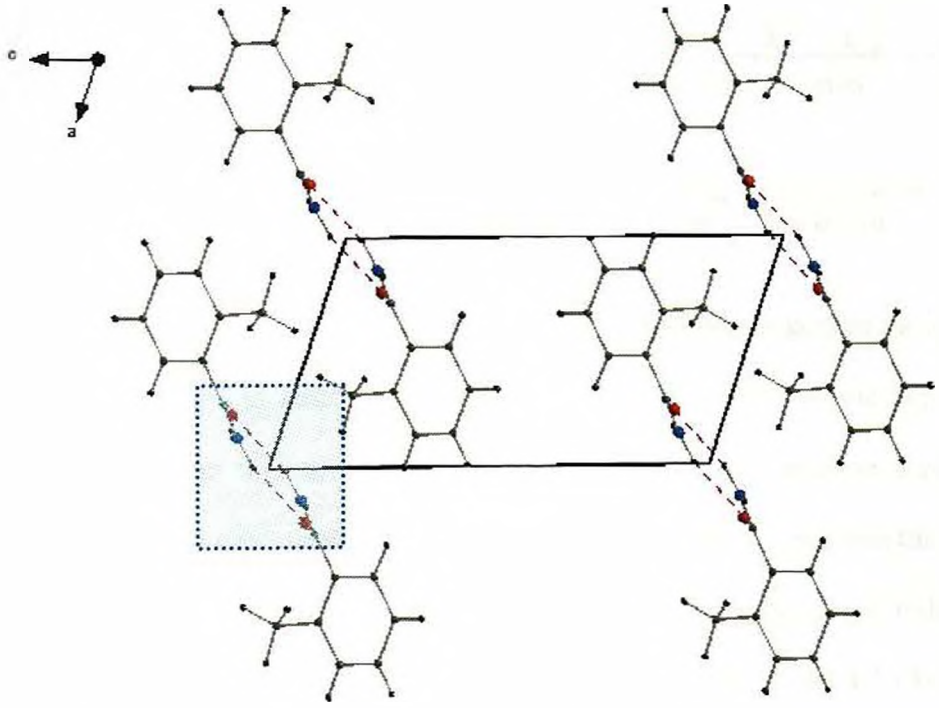

Figure 5.2.10: View of ortho-methylbenzamide structure 10 showing the amide dimers at each of the unit cell corners (blue shaded area).

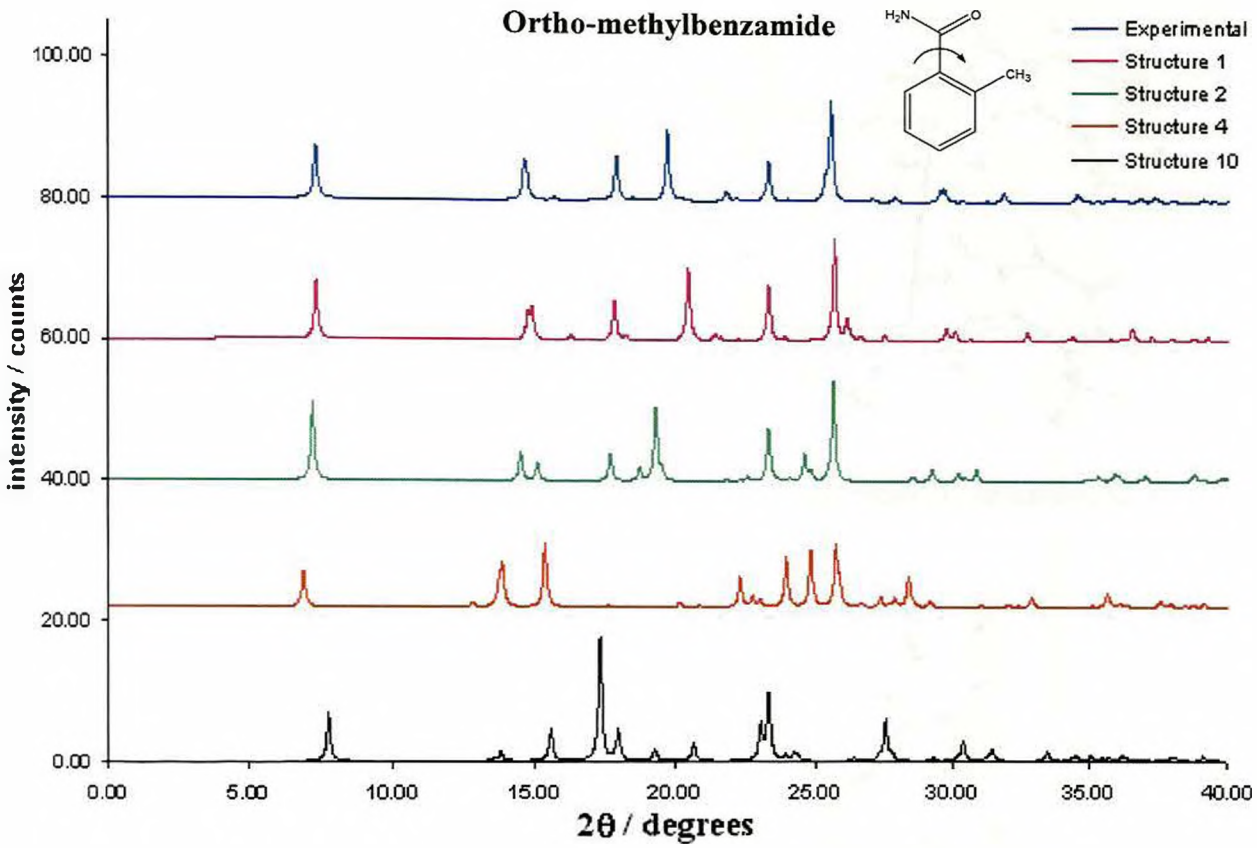

Figure 5.2.11: Comparison of the experimental X-ray diffraction pattern of ortho-methylbenzamide with the simulated powder patterns for ortho-methylbenzamide structures 1, 2, 4 and 10.

From figure 5.2.11 it is evident that the simulated X-ray powder pattern for theoretical ortho-methylbenzamide structure 1 is almost identical to that of the experimental structure, indicating that the differences between structure 1 and the experimental structure do indeed arise from an alternative unit cell setting. To confirm this, the unit cells of both the predicted and experimental crystal structures were reduced and transformed to the same setting and the overlaid (figures 5.2.12 and 5.2.13). The two crystal structures are indeed the same. There are also obvious similarities between the experimental structure and theoretical structure 2 although they are clearly not identical.

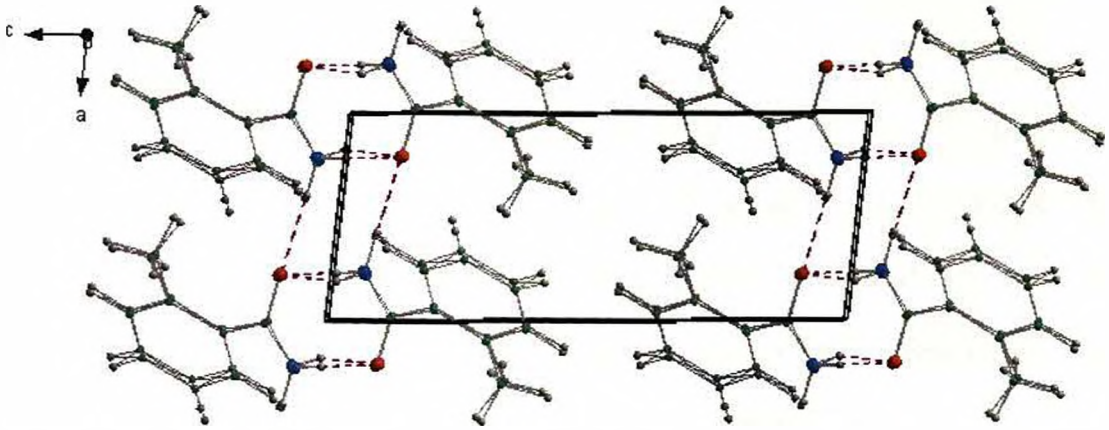

Figure 5.2.12: Ortho-methylbenzamide structure 1 and the experimental structure overlaid showing the ladders along axis a.

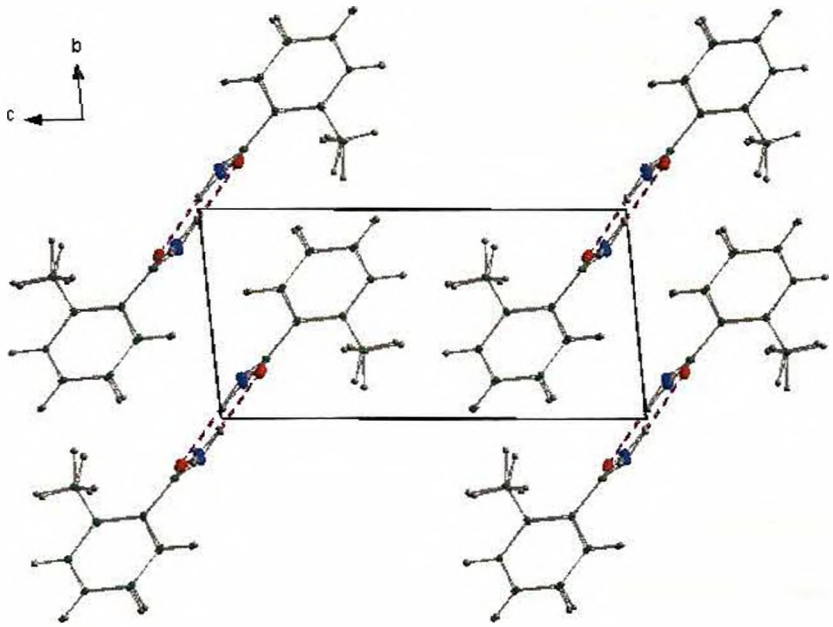

Figure 5.2.13: Ortho-methylbenzamide structure 1 and the experimental structure overlaid showing centrosymmetric amide dimers at each of the unit cell corners.

5.3 Meta-methylbenzamide

5.3.1 Experimental crystal structure

The crystal structure of meta-methylbenzamide (III) [Orii. S. et al. 1963] has been determined using conventional single crystal X-ray diffraction data, although the hydrogen atoms were placed in idealised positions and not refined. The unit cell parameters, space group and single point minimised lattice energy of the experimentally determined crystal structure are given in table 5.3.1.

a (Å)	5.12(1)
b (Å)	16.02(2)
c (Å)	8.93(2)
β (°)	95.00(1)
Volume ($Å^3$)	729.67(2)
Density (gcm^{-3})	1.242(2)
Space group	$P2_1/c$ (14)
Z	4
Single point minimised lattice energy ($kcalmol^{-1}$)	-4.83

Table 5.3.1: The crystallographic and lattice energy data for experimentally determined meta-methylbenzamide.

The crystal structure of meta-methylbenzamide (III) contains the expected centrosymmetric amide $R_2^2(8)$ dimers of type N-H...O=C. The second amino hydrogen atom forms an additional N-H...O=C hydrogen bond to an adjacent dimer forming a C(4) chain. Combination of these two motifs generates the characteristic

secondary network of $R_2^2(8)$ ladders which extend along the [100] direction (figure 5.3.1 and 5.3.2). The ladders then pack in a herringbone-type arrangement.

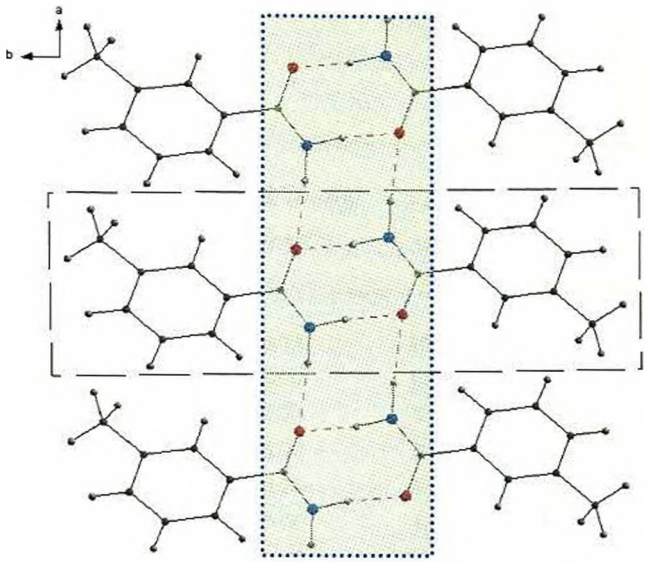

Figure 5.3.1: Crystal structure of meta-methylbenzamide (III) showing ladders running along the [100] direction (green shaded area).

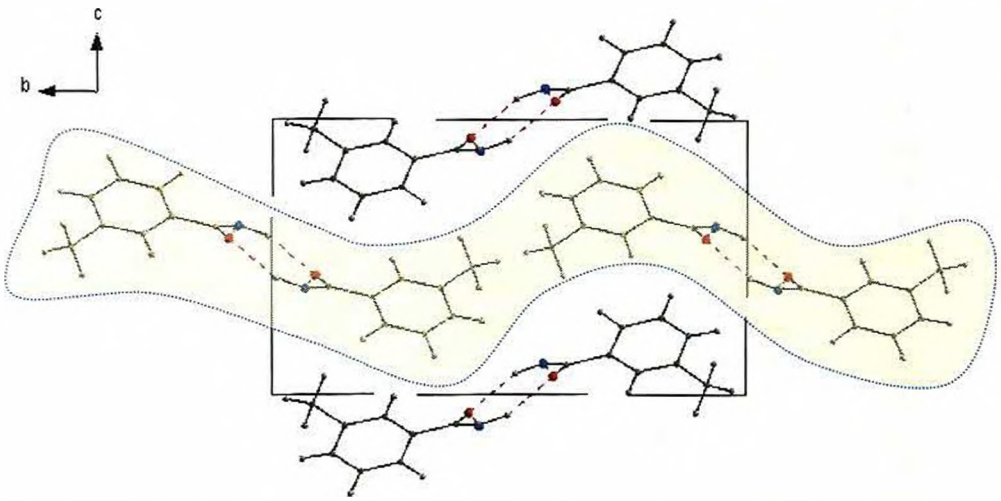

Figure 5.3.2: Crystal structure of meta-methylbenzamide (III) showing the herringbone arrangement of the ladders in projection down the *a* axis as indicated by the yellow shading.

5.3.2 Structure prediction analysis - Meta-methylbenzamide

Crystal structure prediction was performed in the space group $P2_1/c$ (14). No geometrical restraints were placed upon the molecular model, which was allowed to

rotate through all degrees of freedom (as in figure 5.1.1). The prediction calculation generated 250 theoretical crystal structures, ranging in energy from –6.74 to –2.56 kcalmol^{-1}. Table 5.3.2 shows the top 30 predicted models and their corresponding unit cell parameters.

No.	Volume (Å^3)	Density (gcm^{-3})	Lattice energy (kcalmol^{-1})	a (Å)	b (Å)	c (Å)	β (°)
1	717.32	1.25	-6.74	10.10	15.40	15.15	162.29
2	739.02	1.21	-6.33	9.63	8.63	8.90	91.91
3	751.89	1.19	-6.31	5.15	17.21	8.49	86.91
4	730.50	1.23	-6.23	6.25	15.88	7.38	93.46
5	737.09	1.22	-6.20	4.95	29.07	7.14	134.21
6	717.91	1.25	-6.06	4.04	5.90	31.28	105.45
7	720.67	1.25	-5.94	33.36	4.04	31.32	170.16
8	720.66	1.25	-5.92	9.80	31.05	7.07	160.42
9	723.47	1.24	-5.88	4.32	25.61	8.08	126.05
10	725.03	1.24	-5.86	5.76	31.24	7.15	145.71
11	734.13	1.22	-5.71	14.00	27.60	8.02	166.29
12	732.53	1.23	-5.69	7.00	30.55	5.91	144.57
13	733.53	1.22	-5.62	3.98	32.15	5.73	92.22
14	733.20	1.22	-5.60	3.97	30.17	6.15	84.70
15	754.73	1.19	-5.56	12.96	8.05	9.06	52.96
16	754.38	1.19	-5.53	17.24	5.11	13.89	141.91
17	712.55	1.26	-5.53	37.24	4.06	33.97	172.03
18	718.19	1.25	-5.41	5.81	4.09	35.95	122.72
19	756.34	1.19	-5.40	7.27	20.65	8.18	141.97
20	719.02	1.25	-5.40	10.09	4.16	17.17	94.37
21	728.32	1.23	-5.39	13.12	7.64	17.01	154.70
22	731.15	1.23	-5.34	4.15	9.69	19.26	70.56
23	731.33	1.23	-5.32	4.08	19.42	17.38	147.95
24	781.39	1.15	-5.27	26.22	5.06	20.04	162.92
25	742.69	1.21	-5.25	7.43	9.63	10.55	79.57
26	729.65	1.23	-5.20	21.55	6.66	17.74	163.35
27	730.12	1.23	-5.14	10.56	12.16	7.24	51.71
28	725.98	1.24	-5.07	21.47	5.68	22.54	164.68
29	721.00	1.25	-5.06	12.78	4.08	17.32	127.10
30	763.20	1.18	-5.02	18.92	5.14	15.24	148.98

Table 5.3.2: Top 30 predicted structures for meta-methylbenzamide (III).

5.3.3 Re-ranking of structure prediction results - Meta-methylbenzamide

Ranked according to lattice energy ($kcalmol^{-1}$)		Ranked according to Hbonding merit points		Ranked according to graphset merit points	
1	**-6.74**	**2**	**40.00**	**2**	**2**
2	**-6.33**	**3**	**40.00**	**3**	**2**
3	**-6.31**	5	40.00	5	2
4	-6.23	15	40.00	15	2
5	-6.20	16	40.00	16	2
6	-6.06	19	40.00	19	2
7	-5.94	24	40.00	24	2
8	-5.92	**30**	**40.00**	**30**	**2**
9	-5.88	18	39.27	**1**	**1**
10	-5.86	**1**	**34.61**	4	1
11	-5.71	11	33.04	6	1
12	-5.69	26	32.85	7	1
13	-5.62	9	31.90	8	1
14	-5.60	4	30.85	9	1
15	-5.56	25	22.00	10	1
16	-5.53	6	20.00	11	1
17	-5.53	7	20.00	13	1
18	-5.41	8	20.00	14	1
19	-5.40	10	20.00	17	1
20	-5.40	12	20.00	18	1
21	-5.39	13	20.00	22	1
22	-5.34	14	20.00	23	1
23	-5.32	17	20.00	25	1
24	-5.27	20	20.00	26	1
25	-5.25	21	20.00	27	1
26	-5.20	22	20.00	28	1
27	-5.14	23	20.00	29	1
28	-5.07	27	20.00	12	0
29	-5.06	28	20.00	20	0
30	**-5.02**	29	20.00	21	0

Table 5.3.3: Top 30 predicted structures for meta-methylbenzamide (III) re-ranked according to hydrogen bonding and graph set merit points. Highlighted structures show similarity to experimental structure.

The re-ranking procedure (table 5.3.3) shows that a total of 8 theoretical structures have the expected maximum 40 hydrogen bonding merit points and 8 structures have 2 graph set merit points highlighting the presence of the characteristic structural motifs expected in amide crystal structures. All theoretical structures with maximum merit points were examined further. However, only structures 1, 2, 3 and 30 are discussed in more detail (highlighted) either due to their similarity to the experimentally determined structure or due to their behaviour in the re-ranking process.

Meta-methylbenzamide structure 1 is energetically the most favourable structure, but has acquired only 34.61 merit points and moved down the rankings by 9 places in terms of hydrogen bonding and 8 places in terms of graph set assignment points (table 5.3.3). Structure 1 contains centrosymmetric amide $R_2^2(8)$ dimers of type N-H...O=C but rather than the formation of C(4) chains the second amino nitrogen generates $R_2^2(4)$ amino dimers through non-ideal N-H...N type interactions. These combine with the $R_2^2(8)$ dimers to form a network of ladders in the [1, 0, 1] direction (figures 5.3.3 and 5.3.4). The packing of these ladders is similar to that in the experimental structure forming a herringbone type arrangement.

		D-H	H...A	D...A	D-H...A
1	N(66) --H(75) ..O(67)	0.9600	2.0400	2.9988	174.00
2	N(66) --H(76) ..N(66)	0.9600	2.3800	3.2181	145.00

1 N(66) --H(75) ..O(67): 2.04 merit = 10
2 N(66) --H(76) ..N(66): 2.38 merit = 6.76

1 N(66) --H(75) ..O(67): 174 merit = 10
2 N(66) --H(76) ..N(66): 145 merit = 7.85

TOTAL MERIT FOR POLYMORPH 1 = 34.61

Table 5.3.4: Hydrogen bonding merit points generated by the re-ranking strategy for meta-methylbenzamide structure 1.

The molecules within meta-methylbenzamide structure 2 also generate centrosymmetric amide $R_2^2(8)$ dimers of type N-H...O=C at (0, 0, ½). However, the second amino hydrogen forms hydrogen bonds to an adjacent dimer through formation of a C(4) chain generating a secondary network of $R_6^4(16)$ rings, forming an infinite sheet in the (011) plane. The formation of this alternative secondary

network compared to that of the expected $R_4^2(8)$ ladders, arises from the displacement of adjacent dimers by ½ a unit cell along the *c* axis (figure 5.3.5). Although structure 2 is not the same as the experimental crystal structure it has the maximum hydrogen bonding merit points (40 points) and graph set assignment points (2 points) because it contains both the $R_2^2(8)$ dimers and the C(4) chains (see table 5.3.3).

		D-H	H...A	D...A	D-H...A
1	N(66) --H(75) ..O(67)	0.9700	2.0800	3.0267	167.00
2	N(66) --H(76) ..O(67)	0.9600	2.1300	3.0774	166.00

1 N(66) --H(75) ..O(67): 2.08 merit = 10
2 N(66) --H(76) ..O(67): 2.13 merit = 10

1 N(66) --H(75) ..O(67): 167 merit = 10
2 N(66) --H(76) ..O(67): 166 merit = 10

TOTAL MERIT FOR POLYMORPH 2 = 40

Table 5.3.5: Hydrogen bonding merit points generated by the re-ranking strategy for meta-methylbenzamide structure 2.

Meta-methylbenzamide structure 3 is most like the experimental structure both in terms of hydrogen bonding and molecular orientation. It has the maximum number of hydrogen bonding merit and graph set assignment points and has moved up a one place to position 2 (table 5.3.3). The structure contains centrosymmetric amide $R_2^2(8)$ dimers, with the second amino hydrogen atom forming an additional N-H...O=C hydrogen bond on an adjacent molecule to give a C(4) chain. The combination of these motifs gives a secondary network of $R_4^2(8)$ ladders that extend along the [1, 0, 0] direction (figure 5.3.6 and 5.3.7), the ladders again display a herringbone type arrangement. The only obvious difference between structure 3 and the experimental crystal structure is that structure 3 has a different relationship between the ladders, as clearly illustrated by the relative positions of the methyl groups

		D-H	H...A	D...A	D-H...A
1	N(66) --H(75) ..O(67)	0.9600	2.0600	3.0142	169.00
2	N(66) --H(76) ..O(67)	0.9700	2.1300	3.0827	168.00

1 N(66) --H(75) ..O(67): 2.06 merit = 10
2 N(66) --H(76) ..O(67): 2.13 merit = 10

1 N(66) --H(75) ..O(67): 169 merit = 10
2 N(66) --H(76) ..O(67): 168 merit = 10

TOTAL MERIT FOR POLYMORPH 3 = 40

Table 5.3.6: Hydrogen bonding merit points generated by the re-ranking strategy for meta-methylbenzamide structure 3.

Meta-methylbenzamide structure 30, which is 1.72kcalmol^{-1} less stable than the theoretically most stable structure has the maximum number of hydrogen bonding merit and graph set assignment points, moving up 22 places to position 8 (table 5.3.3). The structure contains the characteristic amide $R_2^2(8)$ dimers of type N-H...O=C around (½, ½, ½). Combination of these dimers with C(4) chains gives rise to $R_4^2(8)$ rings and hence to ladders extending along [010] (figure 5.3.8 and 5.3.9). Where as the experimental structure comprised a herringbone arrangement of the ladders, structure 30 simply has chains generated from dimers running along the (102) plane.

		D-H	H...A	D...A	D-H...A
1	N(66) --H(75) ..O(67)	0.9600	2.0600	3.0123	167.00
2	N(66) --H(76) ..O(67)	0.9700	2.1200	3.0598	164.00

1 N(66) --H(75) ..O(67): 2.06 merit = 10
2 N(66) --H(76) ..O(67): 2.12 merit = 10

1 N(66) --H(75) ..O(67): 167 merit = 10
2 N(66) --H(76) ..O(67): 164 merit = 10

TOTAL MERIT FOR POLYMORPH 30 = 40

Table 5.3.7: Hydrogen bonding merit points generated by the re-ranking strategy for meta-methylbenzamide structure 30.

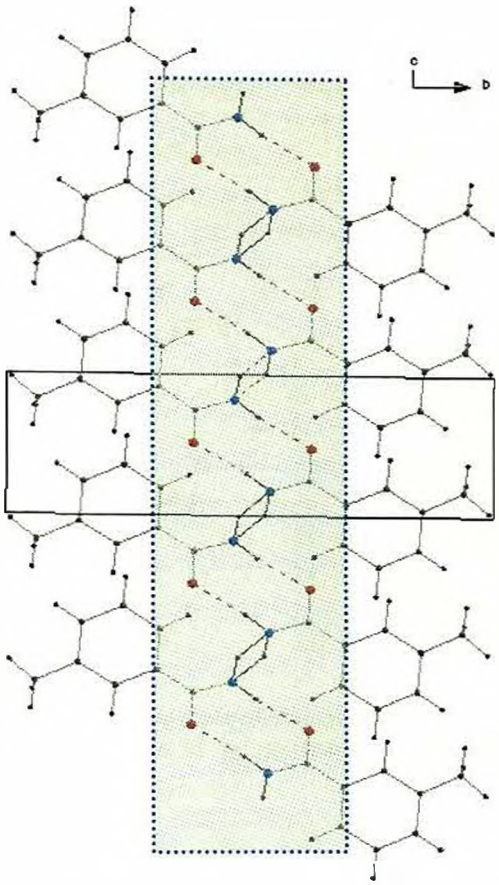

Figure 5.3.3: meta-methylbenzamide structure 1 showing ladders running along the [101] direction (green shaded area).

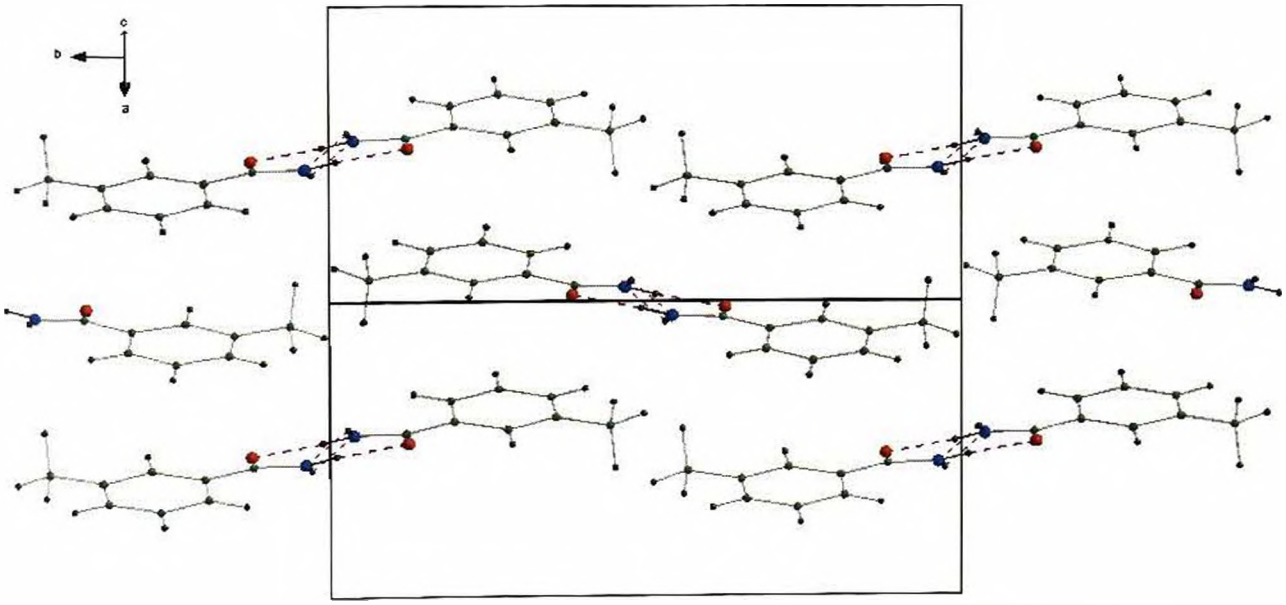

Figure 5.3.4: meta-methylbenzamide structure 1 showing herringbone type arrangement along (101).

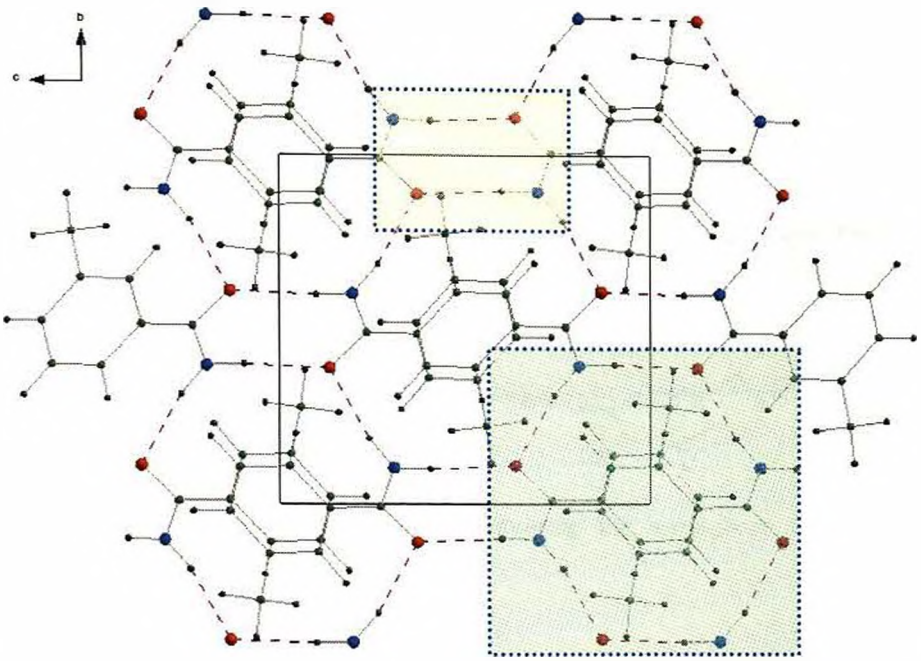

Figure 5.3.5: Packing arrangement of meta-methylbenzamide structure 2 showing the infinite sheet formation along (011) by a combination of $R_2^2(8)$ dimers (yellow shaded area) and $R_6^4(16)$ motifs (green shaded area).

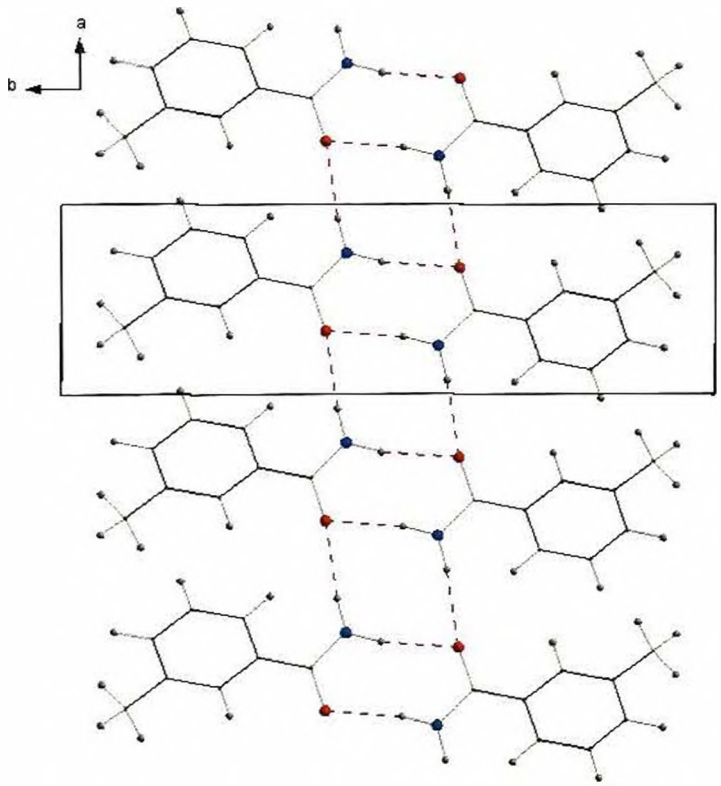

Figure 5.3.6: meta-methylbenzamide structure 3 showing ladders running along the [100] direction.

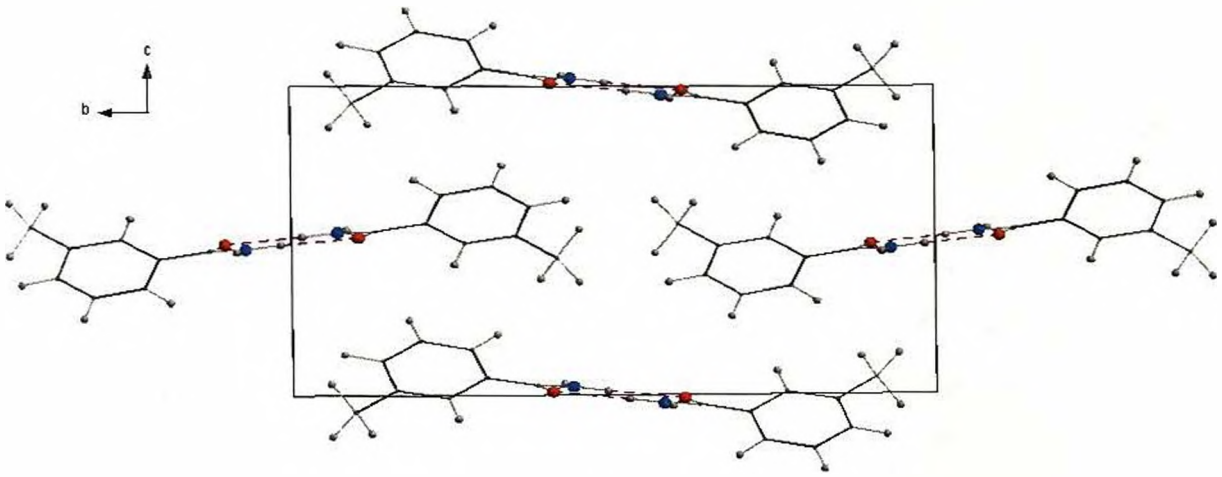

Figure 5.3.7: meta-methylbenzamide structure 3 showing the herringbone type arrangement in projection down the *a* axis.

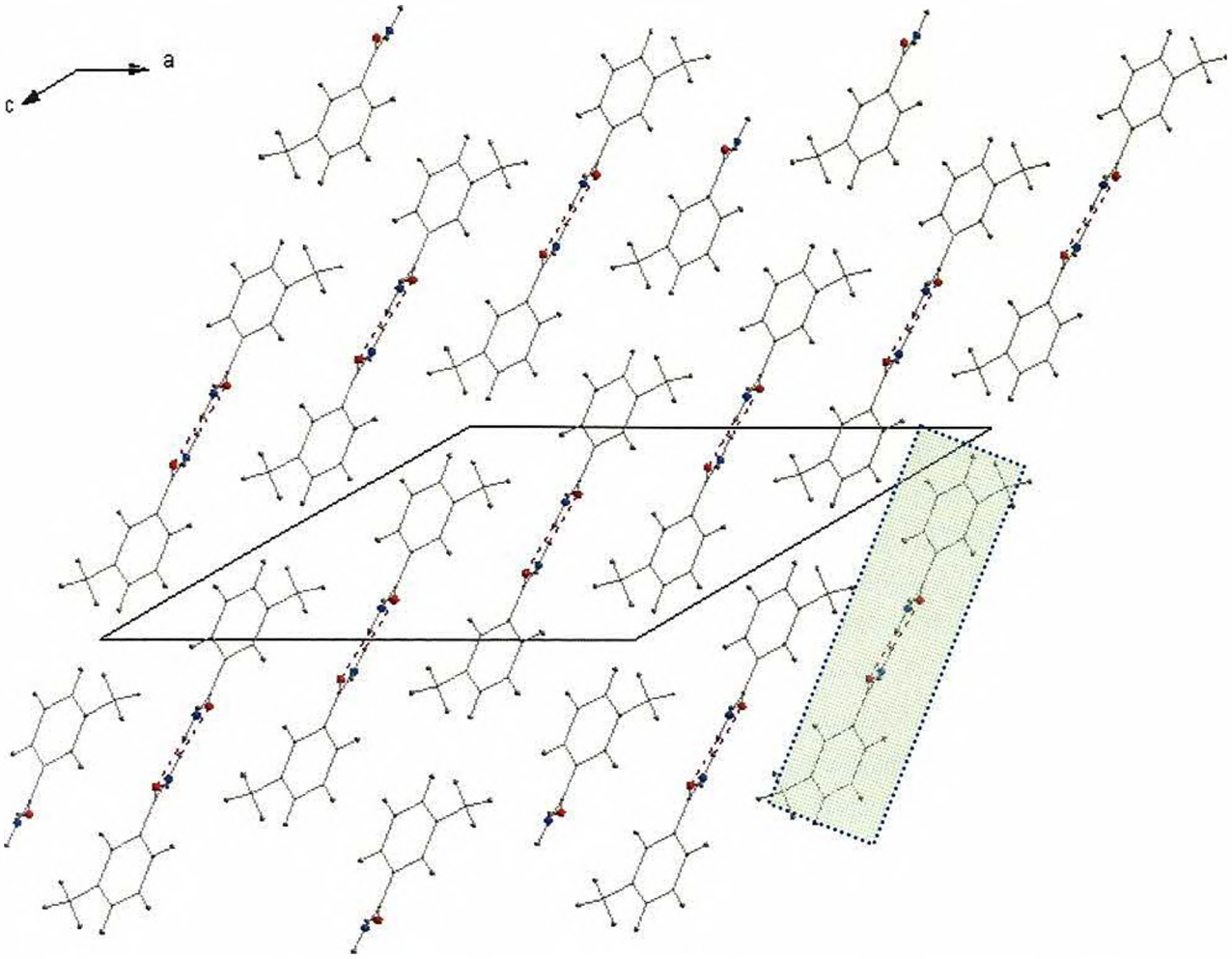

Figure 5.3.8: Layers of ladders of meta-methylbenzamide structure 30 formed along the (102) plane (green shaded area).

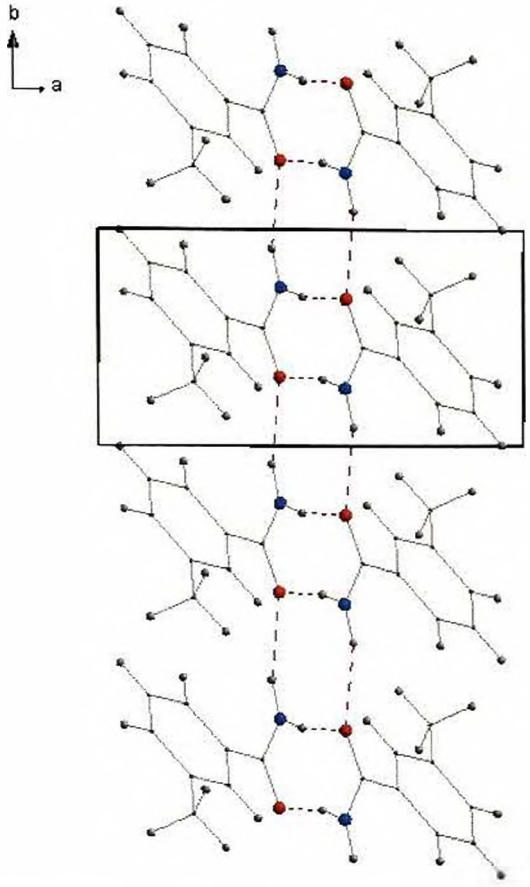

Figure 5.3.9: meta-methylbenzamide structure 30 showing ladders running along the [010] direction.

Simulated powder X-ray diffraction data were used to compare the experimental structure with the predicted meta-methylbenzamide structures 1, 2, 3 and 30 (see figure 5.3.10). The powder patterns of structures 1, 2 and 30 are not comparable to that of the experimental structure, this is not surprising, as they all display features different to the experimental crystal structure. Structure 3 shows some resemblance to the experimental crystal structure, although the structures are clearly not the same.

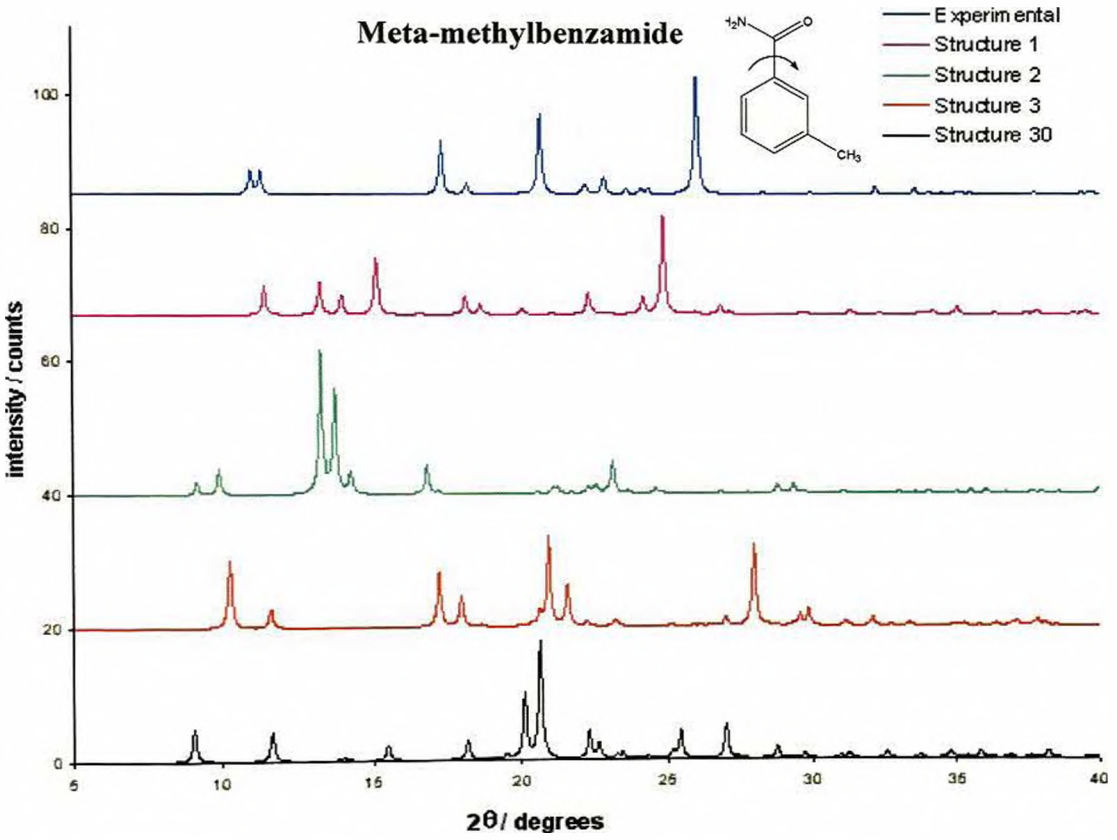

Figure 5.3.10: Comparison of the experimental X-ray diffraction pattern of meta-methylbenzamide with the simulated powder patterns for meta-methylbenzamide structures 1, 2, 3 and 30.

5.4 Para-methylbenzamide

5.4.1 Experimental crystal structure

The crystal structure of para-methylbenzamide (IV) [Kato. Y. et al. 1981] has been determined using conventional single crystal X-ray diffraction data, although the hydrogen atoms were placed in idealised positions and not refined. The unit cell parameters, space group and single point minimised lattice energy of the experimentally determined crystal structure are given in table 5.4.1.

a (Å)	9.858(1)
b (Å)	7.526(1)
c (Å)	10.764(1)
β (°)	111.30(1)
Volume ($Å^3$)	744.0(29)
Density (gcm^{-3})	1.213(2)
Z	4
Space group	$P2_1/c$ (14)
Single point minimised lattice energy ($kcalmol^{-1}$)	-6.81

Table 5.4.1: The crystallographic and lattice energy data for experimentally determined para-methylbenzamide.

The crystal structure of (IV) also contains centrosymmetric $R_2^2(8)$ amide dimers around (000) that are linked by C(4) chains, both through N-H···O=C type hydrogen bonds. However, the combination of these two motifs does not result in the expected $R_4^2(8)$ ladders. The alternating position and orientation of the $R_2^2(8)$ dimers results in each dimer being hydrogen bonded to 4 others through the C(4) chains generating $R_6^4(16)$ rings in a puckered hydrogen bonded sheet in the (110) plane (figure 5.4.1).

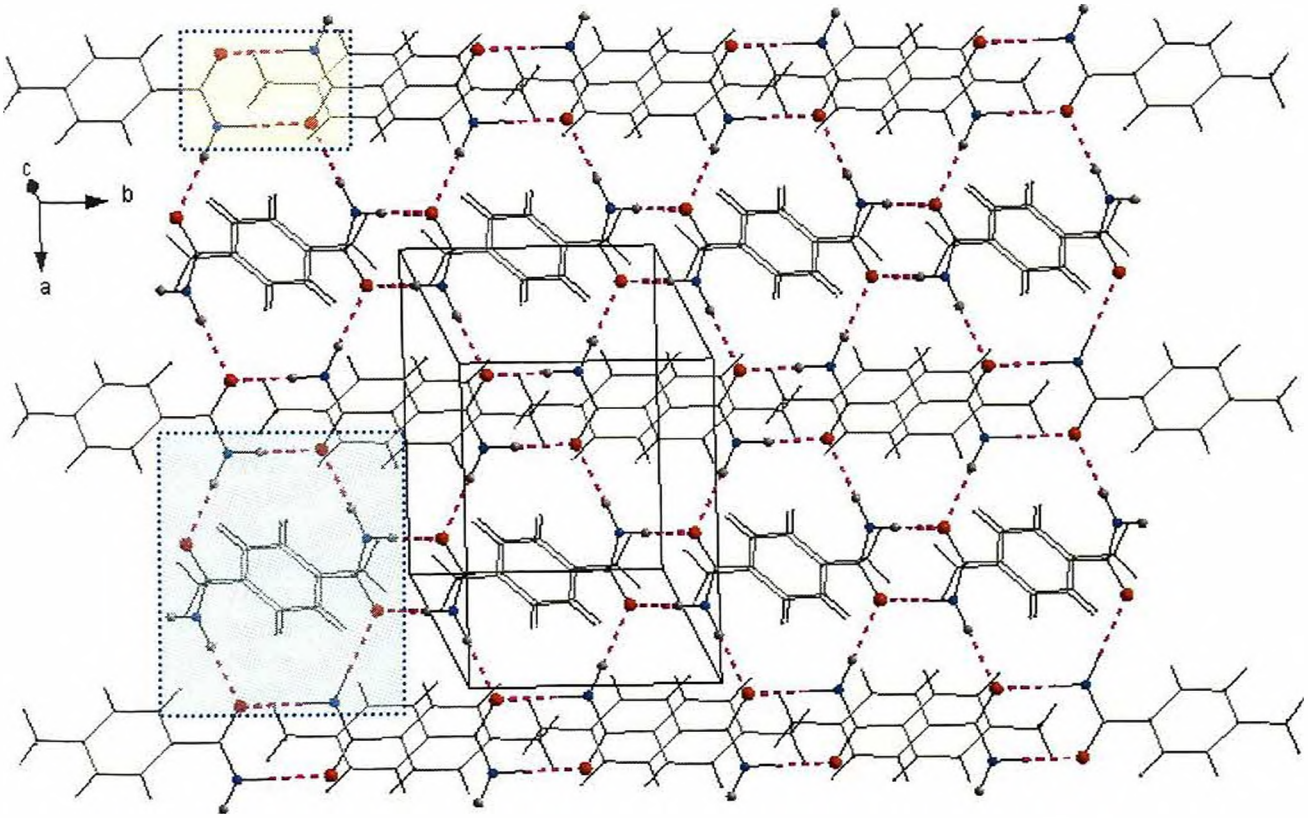

Figure 5.4.1: Puckered hydrogen bonded sheet along (110) plane for para-methylbenzamide, $R_2^2(8)$ and $R_6^4(16)$ motifs are illustrated using green and blue shaded areas respectively.

5.4.2 Structure prediction analysis - Para-methylbenzamide

Crystal structure prediction was performed in the space group $P2_1/c$ (14). No restraints were placed upon the molecular model, which was allowed to rotate through all degrees of freedom (as in figure 5.1.1). The prediction calculation generated 250 theoretical crystal structures, ranging in energy from –7.88 to –4.07 kcalmol^{-1}. Table 5.4.2 shows the top 30 predicted models and their corresponding unit cell parameters.

No.	Volume (Å^3)	Density (gcm^{-3})	Lattice energy (kcalmol^{-1})	a (Å)	b (Å)	c (Å)	β (°)
1	694.21	1.29	-7.89	11.72	9.73	8.63	135.12
2	696.86	1.29	-7.82	8.49	9.62	8.55	87.57
3	722.58	1.24	-7.06	9.62	17.23	13.17	160.67
4	721.19	1.24	-6.87	5.10	6.24	22.87	82.26
5	723.37	1.24	-6.68	5.08	5.36	27.61	106.05
6	730.60	1.23	-6.56	5.15	27.65	5.15	94.08
7	721.11	1.25	-6.55	8.00	6.41	24.13	144.37
8	707.68	1.27	-6.50	33.26	5.86	35.03	174.05
9	711.35	1.26	-6.48	27.22	6.73	20.64	169.16
10	742.74	1.21	-6.46	12.71	8.44	9.48	133.10
11	737.06	1.22	-6.46	5.01	29.04	7.16	134.98
12	724.26	1.24	-6.38	12.74	8.61	9.86	137.92
13	711.61	1.26	-6.38	7.11	30.91	5.75	145.77
14	733.78	1.22	-6.37	5.16	28.16	7.02	134.01
15	744.63	1.21	-6.35	10.00	5.03	14.87	84.29
16	713.74	1.26	-6.34	3.97	31.10	7.11	125.66
17	740.88	1.21	-6.31	7.87	24.02	6.08	139.85
18	743.18	1.21	-6.30	7.18	29.63	11.28	161.95
19	742.99	1.21	-6.29	7.43	28.32	5.25	137.76
20	727.59	1.23	-6.22	5.12	20.99	10.94	141.81
21	744.49	1.21	-6.21	5.16	17.22	12.96	40.26
22	712.19	1.26	-6.20	32.29	5.92	33.91	173.69
23	713.63	1.26	-6.19	24.35	4.47	24.63	164.58
24	746.59	1.20	-6.18	5.08	23.06	6.61	105.27
25	747.92	1.20	-6.15	13.07	6.83	9.19	114.21
26	723.27	1.24	-6.12	9.19	10.33	12.25	141.55
27	706.17	1.27	-6.12	35.09	4.01	32.26	171.05
28	700.27	1.28	-6.11	11.04	9.85	10.18	140.73
29	728.97	1.23	-6.09	8.00	6.40	14.85	106.48
30	724.03	1.24	-6.07	9.25	10.39	11.53	139.24

Table 5.4.2: Top 30 predicted structures for para-methylbenzamide (IV).

5.4.3 Re-ranking of structure prediction results - Para-methylbenzamide

Ranked according to lattice energy ($kcalmol^{-1}$)		Ranked according to Hbonding merit points		Ranked according to graphset merit points	
1	**-7.89**	**10**	**42.00**	**1**	**2**
2	**-7.82**	12	40.56	**2**	**2**
3	**-7.06**	**3**	**40.00**	**3**	**2**
4	-6.87	4	40.00	4	2
5	-6.68	5	40.00	6	2
6	-6.56	6	40.00	**10**	**2**
7	-6.55	11	40.00	11	2
8	-6.50	14	40.00	14	2
9	-6.48	15	40.00	15	2
10	**-6.46**	17	40.00	17	2
11	-6.46	18	40.00	18	2
12	-6.38	19	40.00	19	2
13	-6.38	20	40.00	20	2
14	-6.37	21	40.00	21	2
15	-6.35	24	40.00	24	2
16	-6.34	25	40.00	5	1
17	-6.31	**2**	**39.91**	8	1
18	-6.30	27	39.36	9	1
19	-6.29	**1**	**38.79**	12	1
20	-6.22	29	36.45	16	1
21	-6.21	7	35.25	22	1
22	-6.20	9	30.85	23	1
23	-6.19	8	20.00	25	1
24	-6.18	13	20.00	27	1
25	-6.15	16	20.00	28	1
26	-6.12	22	20.00	29	1
27	-6.12	23	20.00	30	1
28	-6.11	26	20.00	7	0
29	-6.09	28	20.00	13	0
30	-6.08	30	20.00	26	0

Table 5.4.3: Top 30 predicted structures for para-methylbenzamide (IV) re-ranked according to hydrogen bonding and graph set merit points. Highlighted structures show similarity to experimental structure.

The re-ranking procedure (table 5.4.3) shows that a total of 14 theoretical structures have the expected maximum 40 hydrogen bonding merit points and 16 structures have 2 graph set merit points highlighting the presence of the characteristic structural motifs expected in amide crystal structures. All theoretical structures with maximum merit points were examined further. However, only structures 1, 2, 3 and 10 are discussed in more detail (highlighted) either due to their similarity to the experimentally determined structure or due to their behaviour in the re-ranking process.

Para-methylbenzamide structure 1 is clearly the most energetically favourable and despite having the maximum graphset assignment points, it has been re-ranked to position 18 in terms of hydrogen bonding merit points (table 5.4.3). The packing arrangement of structure 1 comprises the amide $R_2^2(8)$ dimers of type N-H...O=C around (0,0,0) which are linked to 4 others by C(4) chains generating a secondary network of $R_6^6(16)$ rings along the (011) plane (figures 5.4.2). However, unlike the experimental crystal structure, the sheets generated in structure 30 are not puckered and is simply due to the orientation of the dimers.

		D-H	H...A	D...A	D-H...A
1	N(66) --H(75) ..O(67)	0.9600	2.0800	3.0295	170.00
2	N(66) --H(76) ..O(67)	0.9700	2.3100	3.2450	164.00

1 N(66) --H(75) ..O(67): 2.08 merit = 10
2 N(66) --H(76) ..O(67): 2.31 merit = 8.79

1 N(66) --H(75) ..O(67): 170 merit = 10
2 N(66) --H(76) ..O(67): 164 merit = 10

TOTAL MERIT FOR POLYMORPH 1 = 38.79

Table 5.4.4: Hydrogen bonding information generated by the re-ranking strategy for para-methylbenzamide structure 1.

Para-methylbenzamide structure 2 has also dropped down the rankings in terms of hydrogen bonding merit points but has maximum graphset assignment points (table 5.4.3). The crystal packing arrangement is similar to that of structure 1: $R_2^2(8)$ dimers of type N-H...O=C are linked through C(4) chains generating a secondary network of $R_6^6(16)$ rings forming infinite sheets running along the (011) plane (figures 5.4.3). The

hydrogen bonding merit points are also reduced for this structure because the NH...O distance within the $R_2^2(8)$ dimers is relatively long (2.23Å).

		D-H	H...A	D...A	D-H...A
1	N(66) --H(75) ..O(67)	0.9600	2.0900	3.0346	167.00
2	N(66) --H(76) ..O(67)	0.9700	2.2300	3.1721	164.00

1 N(66) --H(75) ..O(67): 2.09 merit = 10
2 N(66) --H(76) ..O(67): 2.23 merit = 9.91

1 N(66) --H(75) ..O(67): 167 merit = 10
2 N(66) --H(76) ..O(67): 164 merit = 10

TOTAL MERIT FOR POLYMORPH 2 = 39.91

Table 5.4.5: Hydrogen bonding information generated by the re-ranking strategy for para-methylbenzamide structure 2.

Para-methylbenzamide structure 3 has remained unchanged in ranking terms for both hydrogen bonding and graphset assignment merit points (table 5.4.3). The packing arrangement of structure 3 also contains centrosymmetric amide $R_2^2(8)$ dimers of type N-H...O=C formed around (0, ½, 0). The second amino hydrogen forms an additional N-H...O=C hydrogen bond with adjacent dimers and through formation of a C(4) chain generates a secondary network of $R_4^4(8)$ rings and ladders that run along the [101] direction (figure 5.4.4).

		D-H	H...A	D...A	D-H...A
1	N(66) --H(75) ..O(67)	0.9600	2.0600	3.0175	169.00
2	N(66) --H(76) ..O(67)	0.9700	2.1500	3.0956	165.00

1 N(66) --H(75) ..O(67): 2.06 merit = 10
2 N(66) --H(76) ..O(67): 2.15 merit = 10

1 N(66) --H(75) ..O(67): 169 merit = 10
2 N(66) --H(76) ..O(67): 165 merit = 10

TOTAL MERIT FOR POLYMORPH 3 = 40

Table 5.4.6: Hydrogen bonding information generated by the re-ranking strategy for para-methylbenzamide structure 3.

Para-methylbenzamide structure 10 is most like the experimental structure and consequently has been moved up to position 1 in terms of hydrogen bonding merit points and has remained in the top 5 with respect to graph set assignment points (table 5.4.3). The packing within structure 10 contains characteristic amide $R_2^2(8)$ dimers and C(4) chain motifs linking each dimer to 4 others generating a secondary network of $R_4^4(16)$ rings along the (011) plane. The difference between structure 10 and the experimental crystal structure is a subtle difference in the orientation of the phenyl rings and more obviously the direction of the ladders and the plane along which the puckered sheet runs. An additional 2 hydrogen bonding merit points have been awarded to this structure because of additional C-H...O hydrogen bonds within the packing arrangement (figures 5.4.5).

		D-H	H...A	D...A	D-H...A
1	N(66) --H(75) ..O(67)	0.9700	2.0700	3.0328	175.00
2	N(66) --H(76) ..O(67)	0.9700	2.1400	3.0954	171.00
3	C(59) --H(68) ..O(67)	1.0200	2.5400	3.3640	137.00

1 N(66) --H(75) ..O(67): 2.07 merit = 10
2 N(66) --H(76) ..O(67): 2.14 merit = 10
3 C(59) --H(68) ..O(67): 2.54 merit = 1

1 N(66) --H(75) ..O(67): 175 merit = 10
2 N(66) --H(76) ..O(67): 171 merit = 10
3 C(59) --H(68) ..O(67): 137 merit = 1

TOTAL MERIT FOR POLYMORPH 10 = 40

Table 5.4.7: Hydrogen bonding information generated by the re-ranking strategy for para-methylbenzamide structure 10.

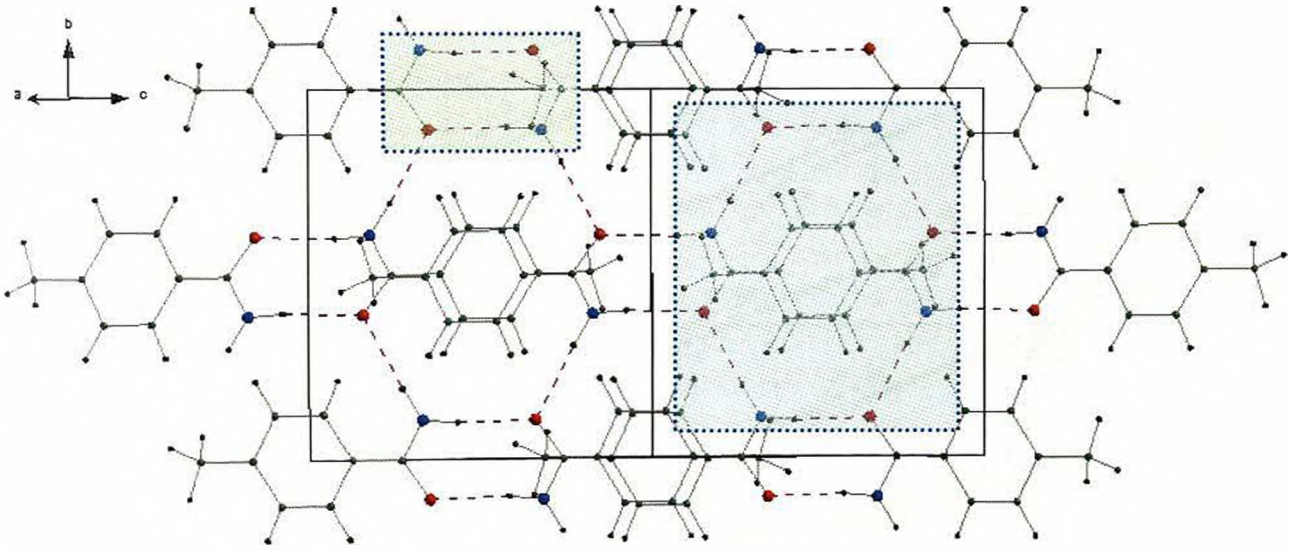

Figure 5.4.2: Formation of sheets in the (011) plane for para-methylbenzamide structure 1. $R_2^2(8)$ dimers and $R_4^4(16)$ motifs are illustrated using green and blue shaded areas respectively.

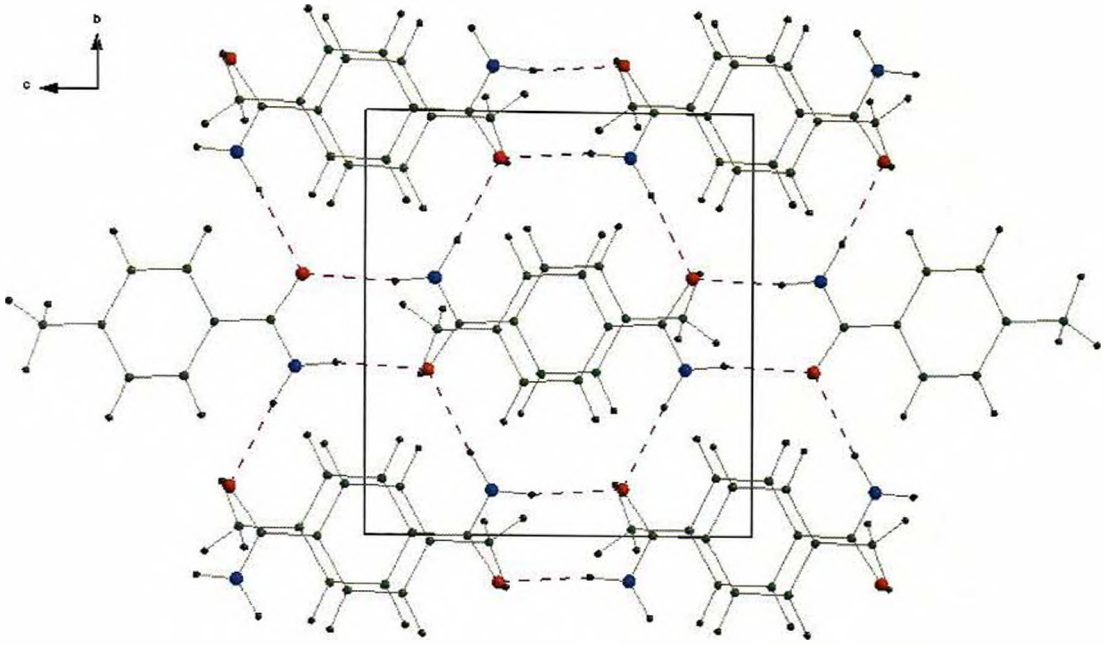

Figure 5.4.3: Sheets in the (011) plane for para-methylbenzamide structure 2.

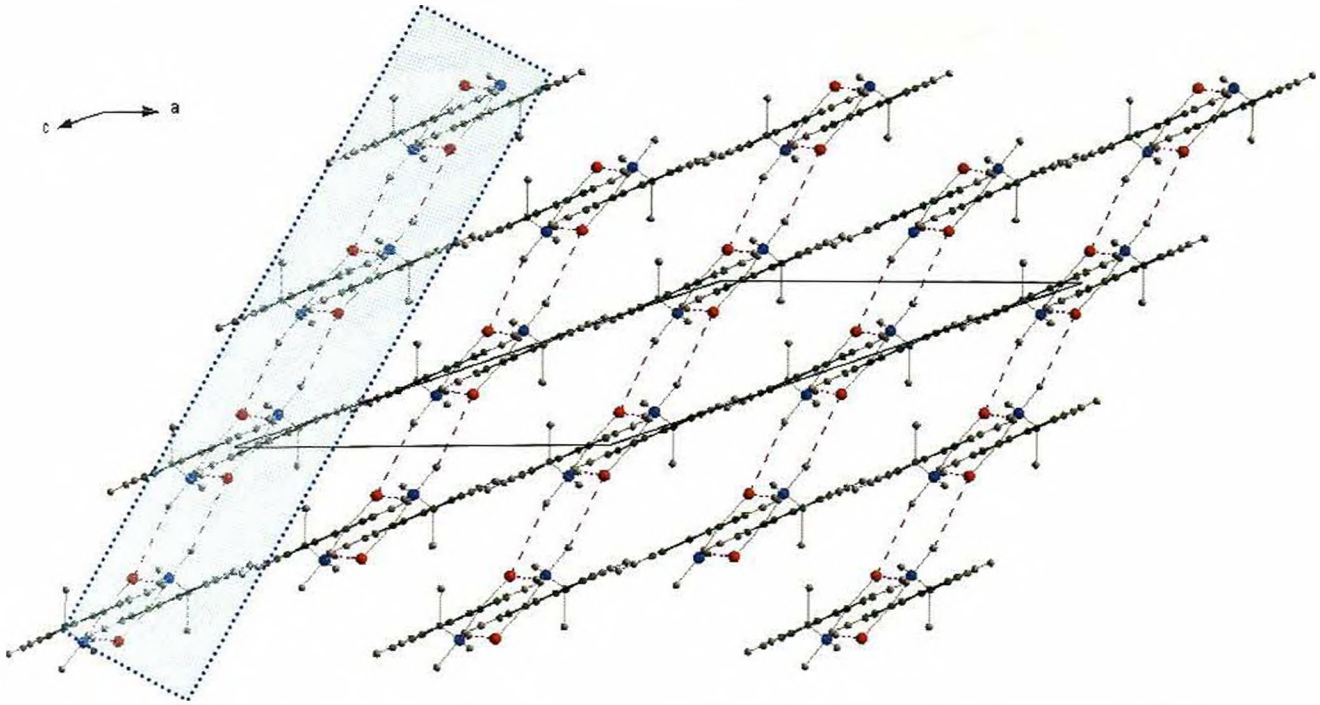

Figure 5.4.4: para-methylbenzamide structure 3 showing the ladders running along the [101] direction (blue shaded area).

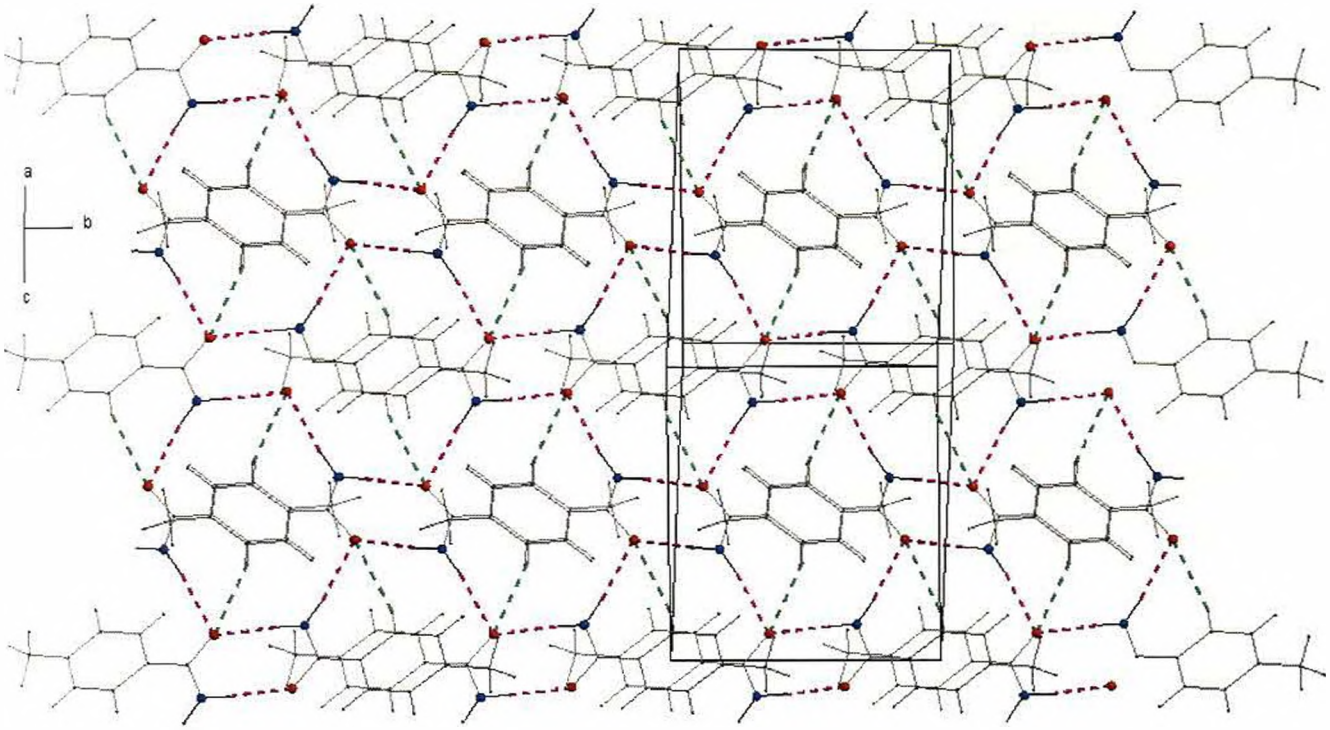

Figure 5.4.5: Hydrogen bonded sheets along (011) plane for para-methylbenzamide structure 10. Green dashed lines illustrate the additional C-H...O hydrogen bonds.

Simulated powder X-ray diffraction data were used to compare the experimental structure with the predicted para-methylbenzamide structures 1,2, 3 and 10 (see figure 5.4.6). On comparison all the powder patterns appear to be different to the experimental X-ray diffraction pattern. It is surprising that the simulated powder pattern for para-methylbenzamide structure 10 isn't similar compared to the experimental X-ray diffraction pattern since there is significant resemblance in the hydrogen bonding between the two structures.

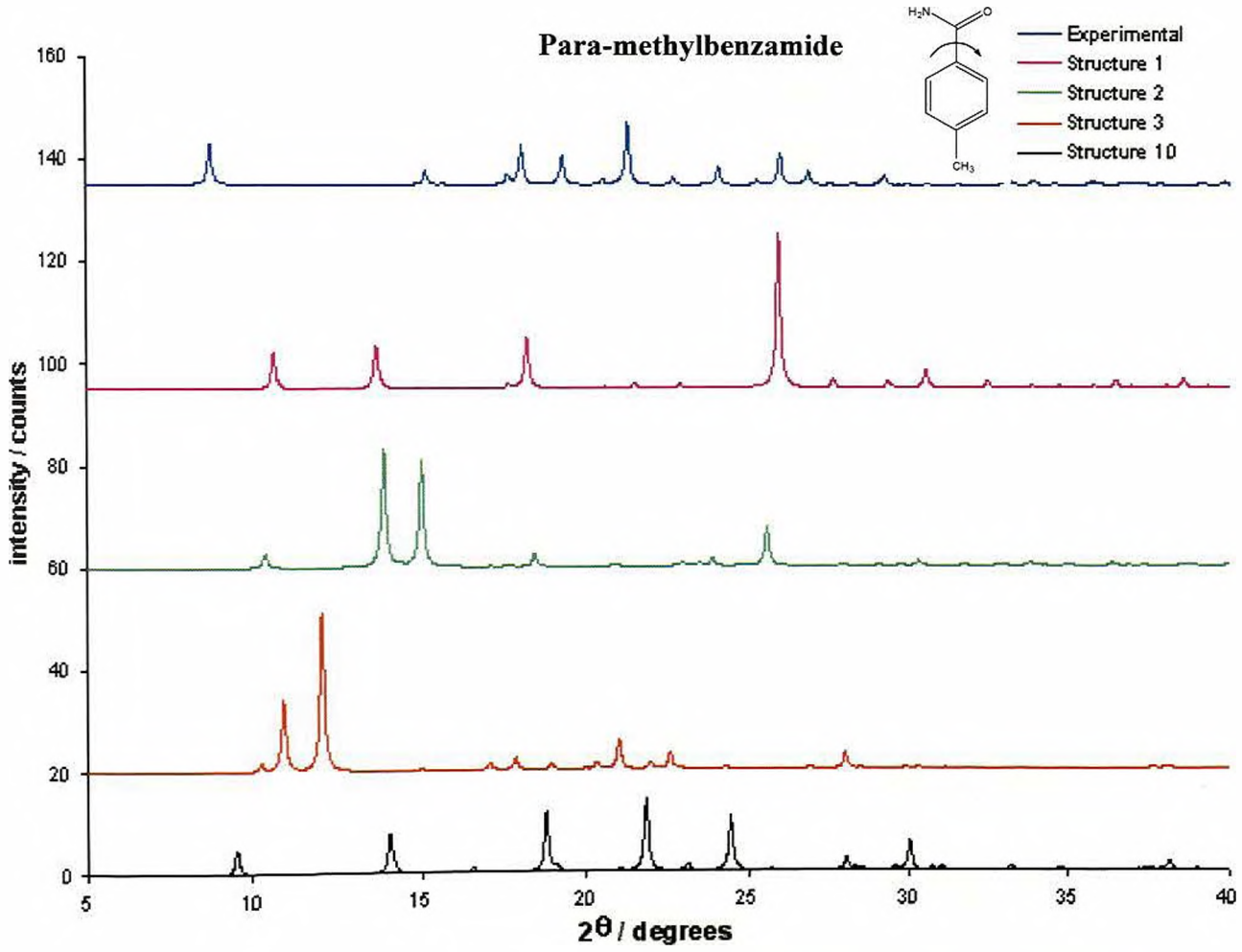

Figure 5.4.6: Comparison of the experimental X-ray diffraction pattern of para methylbenzamide with the simulated powder patterns for para-methylbenzamide structures 1, 2, 3 and 10.

5.5 Oxamide

5.5.1 Experimental crystal structure

The crystal structure of oxamide (V) [Swaminathan. K.S. and Craven. B.M. 1982] has been determined using conventional single crystal X-ray diffraction data, although the hydrogen atoms were placed in idealised positions and not refined. The unit cell parameters, space group and single point minimised lattice energy of the experimentally determined crystal structure are given in table 5.5.1.

a (Å)	3.56(2)
b (Å)	5.17(1)
c (Å)	5.64(1)
α (°)	83.93(2)
β (°)	143.38(1)
γ (°)	115.22(1)
Volume ($Å^3$)	86.654(14)
Density (gcm^{-3})	1.667(2)
Space group	P-1 (2)
Z	1
Single point minimised lattice energy ($kcalmol^{-1}$)	-1.01

Table 5.5.1: The crystallographic and lattice energy data for experimentally determined oxamide.

The crystal structure of oxamide (V) comprises the oxamide molecules lying on a inversion centre (000) and held together in infinite sheets by N-H···O=C hydrogen bonds (see figure 5.5.1). The amino N atom acts as a double hydrogen bond donor forming $R_2^2(8)$ dimers and C(4) chains which combine to form a secondary hydrogen

bonding network of $R_1^2(8)$ rings leading to the formation of ladders that extend in the [010] direction. These ladders are held together through the molecules themselves to form hydrogen bonded sheets parallel to (011). The sheets are stacked such that the $R_2^2(8)$ dimers are situated directly above and below one another by a distance which is exactly the length of axis *a* (d = 3.56Å). This molecular arrangement makes it conducive for π-π stacking of the sheets, see figures 5.5.1 and 5.5.2.

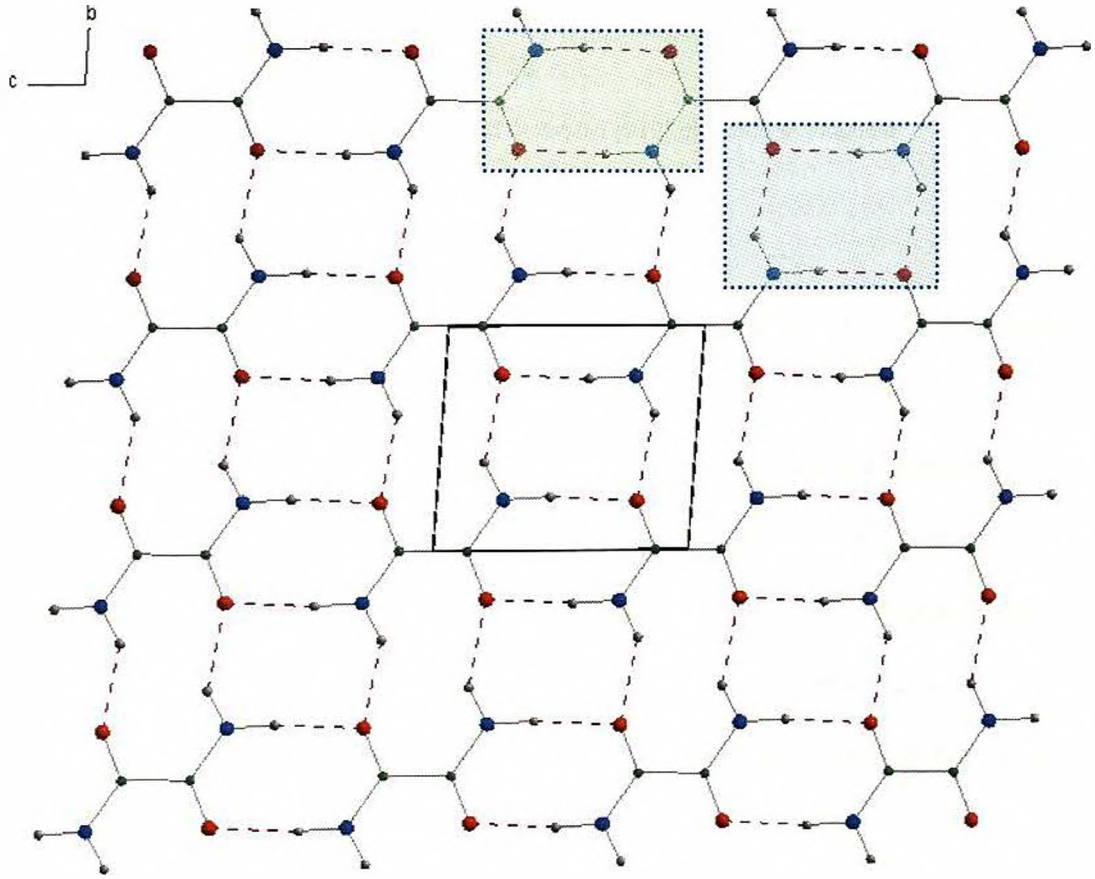

Figure 5.5.1: A hydrogen bonded sheet in the (011) plane for oxamide. Hydrogen bonding $R_2^2(8)$ and $R_1^2(8)$ motifs are also illustrated using green and blue shading respectively.

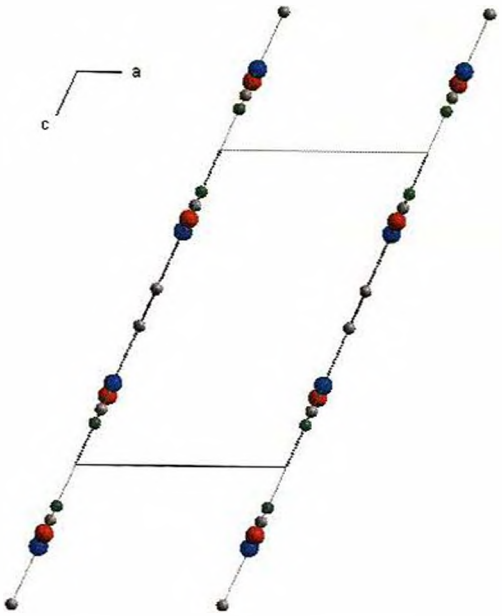

Figure 5.5.2: Hydrogen bonded sheets viewed down the [010] direction in oxamide.

5.5.2 Structure prediction analysis - Oxamide

Crystal structure was prediction was performed in space group P-1 (2). No restraints were placed upon the molecular model, which was allowed to rotate through all degrees of freedom (as in figure 5.1.1). The prediction calculation generated only 1 theoretical crystal structure of energy –3.36 kcalmol^{-1}. The combination of both the sheer simplicity of the oxamide molecule and the space group P-1 (2) is probably why only 1 model was predicted although the prediction was carried out considering a general position of the molecule with no implication of inversion symmetry within the molecular model. Table 5.5.2 gives details of the predicted structure.

No.	Volume (Å^3)	Density (gcm^{-3})	Lattice energy (kcalmol^{-1})	a (Å)	b (Å)	c (Å)	α (°)	β (°)	γ (°)
1	87.93	1.66	-3.36	5.06	4.08	5.80	90.24	102.74	129.82

Table 5.5.2: Predicted structure for oxamide (V).

5.5.3 Re-ranking of structure prediction results - Oxamide

Ranked according to lattice energy ($kcalmol^{-1}$)		Ranked according to Hbonding merit points		Ranked according to graphset merit points	
1	-3.36	1	80.00	1	2

Table 5.5.3: Predicted structure for oxamide (V) according to hydrogen bonding and graph set merit points. Highlighted structure shows similarity to experimental structure.

Assessment of this theoretical structure (table 5.5.3) shows that it has the maximum 80 hydrogen bonding merit points and the 2 graph set assignment merit points. This structure has a packing arrangement, which resembles the experimental crystal structure with the molecule on the centre of inversion (000). A hydrogen bonded network of C(4) chains, centrosymmetric $R_2^2(8)$ dimers and $R_4^2(8)$ rings are generated forming an infinite molecular sheet in the (101) plane. The distance between the sheets is longer at 4.08 Å, exactly the length of *b* axis (figures 5.5.3 and 5.5.4). Table 5.5.4 shows the hydrogen bonding ranking of this structure.

		D-H	H...A	D...A	D-H...A
1	1 N(3) --H(7) ..O(5)	0.9600	2.0500	3.0073	173.00
2	1 N(3) --H(8) ..O(6)	0.9600	2.0500	3.0088	177.00
3	1 N(4) --H(9) ..O(6)	0.9600	2.0500	3.0073	173.00
4	1 N(4) --H(10) ..O(5)	0.9600	2.0500	3.0087	177.00

1	1 N(3) --H(7) ..O(5):	2.05	merit = 10
2	1 N(3) --H(8) ..O(6):	2.05	merit = 10
3	1 N(4) --H(9) ..O(6):	2.05	merit = 10
4	1 N(4) --H(10) ..O(5):	2.05	merit = 10

1	1 N(3) --H(7) ..O(5):	173	merit = 10
2	1 N(3) --H(8) ..O(6):	177	merit = 10
3	1 N(4) --H(9) ..O(6):	173	merit = 10
4	1 N(4) --H(10) ..O(5):	177	merit = 10

TOTAL MERIT FOR POLYMORPH 1 = 80

Table 5.5.4: Hydrogen bonding merit points generated by the re-ranking strategy for oxamide structure 1.

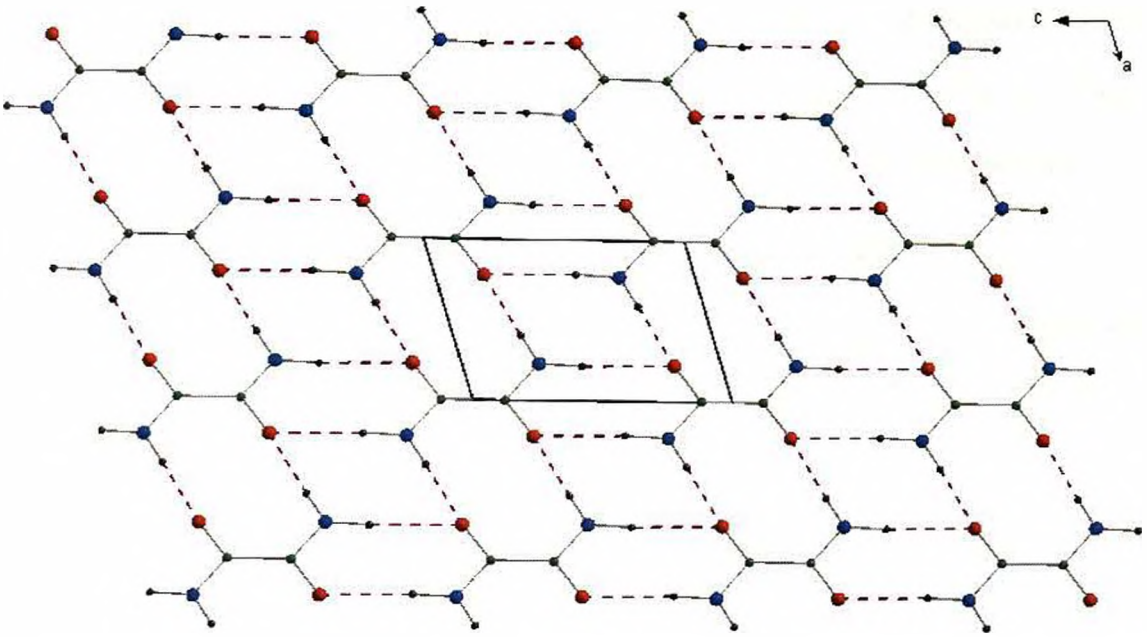

Figure 5.5.3: View of the theoretical structure showing the infinite sheet in the (101) plane in oxamide structure 1.

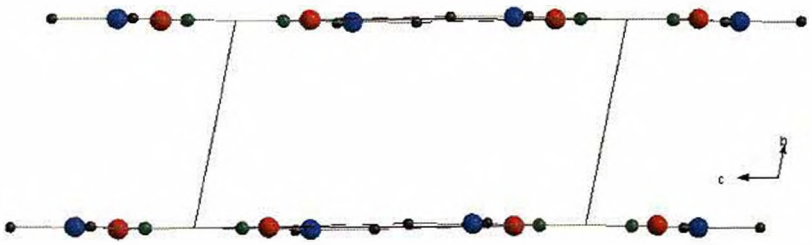

Figure 5.5.4: Hydrogen bonded sheets generated in the [010] direction in oxamide structure 1.

The experimental powder X-ray diffraction pattern of oxamide and simulated powder pattern of in oxamide structure 1.structure 1 is shown in figure 5.5.5. The two powder patterns are clearly different despite the striking similarities in the two structures.

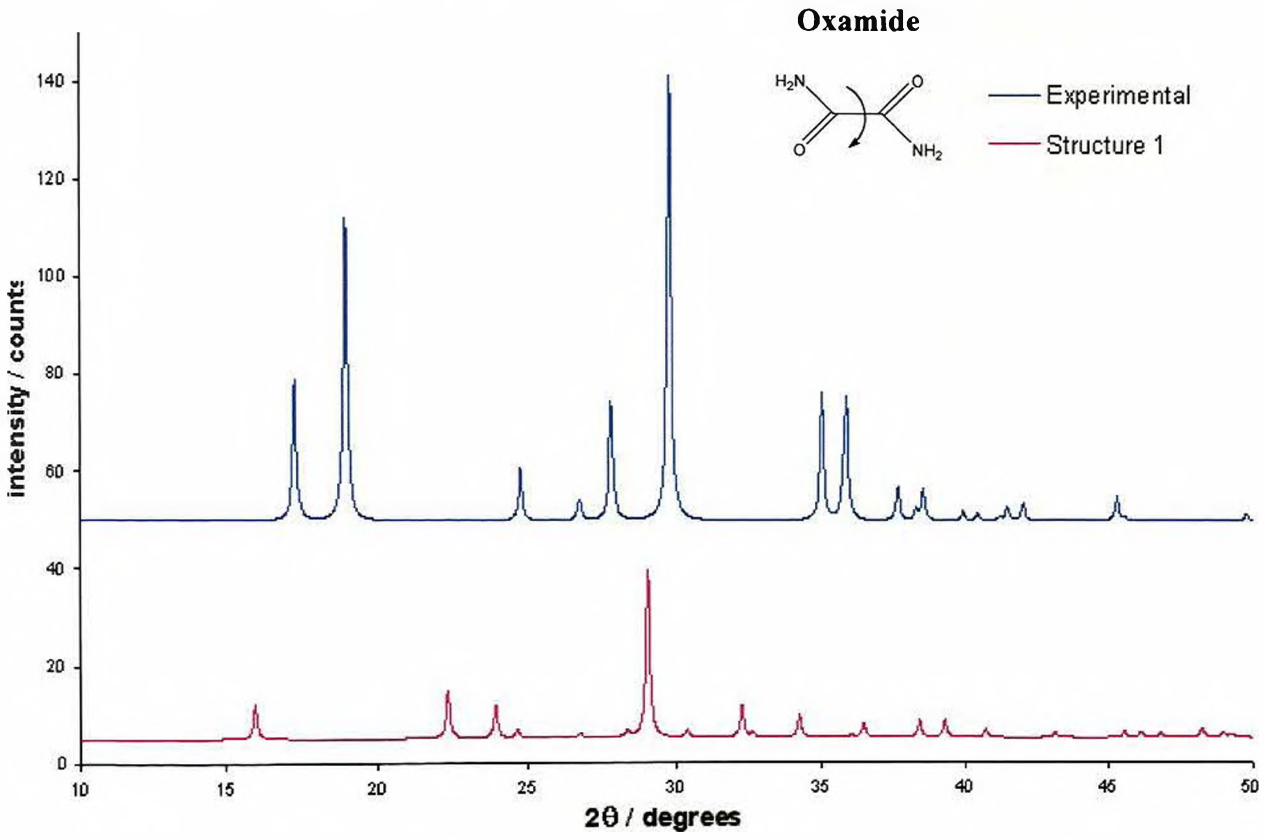

Figure 5.5.5: Comparison of the experimental and simulated X-ray diffraction patterns of oxamide.

5.6 Glutaramide

5.6.1 Experimental crystal structure

The crystal structure of glutaramide (VI) [Hospital. M. and Housty. J. 1966] has been determined using conventional single crystal X-ray diffraction data, although the hydrogen atoms were placed in idealised positions and not refined. The unit cell parameters, space group and single point minimised lattice energy of the experimentally determined crystal structure are given in table 5.6.1.

a (Å)	6.19(1)
b (Å)	8.26(1)
c (Å)	17.46(2)
β (°)	130.840(2)
Volume ($Å^3$)	675.4(16)
Density (gcm^{-3})	1.28(1)
Space group	C2/c (15)
Z	4
Single point minimised lattice energy ($kcalmol^{-1}$)	-35.99

Table 5.6.1: The crystallographic and lattice energy data for experimentally determined glutaramide.

The crystal packing arrangement in glutaramide (VI) is determined by two distinct N-H...O=C type hydrogen bonds. The amino N atom acts as a double donor forming the two characteristic motifs; the $R_2^2(8)$ dimer and C(4) chain, which combine to form a secondary $R_4^2(8)$ ring system. The amide groups within each molecule lie 90° with respect to one another such that an infinite three dimensional network is formed by

combination of ladders running along the [110] direction linked through the molecule itself to ladders along the [001] direction (figure 5.6.1 and 5.6.2).

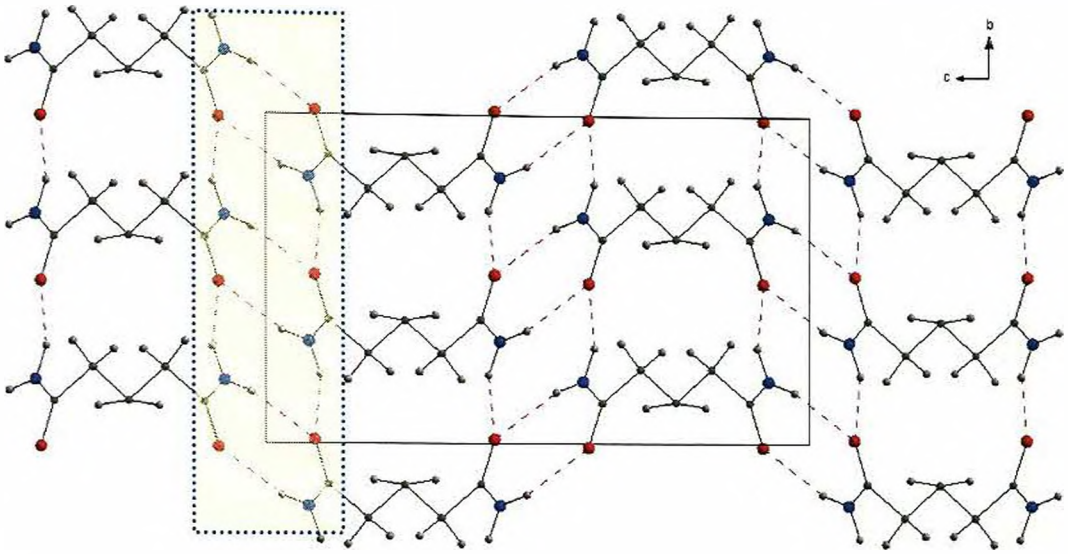

Figure 5.6.1: View of (VI) showing the ladders extending along the [110] direction (yellow shaded area).

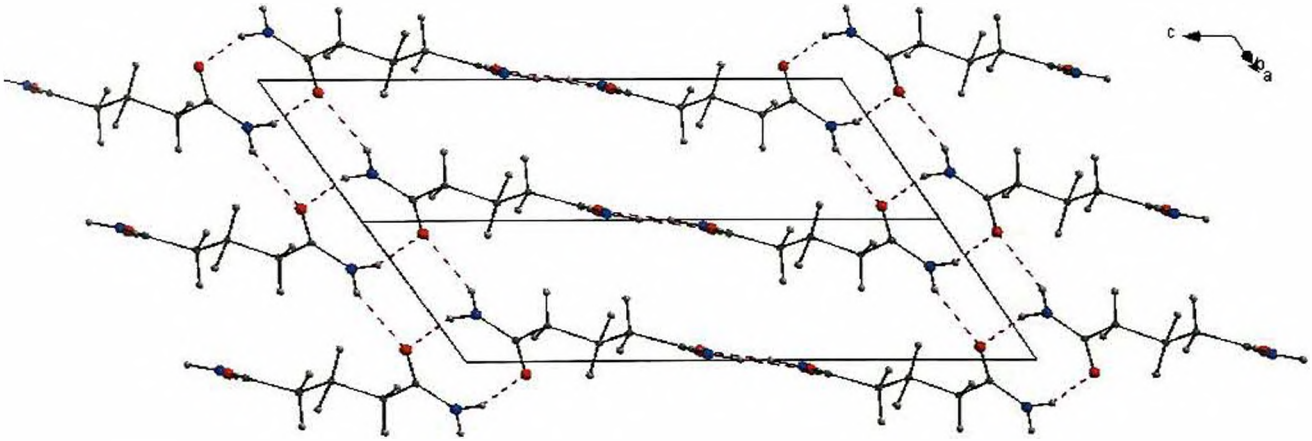

Figure 5.6.2: View of (VI) illustrating the infinite sheets in the [001] direction.

5.6.2 Structure prediction analysis - Glutaramide

Crystal structure prediction was performed in the space group C2/c (15). No geometric restraints were placed upon the molecular model, which was allowed to rotate through all degrees of freedom (as in figure 5.1.1). The prediction calculation

generated 250 theoretical crystal structures, ranging in energy from –39.81 to –34.84 kcalmol^{-1}. Table 5.6.2 shows the top 30 predicted structures for glutaramide and their corresponding unit cell parameters.

No.	Volume (Å^3)	Density (gcm^{-3})	Lattice energy (kcalmol^{-1})	a (Å)	b (Å)	c (Å)	β (°)
1	1324.38	1.31	-39.82	36.63	4.40	39.76	168.08
2	1340.78	1.29	-39.49	14.62	5.11	39.60	153.05
3	1336.84	1.29	-39.36	35.80	4.85	9.29	55.94
4	1382.96	1.25	-39.27	42.15	4.94	37.94	169.92
5	1339.14	1.29	-39.03	23.95	5.11	12.59	119.63
6	1274.31	1.36	-39.02	11.32	9.76	12.05	73.18
7	1389.14	1.24	-38.97	28.95	4.87	9.86	89.02
8	1349.75	1.28	-38.84	23.03	5.08	19.07	142.76
9	1385.93	1.25	-38.80	8.76	4.50	35.51	81.34
10	1278.80	1.35	-38.77	38.02	4.88	21.69	161.47
11	1283.96	1.35	-38.73	20.69	4.88	14.46	118.38
12	1414.88	1.22	-38.62	17.27	7.59	25.72	155.17
13	1363.42	1.27	-38.62	18.16	4.85	23.59	138.95
14	1324.53	1.31	-38.62	35.46	4.89	15.16	149.76
15	1436.39	1.20	-38.58	8.30	4.98	39.89	119.42
16	1352.48	1.28	-38.53	35.95	4.34	9.39	67.28
17	1296.17	1.33	-38.51	14.49	4.88	21.07	119.59
18	1335.80	1.29	-38.45	36.40	5.14	24.44	163.00
19	1457.93	1.19	-38.43	8.57	5.17	33.14	96.17
20	1359.36	1.27	-38.28	36.00	4.89	11.90	139.57
21	1388.74	1.24	-38.23	33.43	4.84	24.38	159.39
22	1354.06	1.28	-38.19	9.69	4.85	38.48	131.53
23	1480.74	1.17	-38.12	4.96	8.54	35.76	102.21
24	1452.42	1.19	-38.00	26.34	10.54	20.89	165.50
25	1301.81	1.33	-37.96	16.48	5.17	20.57	132.00
26	1374.56	1.26	-37.95	14.37	5.04	19.00	93.13
27	1332.92	1.30	-37.82	19.80	4.66	19.11	49.12
28	1324.97	1.30	-37.80	24.57	5.15	39.44	164.60
29	1347.65	1.28	-37.78	35.96	4.40	8.52	89.67
30	1377.84	1.25	-37.76	34.75	4.93	8.04	88.25

Table 5.6.2: Top 30 predicted structures for glutaramide (VI).

5.6.3 Re-ranking of structure prediction results - Glutaramide

Ranked according to lattice energy ($kcalmol^{-1}$)		Ranked according to Hbonding merit points		Ranked according to graphset merit points	
1	**-39.82**	**6**	**101.92**	**2**	**2**
2	**-39.49**	11	101.92	3	2
3	-39.36	17	101.88	4	2
4	-39.27	10	100.55	**7**	**2**
5	-39.03	**1**	**94.37**	8	2
6	**-39.02**	**29**	**93.28**	9	2
7	**-38.97**	**2**	**92.16**	10	2
8	-38.84	22	88.45	11	2
9	-38.80	20	88.39	13	2
10	-38.77	3	87.77	14	2
11	-38.73	25	84.03	15	2
12	-38.62	13	82.00	17	2
13	-38.62	4	80.00	18	2
14	-38.62	5	80.00	19	2
15	-38.58	**7**	**80.00**	21	2
16	-38.53	8	80.00	22	2
17	-38.51	9	80.00	23	2
18	-38.45	12	80.00	24	2
19	-38.43	15	80.00	25	2
20	-38.28	16	80.00	28	2
21	-38.23	19	80.00	**29**	**2**
22	-38.19	21	80.00	30	2
23	-38.12	23	80.00	**1**	**1**
24	-38.00	27	80.00	5	1
25	-37.96	30	80.00	**6**	**1**
26	-37.95	18	79.94	12	1
27	-37.82	24	79.94	16	1
28	-37.80	14	79.91	20	1
29	**-37.78**	16	79.65	26	1
30	-37.76	28	79.45	27	1

Table 5.6.3: Top 30 predicted structures for glutaramide (II) re-ranked according to hydrogen bonding and graph set merit points. Highlighted structures show similarity to experimental structure.

The re-ranking procedure (table 5.6.3) shows that only 13 theoretical structures have the expected maximum 80 hydrogen bonding merit points and 22 structures have 2 graph set merit points highlighting the presence of the characteristic structural motifs expected in amide crystal structures. However, 12 structures had bonding merit points greater than the expected maximum through formation of additional N-H...N type hydrogen bonds. All theoretical structures with maximum merit points were examined further. However, only structures 1, 2, 6, 7 and 29 are discussed in more detail (highlighted) either due to their similarity to the experimentally determined structure or due to their behaviour in the re-ranking process. One important factor to note is that

the volume of all the predicted structures are approximately double that of the experimental structure.

Glutaramide structure 1 is clearly the most energetically favourable structure but has fallen down the rankings to position 5 with respect to hydrogen bonding merit points and position 23 with respect to graph set assignment points (table 5.6.3). The structure comprises N-H...O=C type hydrogen bonds, however due to the orientation of the amide groups two alternative structural arrangements are formed which are joined through the molecule itself. On one side of the molecule, we have C(4) chains and $R_2^2(8)$ dimers that combine to form $R_4^2(8)$ rings and generate ladders. On the other side of the molecule C(4) chains and $R_4^2(8)$ rings combine to generate $R_4^4(16)$ rings (appearing to simulate $R_2^2(8)$ ladders), both arrangements run parallel to the (101) plane. Structure 1 has acquired 94.37 merit points through the presence of additional N-H...N type hydrogen bonds within it packing arrangement (figure 5.6.3).

		D-H	H...A	D...A	D-H...A
1	N(39) --H(49) ..O(41)	0.9600	2.2100	3.1095	155.00
2	N(39) --H(49) ..N(39)	0.9600	2.3900	3.2377	146.00
3	N(39) --H(50) ..O(41)	0.9600	2.0300	2.9881	177.00
4	N(40) --H(51) ..O(42)	0.9600	2.0400	3.0002	172.00
5	N(40) --H(52) ..O(42)	0.9600	2.0600	3.0263	176.00

3	N(39) --H(50) ..O(41):	2.03	merit = 10
4	N(40) --H(51) ..O(42):	2.04	merit = 10
5	N(40) --H(52) ..O(42):	2.06	merit = 10
1	N(39) --H(49) ..O(41):	2.21	merit = 9.99
2	N(39) --H(49) ..N(39):	2.39	merit = 6.39

3	N(39) --H(50) ..O(41):	177	merit = 10
4	N(40) --H(51) ..O(42):	172	merit = 10
5	N(40) --H(52) ..O(42):	176	merit = 10
1	N(39) --H(49) ..O(41):	155	merit = 9.85
2	N(39) --H(49) ..N(39):	146	merit = 8.14

TOTAL MERIT FOR POLYMORPH 1 = 94.37

Table 5.6.4: Hydrogen bonding merit points generated by the re-ranking strategy for glutaramide structure 1.

Glutaramide structure 2 has fallen down the rankings to position 7 with respect to hydrogen bonding merit points and risen to position 1 with respect to graph set assignment points (table 5.6.3). The structure comprises N-H…O=C type hydrogen bonds that generate C(4) chains and $R_2^2(8)$ amide dimers. These 2 motifs combine on a secondary level to form $R_4^4(8)$ rings and consequently very short twisted ladders in the [101] direction (comprising of 1 $R_2^2(8)$ dimer and 2 $R_4^4(8)$ rings), These ladders are then joined to form chains through a complex ring system that run along the [101] direction. Like structure 1, additional N-H…N hydrogen bonds are present within the packing arrangement and are responsible the additional hydrogen bonding merit points (figure 5.6.4).

		D-H	H...A	D...A	D-H...A
1	N(39) --H(49) ..O(41)	0.9600	2.1300	3.0466	159.00
2	N(39) --H(49) ..N(39)	0.9600	2.4300	3.2581	144.00
3	N(39) --H(50) ..O(42)	0.9600	2.0200	2.9843	176.00
4	N(40) --H(51) ..O(41)	0.9700	2.0700	3.0268	169.00
5	N(40) --H(52) ..O(42)	0.9600	2.0500	2.9952	168.00

1	N(39) --H(49) ..O(41):	2.13	merit = 10
3	N(39) --H(50) ..O(42):	2.02	merit = 10
4	N(40) --H(51) ..O(41):	2.07	merit = 10
5	N(40) --H(52) ..O(42):	2.05	merit = 10
2	N(39) --H(49) ..N(39):	2.43	merit = 4.71

3	N(39) --H(50) ..O(42):	176	merit = 10
4	N(40) --H(51) ..O(41):	169	merit = 10
5	N(40) --H(52) ..O(42):	168	merit = 10
1	N(39) --H(49) ..O(41):	159	merit = 9.91
2	N(39) --H(49) ..N(39):	144	merit = 7.54

TOTAL MERIT FOR POLYMORPH 2 = 92.16

Table 5.6.5: Hydrogen bonding merit points generated by the re-ranking strategy for glutaramide structure 2.

Glutaramide structure 6 has risen up the rankings to position 1 with respect to hydrogen bonding merit points and fallen to position 25 with respect graph set assignment points (table 5.6.3). The structure comprises of N-H…O=C type hydrogen bonds that generate C(4) chains and $R_2^2(8)$ amide dimers which form infinite chains along the (101)] plane. These 2 motifs combine on a secondary level to form $R_4^2(8)$ rings and consequently the formation of ladders in the [010] direction. These ladders are linked through the molecule itself to produce infinite sheets in the (101) plane. Structure 6 contains additional N-H…N hydrogen bonds within its packing arrangement and as a consequence has gained a substantial number of hydrogen bonding merit points (figure 5.6.5 and 5.6.6).

Glutaramide structure 7 most closely resembles the experimental crystal structure in that it contains ladders that run in a perpendicular fashion along two different axis. The structure has fallen down the rankings to position 15 with respect to hydrogen bonding merit points and risen to position 4 with respect to graph set assignment points (table 5.6.3). The structure has acquired the expected maximum of 80.00 hydrogen bonding merit points and 2 graph set assignment point indicating the presence of the characteristic amide motifs (table 5.6.7). The packing arrangement comprises of N-H···O=C type hydrogen bonds and form C(4) and $R_2^2(8)$ dimers which form infinite chains along the [010] direction. Combination of these two motifs gives rise to the secondary network of $R_4^2(8)$ rings resulting in the generation of ladders that extend along the *c* axis *b* axis in a perpendicular fashion. Structure 7 contains additional N-H…N hydrogen bonds however, the H…A distance has fallen outside the specified maximum of 2.5Å it has acquired no points, as a result of the merit points accumulated by the corresponding angle have automatically been assigned to

zero. Figures 5.6.7 and 5.6.8 shows the packing arrangement of structure 7 along the planes described.

		D-H	H...A	D...A	D-H...A
1	N(39) --H(49) ..O(41)	0.9600	2.1100	3.0362	160.00
2	N(39) --H(49) ..N(39)	0.9600	2.4500	3.2676	143.00
3	N(39) --H(50) ..O(42)	0.9700	2.1300	3.0522	160.00
4	N(39) --H(50) ..N(40)	0.9700	2.5000	3.0610	117.00
5	N(40) --H(51) ..O(42)	0.9600	2.1100	3.0362	160.00
6	N(40) --H(51) ..N(40)	0.9600	2.4500	3.2676	143.00
7	N(40) --H(52) ..O(41)	0.9700	2.1300	3.0522	160.00
8	N(40) --H(52) ..N(39)	0.9700	2.5000	3.0610	117.00

1	N(39) --H(49) ..O(41): 2.11	merit = 10
3	N(39) --H(50) ..O(42): 2.13	merit = 10
5	N(40) --H(51) ..O(42): 2.11	merit = 10
7	N(40) --H(52) ..O(41): 2.13	merit = 10
2	N(39) --H(49) ..N(39): 2.45	merit = 3.75
4	N(39) --H(50) ..N(40): 2.50	merit = 1 => 0
6	N(40) --H(51) ..N(40): 2.45	merit = 3.75
8	N(40) --H(52) ..N(39): 2.50	merit = 1 => 0

1	N(39) --H(49) ..O(41): 160	merit = 10
3	N(39) --H(50) ..O(42): 160	merit = 10
5	N(40) --H(51) ..O(42): 160	merit = 10
7	N(40) --H(52) ..O(41): 160	merit = 10
2	N(39) --H(49) ..N(39): 143	merit = 7.21
4	N(39) --H(50) ..N(40): 117	merit = 0
6	N(40) --H(51) ..N(40): 143	merit = 7.21
8	N(40) --H(52) ..N(39): 117	merit = 0

TOTAL MERIT FOR POLYMORPH 6 = 101.92

Table 5.6.6: Hydrogen bonding information generated by the re-ranking strategy for glutaramide structure 6.

		D-H	H...A	D...A	D-H...A
1	N(39) --H(49) ..O(41)	0.9600	2.1100	3.0367	162.00
2	N(39) --H(49) ..N(39)	0.9600	2.5400	3.3439	142.00
3	N(39) --H(50) ..O(41)	0.9600	2.0800	3.0118	162.00
4	N(40) --H(51) ..O(42)	0.9600	2.0300	2.9885	176.00
5	N(40) --H(52) ..O(42)	0.9600	2.0500	2.9977	169.00

1 N(39) --H(49) ..O(41): 2.11 merit = 10
3 N(39) --H(50) ..O(41): 2.08 merit = 10
4 N(40) --H(51) ..O(42): 2.03 merit = 10
5 N(40) --H(52) ..O(42): 2.05 merit = 10
2 N(39) --H(49) ..N(39): 2.54 merit = 0

1 N(39) --H(49) ..O(41): 162 merit = 10
3 N(39) --H(50) ..O(41): 162 merit = 10
4 N(40) --H(51) ..O(42): 176 merit = 10
5 N(40) --H(52) ..O(42): 169 merit = 10
2 N(39) --H(49) ..N(39): 142 merit = 6.86 => 0

TOTAL MERIT FOR POLYMORPH 7 = 80.00

Table 5.6.7: Hydrogen bonding merit points generated by the re-ranking strategy for glutaramide structure 7.

Glutaramide structure 29 has shown a very dramatic movement within the re-ranking tables, moving to positions 6 and 21 with respect to hydrogen bonding and graph set assignment merit points respectively (table 5.6.3). The structure comprises of N-H...O=C type hydrogen bonds that like structure 1 form two alternative structural arrangements which are joined through the molecule itself. On one side of the molecule, we have C(4) chains and $R_2^2(8)$ dimers that combine to form $R_4^2(8)$ rings and generate ladders. On the other side of the molecule 4 $R_2^2(8)$ dimers combine to generate $R_4^6(16)$ rings, both arrangements run parallel to the (101) plane. Structure 29 has acquired 93.28 merit points through the presence of additional N-H...N type hydrogen bonds within it packing arrangement (figure 5.6.9).

		D-H	H...A	D...A	D-H...A
1	N(39) --H(49) ..O(41)	0.9600	2.0500	3.0057	170.00
2	N(39) --H(50) ..O(41)	0.9700	2.2100	3.1399	161.00
3	N(40) --H(51) ..O(42)	0.9600	2.1900	3.0937	155.00
4	N(40) --H(51) ..N(40)	0.9600	2.4100	3.2479	145.00
5	N(40) --H(52) ..O(42)	0.9600	2.0300	2.9961	177.00

1	N(39) --H(49) ..O(41):	2.05	merit = 10
3	N(40) --H(51) ..O(42):	2.19	merit = 10
5	N(40) --H(52) ..O(42):	2.03	merit = 10
2	N(39) --H(50) ..O(41):	2.21	merit = 9.99
4	N(40) --H(51) ..N(40):	2.41	merit = 5.59

1	N(39) --H(49) ..O(41):	170	merit = 10
2	N(39) --H(50) ..O(41):	161	merit = 10
5	N(40) --H(52) ..O(42):	177	merit = 10
3	N(40) --H(51) ..O(42):	155	merit = 9.85
4	N(40) --H(51) ..N(40):	145	merit = 7.85

TOTAL MERIT FOR POLYMORPH 29 = 93.28

Table 5.6.8: Hydrogen bonding merit points generated by the re-ranking strategy for glutaramide structure 29.

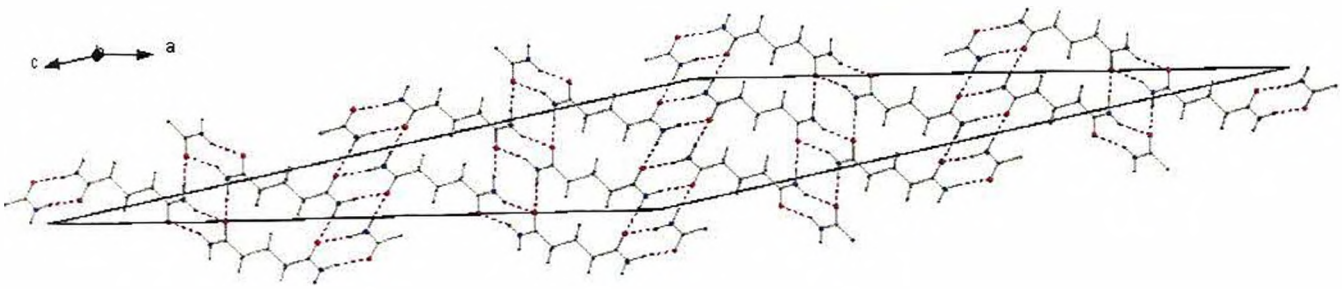

Figure 5.6.3: View of glutaramide structure 1 showing sheets in the (101) plane.

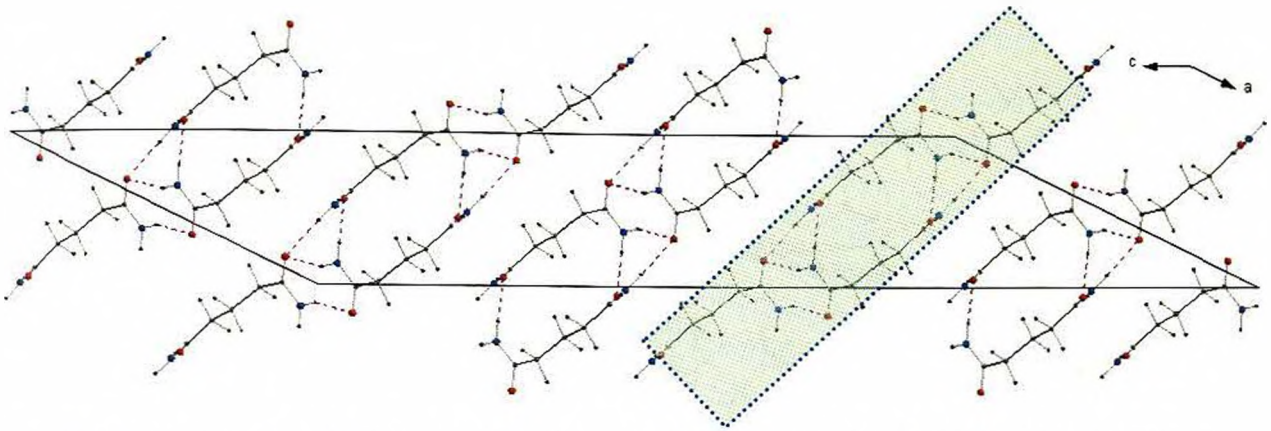

Figure 5.6.4: View of glutaramide structure 2 showing chains running along the [101] direction (green shaded area).

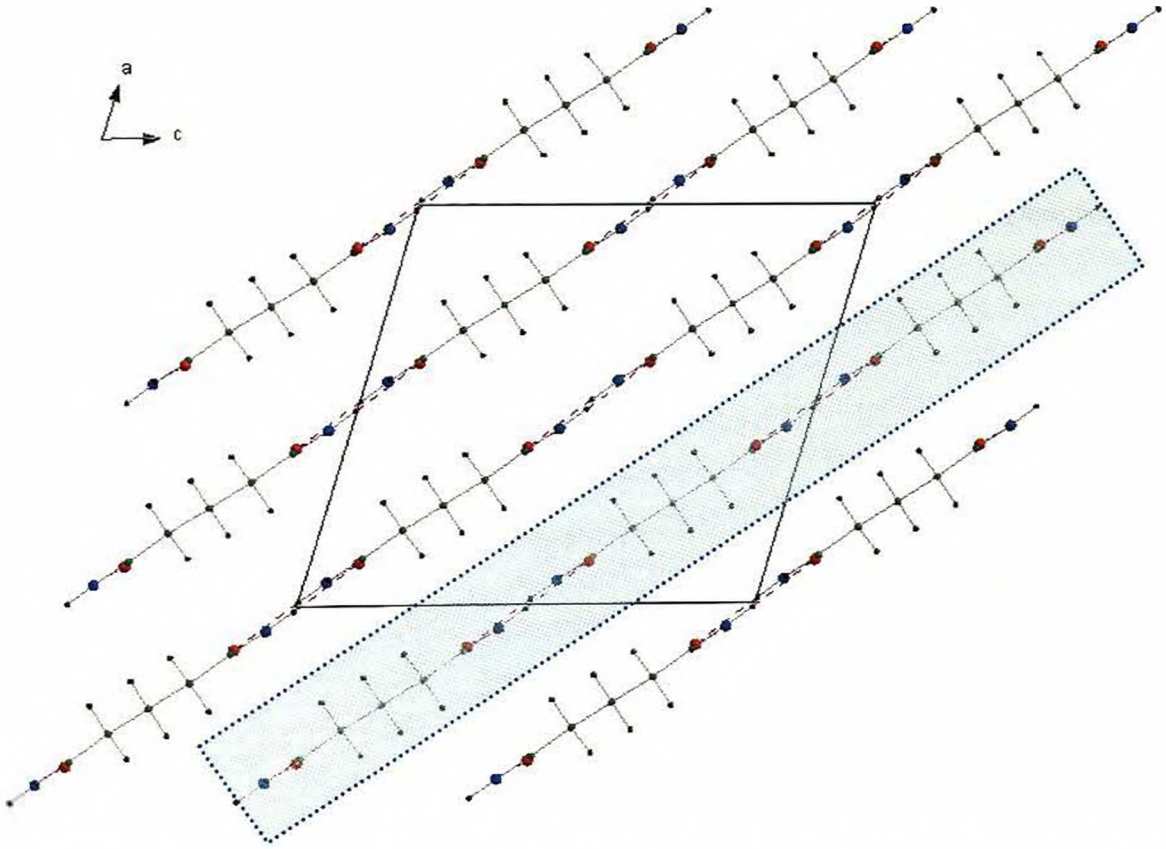

Figure 5.6.5: View of glutaramide structure 6 showing chains along the [101] direction (blue shaded area).

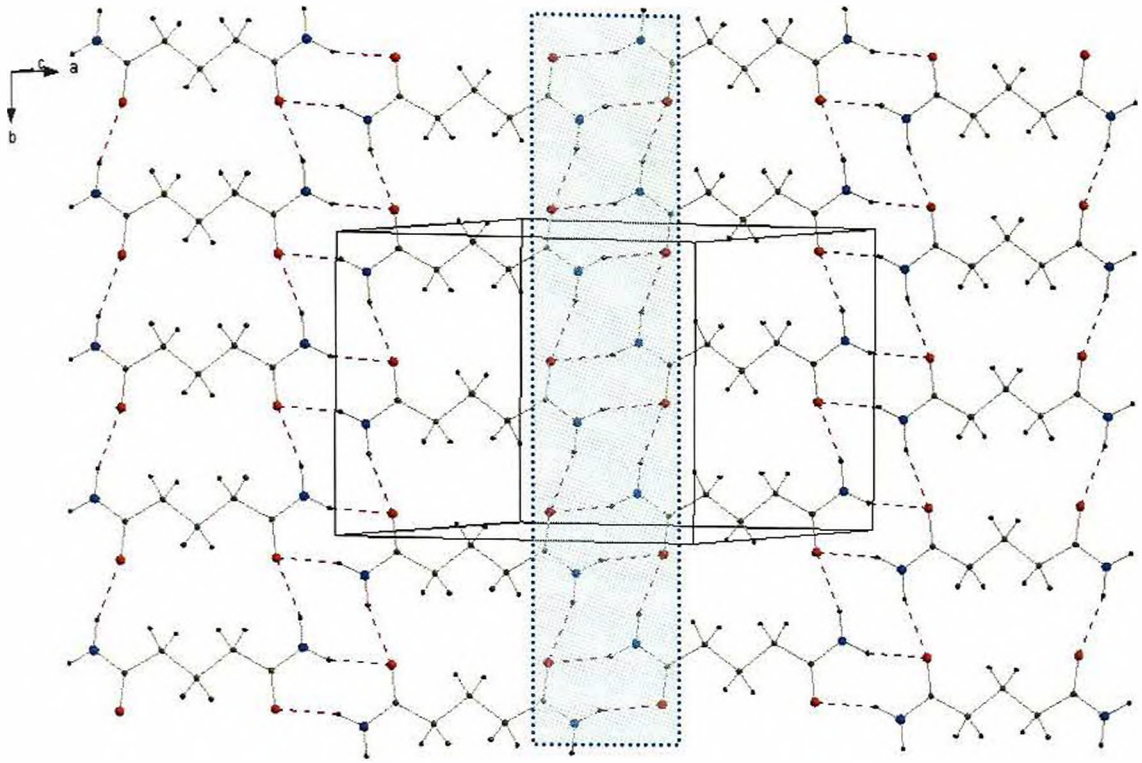

Figure 5.6.6: View of glutaramide structure 6 showing the ladders running along the [010] direction (blue shaded area).

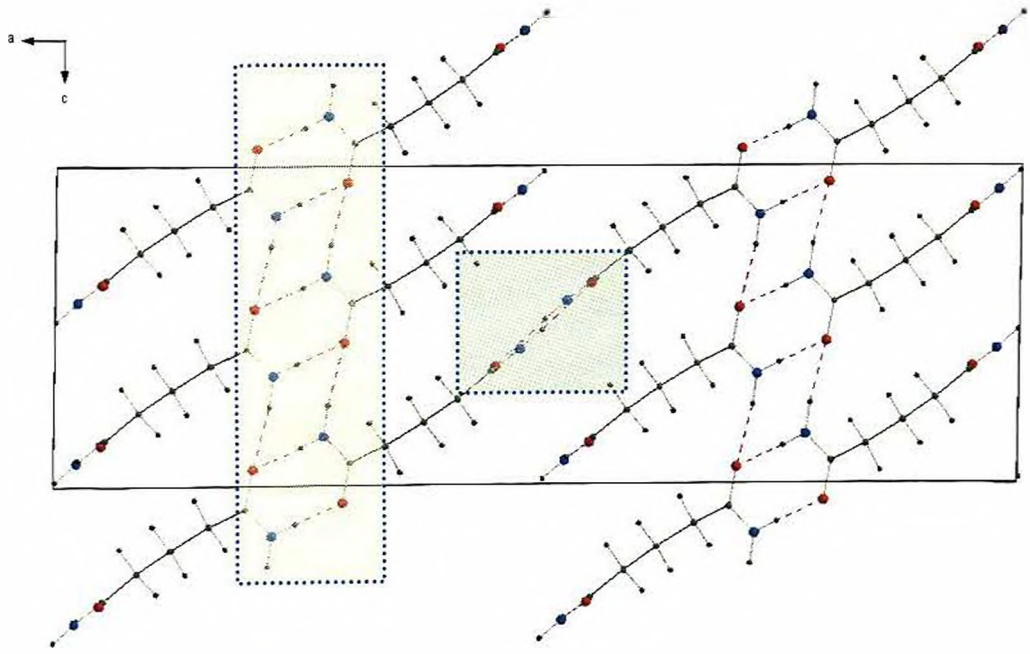

Figure 5.6.7: Glutaramide structure 7 view of ladders alternatively running along axis *c* (yellow shaded area) and perpendicular along axis *b* (green shaded area).

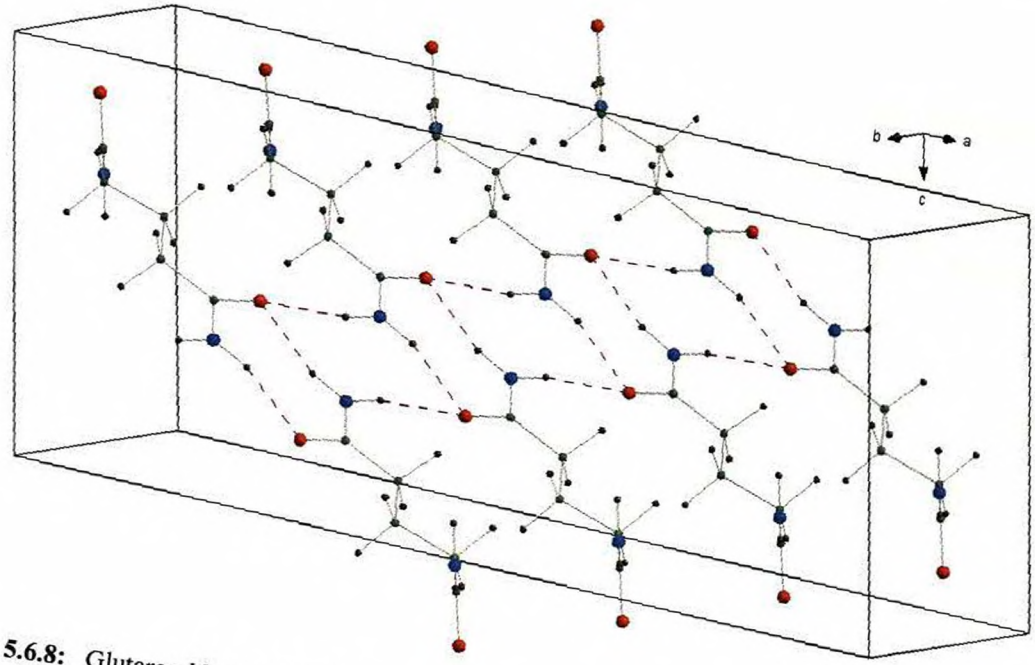

Figure 5.6.8: Glutaramide structure 7 Ladders extending along the *b* axis perpendicular to the ladders running along the *c* axis (purple dashed lines).

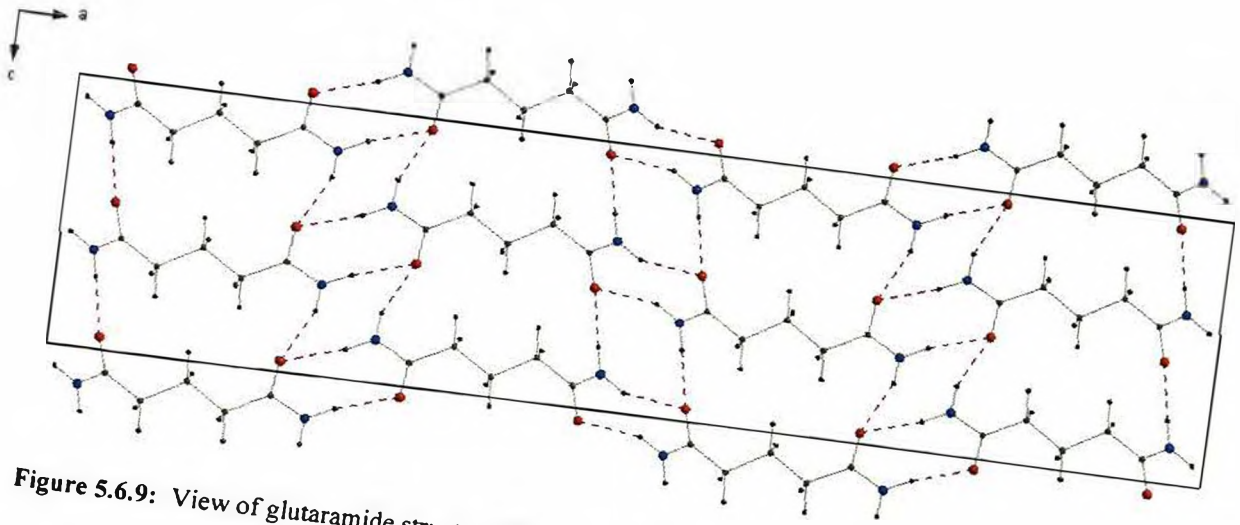

Figure 5.6.9: View of glutaramide structure 29 showing Sheets along the (101) plane.

On comparison of the simulated X-ray diffraction powder patterns for glutaramide structures 1, 2, 6 and 29 with the experimental powder pattern (figure 5.6.10) it is obvious that none of these structures are similar to the experimental structure even though they might contain the characteristic motifs. Structure 7 however does contain similar 2θ intensities, which are comparable to the experimental powder pattern illustrating its resemblance to the experimental crystal structure.

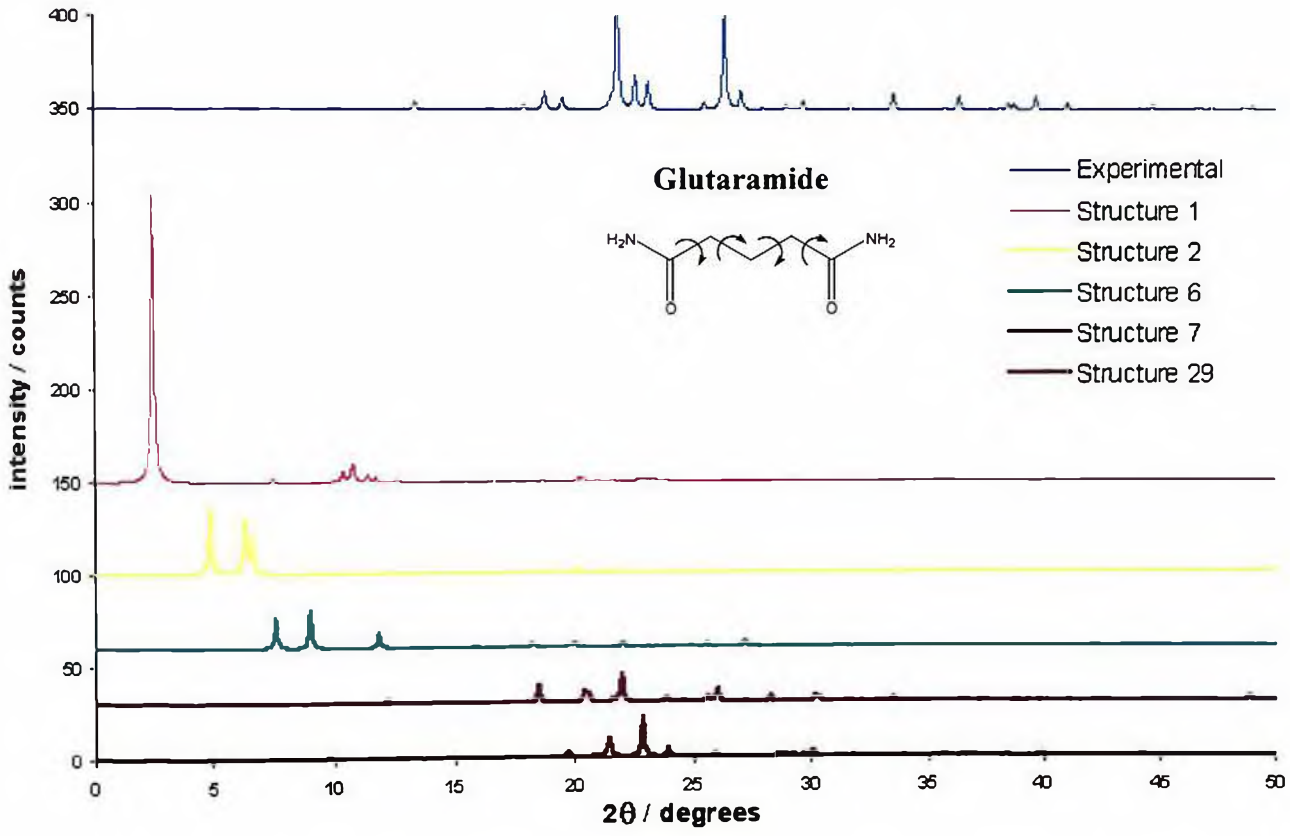

Figure 5.6.10: Comparison of the experimental X-ray diffraction pattern of glutaramide with the simulated powder patterns for glutaramide structures 1, 2, 6, 7 and 29.

5.7 Adipamide

5.7.1 Experimental crystal structure

The crystal structure of adipamide (VII) was initially reported in 1966 [Hospital. M. and Housty. J. 1966] by single crystal X-ray diffraction. However, indications were made of the existence of a second polymorph, which has been elucidated more recently, from laboratory X-ray powder diffraction using the DE 'direct space' global optimisation method [Seaton. C.C. and Tremayne. M. 2002]. The unit cell parameters, space group and single point minimised lattice energy of the experimentally determined crystal structure are given in table 5.7.1.

	Form (I) Monoclinic	Form (II) Triclinic
a (Å)	6.89(1)	5.1097(2)
b (Å)	5.15(1)	5.5722(2)
c (Å)	10.67(1)	7.0472(3)
α (°)	90	69.577(1)
β (°)	111.00(1)	87.120(3)
γ (°)	90	75.465(3)
Volume ($Å^3$)	353.46(1)	181.87(2)
Density (gcm^{-3})	1.7091 (1)	1.243(1)
Space group	P21/c (14)	P-1(2)
Z	2	1
Single point minimised lattice energy ($kcalmol^{-1}$)	-35.65	-37.93

Table 5.7.1: The crystallographic data for the experimentally determined polymorphs of adipamide.

The monoclinic form of adipamide (form I) exhibits a structural arrangement where N-H...O=C interactions form two C(4) chains; one in the [010] direction with the other formed by the molecules propagating about a 2_1 axis. These combine to generate a ladder of $R_3^2(8)$ rings (rather than dimers) linked through the molecule itself forming infinite sheets parallel to the (101) plane (figure 5.7.1).

The triclinic crystal structure of adipamide (from II) is also made up of infinite hydrogen bonded sheets generated by N-H...O=C hydrogen bonds. The molecule itself sits on an inversion centre at (0,0,0) with the amino N atom acting as a double hydrogen bond donor and forms two characteristic motifs; the centrosymmetric $R_2^2(8)$ dimer and the C(4) chain. Combination of these two motifs form a secondary hydrogen bonding network of $R_4^2(8)$ rings which lead to the formation of ladders running in the [100] direction. These ladders are linked through the adipamide molecule itself to produce infinite sheets in the (011) plane (figures 5.7.2 and 5.7.3).

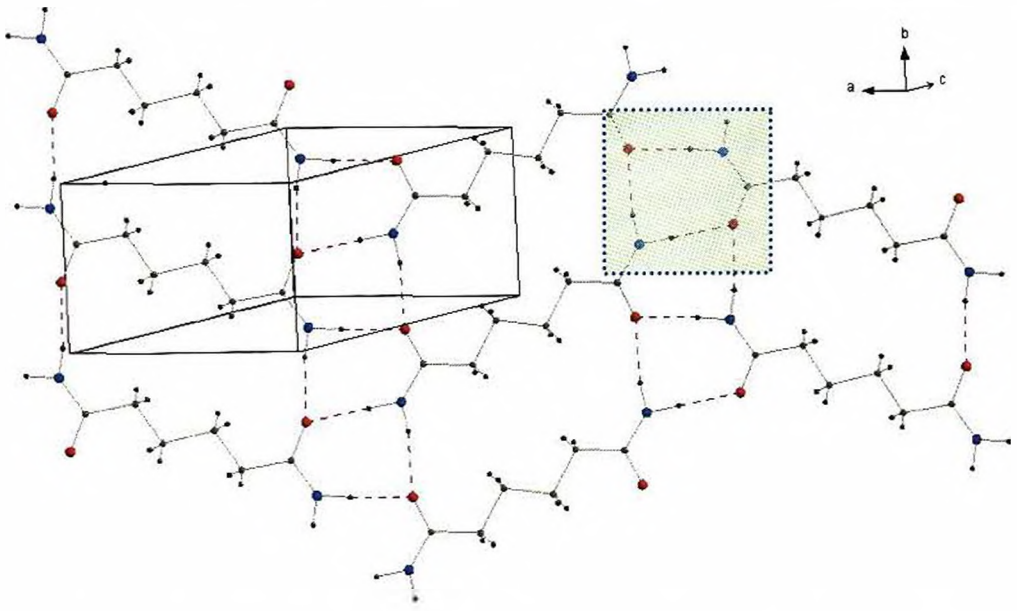

Figure 5.7.1: View of adipamide form (I) sheets parallel to the (101) plane. Also shown is the $R_3^2(8)$ motif (green shaded area).

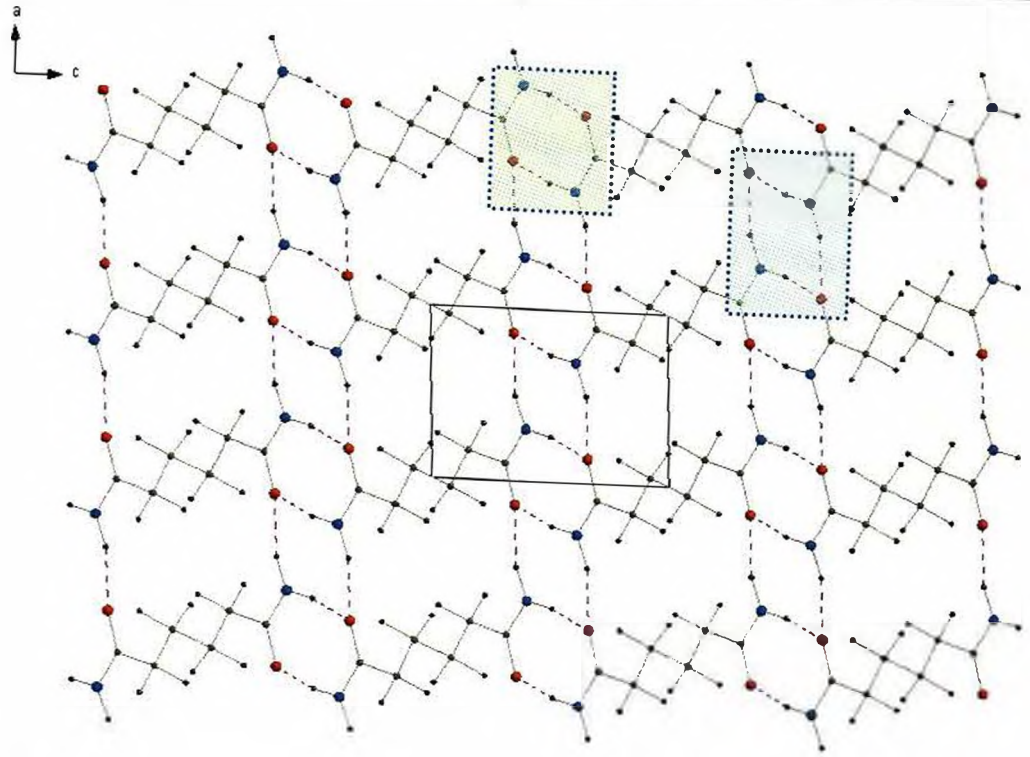

Figure 5.7.2: Combination of $R_2^2(8)$ and $R_4^2(8)$ dimers (green and blue shaded area respectively) in triclinic adipamide form (II) generating a hydrogen bonded sheet.

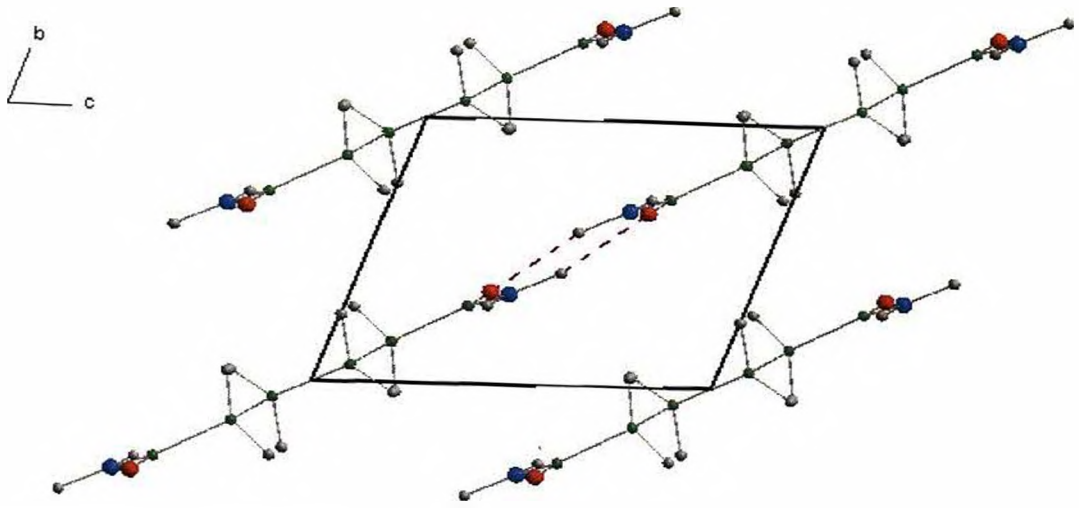

Figure 5.7.3: End-on view of hydrogen bonded sheets in triclinic adipamide form (II))

5.7.2 Structure prediction analysis of adipamide form (II)

Crystal structure prediction was performed in space group P1 (1) rather than P-1 (2), so that no assumption of symmetry was involved. No geometric restraints were placed upon the molecular structure, which was allowed to rotate through all degrees of freedom (as in figure 5.1.1). The prediction calculation generated 13 theoretical crystal structures, ranging in energy from –40.13 to –32.52kcalmol^{-1} (table 5.7.2).

No.	Volume ($Å^3$)	Density (gcm^{-3})	Lattice energy ($kcalmol^{-1}$)	a (Å)	b (Å)	c (Å)	α (°)	β (°)	γ (°)
1	188.22	1.27	-40.13	5.00	7.17	5.72	68.90	95.63	84.42
2	189.31	1.26	-40.12	4.97	8.74	8.31	78.94	80.38	32.25
3	186.94	1.28	-39.92	10.07	5.01	4.58	125.07	97.77	82.81
4	192.52	1.24	-39.64	6.11	8.38	6.87	78.64	69.57	36.27
5	200.35	1.19	-39.22	5.00	8.64	8.75	90.62	96.77	32.71
6	195.10	1.23	-36.23	5.00	4.29	10.52	95.23	84.55	61.59
7	192.48	1.24	-36.07	12.35	4.34	4.78	79.13	56.23	102.46
8	206.41	1.16	-35.10	9.14	5.77	5.07	121.34	112.77	87.50
9	203.11	1.18	-35.01	8.16	4.79	5.37	78.34	99.01	94.28
10	197.66	1.21	-34.77	6.86	4.97	6.82	99.31	120.17	90.00
11	192.40	1.24	-33.44	5.32	7.85	6.80	45.28	83.36	73.76
12	193.92	1.23	-33.40	5.40	5.78	7.65	120.66	71.51	103.71
13	203.21	1.18	-32.52	11.05	4.25	6.12	61.52	76.65	53.74

Table 5.7.2: Top 13 predicted structures for adipamide structure (VII) – triclinic form (II).

5.7.3 Re-ranking of structure prediction results – Adipamide form (II)

Ranked according to lattice energy ($kcalmol^{-1}$)		Ranked according to Hbonding merit points		Ranked according to graphset merit points	
1	**-40.13**	**13**	**99.72**	**1**	**2**
2	**-40.12**	7	90.36	**2**	**2**
3	-39.92	6	88.40	3	2
4	-39.64	9	87.11	4	2
5	-39.22	**1**	**80.00**	5	2
6	-36.23	**2**	**80.00**	6	2
7	-36.07	3	80.00	7	2
8	-35.10	4	80.00	8	2
9	-35.01	5	80.00	9	2
10	-34.77	8	80.00	11	1
11	-33.44	10	69.22	12	1
12	-33.40	11	40.00	**13**	**1**
13	**-32.52**	12	40.00	10	0

Table 5.7.3: Top 13 predicted structures for adipamide (VII) re-ranked according to hydrogen bonding and graph set merit points. Highlighted structures show similarity to experimental structure.

The re-ranking procedure (table 5.7.3) shows that a total of 6 predicted structures have the expected maximum 80 hydrogen bonding merit points and 9 structures have 2 graph set merit points highlighting the presence of the characteristic structural motif expected in amide crystal structures. All theoretical structures with maximum merit points were examined further. However, only adipamide structures 1, 2, and 13 are discussed in more detail (highlighted) either due to their similarity to the experimentally determined structure or due to their behaviour in the re-ranking process. Four theoretical structures have hydrogen bonding merit points greater then the expected maximum of 80. This is due to additional N-H...N type hydrogen bonds present within their packing arrangements.

Adipamide (form II) structure 1 is energetically the most favourable structure and has the expected maximum of 80 hydrogen bonding merit points and 2 graph set assignment points and 2 graphset assignment points (table 5.7.4). This structure is held together by N-H...O=C hydrogen bonds with the amino N atom acting as a

double hydrogen bond donor forming $R_2^2(8)$ dimers and C(4) chains. Combination of these two motifs generates the secondary hydrogen bonding network of $R_4^4(8)$ rings which in turn leads to the formation of ladders that are themselves linked though the adipamide molecule giving rise to sheets which run parallel to the (011) plane (figures 5.7.4 and 5.7.5). This structure is very close to the experimental crystal structure.

		D-H	H...A	D...A	D-H...A
1	N(7) --H(19) ..O(10)	0.9600	2.0600	3.0084	169.00
2	N(7) --H(20) ..O(9)	0.9600	2.0200	2.9843	177.00
3	N(8) --H(21) ..O(9)	0.9600	2.0600	3.0084	169.00
4	N(8) --H(22) ..O(10)	0.9600	2.0200	2.9843	177.00

1	N(7) --H(19) ..O(10):	2.06	merit = 10
2	N(7) --H(20) ..O(9):	2.02	merit = 10
3	N(8) --H(21) ..O(9):	2.06	merit = 10
4	N(8) --H(22) ..O(10):	2.02	merit = 10

1	N(7) --H(19) ..O(10):	169	merit = 10
2	N(7) --H(20) ..O(9):	177	merit = 10
3	N(8) --H(21) ..O(9):	169	merit = 10
4	N(8) --H(22) ..O(10):	177	merit = 10

TOTAL MERIT FOR POLYMORPH 1 = 80

Table 5.7.4: Hydrogen bonding merit points generated by the re-ranking strategy for adipamide form (II) structure 1.

Adipamide (form II) structure 2 is another structure that has acquired the expected maximum number of hydrogen bonding merit points and graphset assignment merit points (table 5.7.3). This structure is similar to structure 1, in that it contains $R_2^2(8)$ dimers, C(4) chains and the secondary $R_4^4(8)$ rings. The structure also forms infinite hydrogen bonded sheets that run parallel to the (011) plane (figures 5.7.6 and 5.7.7), but differs in that these sheets are significantly puckered.

		D-H	H...A	D...A	D-H...A
1	N(7) --H(19) ..O(10)	0.9600	2.0800	3.0277	165.00
2	N(7) --H(20) ..O(9)	0.9600	2.0400	2.9925	172.00
3	N(8) --H(21) ..O(9)	0.9600	2.0800	3.0277	165.00
4	N(8) --H(22) ..O(10)	0.9600	2.0400	2.9925	172.00

1	N(7) --H(19) ..O(10):	2.08	merit = 10
2	N(7) --H(20) ..O(9):	2.04	merit = 10
3	N(8) --H(21) ..O(9):	2.08	merit = 10
4	N(8) --H(22) ..O(10):	2.04	merit = 10

1	N(7) --H(19) ..O(10):	165	merit = 10
2	N(7) --H(20) ..O(9):	172	merit = 10
3	N(8) --H(21) ..O(9):	165	merit = 10
4	N(8) --H(22) ..O(10):	172	merit = 10

TOTAL MERIT FOR POLYMORPH 2 = 80

Table 5.7.5: Hydrogen bonding information generated by the re-ranking strategy for adipamide (form II) structure 2.

Adipamide (form II) structure 13 has more than the expected number of merit points (99.72) and as a result has moved up the rankings to position 1 in terms of hydrogen bonding although it only has 1 graph set assignment point (table 5.7.3). Structure 13 comprises centrosymmetric amide $R_2^2(8)$ dimers of type N-H...O=C which form chains in the [110] direction. The second amino nitrogen generates alternative $R_2^2(4)$ amino dimers through N-H...N type interactions that in combination with the $R_2^2(8)$ dimers form ladders in the [001] direction (figures 5.7.8 and 5.7.9).

Despite the lack of symmetry constraints in the prediction calculation, all these structures were positioned on an inversion centre, implying the higher P-1 symmetry seen in the experimental structure of form (II).

		D-H	H...A	D...A	D-H...A
1	N(7) --H(19) ..O(10)	0.9600	2.1200	3.0325	158.00
2	N(7) --H(19) ..N(8)	0.9600	2.4200	3.2478	144.00
3	N(7) --H(20) ..N(8)	0.9600	2.3200	3.1739	148.00
4	N(8) --H(21) ..O(9)	0.9600	2.1200	3.0325	158.00
5	N(8) --H(21) ..N(7)	0.9600	2.4200	3.2478	144.00
6	N(8) --H(22) ..N(7)	0.9600	2.3200	3.1739	148.00

1	N(7) --H(19) ..O(10):	2.12	merit = 10
4	N(8) --H(21) ..O(9):	2.12	merit = 10
2	N(7) --H(19) ..N(8):	2.42	merit = 5.16
3	N(7) --H(20) ..N(8):	2.32	merit = 8.56
5	N(8) --H(21) ..N(7):	2.42	merit = 5.16
6	N(8) --H(22) ..N(7):	2.32	merit = 8.56

1	N(7) --H(19) ..O(10):	158	merit = 9.94
2	N(7) --H(19) ..N(8):	144	merit = 7.54
3	N(7) --H(20) ..N(8):	148	merit = 8.66
4	N(8) --H(21) ..O(9):	158	merit = 9.94
5	N(8) --H(21) ..N(7):	144	merit = 7.54
6	N(8) --H(22) ..N(7):	148	merit = 8.66

TOTAL MERIT FOR POLYMORPH 13 = 99.72

Table 5.7.6: Hydrogen bonding information generated by the re-ranking strategy for adipamide (form II) structure 13.

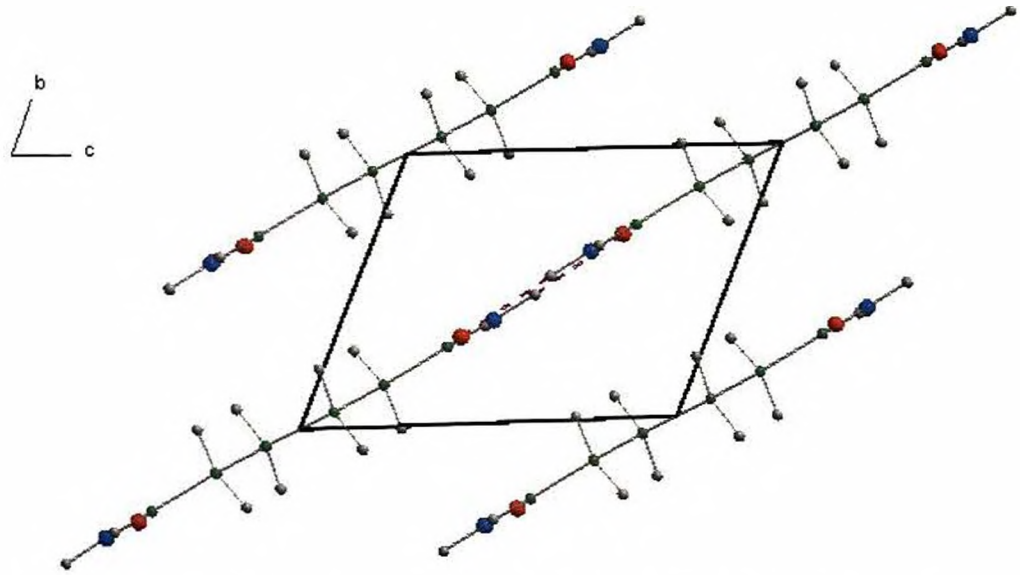

Figure 5.7.4: End-on view of the adipamide sheets along the (011) plane in adipamide (form II) structure 1.

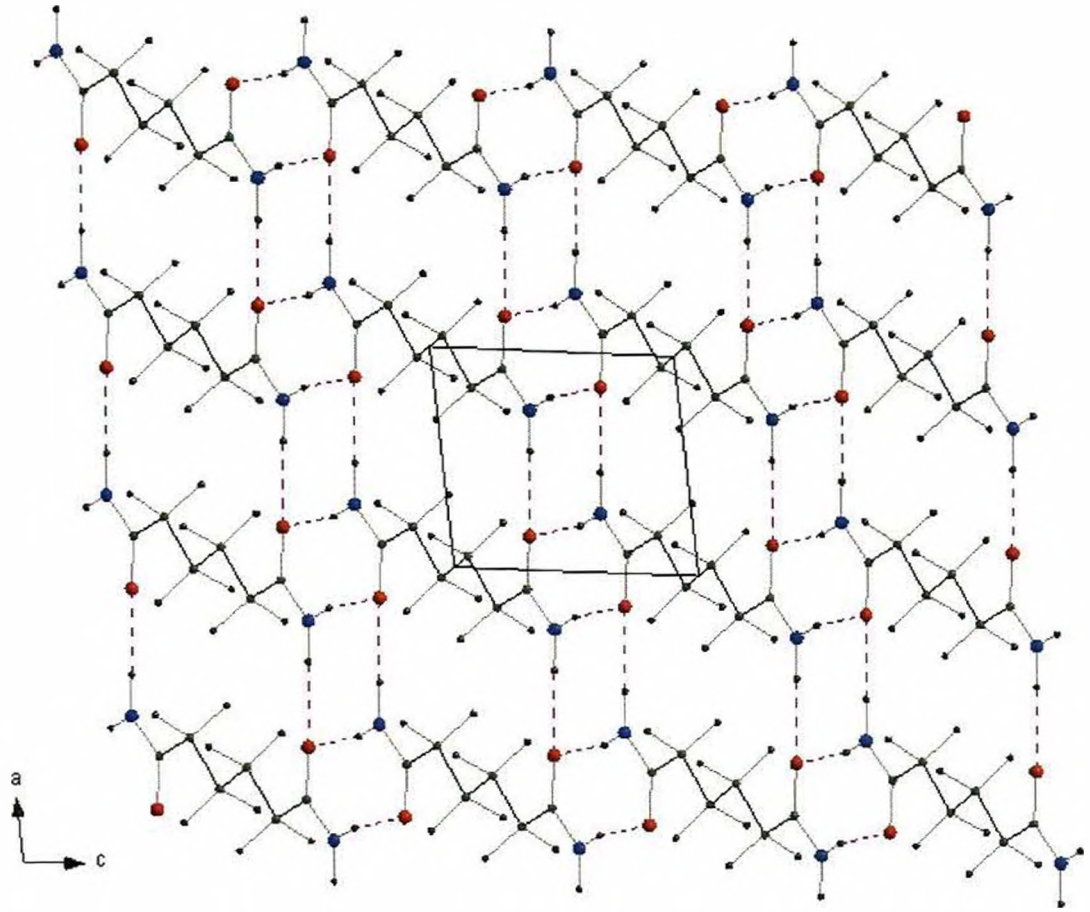

Figure 5.7.5: View of an infinite hydrogen bonded sheet in adipamide (form II) structure 1.

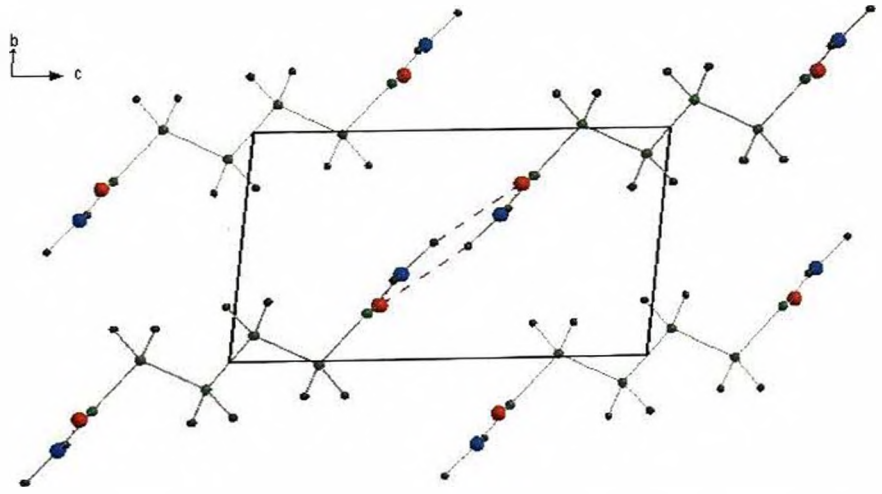

Figure 5.7.6: View of the sheets in adipamide (form II) structure 2 running parallel to the (011) plane.

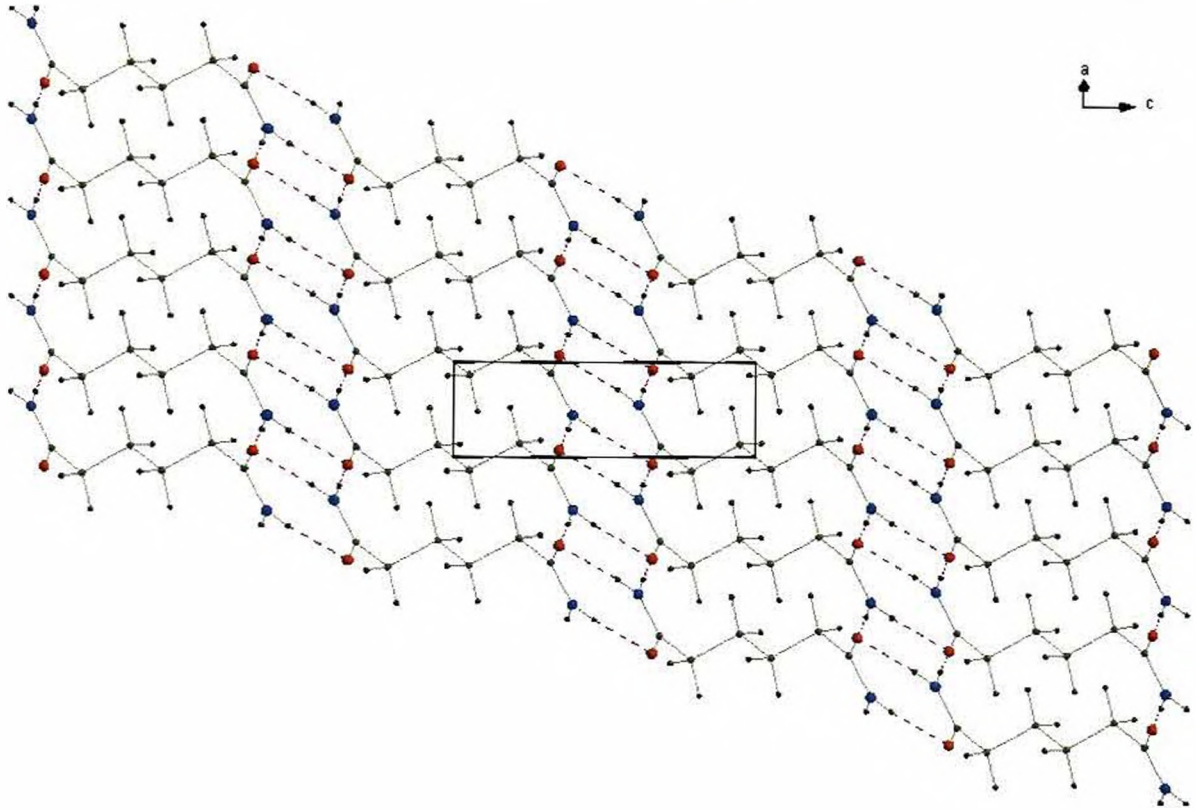

Figure 5.7.7: Infinite hydrogen bonded sheet in adipamide (form II) structure 2.

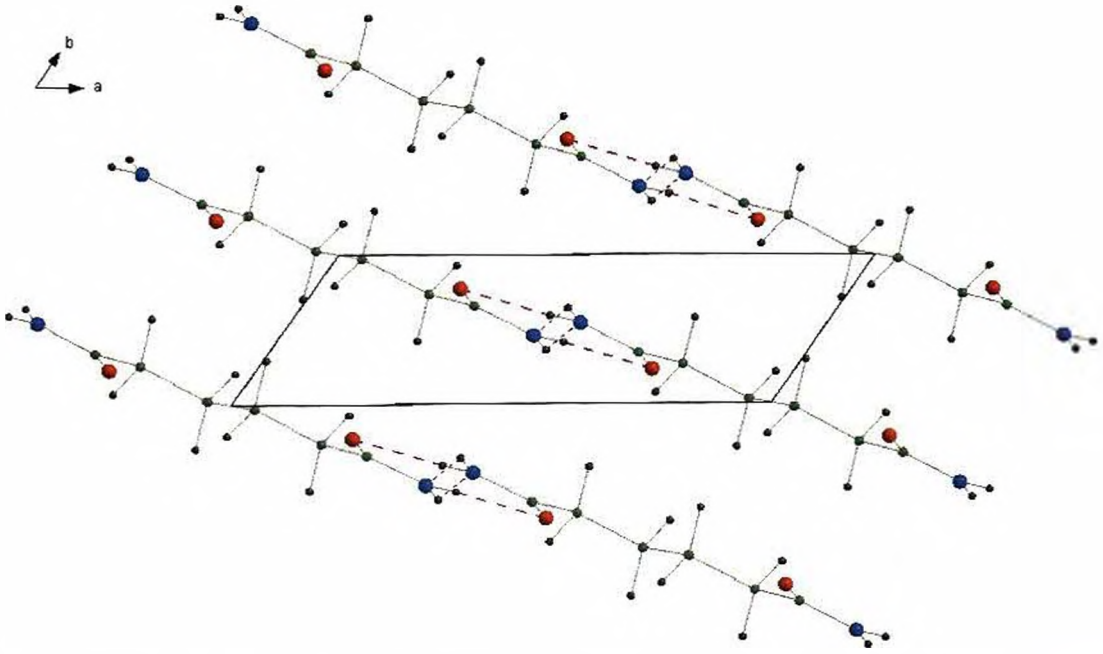

Figure 5.7.8: Packing arrangement of adipamide (form II) structure 13 illustrating the chains extending along the [110] direction.

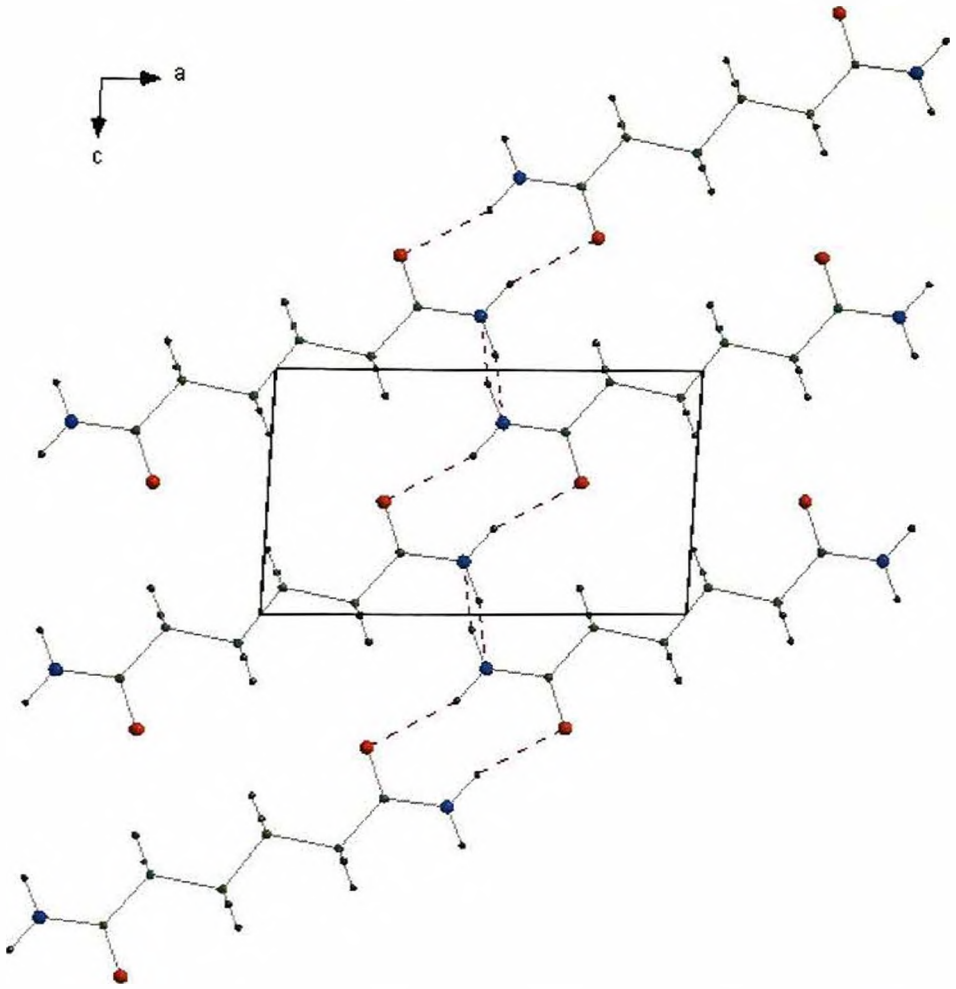

Figure 5.7.9: Adipamide (form II) structure 13 showing ladders running along the [001] direction.

Simulated powder X-ray diffraction data was used to compare the experimental structure with the predicted adipamide (form II) structures 1,2 and 13 (figure 5.7.10). The powder patterns of structures 2 and 13 differ considerably to that of the experimental structure whereas the simulated pattern for structure 1 confirms that this theoretical structure is indeed the same as the experimental crystal structure.

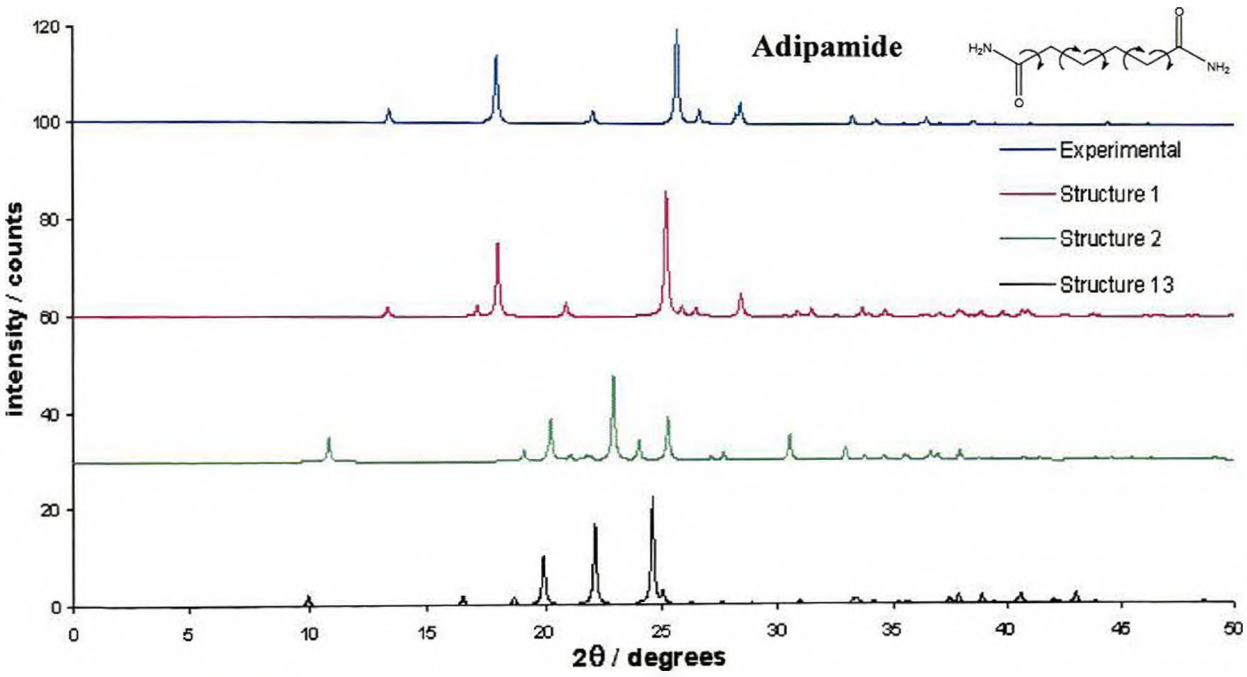

Figure 5.7.10: Comparison of the experimental X-ray diffraction pattern of adipamide (form II) with the simulated powder patterns for adipamide (form II) structures 1, 2, and 13.

5.7.4 Structure prediction analysis of adipamide form (I)

Crystal structure prediction was performed in space group $P2_1/c$ (14). No geometric restraints were placed upon the molecular structure, which was allowed to rotate through all degrees of freedom. The prediction calculation generated 474 theoretical crystal structures, ranging in energy from –40.05 to –26.74kcalmol^{-1} (table 5.7.7). It is also worth noting that predicted structures 15 and 24 have low densities compared to all other structures.

No.	Volume (Å^3)	Density (gcm^{-3})	Lattice energy (kcalmol^{-1})	a (Å)	b (Å)	c (Å)	β (°)
1	751.41	1.27	-40.06	10.66	5.00	22.33	140.92
2	749.86	1.27	-39.99	30.61	5.00	10.99	153.56
3	784.67	1.22	-39.92	4.99	16.13	10.40	69.39
4	760.34	1.25	-39.84	16.86	10.65	14.80	163.39
5	741.53	1.29	-39.83	13.69	5.47	9.948	83.78
6	760.07	1.25	-39.82	10.01	10.65	7.663	111.70
7	753.75	1.27	-39.78	42.93	5.60	39.17	175.41
8	766.46	1.24	-39.76	4.99	14.39	14.50	132.73
9	761.48	1.25	-39.75	5.01	10.65	14.70	75.94
10	751.40	1.27	-39.64	9.99	5.56	17.39	129.05
11	777.72	1.23	-39.55	23.65	7.30	10.65	154.99
12	761.10	1.25	-39.53	13.85	5.66	9.95	102.96
13	767.56	1.24	-39.43	10.65	14.41	11.82	154.99
14	755.77	1.26	-39.39	27.08	4.52	9.73	140.63
15	812.22	1.17	-39.27	9.99	7.83	12.17	121.55
16	772.65	1.23	-39.04	15.20	5.87	9.97	60.06
17	784.10	1.22	-38.99	10.66	9.93	12.97	145.24
18	765.27	1.25	-38.90	14.39	8.60	10.46	143.80
19	751.51	1.27	-38.88	25.85	5.02	11.04	148.42
20	770.34	1.24	-38.86	6.966	13.55	8.13	89.36
21	757.40	1.26	-38.81	7.23	5.03	21.71	73.42
22	753.19	1.27	-38.78	28.07	4.98	14.68	158.52
23	756.91	1.26	-38.75	5.607	4.99	27.05	88.96
24	813.77	1.17	-38.73	16.36	10.56	15.21	161.97
25	751.70	1.27	-38.73	7.819	18.80	7.47	136.86
26	762.09	1.25	-38.65	14.32	10.65	14.85	160.34
27	791.28	1.21	-38.61	18.32	7.42	11.74	150.32
28	765.12	1.25	-38.54	26.48	5.00	18.45	161.75
29	773.57	1.23	-38.44	17.61	10.6	15.33	164.42
30	764.58	1.25	-38.34	9.930	7.90	17.38	145.94

Table 5.7.7: Top 30 predicted structures for adipamide form (I).

5.7.5 Re-ranking of structure prediction results – Adipamide form (I)

Ranked according to lattice energy ($kcalmol^{-1}$)		Ranked according to Hbonding merit points		Ranked according to graphset merit points	
1	**-40.06**	**1**	**80**	**1**	**2**
2	**-39.99**	**2**	**80**	**2**	**2**
3	-39.92	3	80	3	2
4	-39.84	4	80	4	2
5	-39.83	5	80	5	2
6	-39.82	6	80	6	2
7	-39.78	7	80	7	2
8	-39.76	8	80	8	2
9	-39.75	9	80	9	2
10	-39.64	10	80	10	2
11	-39.55	11	80	11	2
12	-39.53	12	80	12	2
13	-39.43	13	80	13	2
14	-39.39	14	80	14	2
15	-39.27	15	80	15	2
16	-39.04	16	80	16	2
17	-38.99	17	80	17	2
18	-38.90	20	80	18	2
19	**-38.88**	24	80	**19**	**2**
20	-38.86	25	80	20	2
21	-38.81	26	80	21	2
22	-38.78	27	80	22	2
23	-38.75	28	80	23	2
24	-38.73	29	80	24	2
25	-38.73	30	80	25	2
26	-38.65	18	79.85	26	2
27	-38.61	21	78.66	27	2
28	-38.54	**19**	**78.41**	28	2
29	-38.44	22	77.81	29	2
30	-38.34	23	77.81	30	2

Table 5.7.8: Top 30 predicted structures for adipamide form (I) re-ranked according to hydrogen bonding and graph set merit points. Highlighted structures show similarity to experimental structure.

The re-ranking procedure (table 5.7.8) shows that a total of 25 predicted structures have the expected maximum 80 hydrogen bonding merit points and all 30 structures have 2 graph set merit points highlighting the presence of the characteristic structural motifs expected in amide crystal structures. All theoretical structures with maximum merit points were examined further. However, only adipamide (form I) structures 1, 2 and 19 are discussed in more detail (highlighted) either due to their similarity to the experimentally determined structure or due to their behaviour in the re-ranking process. Five structures have hydrogen bonding merit points lower then the expected

maximum of 80 due to N-H...O type hydrogen bonding geometry outside the specified limits.

Adipamide (form I) structure 1 is energetically the most favourable structure and has the expected maximum of 80 hydrogen bonding merit points and 2 graph set assignment points based on the presence of $R_2^2(8)$ and C(4) motifs. In the case of this polymorph, this is not preferable as the structure contains $R_3^2(8)$ and not $R_2^2(8)$ dimers (table 5.7.10). Structure 1 is held together by N-H...O=C hydrogen bonds in which the amino N atom acts as a double hydrogen bond donor forming $R_2^2(8)$ dimers and C(4) chains. These two motifs combine and generate a secondary hydrogen bonding network of $R_4^2(8)$ rings in turn giving rise to ladders which extend along the [010] direction. The ladders are themselves linked though the adipamide molecule giving rise to infinite sheets lying in the (110) plane (figures 5.7.10a and 5.7.11). Although this structure is dissimilar to form (I), it has a striking similarity to that of the experimental structure of form (II). This is confirmed by comparison of the interplaner spacing in the 2 structures: predicted structure 5.58Å and experimental structure form (II) 5.57Å.

Adipamide (form I) structure 2 is very much like structure 1; it too has the expected maximum of 80 hydrogen bonding merit points and 2 graph set assignment points which as discussed previously is not a good indication of similarity to form (I) (table 5.7.10). This structure is similar to structure 1, N-H...O=C hydrogen bonds form $R_2^2(8)$ dimers and C(4) chains which in turn generate $R_4^2(8)$ rings and characteristic ladders. These ladders are themselves linked though the molecule giving rise to infinite sheets lying in the (101) plane (figures 5.7.12 and 5.7.13). As before, this

structure has more similarity to form (II) then form (I) with interplaner spacing of 5.50Å.

			D-H	H...A	D...A	D-H...A
1	N(73) --H(85)	..O(75)	0.9600	2.0600	3.0118	169.00
2	N(73) --H(86)	..O(76)	0.9600	2.0200	2.9823	177.00
3	N(74) --H(87)	..O(76)	0.9600	2.0600	3.0101	169.00
4	N(74) --H(88)	..O(75)	0.9600	2.0200	2.9823	178.00

1	N(73) --H(85)	..O(75)	2.06	merit = 10
2	N(73) --H(86)	..O(76)	2.02	merit = 10
3	N(74) --H(87)	..O(76)	2.06	merit = 10
4	N(74) --H(88)	..O(75)	2.02	merit = 10

1	N(73) --H(85)	..O(75)	169	merit = 10
2	N(73) --H(86)	..O(76)	177	merit = 10
3	N(74) --H(87)	..O(76)	169	merit = 10
4	N(74) --H(88)	..O(75)	178	merit = 10

TOTAL MERIT FOR POLYMORPH 1 = 80

Table 5.7.9: Hydrogen bonding merit points generated by the re-ranking strategy for adipamide (form I) structure 1.

			D - H	H...A	D...A	D - H...A
1	N(73) --H(85)	..O(76)	0.9600	2.0600	3.0154	169.00
2	N(73) --H(86)	..O(76)	0.9600	2.0200	2.9819	177.00
3	N(74) --H(87)	..O(75)	0.9600	2.0600	3.0154	169.00
4	N(74) --H(88)	..O(75)	0.9600	2.0200	2.9819	177.00

1	N(73) --H(85)	..O(76)	2.06	merit = 10
2	N(73) --H(86)	..O(76)	2.02	merit = 10
3	N(74) --H(87)	..O(75)	2.06	merit = 10
4	N(74) --H(88)	..O(75)	2.02	merit = 10

1	N(73) --H(85)	..O(75)	169	merit = 10
2	N(73) --H(86)	..O(76)	177	merit = 10
3	N(74) --H(87)	..O(75)	169	merit = 10
4	N(74) --H(88)	..O(75)	177	merit = 10

TOTAL MERIT FOR POLYMORPH 1 = 80

Table 5.7.10: Hydrogen bonding merit points generated by the re-ranking strategy for adipamide (form I) structure 2.

Adipamide (form I) structure 19 has fallen down the rankings to position 28 with respect to hydrogen bonding merit points, but is most like the experimental form (I) crystal structure. It is the only one that contains N-H...O=C hydrogen bonds which form the characteristic $R_3^2(8)$ ring system as well as the C(4) chain. These two motifs form the characteristic staggered ladder motifs seen as in the monoclinic polymorph of adipamide. However, this predicted structure also contains $R_2^2(8)$ dimers and C(4) chains generating the alternate network of $R_4^2(8)$ rings and the resulting ladders. These two ladder systems are linked alternatively through the adipamide molecule giving rise to infinite sheets which run in the (201) plane (figures 5.7.14 and 5.7.15). The hydrogen bonding merit points are reduced for this structure because the NH...O angle is relatively short (147°).

		D - H	H...A	D...A	D - H...A
1	N(73) -- H(85) .. O(76)	0.9635	2.0611	3.0134	169.44
2	N(73) -- H(86) .. O(76)	0.9628	2.0183	2.9806	177.71
3	N(74) -- H(87) .. O(75)	0.9658	2.1751	3.0365	147.83
4	N(74) -- H(88) .. O(75)	0.9616	2.0007	2.9593	174.46

1	N(73) -- H(85) .. O(76)	2.06	merit = 10
2	N(73) -- H(86) .. O(76)	2.01	merit = 10
3	N(74) -- H(87) .. O(75)	2.17	merit = 10
4	N(74) -- H(88) .. O(75)	2.00	merit = 10

1	N(73) -- H(85) .. O(76)	169	merit = 10
2	N(73) -- H(86) .. O(76)	177	merit = 10
3	N(74) -- H(87) .. O(75)	147	merit = 8.41
4	N(74) -- H(88) .. O(75)	174	merit = 10

TOTAL MERIT FOR POLYMORPH 1 = 78.41

Table 5.7.11: Hydrogen bonding merit points generated by the re-ranking strategy for adipamide (form I) structure 19.

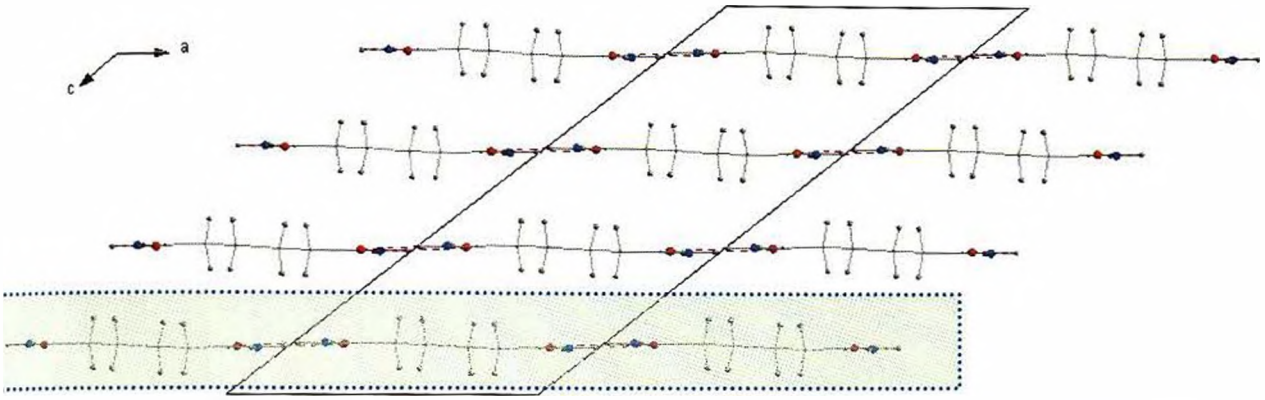

Figure 5.7.10a: End-on view of adipamide (form I) structure 1 showing the sheets along the (110) plane (green shaded area).

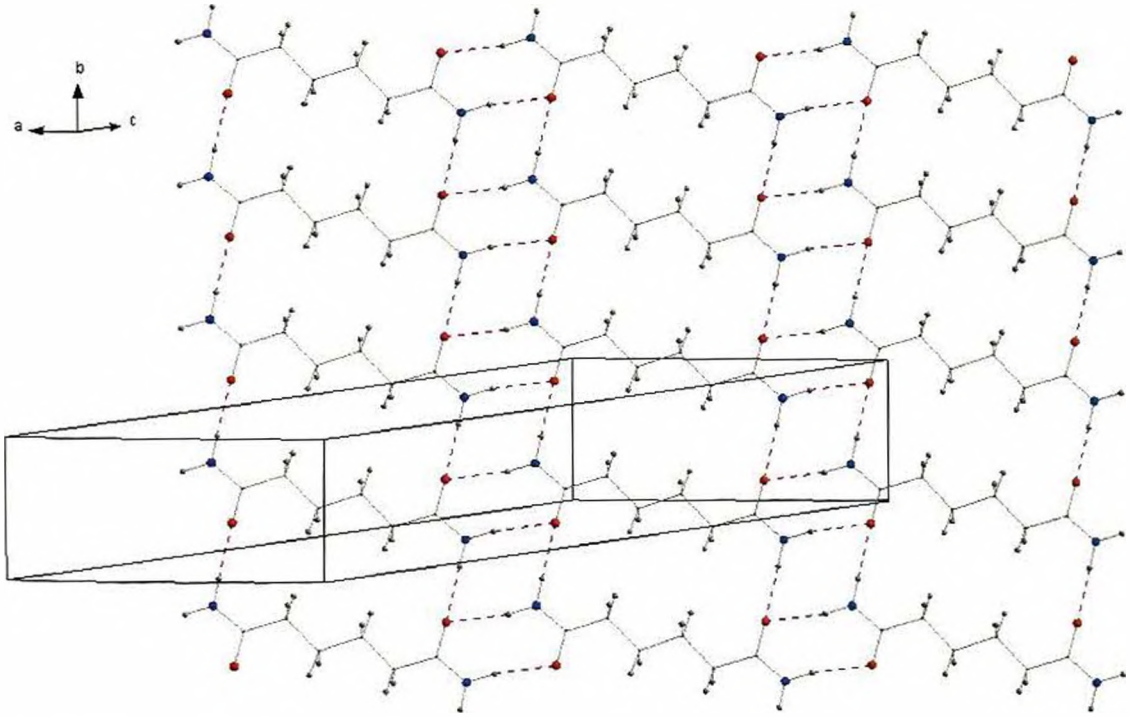

Figure 5.7.11: View of an infinite hydrogen bonded sheet in adipamide (form I) structure 1.

Figure 5.7.12: End-on view of adipamide (form I) structure 2 showing the adipamide sheets along the (101) plane within.

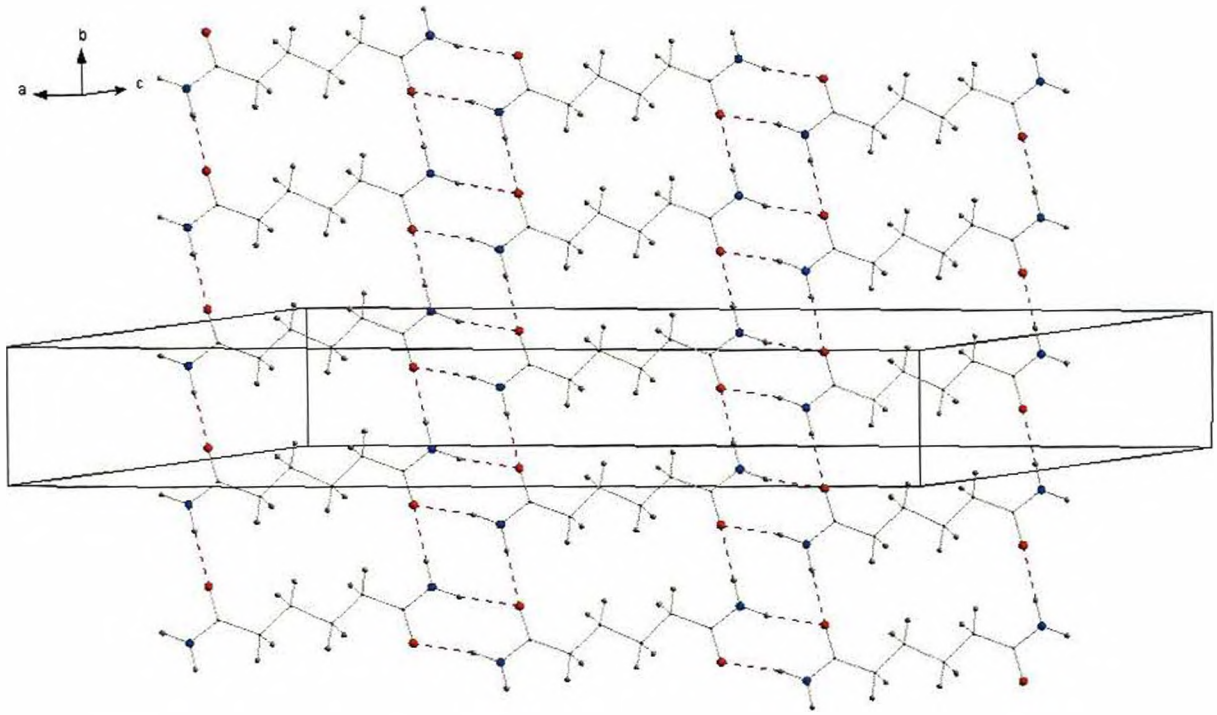

Figure 5.7.13: View of an infinite hydrogen bonded sheet in adipamide (form I) structure 2.

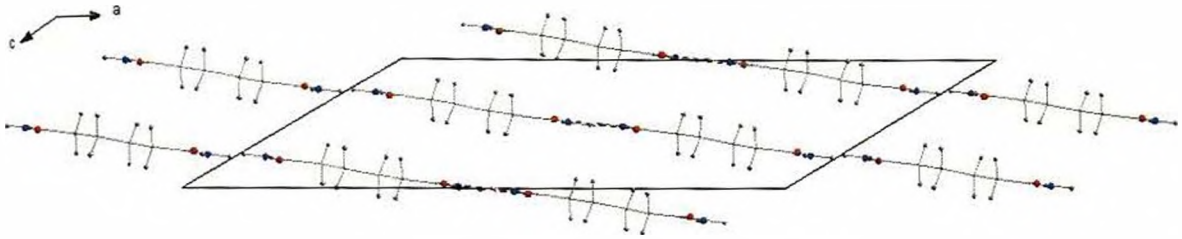

Figure 5.7.14: End-on view of adipamide (form I) structure 19 showing the adipamide sheets along the (201) plane.

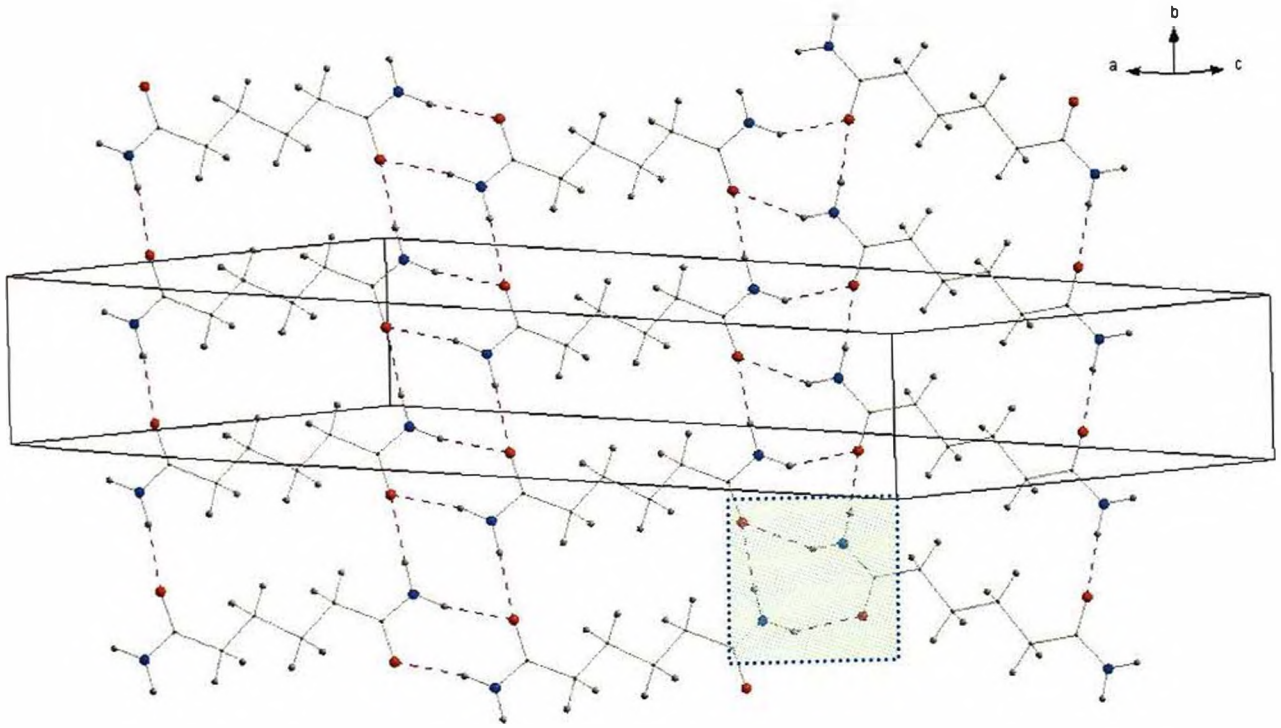

Figure 5.7.15: View of an infinite hydrogen bonded sheet in adipamide (form I) structure 19. The $R_3^3(8)$ dimer is illustrated in the green shaded area

Simulated powder X-ray diffraction data was used to compare the experimental structure with the predicted adipamide (form I) structures 1,2 and 19 (figure 5.7.16). The powder patterns of all the structures differ somewhat to that of the experimental form (I) powder pattern, however there is more resemblance of the predicted structures with the form (II) simulated powder pattern. It is not surprising since the interplaner distances of the predicted structures bared more similarity to the form (II) crystal structure as did the structural hydrogen bonding motifs generated.

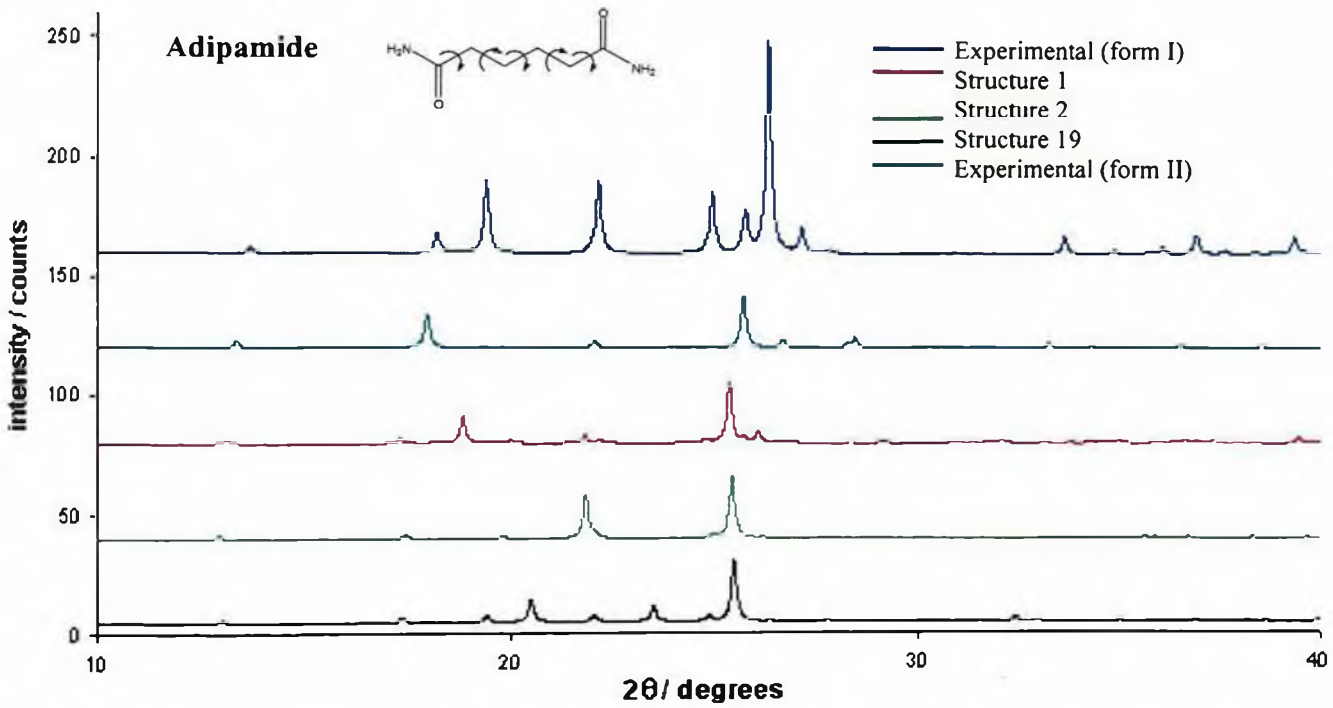

Figure 5.7.16: Comparison of the experimental X-ray diffraction pattern of adipamide form (I and II) with the simulated powder patterns for adipamide (form I) structures 1, 2, and 19.

5.7.6 Stability of adipamide form (I) and (II)

The relative stabilities of the two polymorphs of adipamide were explored experimentally. Adipamide powder was purchased from Aldrich [CAS no. 628-94-4] and re-crystallised from solution using a variety of laboratory solvents. All resulting solids were ground to a powder and characterised by powder X-ray diffraction. Initial attempts to re-crystallise form (I) proved unsuccessful; on each occasion only form (II) was obtained. Mixed solvents were also used for recrystallisation with both slow and rapid cooling techniques. In the original publication [Hospital. M. and Housty. J. 1966] sublimation had been used to prepare this form (*using a cold finger*). However we made several attempts at reproducing this synthesis but without success. Form (I) of adipamide does seem to be elusive and may be an example of a disappearing polymorph [Dunitz, J. D and Bernstein. J. 1995]. No further experimental work was carried out on this material as experimental evidence clearly showed that the triclinic form (II) is the most stable polymorph. This may also explain why the structure was not predicted in out calculations.

5.8 Pimelamide

5.8.1 Experimental crystal structure

The crystal structure of pimelamide (VIII) [Pedireddi, V.R. 2002] has been determined using conventional single crystal X-ray diffraction data, although the hydrogen atoms were placed in idealised positions and not refined. The unit cell parameters, space group and single point minimised lattice energy of the experimentally determined crystal structure are given in table 5.8.1.

a (Å)	5.92 (1)
b (Å)	8.49(2)
c (Å)	22.55(2)
β (°)	131.55(1)
Volume ($Å^3$)	850.03(12)
Density (gcm^{-3})	1.211(2)
Z	4
Space group	C2/c (15)
Single point minimised lattice energy ($kcalmol^{-1}$)	-34.34

Table 5.8.1: The crystallographic and lattice energy data for experimentally determined pimelamide.

The crystal packing arrangement in pimelamide (VIII) is determined by two distinct N-H...O=C type hydrogen bonds. The amino N atom acts as a double donor forming the two characteristic motifs; the $R_2^2(8)$ dimer and C(4) chain, which combine to form a secondary $R_4^4(8)$ ring system. The amide groups within each molecule lie 90° with

respect to one another such that an infinite three dimensional network is formed by combination of ladders running along the [110] direction linked through the molecule itself to ladders along the [001] direction (figure 5.8.1 and 5.8.2).

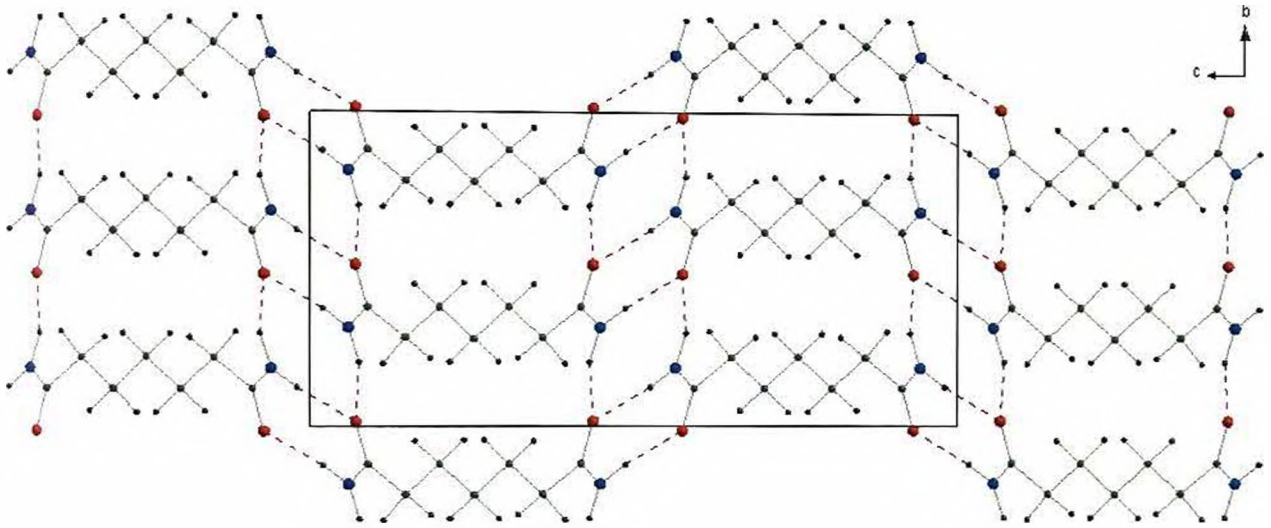

Figure 5.8.1: View of pimelamide (VIII) showing the ladders extending along the [110] direction.

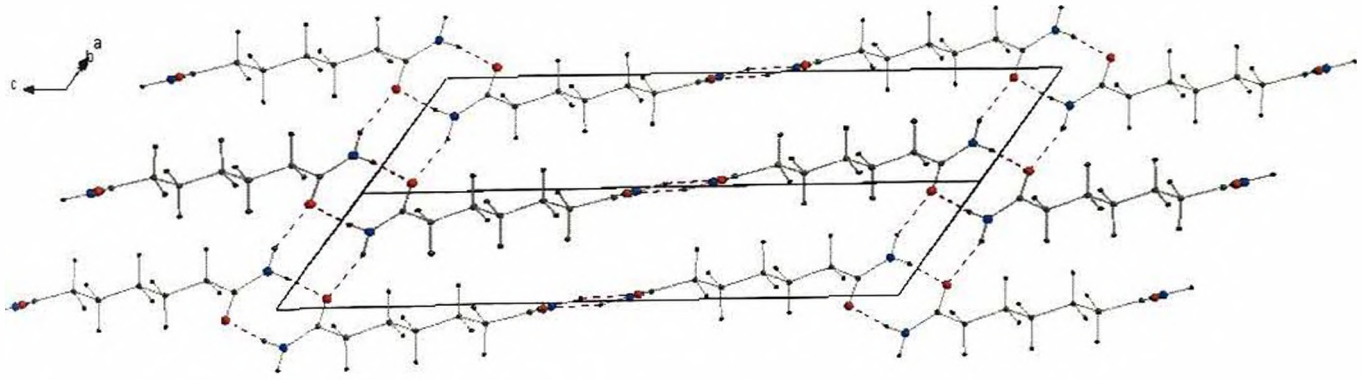

Figure 5.8.2: View of pimelamide (VIII) illustrating the infinite sheets in the [001] direction.

5.8.2 Structure prediction analysis – Pimelamide

Crystal structure prediction was performed in the space group C2/c (15). No restraints were placed upon the molecular model, which was allowed to rotate through all degrees of freedom (as in figure 5.1.1). The prediction calculation was carried out 3 times, however on each occasion the calculation failed and no structures were generated. One possible reason for the failure of the prediction calculation may be the extent of flexibility and the large number of degrees of freedom present within the molecule.

However, considering the fact that the aliphatic chain length contains 7 carbon atoms it is a possibility that an odd number of carbon atoms could of posed an excessive demand on computing power when considering the high degree of flexibility in the molecule and resulting in the failure of this structure prediction.

5.9 Suberamide

5.9.1 Experimental crystal structure

The crystal structure of suberamide (IX) [Hospital. M. and Housty. J. 1966] has been determined using conventional single crystal X-ray diffraction data, although the hydrogen atoms were placed in idealised positions and not refined. The unit cell parameters, space group and single point minimised lattice energy of the experimentally determined crystal structure are given in table 5.9.1.

a (Å)	14.44(2)
b (Å)	5.13(1)
c (Å)	14.17(2)
β (°)	117.50(1)
Volume ($Å^3$)	931.07(2)
Density (gcm^{-3})	1.151(2)
Space group	C2/c (15)
Z	4
Single point minimised lattice energy ($kcalmol^{-1}$)	-37.48

Table 5.9.1: The crystallographic and lattice energy data for experimentally determined suberamide.

The three dimensional hydrogen bonding network within (IX) consists of infinite hydrogen bonded sheets generated by N-H...O=C hydrogen bonds. The amino N atom acts as a double donor and forms the two characteristic motifs, the $R_2^2(8)$ dimer and the C(4) chain. Combination of these two motifs forms a secondary hydrogen bonding network of $R_4^2(8)$ rings which leads to the formation of ladders running in the [010] direction. These ladders are linked through the molecule itself to produce infinite sheets in the (011) plane (figures 5.9.1 and 5.9.2).

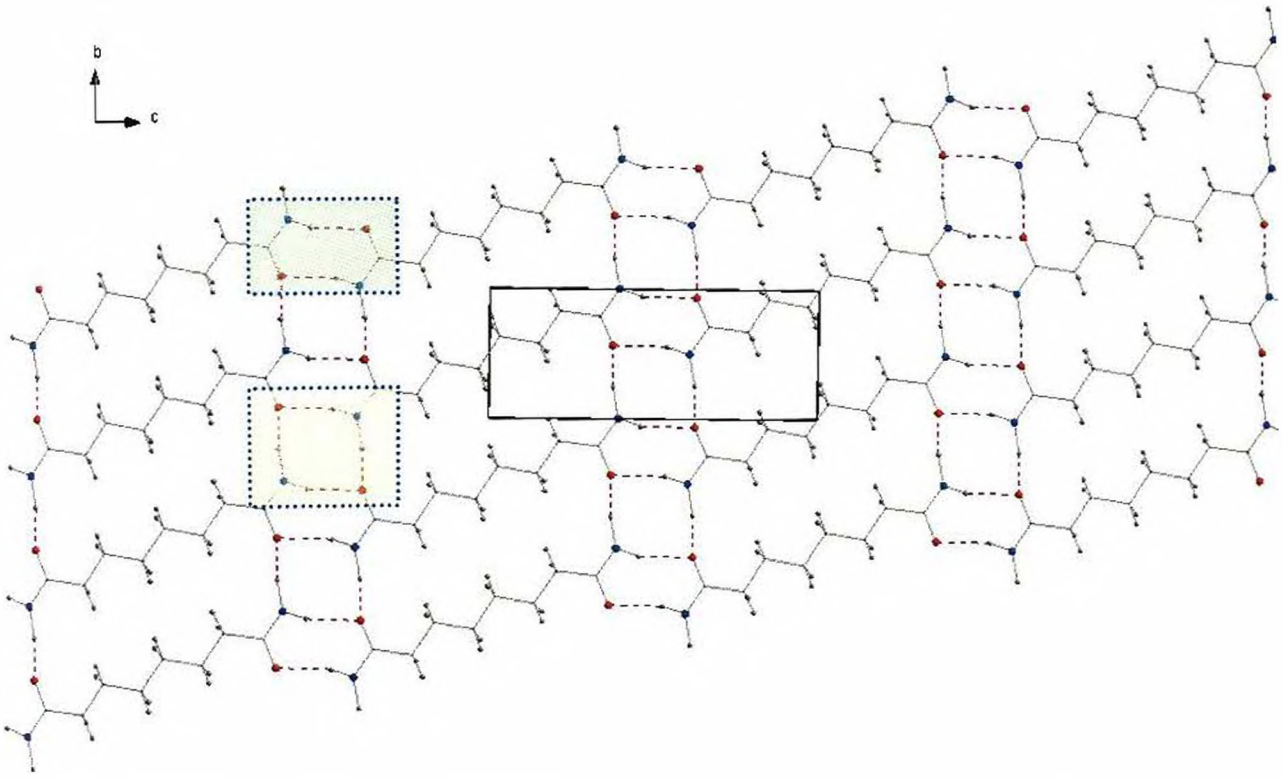

Figure 5.9.1: View suberamide (IX) showing a combination of dimers and chains to form the hydrogen bonded sheet. The $R_2^2(8)$ and $R_4^2(8)$ motifs are shown using green and yellow shading respectively.

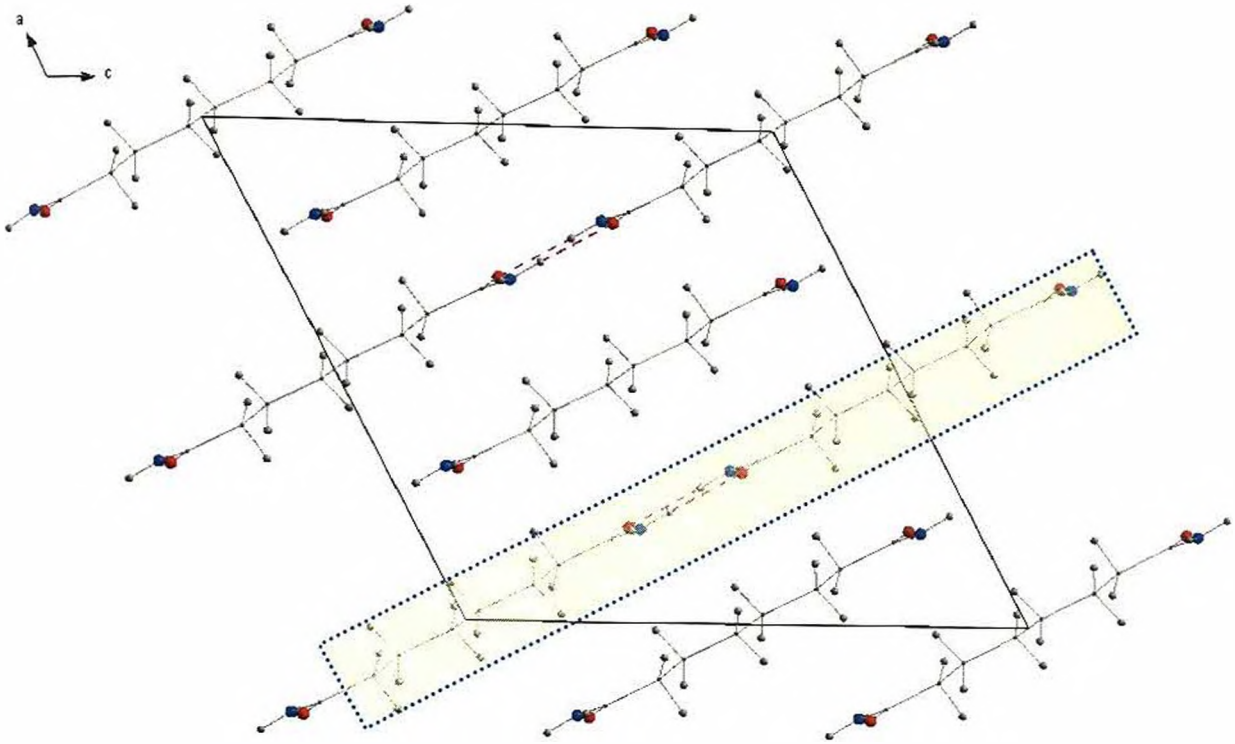

Figure 5.9.2: End-on view of hydrogen bonded sheets in suberamide (IX) as illustrated by the yellow shading.

5.9.2 Structure prediction analysis - Suberamide

Crystal structure prediction was performed in the space group C2/c (15). No geometric restraints were placed upon the molecular model, which was allowed to rotate through all degrees of freedom (as in figure 5.1.1). The prediction calculation generated 250 theoretical crystal structures, ranging in energy from –38.94 to –34.76 kcalmol^{-1}. Table 5.9.2 shows the top 30 predicted models and their corresponding unit cell parameters.

No.	Volume ($Å^3$)	Density (gcm^{-3})	Lattice energy ($kcalmol^{-1}$)	a (Å)	b (Å)	c (Å)	β (°)
1	1970.74	1.16	-38.94	16.77	7.50	26.40	143.60
2	1965.76	1.16	-38.84	21.02	5.30	20.14	118.83
3	1945.07	1.18	-38.78	25.71	4.56	16.59	88.88
4	1945.13	1.18	-38.67	35.40	5.05	35.49	162.14
5	1926.66	1.19	-38.63	21.56	5.05	19.60	115.35
6	1971.00	1.16	-38.60	30.94	5.05	14.65	120.52
7	1946.09	1.18	-38.44	19.32	4.53	30.06	132.25
8	1889.85	1.21	-38.39	25.71	5.11	17.40	124.28
9	1974.84	1.16	-38.27	21.07	5.25	25.99	43.44
10	1945.29	1.18	-38.17	25.75	5.12	29.77	150.27
11	2002.37	1.14	-38.14	25.65	4.96	47.24	160.56
12	1976.17	1.16	-38.12	13.15	7.68	24.00	125.34
13	1985.27	1.15	-38.11	26.45	9.87	18.02	155.04
14	1974.78	1.16	-38.11	25.42	4.97	26.35	143.58
15	1918.12	1.19	-37.97	25.66	5.12	21.53	137.29
16	1991.62	1.15	-37.95	13.63	7.60	20.75	67.93
17	1992.82	1.15	-37.95	29.31	7.59	14.41	141.55
18	2071.31	1.10	-37.94	18.92	8.88	12.94	72.39
19	1935.41	1.18	-37.82	25.71	5.12	24.81	143.67
20	1957.30	1.17	-37.80	42.53	4.82	9.71	100.57
21	2012.11	1.14	-37.79	23.42	4.98	21.38	126.22
22	1919.48	1.19	-37.78	34.99	5.07	19.27	145.82
23	1946.71	1.18	-37.77	25.73	5.11	25.35	144.30
24	1944.29	1.18	-37.76	25.73	5.12	15.54	71.84
25	1908.38	1.20	-37.73	39.16	4.86	11.18	116.29
26	1907.70	1.20	-37.73	19.30	5.55	20.62	120.21
27	1998.79	1.14	-37.69	20.43	7.53	13.94	68.65
28	1929.39	1.19	-37.69	10.22	5.04	37.95	99.24
29	1983.16	1.15	-37.69	20.16	9.89	10.04	97.97
30	1944.43	1.18	-37.60	35.20	5.06	35.14	161.92

Table 5.9.2: Top 30 predicted structures for suberamide (IX).

5.9.3 Re-ranking of structure prediction results - Suberamide

Ranked according to lattice energy ($kcalmol^{-1}$)		Ranked according to Hbonding merit points		Ranked according to graphset merit points	
1	**-38.94**	**1**	**80.00**	**1**	**2**
2	**-38.84**	**2**	**80.00**	**2**	**2**
3	-38.78	3	80.00	3	2
4	-38.67	4	80.00	4	2
5	-38.63	5	80.00	5	2
6	-38.60	6	80.00	6	2
7	-38.44	7	80.00	7	2
8	-38.39	8	80.00	8	2
9	**-38.27**	**10**	**80.00**	**9**	**2**
10	**-38.17**	11	80.00	**10**	**2**
11	-38.14	12	80.00	11	2
12	-38.12	13	80.00	14	2
13	-38.11	14	80.00	15	2
14	-38.11	15	80.00	19	2
15	-37.97	16	80.00	20	2
16	-37.95	17	80.00	21	2
17	-37.95	18	80.00	23	2
18	-37.94	19	80.00	24	2
19	-37.82	20	80.00	25	2
20	-37.80	21	80.00	26	2
21	-37.79	23	80.00	30	2
22	-37.78	24	80.00	12	1
23	-37.77	25	80.00	13	1
24	-37.76	26	80.00	16	1
25	-37.73	29	80.00	17	1
26	-37.73	**9**	**79.94**	18	1
27	-37.69	27	79.74	22	1
28	-37.69	22	79.29	27	1
29	-37.69	30	79.29	28	1
30	-37.60	28	78.89	29	1

Table 5.9.3: Top 30 predicted structures for suberamide (IX) re-ranked according to hydrogen bonding and graph set merit points. Highlighted structures show similarity to experimental structure.

The re-ranking procedure (table 5.9.3) shows that only 25 theoretical structures have the expected maximum 80 hydrogen bonding merit points and 20 structures have 2 graph set merit points highlighting the presence of the characteristic structural motifs expected in amide crystal structures. All theoretical structures with maximum merit points were examined further. However, only structures 1, 2, 9 and 10 are discussed in more detail (highlighted) either due to their similarity to the experimentally determined structure or due to their behaviour in the re-ranking process.

Suberamide structure 1 is energetically the most favorable structure and has remained at position 1 with the maximum hydrogen bonding merit points and graph set assignment merit points (table 5.9.3). The structure comprises N-H...O=C type hydrogen bonds that generate $R_2^2(8)$ dimers and C(4) chains which combine to form a secondary network of $R_2^2(8)$ rings. These motifs give rise to ladders in the [201] direction that are themselves linked though the molecule giving rise to staggered sheets which run parallel to the (101) plane (figures 5.9.3 and 5.9.4). The obvious difference between the experimental crystal structure and predicted structure 1 is that the latter contains molecules which occupy positions at each of the unit cell edges and ½ the distance along each of the axis *a* and *c*. In the former the molecules are arranged more horizontally and hence form sheets along the (101) plane.

				D-H	H...A	D...A	D-H...A
1	N05	--H21	..O07	0.9600	2.0700	3.0166	168.00
2	N05	--H22	..O07	0.9600	2.0200	2.9777	176.00
3	N06	--H23	..O08	0.9600	2.0700	3.0167	168.00
4	N06	--H24	..O08	0.9600	2.0200	2.9776	176.00

1	N05	--H21	..O07:	2.07	merit = 10
2	N05	--H22	..O07:	2.02	merit = 10
3	N06	--H23	..O08:	2.07	merit = 10
4	N06	--H24	..O08:	2.02	merit = 10

1	N05	--H21	..O07:	168	merit = 10
2	N05	--H22	..O07:	176	merit = 10
3	N06	--H23	..O08:	168	merit = 10
4	N06	--H24	..O08:	176	merit = 10

TOTAL MERIT FOR POLYMORPH 1 = 80

Table 5.9.4: Hydrogen bonding information generated by the re-ranking strategy for suberamide structure 1.

Suberamide structure 2 is another structure that has the maximum number of merit points and whose relative position in the rankings has remained unchanged with respect to hydrogen bonding and graph set assignment merit points (table 5.9.3). The hydrogen bonding arrangement of structure 2 consists of $R_2^2(8)$ dimers and C(4) chains running in the [001] direction. Although projection down the *b* axis gives the illusion of infinite ladders in the [001] direction, alternating dimers lie perpendicular to each other, such that the combination of these two characteristic motifs gives rise to larger $R_6^6(24)$ rings in an infinite three dimensional network (figures 5.9.5 and 5.9.6).

				D-H	H...A	D...A	D-H...A
1	N05	--H21	..O07	0.9600	2.0700	3.0204	168.00
2	N05	--H22	..O07	0.9600	2.0300	2.9866	172.00
3	N06	--H23	..O08	0.9600	2.1000	3.0481	169.00
4	N06	--H24	..O08	0.9600	2.0300	2.9907	173.00

1	N05	--H21	..O07:	2.07	merit = 10
2	N05	--H22	..O07:	2.03	merit = 10
3	N06	--H23	..O08:	2.10	merit = 10
4	N06	--H24	..O08:	2.03	merit = 10

1	N05	--H21	..O07:	168	merit = 10
2	N05	--H22	..O07:	172	merit = 10
3	N06	--H23	..O08:	169	merit = 10
4	N06	--H24	..O08:	173	merit = 10

TOTAL MERIT FOR POLYMORPH 2 = 80

Table 5.9.5: Hydrogen bonding information generated by the re-ranking strategy for suberamide structure 2.

Suberamide structure 9 is analogous to structure 2 in that the hydrogen bonding arrangement also consists of $R_2^2(8)$ dimers and C(4) chains, and like structure 2 when projected down the *b* axis these motifs combine to give the illusion of infinite ladders along the [10-1] direction. Again like structure 2, alternating dimers lie perpendicular

to each other, such that the combination of these two characteristic motifs gives rise to larger $R_6^8(24)$ rings in an infinite three dimensional network (figures 5.9.7 and 5.9.8). Structure 9 has moved down to position 26 with respect to hydrogen bonding merit points due to a non-ideal N-H...O angle (table 5.9.3); it has however remained at position 9 with respect to graph set assignment points.

				D-H	H...A	D...A	D-H...A
1	N05	--H21	..O07	0.9700	2.1300	3.0701	164.00
2	N05	--H22	..O07	0.9600	2.0400	2.9935	173.00
3	N06	--H23	..O08	0.9600	2.0800	2.9983	158.00
4	N06	--H24	..O08	0.9600	2.0100	2.9571	169.00

1	N05	--H21	..O07:	2.13	merit = 10
2	N05	--H22	..O07:	2.04	merit = 10
3	N06	--H23	..O08:	2.08	merit = 10
4	N06	--H24	..O08:	2.01	merit = 10

1	N05	--H21	..O07:	164	merit = 10
2	N05	--H22	..O07:	173	merit = 10
4	N06	--H24	..O08:	169	merit = 10
3	N06	--H23	..O08:	158	merit = 9.94

TOTAL MERIT FOR POLYMORPH 9 = 79.94

Table 5.9.6: Hydrogen bonding information generated by the re-ranking strategy for suberamide structure 9.

The three dimensional hydrogen bonding network within suberamide structure 10 comprises N-H...O=C hydrogen bonds which generate $R_2^2(8)$ dimers and C(4) chains. The combination of these two motifs gives rise to a secondary network of $R_4^4(8)$ rings that generate ladders along the [010] direction. This analogous to that of the experimental crystal structure, however differs to predicted structure 1, which has ladders extending along the [201] direction. Structure 10 also generates infinite hydrogen bonded sheets along the (110) plane; this is unlike structure 1 and the

experimental crystal structure, which have infinite sheets running along (101) and (011) respectively (figures 5.9.9 and 5.9.10). Structure 10 has the maximum number of hydrogen bonding merit points but has only moved up the rankings by 1 position (table 5.9.3).

				D-H	H...A	D...A	D-H...A
1	N05	--H21	..O07	0.9600	2.0500	3.0008	170.00
2	N05	--H22	..O08	0.9600	2.0400	2.9805	165.00
3	N06	--H23	..O08	0.9600	2.0600	3.0117	170.00
4	N06	--H24	..O07	0.9600	2.0400	2.9782	164.00

1	N05	--H21	..O07:	2.05	merit = 10
2	N05	--H22	..O08:	2.04	merit = 10
3	N06	--H23	..O08:	2.06	merit = 10
4	N06	--H24	..O07:	2.04	merit = 10

1	N05	--H21	..O07:	170	merit = 10
2	N05	--H22	..O08:	165	merit = 10
3	N06	--H23	..O08:	170	merit = 10
4	N06	--H24	..O07:	164	merit = 10

TOTAL MERIT FOR POLYMORPH 10 = 80

Table 5.9.7: Hydrogen bonding information generated by the re-ranking strategy for suberamide structure 10.

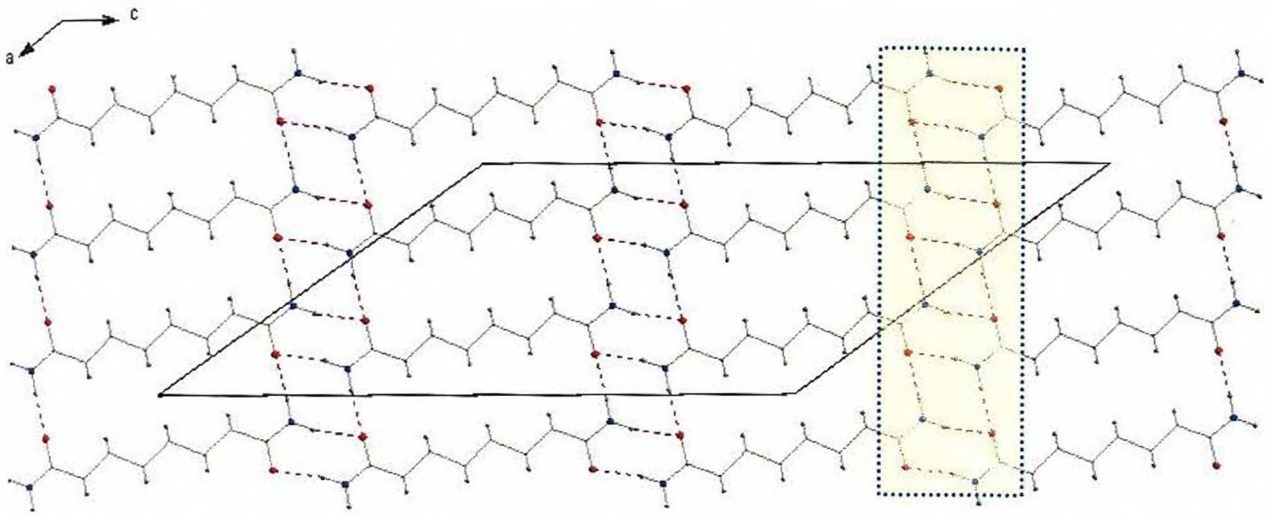

Figure 5.9.3: View of suberamide structure 1 showing ladders in the [201] direction (yellow shaded area).

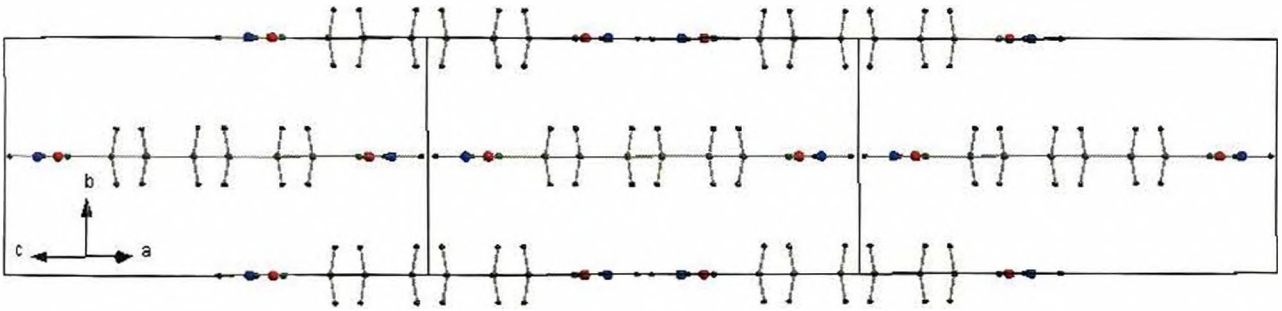

Figure 5.9.4: End on view of suberamide structure 1 showing the sheets along (101) plane.

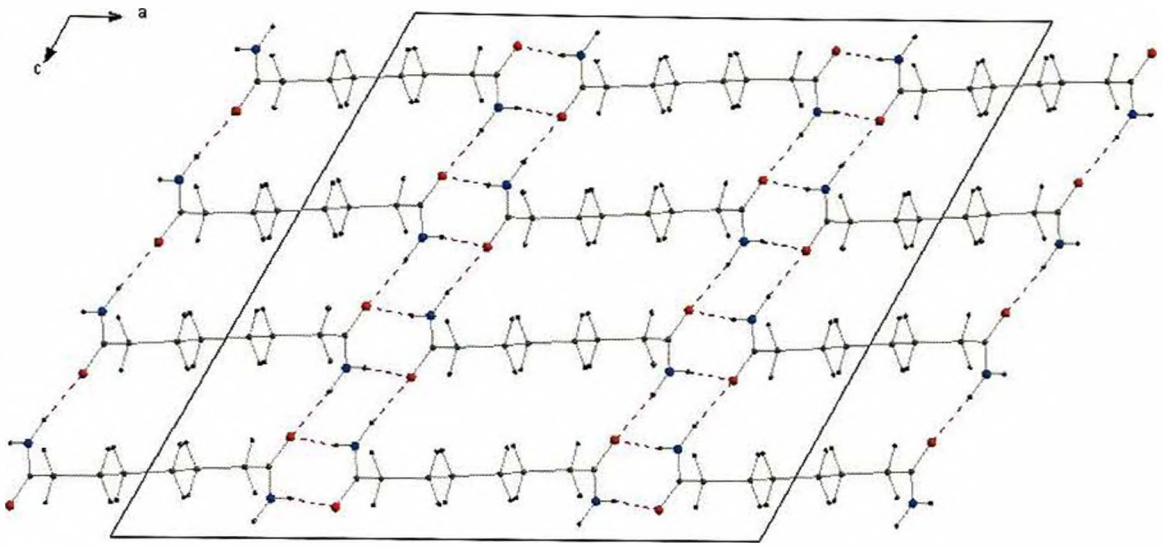

Figure 5.9.5: Suberamide structure 2 showing the combination of dimers and chains giving the illusion of ladders.

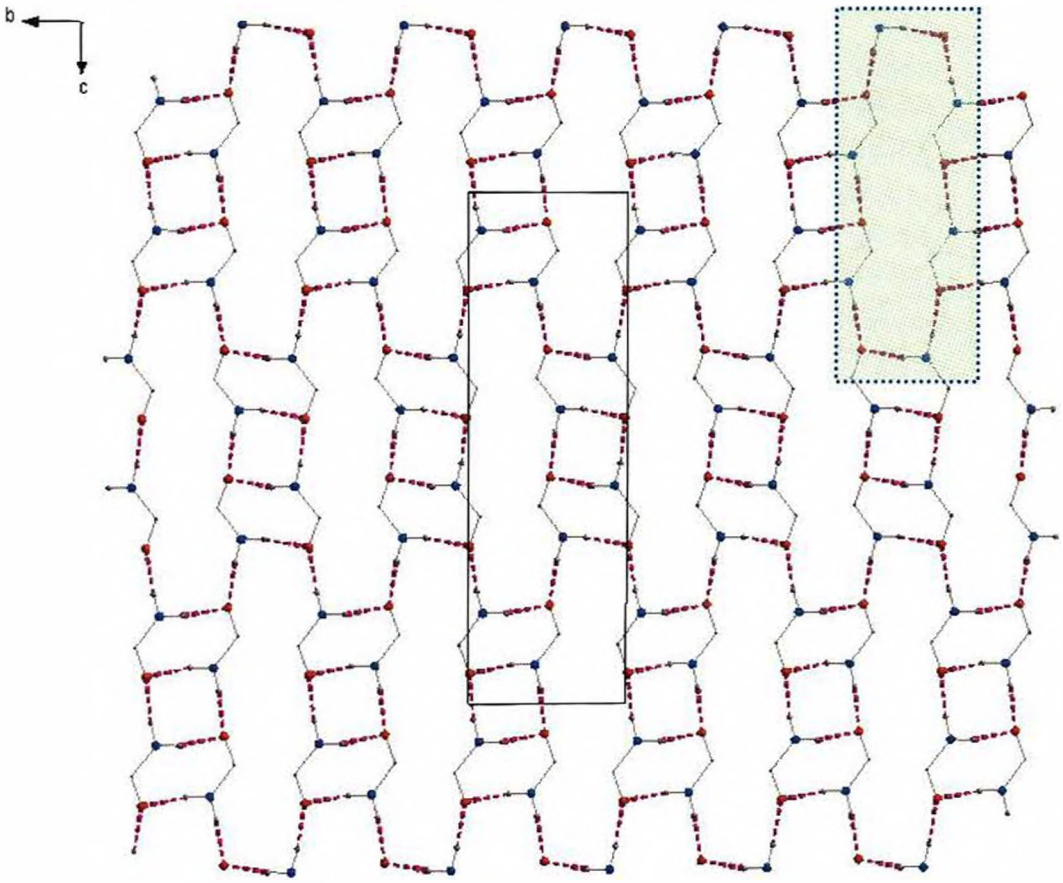

Figure 5.9.6: View of suberamide structure 2 (aliphatic carbon atoms omitted for clarity) showing the hydrogen bonded sheet along (011). The $R_6^8(24)$ motif is illustrated using green shading.

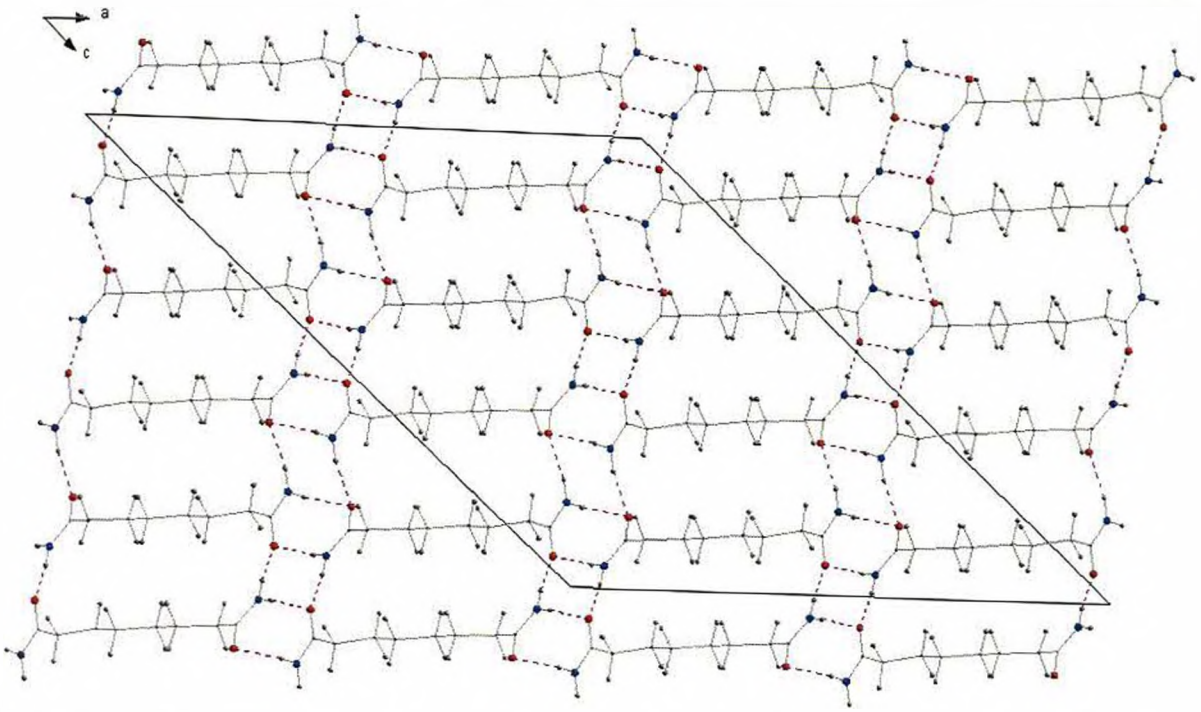

Figure 5.9.7: View of suberamide structure 9 showing the combination of dimers and chains giving the illusion of ladders.

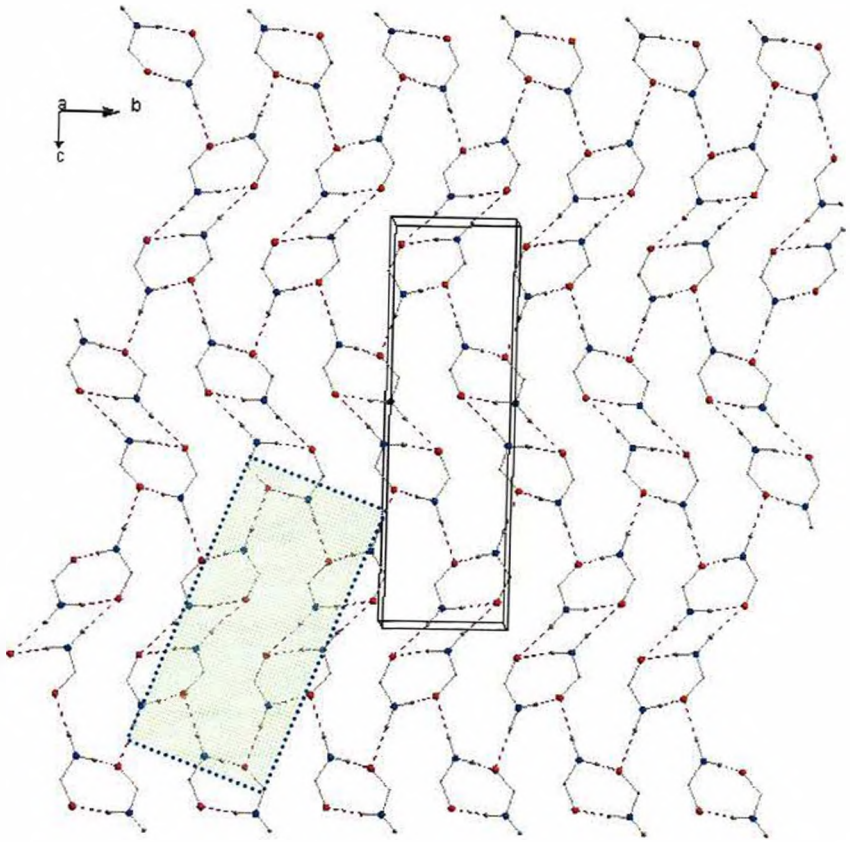

Figure 5.9.8: View of suberamide structure 9 (aliphatic carbon atoms omitted for clarity) showing the hydrogen bonded sheet along (011). The $R_6^8(24)$ motif is illustrated using green shading.

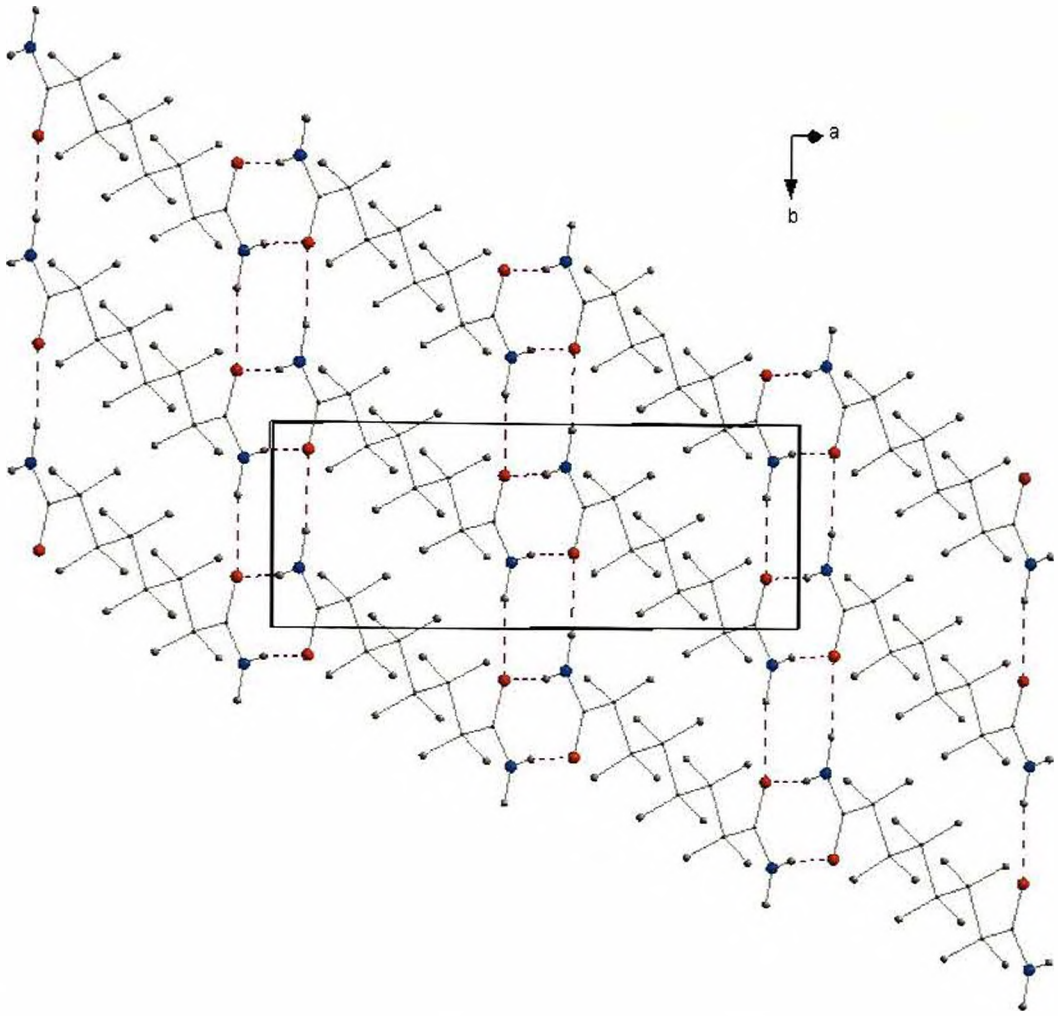

Figure 5.9.9: View of suberamide structure 10 showing the combination of dimers and chains to form the hydrogen bonded sheet.

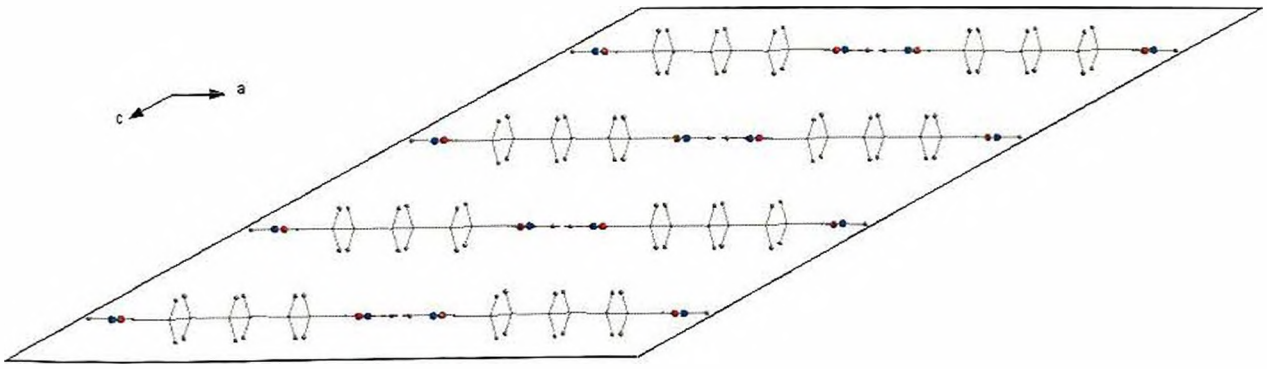

Figure 5.9.10: End-on view of suberamide structure 10 showing hydrogen bonded sheets along (110).

Simulated powder X-ray diffraction data were used to compare the experimental structure with the predicted suberamide structures 1, 2, 9 and 10 (see figure 5.9.11). The powder patterns of structures 2 and 9 are comparable to one another but dissimilar to the experimental structure. This is not surprising since the three dimensional arrangements of structures 2 and 9 form the same structural motifs which are consequently not formed in the experimental crystal structure. The simulated X-ray diffraction patterns for structure 1 and 10 also show some resemblance to the experimental crystal structure in that similar characteristic motifs are present in both structures. However, on inspection of their packing arrangements and their simulated powder patterns it is clear that they are not the same.

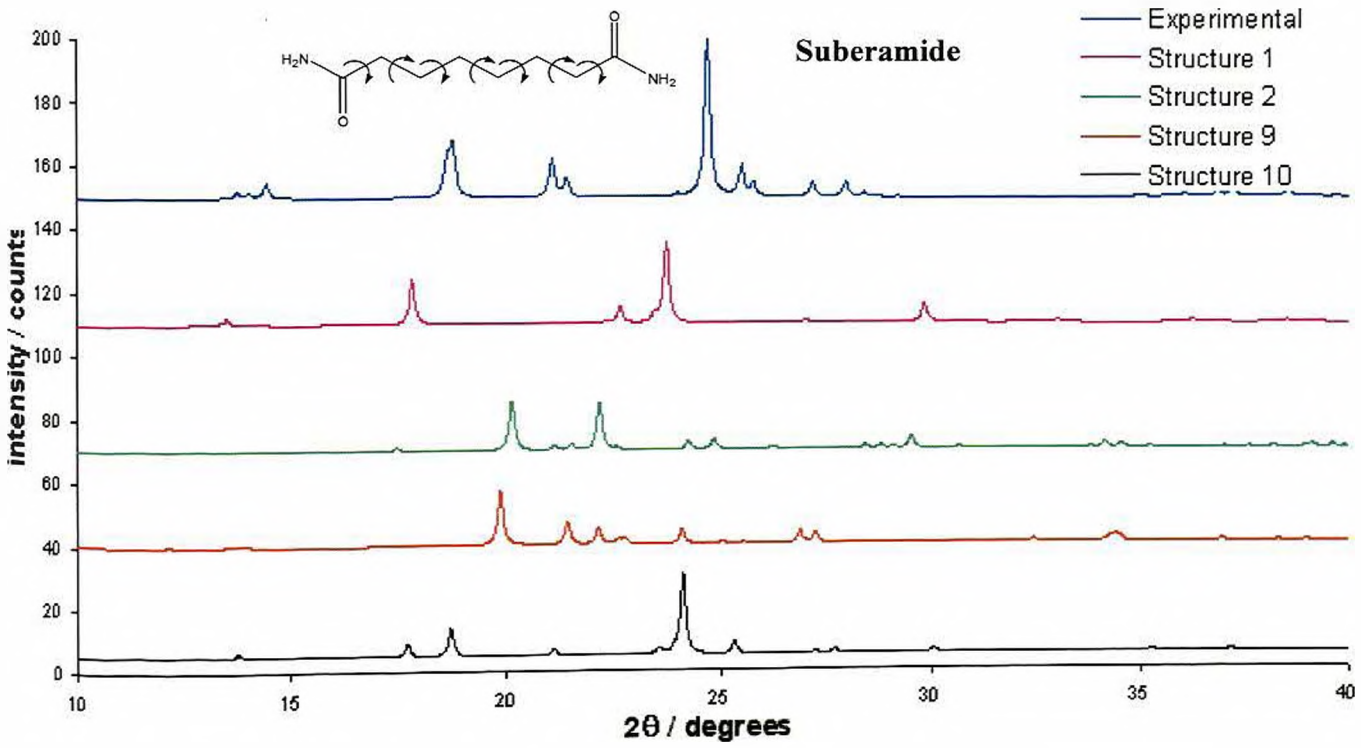

Figure 5.9.11: Comparison of the simulated experimental X-ray diffraction pattern of suberamide with predicted suberamide structures 1, 2, 9 and 10.

5.10 Azelamide

5.10.1 Experimental crystal structure

The crystal structure of azelamide (X) [Hospital. M. 1971] has been determined using conventional single crystal X-ray diffraction data, although the hydrogen atoms were placed in idealised positions and not refined. The unit cell parameters, space group and single point minimised lattice energy of the experimentally determined crystal structure are given in table 5.10.1.

a (Å)	5.782(6)
b (Å)	8.641(9)
c (Å)	27.687(15)
β (°)	131.75(33)
Volume ($Å^3$)	1032.025(16)
Density (gcm^{-3})	1.196(6)
Z	4
Space group	C2/c (15)
Single point minimised lattice energy ($kcalmol^{-1}$)	-34.96

Table 5.10.1: The crystallographic and lattice energy data for experimentally determined Azelamide.

The crystal packing arrangement in azelamide (X) is also determined by two distinct N-H...O=C type hydrogen bonds. The amino N atom acts as a double donor and forms the two characteristic motifs; the $R_2^2(8)$ dimer and C(4) chain, which combine to form a secondary $R_4^2(8)$ ring system resulting in the formation of ladders extending

along [110] direction. The amide groups within each molecule lie 90° with respect to one another such that an infinite three dimensional network is formed by combination of ladders running along the [110] direction linked through the molecule itself to ladders along the [001] direction (figure 5.10.1 and 5.10.2).

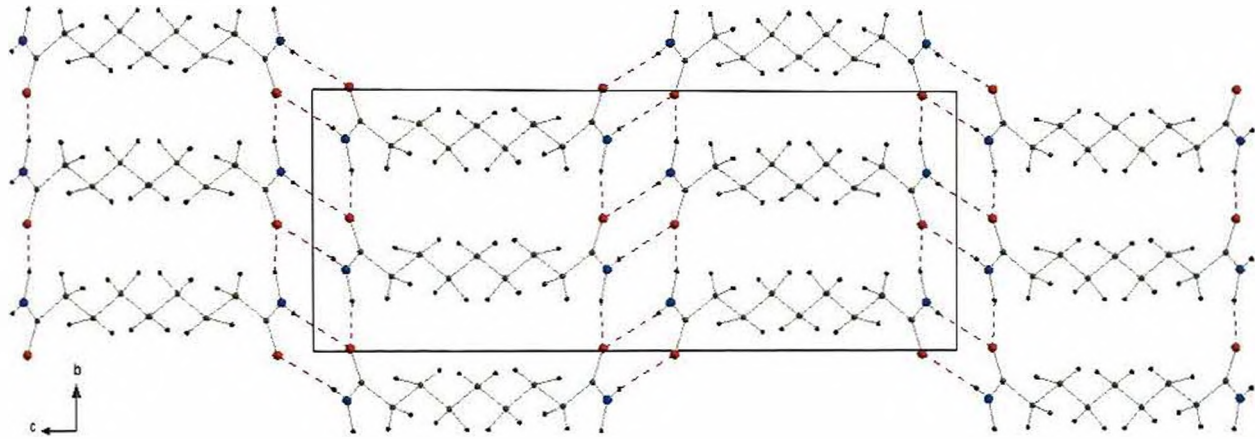

Figure 5.10.1: View of azelamide (X) showing the ladders extending along the [110] direction.

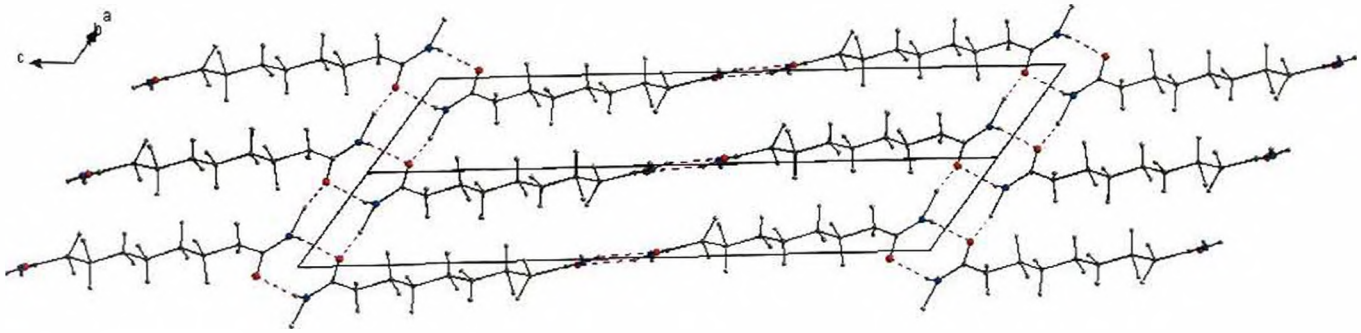

Figure 5.10.2: View of azelamide (X) illustrating the infinite sheets in the [001] direction.

5.10.2 Structure prediction analysis - Azelamide

Crystal structure prediction was performed in the space group C2/c (15). No restraints were placed upon the molecular model, which was allowed to rotate through all degrees of freedom (as in figure 5.1.1). As in pimelamide (section 5.8) it is obvious to suspect that an odd number of carbon atoms in the aliphatic chain and high flexibility could be attributed to the failure of this structure prediction.

5.11 Sebacamide

5.11.1 Experimental crystal structure

The crystal structure of sebacamide (XI) [Heraud J. et al. 1966] has been determined using conventional single crystal X-ray diffraction data, although the hydrogen atoms were placed in idealised positions and not refined. The unit cell parameters, space group and single point minimised lattice energy of the experimentally determined crystal structure are given in table 5.11.1.

a (Å)	10.36(1)
b (Å)	5.66(1)
c (Å)	9.83(1)
β (°)	95(1)
Volume ($Å^3$)	574.214(1)
Density (gcm^{-3})	1.127(1)
Space group	$P2_1/c$ (14)
Z	2
Single point minimised lattice energy ($kcalmol^{-1}$)	-38.26

Table 5.11.1: The crystallographic and lattice energy data for experimentally determined sebacamide.

The crystal structure of (XI) has a hydrogen bonding arrangement comprising $R_2^2(8)$ dimers and C(4) chains running in the [001] direction. Although projection down the *b* axis gives the illusion of infinite ladders in the [001] direction, alternating dimers lie perpendicular to each other, such that the combination of these two characteristic

motifs gives rise to larger $R_4^6(16)$ rings in an infinite three dimensional network (figures 5.11.1 and 5.11.2).

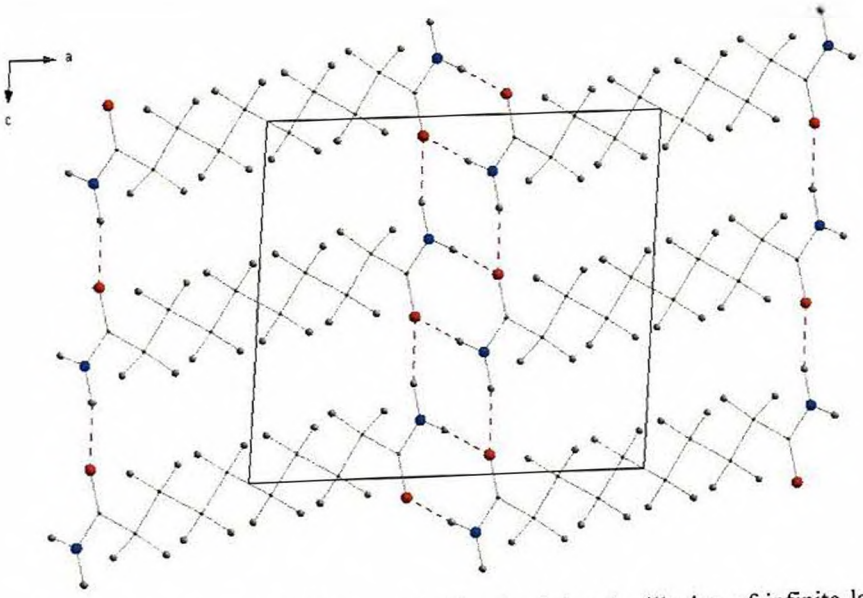

Figure 5.11.1: Projection of sebacamide (XI) down the *b* axis giving the illusion of infinite ladders in the [001] direction.

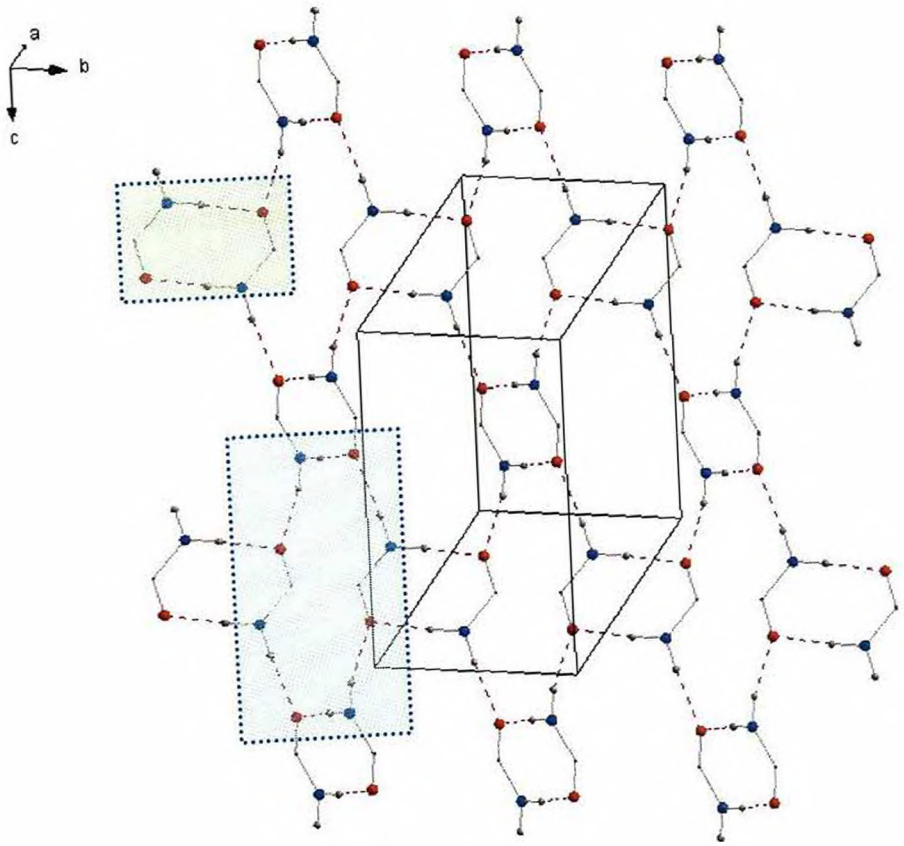

Figure 5.11.2: View of sebacamide (XI) showing the hydrogen bonded sheet along (011). Aliphatic carbon atoms are omitted for clarity. The $R_2^2(8)$ dimer and the $R_4^6(16)$ motif is shown using green and blue shading respectively.

5.11.2 Structure prediction analysis - Sebacamide

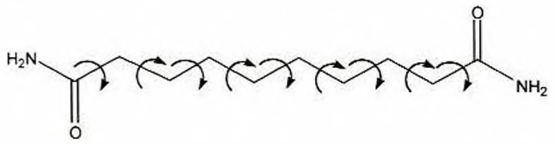

Crystal structure prediction was performed in the space group $P2_1/c$ (14). No restraints were placed upon the molecular model, which was allowed to rotate through all degrees of freedom (as in figure 5.1.1). The prediction calculation for sebacamide was attempted 3 times, but like pimelamide (section 5.8) and azelamide (section 5.10), the calculation failed to complete. Again there is no obvious reason why the calculation failed since it the molecule does not contain an odd number of carbon atoms in the aliphatic chain. Perhaps the high degree of flexibility simply posed too much demand computationally, resulting in the failure of this structure prediction.

5.12 Discussion

A computational strategy that is capable of automatically re-ranking a traditional polymorph prediction output on the basis of structural geometry has been successfully developed. Eleven test cases (aromatic and aliphatic) were selected from the Cambridge Structural Database and used in the development of the re-ranking strategy. All eleven structures showed a preference towards the generation of characteristic $R_2^2(8)$ amide dimers and C(4) chain motifs. The hydrogen bonding geometry of these motifs was used to award hydrogen bonding merit points to favourable crystal structures with the intention of moving them higher up the prediction rankings. Another effective method that was developed to work in tandem was the detection of the characteristic motifs within predicted structures and use this as a basis to award graph set merit points, again with an intention of moving more plausible theoretical structures higher up the rankings.

Examination of prediction data clearly demonstrated that ranking hypothetically according to lattice energy alone is not reliable. Within the re-ranked prediction tables there was some significant movement in the relative positions of some theoretical structures compared to their original lattice energy position. Structures with the maximum number (or greater) of hydrogen bonding and graphset assignment merit points were inspected manually and compared to their corresponding experimental structures. In terms of the aromatic predictions, a significant number of predictions showed the presence of the 2 characteristic $R_2^2(8)$ amide dimer and C(4) chain motifs which combine to form a secondary network of $R_4^4(8)$ rings and consequently ladders. However, some unexpected motifs were also generated, e.g. in

the benzamide prediction, structure 9 fell down 17 places following re-ranking due to it containing an alternative N-H...N dimer leading to the formation of spirals. In the cases of meta and para-methylbenzamide the generation of a secondary network of $R_6^4(16)$ rings was evident in some structures, this was totally unexpected as it was not considered a typical motif characteristic of these structures.

The aliphatic predictions were not as successful as the aromatic, in that the polymorph prediction calculation of 3 structures, namely pimelamide (VIII), azelamide (X) and sebacamide (XI) failed to complete and as a consequence generated no prediction data. This failure could possibly be attributed to the extent of flexibility and the large number of degrees of freedom present within the molecules; also two of the structures had an odd number of carbon atoms within their aliphatic chains and could of also accredited to their failure. Of the successfully predicted aliphatic structures all showed preference for the characteristic $R_2^2(8)$ amide dimer and C(4) chain motifs combining on a secondary level to generate $R_4^2(8)$ rings and ladders. It was envisaged that aliphatic amide structures hydrogen bond in a planar fashion and very little rotation would be seen of the amide functional group. This however was not the case, with a number of structures showing preference for the formation of puckered three dimensional hydrogen bonded sheets. The adipamide triclinic polymorph is seen as being typical of amide structures, however its monoclinic polymorph exhibits an alternative hydrogen bonding arrangement and generates ladders of $R_3^2(8)$ rings. Within the structures suberamide and sebacamide $R_2^2(8)$ amide dimer and C(4) chain motifs are present but rather than combination on a secondary level to generate ladders, larger ring systems, namely $R_6^8(24)$ and $R_4^6(16)$ rings are generated. The characterisation and application of unitary motifs to guide the re-ranking strategy has enabled successful movement of plausible structures higher up the prediction

rankings. However, secondary motif data could not be incorporated into the re-ranking strategy because these larger motifs are were not characteristic within the family of structures studied.

The lattice energies of the experimental crystal structures and the equivalent 'best' prediction were also compared in order to confirm that the polymorph prediction sequence was searching the surface effectively, and that the experimental plus theoretical results are comparable. Table 5.12.1 illustrates that the optimal predicted structure in each case is lower in lattice energy than the experimental counterpart. This is certainly a cause for concern, as it raises questions of whether the experimental structure is indeed the most stable polymorph or that optimisation during calculation of the lattice energy of the experimental structure was not entirely effective. i.e. could the predicted theoretical structures be new undiscovered polymorphs.

Molecular system investigated	Lattice energy of CCD structure ($kcalmol^{-1}$)	Lattice energy of predicted structure 1 ($kcalmol^{-1}$)
Benzamide	-6.00	-6.64
Ortho-methylbenzamide	-1.81	-2.06
Meta-methylbenzamide	-4.83	-6.74
Para-methylbenzamide	-6.81	-7.89
Oxamide	-1.01	-3.36
Glutaramide	-35.99	-39.82
Adipamide (triclinic)	-37.93	-40.13
Adipamide (monoclinic)	-35.65	-40.06
Pimelamide	-34.34	-
Suberamide	-37.48	-38.94
Azelamide	-34.96	-
Sebacamide	-38.26	-

Table 5.12.1: Comparison of the lattice energy of the experimental single crystal structures with that of their corresponding theoretically predicted structures.

Development and application of this re-ranking strategy has clearly demonstrated some success on re-ranking theoretically plausible structures that possibly would not have otherwise been examined. Awarding points to favourable structures through the examination of hydrogen bonding geometry and the graph set assignments has proved invaluable and from the eleven test structures selected and downloaded from the Cambridge Structural Database the prediction sequence completely failed for only three structures. Consequently the 'best' predicted theoretical structure was not always identical when compared to the experimental test structure. However, in some cases the predicted structure contained a molecular distribution within the unit cell that contained certain structural characteristics in comparison with the experimental structure. Certainly more success has been seen here than actual failure, looking not only at the number of structures that were correctly predicted, but also the relative success in the applications ability to work towards extracting vital geometrical and structural data and moving structures up and down the rankings to more realistic positions.

6.0 Conclusion

The research contained within this thesis is based on two main areas of structural chemistry, crystal structure determination from powder diffraction and theoretical crystal structure prediction.

Firstly, the successful application of the 'direct space' differential evolution (DE) global optimisation technique for structure solution from the combined use of powder X-ray, synchrotron and neutron diffraction has been clearly demonstrated within this thesis using two examples. The use of this technique to determine molecular crystal structures directly from powder X-ray diffraction data has become a real capability, and it is envisaged that the crystal structures of even more complex systems will be elucidated using this method in the near future. Although not complex in terms of conformational flexibility or number of optimisation parameters, both examples demonstrate the limitations and complementary of powder X-ray and neutron diffraction data in the study of organic materials. 2,4-dichloro-5-sulfamoylbenzoic acid and oxamic acid are two such examples investigated using the techniques and methods as described. In both cases powder X-ray diffraction data were not sufficient to ensure that the correct solution had been obtained and as a result additional neutron and synchrotron datasets were recorded.

In the case of 2,4-dichloro-5-sulfamoylbenzoic acid neutron data was used to accurately define the relative positions of hydrogen atoms and hence determine the orientation of the sulfonyl group. Force field based energy calculations were also used as a complimentary tool to give invaluable clues as to the most energetically stable crystal structure.

In the case of oxamic acid, synchrotron data have confirmed the *trans* conformation as being the most likely structure solution. Further structural analysis is needed to distinguish the exact location of the amine and hydroxyl groups and information that would help in distinguishing between the oxygen and nitrogen atoms. Hence a neutron dataset was recorded, however due to time restrictions the dataset has not yet been analysed. It is envisaged that this data will enable completion of this investigation through further structure refinement.

Secondly, a computational re-ranking strategy has been developed that is capable of automatically examining a traditional theoretical polymorph prediction output and re-rank 'structurally favourable' crystal structures. Crystal structure prediction aims to predict the three dimensional packing arrangement of a substance on the basis of its molecular structure only. Given the inherent 'phase problem' with crystal structure determination, theoretical prediction is a major facet to structural solid state and provides an alternative route to structure elucidation. The method developed here overcomes the problem of unreliable ranking based purely on lattice energy, the application extracts both hydrogen bonding geometry and graph set assignment information and awards merit points based on the comparison to predefined geometry values and motifs. The re-ranking strategy has been developed by selection of eleven experimental test structures (aromatic and aliphatic amides) whose three dimensional crystal arrangements had been previously determined experimentally. The application has proved to be successful, in that the most plausible theoretical predictions with the expected structural features were re-ranked to higher positions in the rankings. This computational re-ranking method is relatively simple in its construct; only hydrogen bonding geometry and graph set assignment information were incorporated into the merit point scheme and hence guide the re-ranking procedure.

It was envisaged that the hydrogen bonding and graph set merit points system was to be combined in order to obtain an overall 'figure of merit', but this proved difficult within the time available. It is also clear that this type of merit system may only be applicable to well-defined families of compounds with clear structural systematics, and care must be taken in implementation (i.e. a possible use of secondary networks) to ensure reliable results.

Another issue raised from this work was whether or not it would have been more advantageous to carry out the prediction calculations in the top 8 space groups for each of the eleven structures, rather then the space group the crystal structure was experimentally determined in. This certainly would have allowed more theoretical structures to be evaluated with the possibility of identifying crystal structures more characteristic to the experimental crystal structure. However, this clearly would have taken more significant time and considerable effort and unquestionably introduced the concept of polymorphism, which in itself is a whole new ball game.

Given the current exponential advancements in computer hardware and software it is inevitable that crystal structure prediction algorithms will get increasingly powerful leading to exceptionally accurate search methods. Certainly the incorporation of additional geometrical and crystallographic information into prediction calculations has been demonstrated here to be advantageous in identifying the most plausible crystal structure. However, the disadvantage at present is that current prediction programs only model the thermodynamic (enthalpic) factors, and so do not take into account kinetic (entropic) factors such as nature of solvent or nucleation. It is envisaged that when all these energetic factors can be mathematically modelled accurately and combined constructively, only then will we see exceptionally accurate crystal structure predictions.

7.0 Appendices

7.1 Appendix 1

Deuteration of 2,4-dichloro-5-sulfamoylbenzoic acid

JPA - DR JON PREECE PROJECT STUDENTS

BRUKER

OC180S.109
AU PROG:
X00.AU
DATE 18-10-74

SA.NA 801927
SA.NO OC18 109
SF 300.135
SY 299.0
O1 6730.099
SI 32768
TD 32768
SW 6024.096
HZ/PT .368

PW 0.0
RD 0.0
AQ 2.720
RG 200
NS 32
TE 297

FW 7600
O2 0.0
DP 63L PO

LB .300
GB 0.0
CX 40.00
CY 20.00
F1 11.001P
F2 -1.498P
HZ/CM 93.786
PPM/CM .312
SR 4925.88

gerla

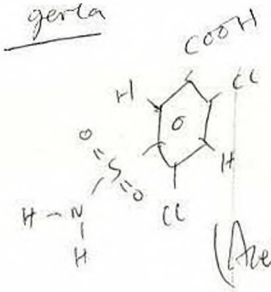

(Acetone-d)

2,4-dichloro-5-sulfamoylbenzoic acid

Ar-H

Ar-H

NH_2

Ar-H : NH_2

1 : 1.37

62

62

85

Acetone

B

INTEGRAL

18.367 17.787 24.448 2.932 60.698

10.5 10.0 9.5 9.0 8.5 8.0 7.5 7.0 6.5 6.0 5.5 5.0 4.5 4.0 3.5 3.0 2.5 2.0 1.5 1.0 .5 0.0 -.5 -1.0

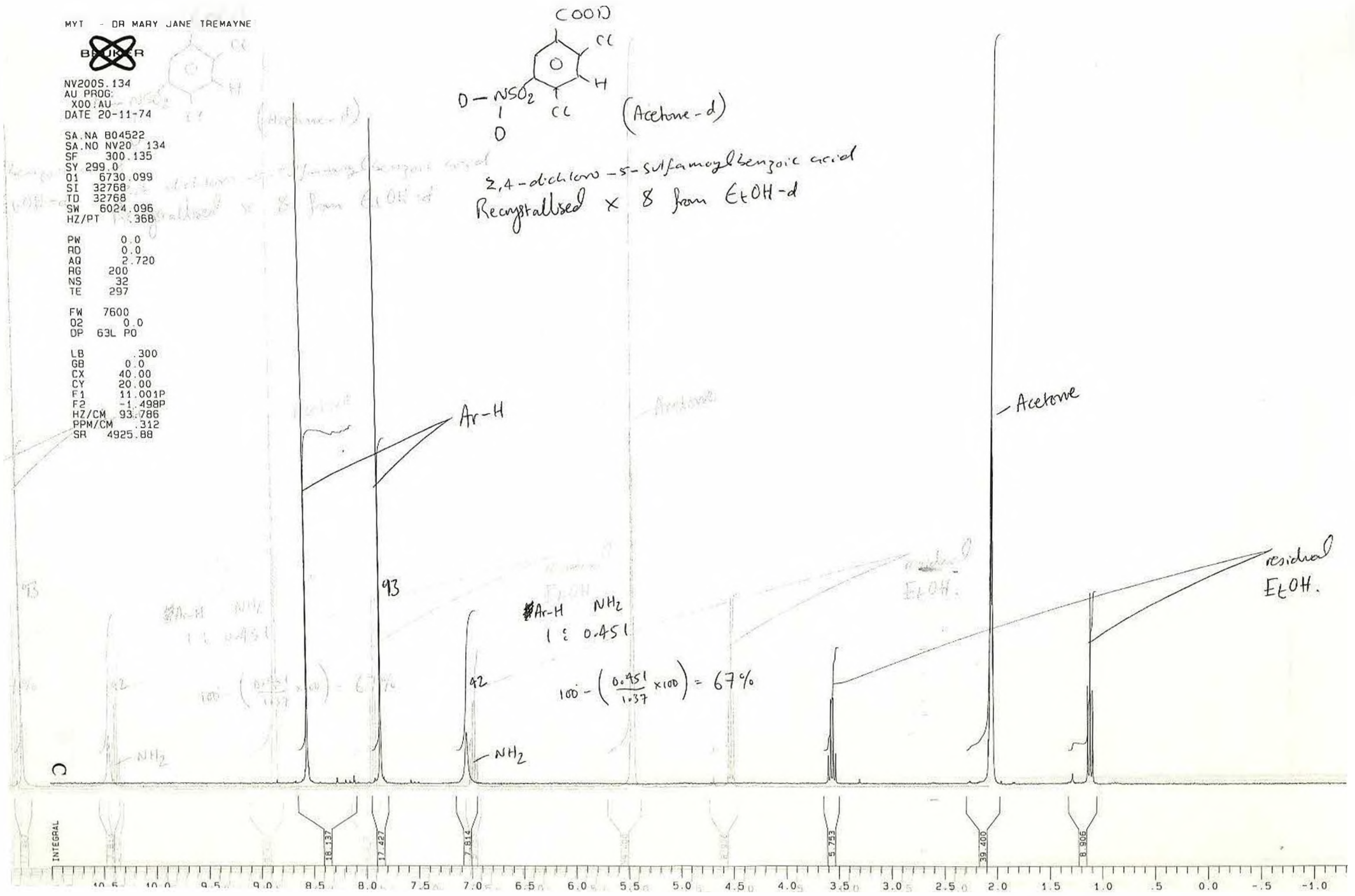
MYT - DR MARY JANE TREMAYNE
BRUKER
NV200S.134
AU PROG:
X00.AU
DATE 20-11-74
SA.NA B04522
SA.NO NV20 134
SF 300.135
SY 299.0
O1 6730.099
SI 32768
TD 32768
SW 6024.096
HZ/PT .368
PW 0.0
RD 0.0
AQ 2.720
RG 200
NS 32
TE 297
FW 7600
O2 0.0
OP 63L PO
LB .300
GB 0.0
CX 40.00
CY 20.00
F1 11.001P
F2 -1.498P
HZ/CM 93.786
PPM/CM .312
SR 4925.88
COOD
Cl
O
H
Cl
D—NSO2
O
(Acetone-d)
2,4-dichloro-5-sulfamoylbenzoic acid
Recrystallised x 8 from EtOH-d
Ar-H
Acetone
residual EtOH.
93
42
NH2
NH2
#Ar-H NH2
1 : 0.451
100 - (0.451/1.37 x100) = 67%
INTEGRAL
18.137
17.427
7.814
5.753
39.400
8.906
10.5 10.0 9.5 9.0 8.5 8.0 7.5 7.0 6.5 6.0 5.5 5.0 4.5 4.0 3.5 3.0 2.5 2.0 1.5 1.0 .5 0.0 -.5 -1.0

7.2 Appendix 2

Deuteration of oxamic acid

Infra-red spectra of oxamic acid before and after deuteration

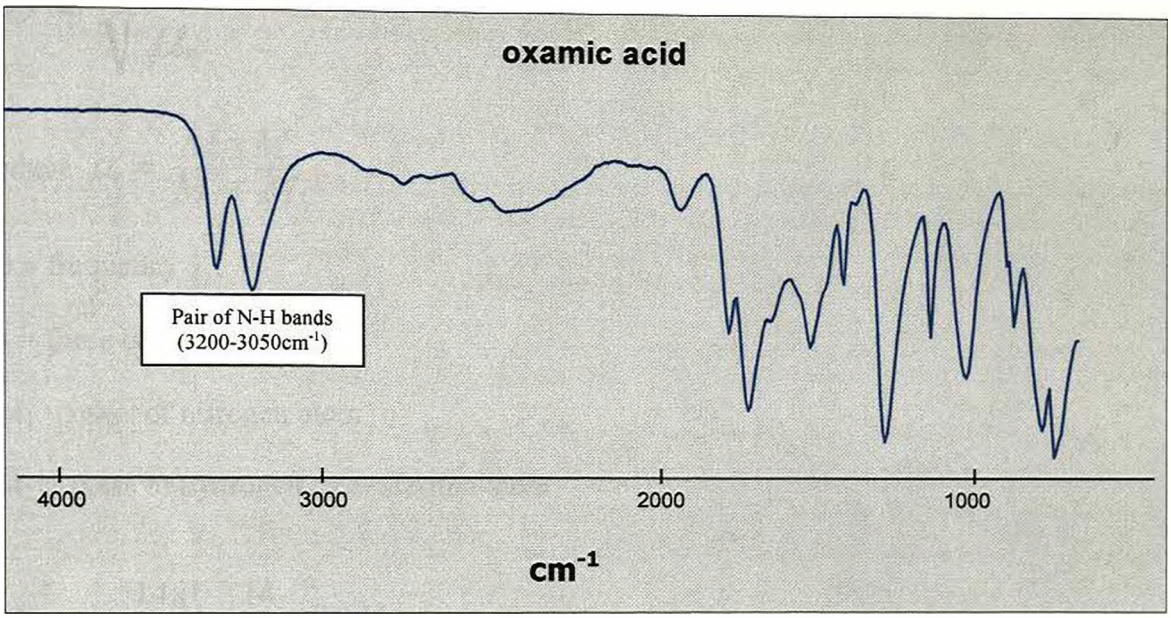

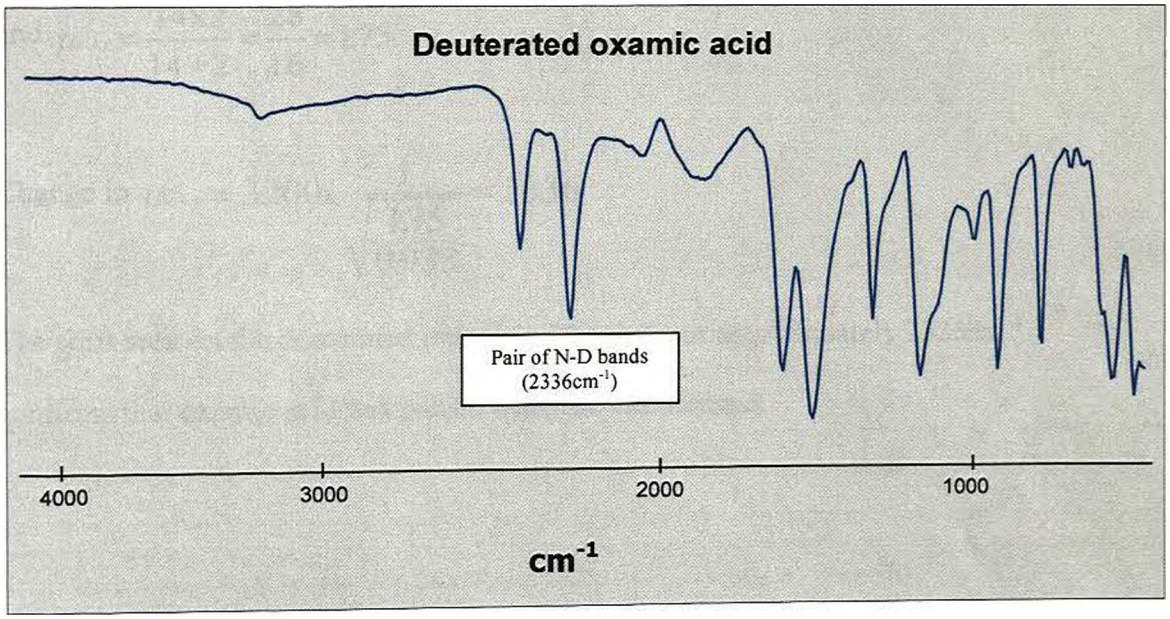

$$\upsilon = \sqrt{\frac{k}{\mu_m}}$$

where $\mu_m = \frac{M_1 x M_2}{M_1 + M_2}$

υ = frequency

k = force constant of a bond

M_1 = mass of nitrogen atom

M_2 = mass of hydrogen or deuterium atom

so $\mu_{N-H} = \frac{14x1}{14+1} = \frac{14}{15} = 0.933$

and $\mu_{N-D} = \frac{14x2}{14+2} = \frac{28}{16} = 1.75$

Change in $\upsilon_{N-D} = 3200x\frac{1}{\sqrt{\frac{1.75}{0.933}}} = 2336$

The shift seen on the deuterated oxamic acid spectra at approximately 2336cm^{-1} confirms that oxamic acid has indeed been fully deuterated.

7.3 Appendix 3

Structural analysis of Single crystal dihydrate
2,4-dichloro-5-sulfamoylbenzoic acid

The dihydrate crystal structure contains 16 molecules in the unit cell and the extensive hydrogen bonding results in a complex packing mode within the crystal that is not easily visualized. Figure 7.3.1 illustrates the molecular structure of the dihydrate, also shown are the water molecules.

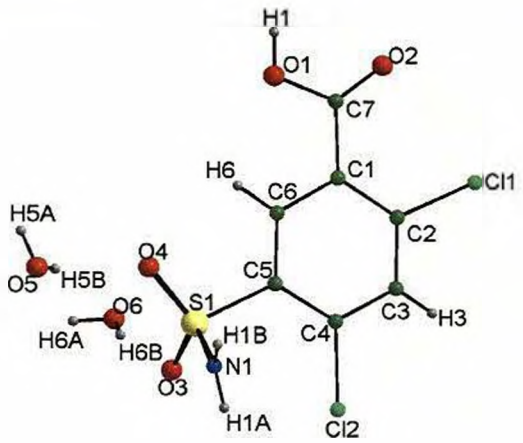

Figure 7.3.1: Molecular conformation of dihydrate structure. Also shown here are the water molecules.

The dihydrate molecules sit end to face and form chains through a complex hydrogen bonding arrangement involving two water molecules. These chains form layers of type N-H...O by the formation of a bond between a single amino hydrogen and an oxygen atom from a water molecule. Within sulfonamide crystal structures the presence of the C(4) motif of type N-H...O=S is extremely common as is the $R_2^2(8)$ motif. However within this dihydrate crystal structure because of the presence of two water molecules, these commonly observed motifs are no longer a feature and are substituted by more complex arrangements (see figure 7.3.2).

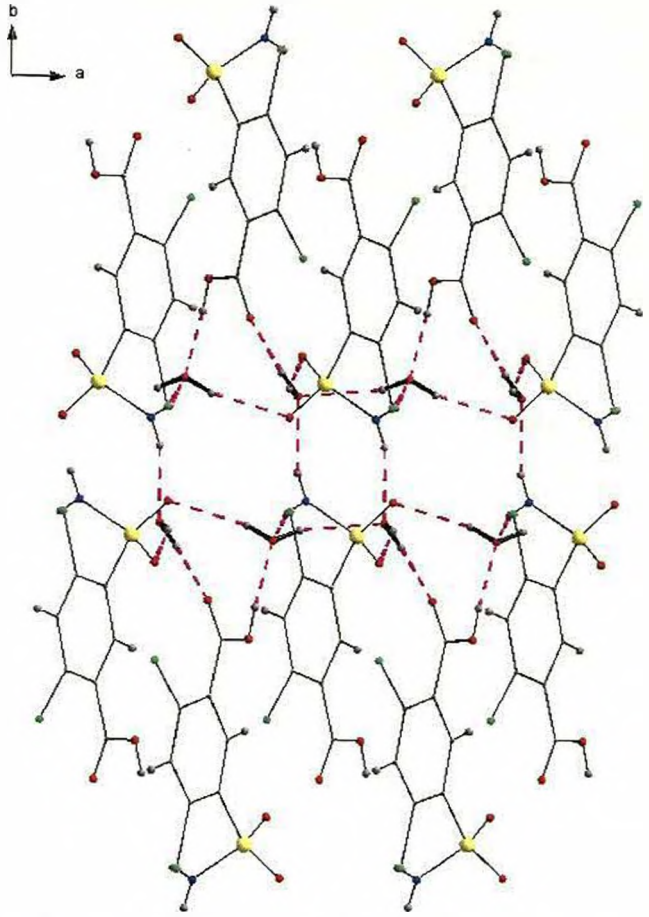

Figure 7.3.2: The complex crystal structure of the dihydrate formed through extensive hydrogen bonding via water molecules

The sulfonamide oxygen (O_3), through a network of three water molecules and the carboxylate group forms a C(14) chain whereas the (O_4) sulfonamide oxygen forms a C(12) motif via two water molecules, the carboxylate functional group and a single amino hydrogen. These sulfonamide interactions join adjacent molecules (which sit head to tail) together to form long chains; the remaining amino hydrogen joins together these chains to form the overall layered crystal structure by the formation of N-H...O type hydrogen bonds through a molecule of water. The hydrogen bonding within the dihydrate is illustrated in table 7.3.1.

Donor --- H....Acceptor	[symmetry]	D - H (Å)	H...A (Å)	D...A (Å)	D - H...A(Å)
O(1) -- H(1) .. O(6)	[-1/4+x , 1/4-y , -1/4+z]	1.0771	2.2958	3.2515	146.86
N(1) -- H(1a) .. O(5)	[-1/2+x , y , -1/2+z]	1.0771	2.5310	3.3532	132.42
N(1) -- H(1b) .. O(6)	[-1/2-x , 1/2-y , z]	1.0771	2.2958	3.2515	146.86
O(5) -- H(5a) .. O(2)	[3/4+x , 1/4-y , -1/4+z]	1.0771	2.5310	3.3532	132.42
O(5) -- H(5b) .. O(4)	[-1/2+x , y , 1/2+z]	1.0771	2.2958	3.2515	146.86
O(6) -- H(6a) .. O(5)	[x , y , z]	1.0771	2.5310	3.3532	132.42
O(6) -- H(6b) .. O(3)	[x , y , z]	1.0771	2.2958	3.2515	146.86

Table 7.3.1 Hydrogen bonding geometry within the dihydrate structure

7.4 Appendix 4

Final refined atomic coordinates for 2,4-dichloro-5-sulfamoylbenzoic acid.

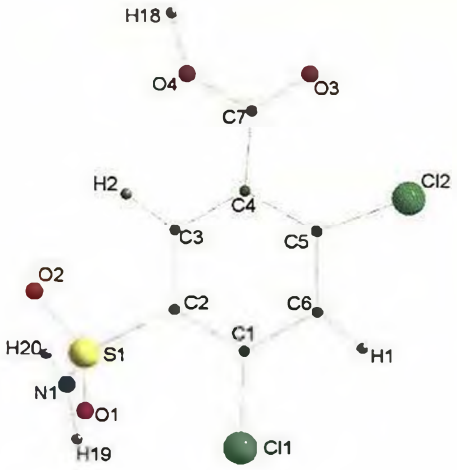

Name	*x*	*y*	*z*	Fraction	U_{iso}
C_1	0.3458(2)	0.1904(2)	0.9412(2)	1.00	0.030(1)
C_2	0.3890(2)	0.1841(2)	0.7711(2)	1.00	0.030(1)
C_3	0.5482(2)	0.2470(2)	0.7891(2)	1.00	0.030(1)
C_4	0.6434(2)	0.3480(2)	0.9791(2)	1.00	0.030(1)
C_5	0.6093(2)	0.3465(2)	1.1524(2)	1.00	0.030(1)
C_6	0.4785(2)	0.2434(2)	1.1334(2)	1.00	0.030(1)
C_7	0.8174(2)	0.3978(20	1.0121(2)	1.00	0.030(1)
Cl_1	0.1696(1)	0.0880(1)	0.9086(1)	1.00	0.036(11)
Cl_2	0.7229(1)	0.4326(1)	1.3968(1)	1.00	0.036(11)
S_1	0.2536(2)	0.0958(2)	0.5316(2)	1.00	0.052(12)
O_1	0.2316(3)	-0.0691(3)	0.5092(3)	1.00	0.037(2)
O_2	0.3486(2)	0.1186(2)	0.4200(2)	1.00	0.037(2)
O_3	0.9342(3)	0.4458(3)	1.1663(3)	1.00	0.037(2)
O_4	0.8188(2)	0.4369(2)	0.8589(2)	1.00	0.037(2)
N_1	0.0757(2)	0.2041(2)	0.4964(2)	1.00	0.037(3)
H_1	0.423(4)	0.252(4)	1.243(4)	1.00	0.05000
H_2	0.588(4)	0.256(4)	0.673(4)	1.00	0.05000
D / H_{18}	0.917(6)	0.494(6)	0.834(6)	0.67 / 0.33	0.05000
D / H_{19}	-0.027(3)	0.168(3)	0.511(3)	0.67 / 0.33	0.05000
D / H_{20}	0.055(5)	0.311(5)	0.461(5)	0.67 / 0.33	0.05000

Final refined atomic coordinates, isotropic displacement parameters, fraction and atomic numbering scheme for 2,4-dichloro-5-sulfamoylbenzoic acid.

Intramolecular distances and angles

$C_1 - C_2$	1.45(1) Å	$C_1 - C_6$	1.45(1) Å	$C_1 - Cl_1$	1.73(1) Å
$C_2 - C_3$	1.45(1) Å	$C_2 - S_1$	1.76(1) Å	$C_3 - C_4$	1.45(1) Å
$C_3 - H_2$	1.07(1) Å	$C_4 - C_5$	1.45(1) Å	$C_4 - C_7$	1.48(1) Å
$C_5 - C_6$	1.45(1) Å	$C_5 - Cl_2$	1.73(1) Å	$C_6 - H_1$	1.08(1) Å
$S_1 - O_1$	1.43(1) Å	$S_1 - O_2$	1.43(1) Å	$S_1 - N_1$	1.60(1) Å
$N_1 - H_{19}$	1.01(1) Å	$N_1 - H_{20}$	1.01(1) Å	$C_7 - O_3$	1.21(1) Å
$C_7 - O_4$	1.31(1) Å	$O_4 - H_{18}$	1.12(1) Å		

$C_2 - C_1 - C_6$	117(1) °	$C_1 - C_2 - C_3$	122(1) °	$C_1 - C_2 - S_1$	121(1) °
$C_1 - C_6 - H_1$	108(1) °	$C_2 - C_1 - Cl_1$	118(1) °	$C_2 - C_3 - H_2$	127(1) °
$C_2 - S_1 - O_1$	111(1) °	$C_2 - S_1 - O_2$	100(1) °	$C_2 - S_1 - N_1$	104(1) °
$C_2 - C_3 - C_4$	116(1) °	$S_1 - N_1 - H_{19}$	119(1) °	$S_1 - N_1 - H_{20}$	125(1) °
$C_1 - C_6 - C_5$	118(1) °	$O_3 - C_7 - O_4$	116(1) °	$O_1 - S_1 - O_2$	113(1) °
$N_1 - S_1 - O_1$	113(1) °	$N_1 - S_1 - O_2$	111(1) °	$C_3 - C_2 - S_1$	116(1) °
$C_3 - C_4 - C_5$	120(1) °	$C_3 - C_4 - C_7$	118(1) °	$C_4 - C_5 - C_6$	119(1) °
$C_4 - C_5 - Cl_2$	129(1) °	$C_4 - C_7 - O_3$	128(1) °	$C_4 - C_7 - O_4$	111(1) °
$C_4 - C_3 - H_2$	113(1) °	$C_7 - O_3 - H_{18}$	119(1) °	$C_7 - O_4 - H_{18}$	132(1) °
$C_5 - C_6 - H_1$	124(1) °	$H_{19} - N_1 - H_{20}$	114(1) °	$O_3 - H_{18} - O_4$	168(1) °
$C_5 - C_4 - C_7$	116(1) °	$C_6 - C_5 - Cl_2$	110(1) °	$C_6 - C_1 - Cl_1$	121(1) °

Geometric analysis including distances (Å) and angles (°) for the final refined structure of anhydrous 2,4-dichloro-5-sulfamoylbenzoic acid.

7.5 Appendix 5

Structure determination of oxamic acid from single crystal X-ray diffraction

Data were recorded at room temperature on a Bruker Smart 6000 diffractometer equipped with a CCD detector and a copper tube source. The structure was solved and refined using SHELXL (Sheldrick, G.M. SHELXL. Program package for crystal structure determination. University of Gottingen, Germany).

Empirical formula	$C_2 H_3 N_3 O$
Formula weight	85.07
Temperature	293(2) K
Wavelength	1.54178 A
Crystal system, space group	Monoclinic, Cc
a	9.530(5) A
b	5.424(3) A
c	6.866(4) A.
β	107.18(4) deg.
Volume	339.1(3) A^3
Z, Calculated density	3, 1.250 Mg/m^3
Crystal size	0.20 x 0.12 x 0.08 mm
Final R indices [I>2sigma(I)]	
R1	0.2160
wR2	0.4178

Crystal data and structure refinement.

	x	y	z	U(eq)
O(3)	0.4527(7)	0 .8718(16)	0.7305(9)	0.021(2)
O(4)	0.6696(9)	0.8769(17)	0.9767(12)	0.034(3)
O(1)	0.6856(10)	1.3607(19)	0.9763(15)	0.052(3)
O(2)	0.4573(8)	1.3766(18)	0.7417(11)	0.027(2)
C(2)	0.5520(20)	0.9803(18)	0.8390(40)	0.028(3)
C(1)	0.5540(20)	1.2669(18)	0.8390(40)	0.029(3)

Atomic coordinates and equivalent isotropic displacement parameters (A^2).

8.0 References

Aakeroy. C. B. and Seddon. K. R., *Chem. Soc. Rev*, **(1993)**, 22, 397-407

Accelrys, Cambridge, UK

Allen. F. A., Kennard. O., Cambridge Crystallographic Data Centre: *Chem. Des. Autom. News.* **(1993)**, 8, 31-37

Andreev. Y. G., Lightfoot. P., Bruce. P. G., *Chem. Commun.* **(1996)**, 2169-2170

Andrews. D.H., *Phys. Rev.* **(1930)**, 36, 544-554

Berstein. J. Polymorphism in molecular crystals, Clarendon press, Oxford, **(2002)**

Berstein. J., Davis. R. E., Shimoni. L., Chang. N., *Angew. Chem. Int. Ed. Engl.* **(1995)**, 34, 15, 1555-1573

Beyer. T., Lewis. T., Price. S. L., *Cryst Eng Comm.* **(2001)**, 44, 1-35

Bouke. P., van Eijck., Kroon. J., *Acta Cryst.* **(2000)**, B56, 535-542

Boultif. A., Louer. D. J., *Appl. Crystallogr.* **(1991)**, 24, 987-993

Bruno. I.J., Cole. J.C., Lommerse. J.P.M., Rowland. R.S., Taylor. R. and Verdonk. M.L. J., *Comput.-Aided. Molec. Design.* **(1997)**, 11, 525

Caira. M. R., *Top. Curr. Chem.* **(1998)**, 198, 164

Carvajal-Rodriguez. J in collected Abstracts of Powder Diffraction Meeting, Toulouse, France. **(1990)**, 127

Cheetham. A. K., Day. P. (ed), Solid state chemistry;techniques. OUP Oxford, **(1987)**

Cockcroft. J. K, PROFIL, Version 5.17, Department of Crystallography, Birkbeck College, UK, **(1994)**

Coelho. A . A., *J. Appl. Cryst.* **(2000)**, 36, 86-95

Curran. C. J., *Am. Chem. Soc.* **(1945)**, 67, 1835-1837

Dauber-Osguthorpe. P., Roberts. V. A., Osguthorpe. D. J., Wolff. J., Genest. M., Hagler. A. T. *Proteins: Structure, Function and Genetics.* **(1988)**, 4, 31-47

Davey. R. J., *Chem Comm.* **(2003)**, 1463 – 1467

David. W. I. F., Shankland. K., Shankland. N., *Chem. Commun.* **(1998)**, 931

David. W. I. F., Shankland. K., Pulham. C. R., Balgden. N., Davey. R. J., Song. M., *Angew. Chem. Int. Ed.* **(2005)**, 44, 7032 - 7035

David. W. I. F., Shankland. K., McCusker. L. B., Baerlocher. C. H. *Structure determination from powder difrraction data (International Union of Crystallography - Monographs on crystallography).* Oxford University Press **(April 4, 2002)**.
Day. G. M., Motherwell. W. D. S., Ammon. H. L., Boerrigter. S. X. M., Della Valle. R. G., Venuti. E., Dzyabchenko. A., Dunitz. J. D., Schweizer. B., van Eijck. B. P., Erk. P., Facelli. J. C., Bazterra. V. E., Ferraro. M. B., Hofmann. D. W. m., Leusen. F. J. j., Liang. C., Pantelides. C. C., Karamertzanis. P. G., Preice. S. L., Lewis. T. C., Nowell. H., Torrisi. A., Scheraga. H. A., Arnautova. Y. A., Schmidt. M. U. and Verwer. P. *Acta Cryst.* **(2005)**, B61, 511-527

Desiraju. G. R., Steiner. T., *The weak Hydrogen Bond in structural chemistry and biology*, Oxford Science Publications, **(1999)**

Dunitz, J. D and Bernstein, J,. *Acc. Chem. Res.* **(1995)**, 28, 193

Dunitz. J. D., *Pure Appl. Chem.* **(1991)**, 63, 177

Etter, M. C., *Acc. Chem. Res.* **(1990)**, 23(4), 120-126

Etter. C. E., MacDonald. J. C., Bernstein. J., *Acta Cryst.* **(1990)**, B46, 256-262

Gavezzotti. A., *Acc. Chem. Res.* **(1994)**, 27, 309-14

Giacovazzo. C., *Acta. Cryst.* **(1996)**, A52, 331

Gordy. W. and Stanford. S. C., *J. Am. Chem. Soc.* **(1941)**, 63, 1094-1096

Gordy. W. and Stanford. S. C., *J. Chem. Phys.* **(1940)**, 8, 170-177

Grell. J., Bernstein. J., Tinhofer. G., *Acta. Cryst.* **(1999)**, B55, 1030-1043

Haleblian. J. K., McCrone. W., Pharmaceutical applications of polymorphism. *J. Pharm. Sci.* **(1969)**, 58(8), 911 - 929

Halgren. T. A. J., *Comput. Chem.* **(1996)**, 17, 490-586

Hammett. L. P, J. *Chem. Educ.* **(1940)**, 17, 131-132

Hanna. S., Coulter. P. D., Windle. A. H., J., *Chem. Soc. Faraday Trans.* **(1995)**, 91, 2615

Harris, K.D.M., Johnston, R.L., Kariuki, B.M. *Acta Cryst.* **(1998)**, A54, 632

Harris. K. D. M., Kariuki. B. M., Tremayne. M. *Sci. Forum.* **(1998)**, 32, 278

Harris. K. D. M., Tremayne. M., Lightfoot. P., Bruce. P.G., *J. Am. Chem. Soc.* **(1994)**, 116, 3543

Harris. K. D. M., Tremayne. M. *Chem. Mater.* **(1996)**, 8, 2554

Harris. K.D.M., Tremayne. M., Kariuki. B.M., *Angew. Chem. Int. Ed* **(2001)**, 40, 1626 - 1651

Hendrickson. J. B., *J. Am. Chem. Soc.* **(1961)**, 83, 4537-4547

Heraud. J., Hospital. M., Housty. J., *C. R. Acad. Sci. Ser.C (Chim).* **(1966)**, 263, 1126

Hilfiker. R. (ed). *Polymorphism in the pharmaceutical industry.* Wiley- VCH, Germany, Weinheim. **(2006).**

Hill. T. L., *J. Chem. Phys.* **(1946)**, 14, 465

Hospital. M., *Acta Crystallogr.B:Struct.Crystallogr.Cryst.Chem.* **(1971)**, 27, 484

Hospital. M., Housty. J., *Acta. Cryst.* **(1966)**, 20, 626

Hospital. M., Housty. J., *Acta. Cryst.* **(1966)**, 20, 368

Hospital. M., Housty. J., *Acta Cryst.* **(1966)**, 21, 413

Izumi. F., Asano. H., Murata. H., Watanabe. N., *J. Appl. Cryst.* **(1987)**, 20, 411

Jeffrey. G. A., *Introduction to hydrogen bonding*, Oxford University Press Inc, **(1997)**

Kariuki. B.M., Serrano-Gonzalez. H., Johnson. R. L., Harris. K.D.M., *Chem. Phys. Lett.* **(1997)**, 280, 189

Kato. Y., Oguro. N., Yagi. K., *Mem. Osaka. Kyoiku. Univ. Ser3.* **(1981)**, 29, 91

Kato. Y., Yamazaki. M., Yokota. M., *Mem. Osaka. Kyoiku. Univ. Ser3.* **(1979)**, 27, 125

Khoshkhoo. S., Anwar. J., *J. Phys. D:Appl. Phys.* **(1993)**, B90, 26

Kobayashi. K., Sato. A., Sakamoto. S., Yamaguchi. K. *J. Am. Chem. Soc.* **(2003)**, 125, 3035

Wall. L., Christiansen. T., Orwant. J. *Programming Perl (3rd Ed.), O'Reilly*, Sebastopol, USA. **(2000)**

Ladd. M. F. C., Palmer. R. A. *Structure Determination by X-ray crystallography, 2nd edition,* Springer New York, **(1995)**

Larson. A.C., Von Dreele. R.B. *Report Number LAUR-86-748.* Los Alamos National Laboratory, Los Alamos, New Mexico, USA. **(1997)**

Latimer. M. W., Rodebush. H. W., *J. Am. Chem. Soc.* **(1920)**, 42, 1419-33

Le Bail. A., Duroy. H., Fourquet. J. L., *Mater. Res. Bull.* **(1988)**, 23, 447-452

Leusen, F. J. J., *Cryst. Growth.* **(1996)**, 166, 900

Lommerse. J. P. M., Motherwell. W. D. S., Ammon. H. L., Dunitz. J. D., Gavezzotti. A., Hofmann. D. W. M., Leusen. F. J. J., Mooij. W. T. M., Price. S. L., Schweizer. B., Schmidt. M. U., van Eijck. B. P., Verwer. P., Williams. D. E., *Acta Cryst.* **(2000)**, B56, 697-714

Maddox. J., *Nature.* **(1988)**, 335, 201

Mayo. S. L., Olafson. B. D., Goddard III. W. A., *J. Phys. Chem.* **(1990)**, 94, 8897-909

Mayo. S. L., B. D. Olafson., *J. Phys. Chem.* **(1990)**, 94, 8897-8909

McClusker. L. B., Von Dreele. R. B., Cox. D. E., Louer. D., Scardi. P., *J. Appl. Cryst.* **(1999)**, 32, 36-50

McCrone. W. C., *Polymorphism in physics and chemistry of the organic solid state*, vol. II, ed. D. Fox, M. M Labes and A Weissberger, Wiley Interscience, New York, **(1965),** 725 - 767

Metropolis. N., *J. Chem. Phys.* **(1953)**, 21, 1087

Millar. G. R., Garroway. A. N., *Navel Research Lab Washington DC, Subject matter report. Part II.* **(2001)**, 33

Mooij. W. T. M., Leusen. F. J. J., *Phys. Chem. Chem. Phys.* **(2001)**, 3, 5063-5066

Mooij. W. T. M., van Eijck. B. P., Price. S. L., Verwer. P., Kroon. J. *J. Comp. Chem.* **(1999)**, vol 19, no 4, 459-474

Mooij. W. T. M.; van Eijck. B. P.; Price. S. L.; Verwer. P. and Kroon. J., *J. Comput. Chem.* **(1998)**, 19, 459-74

Motherwell. W. D. S., Shields. G. P., Allen. F. H., *Acta Cryst.* **(2000)**, B56, 466-473

Motherwell. W. D. S., Ammon. H. L., Dunitz. J. D., Dzyabchenko. A., Erk. P., Gavezzotti. A., Hofmann. D. W. M., Leusen. F. J. J., Lommerse. J. P. M., Mooij. W. T. M., Price. S. L., Scheraga. H., Schweizer. B., Schmidt. M. U., van Eijck. B. P., Verwer. B. P. and Williams. D. E., *Acta Cryst.* **(2002)**, B58, 647-661

Motherwell. W. D. S., Shields. G. P., Allen. F. H. *Acta Cryst.* **(1999)**, B55, 1044-1056

Neuman. M. A., *J. Appl. Cryst.* **(2003)**. 36, 356-365

Nyburg. S. C ., Faerman. C. H., *Acta. Cryst.* **(1985)**, B41, 274-279

Orii. S., Nakamura. T., Takaki. Y., Sasada. Y., Kakudo. M., *Bull. Chem. Soc. Jpn.* **(1963)**, 36, 788

Ostwald. W. *Z. Phys. Chem.* **(1987)**, 22, 289 - 330

Patterson. A. L., *Phys. Revs.* **(1934)**, 46, 372

Pawley. G. S., *J. Appl. Cryst.* **(1981)**, 14, 357

Pazur. R. J., Hocking. P. J., Raymond. S., Marchessault. R. H., *Macro-molecules.* **(1998)**, 31, 6585

Pedireddi. V.R., *Cryst. Eng. Comm.* **(2002)**, 4, 315

Penfold. B. R., White. J. C. B., *Acta Cryst.* **(1959)**, 12, 130 - 135

Pillardy. J., Arnautova. Y. A., Czaplewski. C., Gibson. K. D., Scheraga. H., *Proc. Natl. Acad. Sci. USA.* **(2001)**, 98(22), 12351-56

Price. S. L. *Cryst. Eng. Comm.* **(2004)**, 6, (61), 344-353

Price. S. L. Toward more accurate model intermolecular potentials for organic molecules. In Lipkowitz. K. B. and Boyd. D. B. (eds.), *Reviews in Computational Chemistry.* John Wiley & Sons, New York. **(2000)**, 14, 225-289

Rietveld. H. M., *J. Appl. Cryst.* **(1969)**, 2, 65

Rosenfield. R. E. Jr., Swanson. S. M., Meyer. E. F. Jr., Carrell. H. L., Murray-Rust. P., *J. Mol. Graphics.* **(1984)**, 2, 43

Sarma. J. A., Desiraju. G. R., *Crystal growth and design.* **(2002)**, 2(2), 93-100

Sato. K., *J. Phys. D:Appl. Phys.* **(1993)**, B77, 26

Seaton. C. C., Tremayne. M. *POSSUM: Programs for direct space structure solution,* University of Birmingham. **(2002)**

Seaton. C.C., Tremayne. M., *Chem. Commun.* **(2002)**, 880

Shirley. R. A., *The CRYSFIRE system for Automatic Powder Indexing: User's Manual.* Lattice Press, Cambridge, England, UK. **(2000)**

Spek. A. L., *Acta. Cryst.* **(1990)**, A46 (supplement), C34

Spek. A. L., *J. Appl. Cryst.* **(2003)**, 36, 7-13

Stockton. G. W., Godfrey. R. J., *Chem. Soc. Perkin Trans.* **(1998)**, 2, 2061

Swaminathan. K. S., Craven. B. M., *ACA*, Ser.2, **(1982)**, 10, 13

Taylor. R., Mullaley. A., Mullier. G. W., *Pestic. Sci.* **(1990)**, 29, 197

Tedesco. E., Turner. G. W., Harris. K. D. M., Johnson. R. L., Kariuki. B. M., *Angew. Chem. Int. Ed.* **(2000)**, 39, 4488

Thomas. J. M., *Angew. Chem.* **(1994)**, 106, 963

Thomas. J. M., *Angew. Chem.* **(1998)**, 100, 1735

Thomas. J. M., *Angew. Chem.* **(1999)**, 111, 3800

Thomas. J. M., *Angew. Chem. Int. Ed. Engl.* **(1988)**, 27, 1673

Thomas. J. M., *Angew. Chem. Int. Ed. Engl.* **(1994)**, 33, 913

Thomas. J. M., *Angew. Chem. Int. Ed. Engl.* **(1999)**, 38, 3588

Tremayne. M., Seaton. C. C., *Chem. Comm.* **(2002)**, 880-881

Tremayne. M., Seaton. C. C., Glidewell. C., *American Crystallographic Association.* **(2002)**, 37, 35-50

Tremayne. M., Glidewell. C., *Chem. Commun.* **(2000)**, 2425

Visser. J. W., *J. Appl. Crystallogr.* **(1969)**, 2, 89

Von Dreele. R. B., *J. Appl. Cryst.* **(1999)**, 32, 1084-1089

Von Dreele. R. B., *Acta Cryst.* **(2000)**, D56, 1549-1553

Weissbuch. I., Popovitz-Biro. R.,Leiserowitz. L., *Acta Crystallogr.* **(1995)**, B51:115

Werner. P-E., Eriksson. L., Westdahl. M., *J. Appl. Crystallogr.* **(1985)**, 18, 367

West. A. R. *Basic Solid State Chemistry, 2nd edition*, John Wiley & Sons, **(1999)**

Westeimer. F. H. '*Steric effects in organic chemistry*', ed. M. S. Newman, Wiley, New York, **(1956)**

Wiles. D. B., Young. R. A., *J. Appl. Cryst.* **(1981)**, 14, 149

Willock. D. J, Price. S. L., Leslie. M., Catlow. C. R. A. *J. Comput. Chem.* **(1995)**, 16 (5), 628 - 647

Zollinger. H., *Color Chemistry*, 2. Aufl, VCH, Weinheim, **(1991)**

Zorky. P. M., Kuleshova. L. N., *Acta.Cryst.* **(1980)**, B36; 2113 - 2115